Université Sorbonne Paris Cité

Thèse de doctorat

de l'Université Sorbonne Paris Cité

Préparée à l'Université Paris Diderot

Ecole doctorale BioSPC - 562

U1163 - Molecular Bases of Hereditary Kidney Diseases: Nephronophthisis and Hypodysplasia

Identification and Characterisation of Loss of Function Mutations in *KIF14* leading to Syndromic Renal Hypodysplasia

Par Madeline Louise REILLY

Thèse de doctorat de Biologie Cellulaire

Dirigée par Alexandre BENMERAH

Présentée et soutenue publiquement à Paris le 24/10/2018

Président du Jury : Dr. Jeanne Amiel - Institut Imagine

Rapporteurs : Dr. Sylvie Schneider-Maunoury - Institute of Biology Paris-Seine

Dr. Arnaud Echard - Institut Pasteur

Examinateurs : Dr. Renata Basto - Institut Curie

Dr. Evelyne Fischer - Institut de Biologie de l'Ecole Normale Supérieure

Directeur de thèse : Dr. Alexandre Benmerah - Institut Imagine

Titre : Identification et caractérisation de mutations perte de fonction du gène KIF14 impliquées dans une forme syndromique d'hypodysplasie rénale

Résumé : Des mutations dans le gène *KIF14* ont été précédemment identifiées dans des individus présentant soit une microcéphalie isolée soit une forme syndromique développementale et létale associant une microcéphalie sévère à une hypodysplasie rénale (RHD). Ce dernier phénotype a été considéré comme une ciliopathie, un semble de maladies génétiques liées à des défauts du cil primaire, un organite avec un rôle important dans des voies de signalisation et présent à la surface de nombreuses cellules quiescentes. Le gène *KIF14* code une kinésine mitotique qui joue un rôle clé pendant la cytocinèse mais qui n'a pas été décrite comme protéine ciliaire auparavant. Nous avons analysé les effets des mutations de *KIF14* retrouvées chez des fœtus de quatre familles présentant la forme syndromique. Nos analyses fonctionnelles montrent que les variations identifiées ont un impact sévère sur l'activité de la protéine et correspondent probablement à des mutations de perte de fonction (LOF). Notre analyse des tissus rénaux de fœtus humains a montré une accumulation des 'midbodies' positifs pour KIF14 dans la lumière des bourgeons urétéraux, mettant en évidence des similarités entre les événements mitotiques au début du développement cérébral et rénal. En analysant une lignée de poisson zèbre présentant une mutation non-sens précoce dans le gène *kif14* on a pu montrer un rôle conservé pour cette kinésine mitotique dans le développement rénal et cérébral. De manière intéressante, on a également observé des phénotypes associés à une ciliopathie chez les embryons mutants, suggérant encore une fois que kif14 pourrait jouer un rôle au cil. Cependant, nos analyses *in vitro* et *in vivo* ont finalement démontré que KIF14 n'a pas de rôle direct dans la ciliogenèse et que la perte de *kif14* chez le poisson zèbre phénocopie une ciliopathie par l'accumulation de cellules mitotiques et non ciliées dans les tissus ciliés. Nos résultats montrent que les mutations dans le gène *KIF14* entraînent un syndrome sévère associant une microcéphalie et RHD grâce à une fonction conservée dans la cytocinèse lors du développement du rein et du cerveau.

Mots clefs : KIF14 Cil Ciliopathie Rein Cerveau Microcéphalie Mitose Poisson zèbre Développement

Title : Identification and Characterisation of Loss of Function Mutations in KIF14 leading to Syndromic Renal Hypodysplasia

Summary : Mutations in KIF14 were previously shown to lead to either isolated microcephaly or to a developmental and lethal syndromic form associating severe microcephaly with renal hypodysplasia (RHD). The latter phenotype was considered reminiscent of a ciliopathy, relating to defects of the primary cilium, a signalling organelle present on the surface of many quiescent cells. KIF14 encodes a mitotic kinesin which plays a key role at the midbody during cytokinesis, and was not previously shown to be involved in cilia-related functions. Here, we have analysed four families with foetuses presenting with the syndromic form and harbouring variations in KIF14. Our functional analyses show that the identified variations severely impact the activity of KIF14 and likely correspond to loss-of-function (LOF) mutations. 0ur analysis on human foetal kidney tissues revealed the accumulation of KIF14-positive midbody remnants in the lumen of ureteric bud tips, highlighting similarities between mitotic events during early brain and kidney development. Subsequently, analysis of a kif14 mutant zebrafish line showed a conserved role for this mitotic kinesin. Interestingly, additional ciliopathy-associated phenotypes were also present in these mutant embryos, supporting a potential novel role for kif14 at cilia. However, our in vitro and in vivo analyses ultimately indicated that KIF14 does not have a direct role in ciliogenesis and that kif14 LOF in zebrafish phenocopies ciliopathies through an accumulation of mitotic, non-ciliated cells in ciliated tissues. Altogether, our results demonstrate that KIF14 mutations result in a severe syndrome associating microcephaly and RHD through a conserved function in abscission during kidney and brain development.

Keywords: KIF14 Cilia Ciliopathy Kidney Brain Microcephaly Mitosis Zebrafish Development

“Fish really are just little people with fins”

Nancy Hopkin

Acknowledgements

After three and a half years in the lab it's time to move on to pastures new. Firstly, thanks to Alex for the opportunity to work on this interesting project, as well as for putting up with me for all that time. We looked at lots of kinesins and at some points it did feel as though we were attempting to get through all 45. I've had the opportunity to learn so much and am especially grateful for having the chance to work with zebrafish. A special thank you to Sophie Saunier for accepting me in her lab for the M2 and unexpectedly for the PhD. Also for good naturedly accepting all my sarcasm over the years. Thanks to Cécile for her help with the paper, the project and reading the discussion at the last minute. Thanks to Corinne for regularly checking that myself and Lara were still alive during our weekend thesis writing sessions at the other end of the institute, and thanks to GéGé for keeping Christelle in line.

Working in this lab has been a lot of fun, and that's down to the amazing people in it. Of course a lot of people come and go, and I've seen many a PhD defence. The first was Evelyne, who set an incredibly high standard, just a pity about her terrible music choices with Alby. Some peoples don't find death metal a relaxing background to their experiments. At least it's impossible to 'sing along' to. We all know how sensitive the cells are to bad singing, although not as sensitive as they are to bad dancing. I still hold both Alby and Max responsible for killing my RPE1. You should probably come back and wear the wig and cape in the L2 to see if the cells die then, we still need N égal 2 after all. Although we may be in risk of an angry Christelle email. Despite all that special thanks do go to Alby for her amazing knowledge of literally everything you could ever need to do in the lab, Team Finger for all his support and enthusiasm, and Christelle for her endless help and for teaching me never to defrost two bottles of serum at the same time!

The list of people to thank is rather long, but here goes, thanks so much to Camille for all her support and jokes, from helping me with Minouche, to introducing the name LouLou and laughing about Manuel, it's been a lot of fun. Thanks to Marion for starting the KIF14 project, supervising my M2 and for all her support throughout. Rebecca Ryan for awesome advices, discussions about Marks and Spencer food, and gentle reminders about the 800 years of oppression. I look forward to opening our joint lab together in 2022. Marion Delous for her limitless fishes knowledge and amazing advice, although perhaps not for her Picard TeaTime offerings. Meriem for all her laughter and the occasional microscopy advice, still only 1* though. Gweltas and Charline, it was a genuine pleasure to work with one of you. Sara for teaching me so many new words and phrases in English and French, and of course for the secret friend's group. Olivier for determinedly fixing everything Meriem breaks in the lab and his occasional angry emails. Flora for being my guarantor despite my crazy landlady and the constant need to redo the paperwork for all the new flatmates. Hugo, Daniel and Guillaume for their jokes,

Potatoes and Vale for their enthusiasm, Gaëlle for beating Gweltas at Uno, Esther for all the cat pictures, Marina for her extremes of enthusiasm and depression, Stephanie – thanks fish lady, and Mélinda for organising anything you could ever need, including a last minute, new passport.

I've changed offices a few times but shared them with so many great people. From the original 508 with Nathalie and her Belgian Western blots, Laurine and her plans to move to Scotland and become a DJ, to the displaced 508 in the new lab with Sonia, Bruno and Julie, the thesis writing office with Lara, and finally the greenhouse with Franchies. It's been a pleasure. A special thanks to Franchies for showing me up with her perfect Queen-like English. I trust you to fly the British flag alone now that myself and Rebec have left ;)

Of course the biggest thank you is reserved for my fellow triplets, Lara De Tomasi and Marie Dupont! We started our M2 projects together, applied for three PhD grants for the same lab (and got them), and you've always been there in times of need. As everyone knows, doing a PhD is a stressful business, but with my two little buddies, I knew I always had a shoulder to lean on. Marie your enthusiasm for gossip is limitless, your organisational skills are incredible and your pronunciation of certain English TV programs is adorable. I look forward to coming back for the 29th March. Lara De Tomasi, where to start? You've helped me with so much, both in the lab and out of it. I'm so grateful that we've gone through all of this stress at the same time! I look forward to hearing about your future post-doc in England and sharing some fish and chips in Brighton.

So many of the people in this lab have amazing non-science talents. Charline and Alby have some amazing creative inspirations to transform giant cardboard boxes into much loved constructions, like Lara's life size car. Special mentions for Esther's mad drawing skills, Rebecca Ryan's crazy knitting and Gweltas's running…oh no wait, scratch that last one, I won, didn't I? But perhaps the most collective and amazing skill is everyone's baking abilities. From Hobbit-themed cakes, to Halloween, Christmas and even Rebecca Ryan, we've had some awesome Bake-Off creations. Of course, caking wasn't restricted to those special editions, and I'm so happy that so many people responded to our bullying to participate in Friday TeaTime every week. It's become a lab tradition and I hope someone takes over the ceremonial teapot once I've left. Although I still feel like you should carry on making a gluten free version to keep up the challenge.

None of this would have been possible without the amazing support of my family and friends. Since moving to Paris 5 years ago you've always been there to listen to my complaints, and made my day multiple times with surprise post packages. I look forward to seeing you all in Brighton shortly.

Finally, I would like to thank the jury, Sylvie Schneider-Maunoury, Arnaud Echard, Renata Basto, Evelyne Fischer and Jeanne Amiel for agreeing to evaluate my thesis work.

Table of Contents

Summary

Congenital abnormalities of the kidney and urinary tract (CAKUT) comprise a broad spectrum of renal and urinary tract malformations of varying severity. CAKUT affects around 3-6 per 1000 live births, represents approximately one fifth of all congenital abnormalities detected prenatally and is the leading cause of end-stage renal disease during childhood. Although the severity of CAKUT phenotypes is variable, the most severe forms are associated with foetal or perinatal death. Kidney defects, grouped under the term of renal hypodysplasia (RHD), range from unilateral or bilateral renal agenesis to renal hypoplasia and dysplasia or multicystic kidney dysplasia. These defects can occur in isolation, or when combined with extra-renal phenotypes are termed syndromic. Environmental factors, such as obesity and maternal diabetes, have been suggested to contribute to CAKUT, however, the identification of familial cases, with both autosomal dominant and recessive modes of inheritance, has revealed the importance of genetic factors. The analysis of these familial cases of CAKUT is complicated by incomplete penetrance and variable expressivity, whereby the same mutation in the same gene can give different phenotypes in different individuals. To date, mutations resulting in RHD in humans have been identified in more than 50 genes, revealing a great genetic heterogeneity. Most of these genes encode transcription factors and actors in key signalling pathways implicated in kidney development. Both targeted- and whole-exome sequencing are widely used techniques in the identification of novel candidate genes causing CAKUT.

Biallelic loss-of-function mutations in *KIF14*, encoding a mitotic kinesin required for cytokinesis, were found in foetuses presenting with bilateral renal agenesis or RHD associated with very severe microcephaly. The clinical aspects of these foetuses overlapped with the phenotypic spectrum of ciliopathies, a group of disorders related to defects in the structure or function of the primary cilium, a sensory organelle present on the surface of most cell types. KIF14 was subsequently proposed to have a thus far uncharacterised ciliary function. Using a combination of whole- and targeted-exome sequencing approaches, we identified biallelic damaging variations in *KIF14* in four additional families. These mutations were predicted to be damaging and absent from both in-house and public databases. All the affected foetuses presented with strikingly similar brain and kidney phenotypes, with severe microcephaly and either bilateral renal agenesis, severe non-cystic or cystic RHD, and demonstrated that biallelic mutations in *KIF14* lead to a new syndrome.

Kinesins are molecular motors known to bind their respective cargos through their C-terminal domain and microtubules through their motor domain. As a result of these interactions, the kinesin hydrolyses ATP to proceed along microtubules, usually in a plus-end directed manner. KIF14 is a member of the kinesin-3 family, which is highly conserved during evolution. It was identified as a key actor in

cytokinesis through interactions with PRC1 and citron kinase. KIF14 and citron kinase act reciprocally to ensure correct localisation at the midbody. Unsurprisingly, depletion of KIF14 was shown to lead to cytokinesis defects and binucleated cells.

Using *in vitro* approaches we have shown that the identified mutations affect both protein localisation and function and result in cytokinesis defects. However, the loss of *Kif14* in a murine cell line widely used to examine ciliary functions did not impact upon cilia. The use of the zebrafish as an *in vivo* model revealed that the loss of *kif14* recapitulated the phenotype observed in the affected foetuses in addition to a number of known ciliopathy-related phenotypes. Further analysis of *kif14*$^{-/-}$ embryos showed an accumulation of mitotic cells in numerous organs. We could determine that this mitotic block reduced ciliogenesis and thus the loss of *kif14* phenocopied a ciliopathy. Finally, the analysis of human foetal kidney sections has confirmed the role of KIF14 in cytokinesis in this organ, and highlighted parallels between brain and kidney development.

Abbreviations

ANB: Anterior Neural Boundary

ANR: Anterior Neural Ridge

aRGC: Apical Radial Glial Cell

CAKUT: Congenital Anomalies of the Kidney and Urinary Tract

CC: Coiled-coil

CIT: Citron Kinase

CNS: Central Nervous System

CP: Cortical Plate

CR: Cajal-Retzius

Dc: Central Pallium

Dl: Lateral Pallium

dLGE: Dorsal Ganglionic Eminence

Dm: Medial Pallium

Dp: Posterior Pallium

dpf: Days post-fertilisation

E#: Embryonic Day #

FHA: Forkhead-Homology Associated

GW#: Gestational Week #

hpf: Hours post-fertilisation

IFT: Intraflagellar Transport

INM: Interkinetic Nuclear Migration

iSVZ: Inner Subventricular Zone

IZ: Intermediate Zone

KD: Knockdown

KI: Knock-in

KIF: Kinesin Superfamily Member

KO: Knockout

LGE: Lateral Ganglionic Eminence

MBT: Midblastula Transition

MGE: Medial Ganglionic Eminence

MM: Metanephric Mesenchyme

mpf: Months post-fertilisation

MST: Mitotic Somal Translocation

MZ: Marginal Zone

NEC: Neuroepithelial Cell

oRG: Outer Subventricular Zone Radial Glial Cell

oSVZ: Outer Subventricular Zone

PNS: Peripheral Nervous System

PP: Preplate

PSB: Pallial-Subpallial Boundary

RGC: Radial Glial Cell

SHH: Sonic Hedgehog

SNP: Short Neuron Precursor

SP: Subplate

SVZ: Subventricular Zone

UB : Ureteric Bud

VZ: Ventricular Zone

WES: Whole Exome Sequencing

WGS: Whole Genome Sequencing

Introduction

Chapter One - Development of the Brain

The human brain is a highly complex organ whose development begins early during embryogenesis, continuing pre- and postnatally and thought to be complete by early adulthood. The brain and spinal cord form the central nervous system (CNS), connected to the rest of the body by the peripheral nervous system (PNS). The brain is principally composed of two cell types, neurons and support cells, or glia. The adult brain is composed of around 100 billion neurons, and the same number of glial cells. (von Bartheld *et al.*, 2016). Neurons are usually formed of a nucleus-containing cell body, an axon and many dendrites. Neurons transmit electrical and chemical impulses along the length of the axon and via synapses formed with the dendrites of other cells. These transmissions are aided by the addition of myelin sheaths by glial cells, which additionally act to maintain the neuronal environment. The combination of different connections generates signalling networks within the nervous system.

Neurons are generally divided into classes depending on their function. Afferent neurons transmit information from sensory organs back to the CNS, while efferent neurons signal from the CNS to muscles and organs within the body. Interneurons form connections between neurons, aiding in the formation of neural circuits. Additionally, neurons can also be divided into excitatory and inhibitory neurons which combine to finely balance the various signals within the nervous system.

The brain is broadly organised into three different domains, the forebrain, midbrain and hindbrain, which are roughly symmetrical along the longitudinal axis. The forebrain consists of the cerebrum, the thalamus and hypothalamus, while the hindbrain is composed of the pons, cerebellum and medulla oblongata (Figure 1). Each structure has distinct functions and is formed of specific arrangements of various subtypes of cells. In humans, the cerebrum is the largest domain of the brain and is crucial for higher functions, while the cerebellum is important for the coordination of fine movements. The two cerebral hemispheres are incompletely separated by the longitudinal fissure, within which lies the corpus callosum, a structure composed of axons signalling contralaterally from one hemisphere to the other.

During evolution, the folding of the cortex, present within the cerebrum, is thought to have been important in the development of higher cognitive functions. The cortex is formed of many folds, or gyri, and grooves, or sulci, allowing for a significant increase in surface area and neuron number. The cortex is a highly ordered structure, with neurons forming six defined layers. These layers are composed of different types of neurons and have specific functions in neural signalling, such as the interactions between neurons of layer VI and the thalamus. The formation of these structures and

connections is highly controlled throughout development, and any failures in these processes can lead to a broad range of defects.

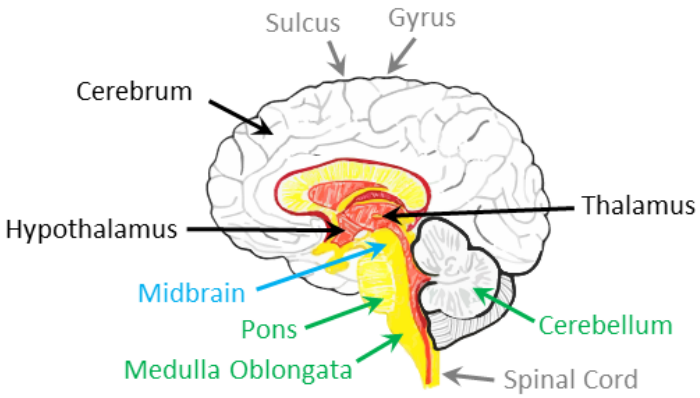

Figure 1. Schematic representation of the organisation of the brain. *Sagittal section, black lines indicate forebrain derived structures, blue lines for the midbrain and green for the hindbrain. Inspired by Bangalore et al. (2009)*

I. Early Human Embryonic Development

The architecture of the adult brain becomes clearer through an understanding of the early developmental origins of neural tissues. At two weeks gestation (2GW) the human embryo consists of an oval-shaped disc, formed of two layers, the epiblast and the hypoplast. The process of gastrulation transforms this bilaminar germ disc into a trilaminar germ disc. A transient structure, known as the primitive streak, appears on the dorsal surface of the disc. A crucial organising centre, the node, forms at the cranial end of the primitive streak and is important in establishing the various axes of the body. Cells surrounding the primitive streak undergo an epithelial-to-mesenchymal transition, migrating through the primitive streak in a process known as ingression (Burdsal *et al.*, 1993), resulting in the formation of the endoderm, mesoderm and ectoderm.

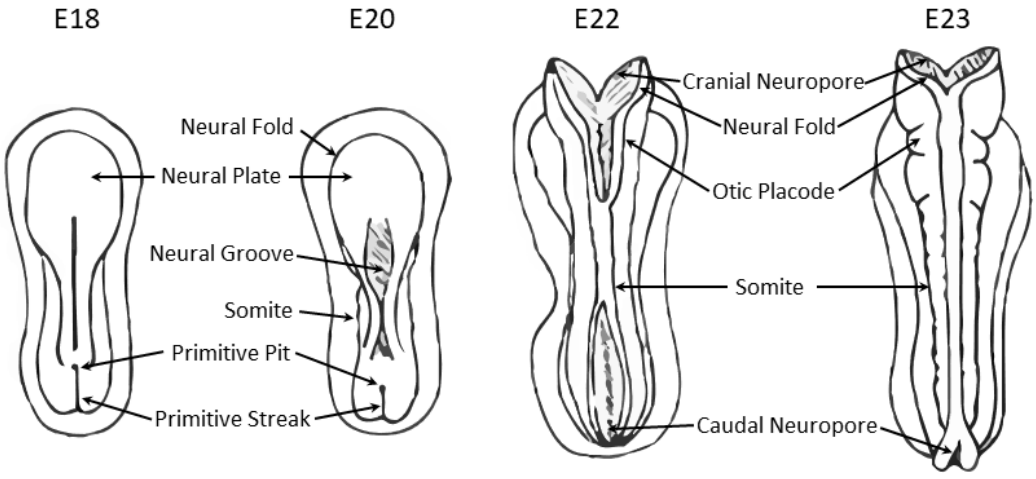

Figure 2. Dorsal view of forming neural tube in developing embryo. *Day of development indicated above each scheme. Inspired by Hawryluk et al. (2012).*

Ingressing cells which remain at the midline form both the prechordal plate and the notochordal process, both of which induce the overlying ectoderm to form the neural plate, at around embryonic day 18 (E18; Figure 2). The notochordal process will transform from a hollow tube to a solid rod, the notochord, which subsequently plays an essential role in the development of the central nervous system (G.C. Schoenwolf *et al.*, 2014). BMP signalling is important in the specification of cells of the ectoderm, with low levels inducing the formation of the neural plate. Within the cells of the neural plate, BMP signalling is additionally repressed through expression of the Sox family of transcription factors (S. I. Wilson *et al.*, 2001).

The cells of the neural plate subsequently form the neural tube, which occurs at the anterior end through primary neurulation, and at the posterior end via secondary neurulation (Harrington *et al.*, 2009). In primary neurulation, the notochord induces the lateral cells of the neural plate to thicken and elevate forming the neural folds, causing a shallow groove to develop ventrally along the midline. This groove deepens and is known as the neural groove. The neural folds continue to elevate and will initially fuse at the midline towards the middle of the anteroposterior axis at E22-24 (Figure 2). The fusion of the neural folds along the midline results in the formation of the neural tube. There may be up to 5 sites of neural tube fusion in humans (O'Rahilly *et al.*, 2008). Closure of the anterior end of the neural tube occurs slightly earlier than the posterior end, at E24-26 and E26-28 respectively (Copp *et al.*, 2013).

Secondary neurulation involves the mesenchymal-to-epithelial transition of cells from both the endoderm and ectoderm layers to form a medullary cord, which hollows to form a lumen (G. C. Schoenwolf *et al.*, 1980). Formation of the neural tube at the junction between the sites of primary and secondary neurulation occurs through a coalescing of the lumens and bending of the neural plate. Through the differential regulation of various adhesion molecules, the neural tube will separate from the overlying ectoderm.

Before the complete closure of the neural tube the cranial end undergoes several morphological changes resulting in the formation of the primary, followed by secondary, brain vesicles (Figure 3). At approximately E19, the neural tube dilates cranially at three paired sites along the midline. These dilations give the three primary brain vesicles, rostrally to caudally, the prosencephalon, the mesencephalon, and the rhombencephalon. The neural tube expands through proliferation and the secretion of cerebrospinal fluid into the lumen, contributing to the formation, by E33, of the five secondary brain vesicles. The prosencephalon subdivides to give, anteriorly, the telencephalon and posteriorly, the diencephalon. The telencephalon will become the cerebral hemispheres, while the diencephalon will become the thalamus and hypothalamus. The mesencephalon becomes the

midbrain, while the rhombencephalon also subdivides giving both the metencephalon and the myelencephalon. The metencephalon will become the pons and cerebellum, while the myelencephalon will give rise to the medulla oblongata. The caudal region of the neural tube will become the spinal cord (G.C. Schoenwolf *et al.*, 2014).

Over the course of the development of these primary and secondary brain vesicles, the neural tube undergoes further morphological changes which will remodel the initially straight tube (Figure 3). Both the cephalic flexure, between the mesencephalon and the rhombencephalon, and the cervical flexure between the rhombencephalon and the spinal cord, bend the expanding neural tube along the longitudinal axis. The developing brain is further bent during the formation of the secondary brain vesicles by the pontine flexure, between the metencephalon and the myelencephalon (Moore *et al.*, 2011).

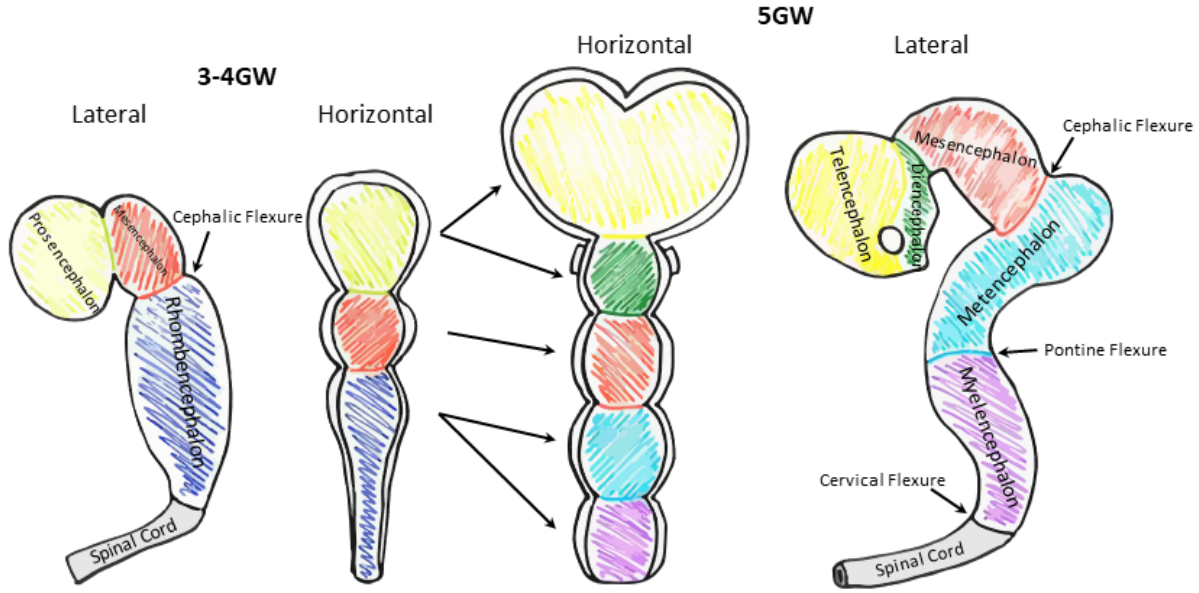

Figure 3. Development of primary and secondary brain vesicles. *Lateral and horizontal views, with gestational age indicated in weeks above each scheme*

II. Patterning of Early Human CNS

Although the events which lead to the formation of these developing brain structures are only partially understood, their patterning and specification are known to begin early during development. Three crucial secondary organising centres have thus far been identified in these early events, the Anterior Neural Ridge (ANR), the zona limitans intrathalamica and the isthmic organiser. Those cells which will give rise to the telencephalon, the future cerebral hemispheres, are positioned at the anterior end of the neural plate (Hebert *et al.*, 2008), and their induction is controlled by the ANR. The zona limitans intrathalamica is present in the diencephalon, while the isthmic organiser is positioned at the

midbrain-hindbrain boundary, with both controlling cell fate and specialisations within their respective regions.

The ANR is formed at anterior end of the embryo from cells at the edge of the neuroectoderm expressing Fibroblast Growth Factor 8, *FGF8* (Figure 4). These cells induce the expression of Forkhead Box G1, *FOXG1,* in the adjacent anterior neuroepithelial cells (Shimamura *et al.*, 1997). The loss of either FGF receptors (FGFR1, FGFR2 and FGFR3), or FGF signalling results in the loss of *FOXG1* expressing cells, and an absence of telencephalon development (Houart *et al.*, 1998; Paek *et al.*, 2009). FOXG1 and FGFs are known to create a positive feedback loop, whereby expression of one promotes the expression of the other, ensuring development of the telencephalon (Paek *et al.*, 2009). In addition to FGF, the antagonism of Wnt signalling is also known to be important in the formation of the telencephalon. Sine oculis homeobox 3, SIX3, acts to repress certain Wnt genes, and upon loss of SIX3 expression the telencephalon fails to form (Lagutin *et al.*, 2003). SIX3 additionally plays a role in promoting Sonic Hedgehog, SHH, expression, required for the formation of the ventral telencephalon (Geng *et al.*, 2008).

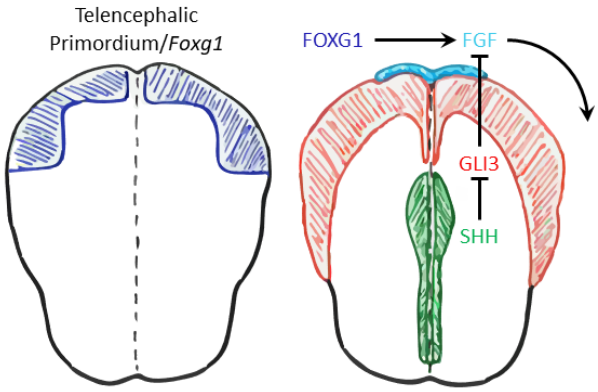

Figure 4: Signalling during early telencephalon development. *Anterior neural ridge is present at the anterior edge and expresses FGF (blue). Interactions between the ventralising signal sonic hedgehog (SHH; green) and the dorsalising signal GLI3 (red) are indicated. Inspired by Hebert et al. (2008)*

In addition to the specification of the anterior-posterior axis, significant signalling events define the mediolateral axis of the neural plate. Following the formation of the neural tube, the mediolateral patterning of the neural plate will become the dorsoventral patterning of the neural tube (Kiecker *et al.*, 2012). SHH is expressed by the underlying notochord and is therefore an important ventralising signal (Echelard *et al.*, 1993). Conversely, Bone Morphogenetic Protein 4 and 7, BMP4 and BMP7, are expressed by the overlying ectoderm, inducing expression of opposing dorsalising signals, such as GLI3 (Liem *et al.*, 1995; Litingtung *et al.*, 2000). SHH expression represses GLI3 and acts to ventralise the neural tube by inhibiting dorsalisation (Rallu *et al.*, 2002). These dorsoventral signals will have varying effects depending on the craniocaudal position along the neural tube. Caudally, where the neural tube

will give the spinal cord, the ventral-most cells will differentiate to give motor neurons, while the dorsal-most cells differentiate into sensory neurons (L. Wilson *et al.*, 2005).

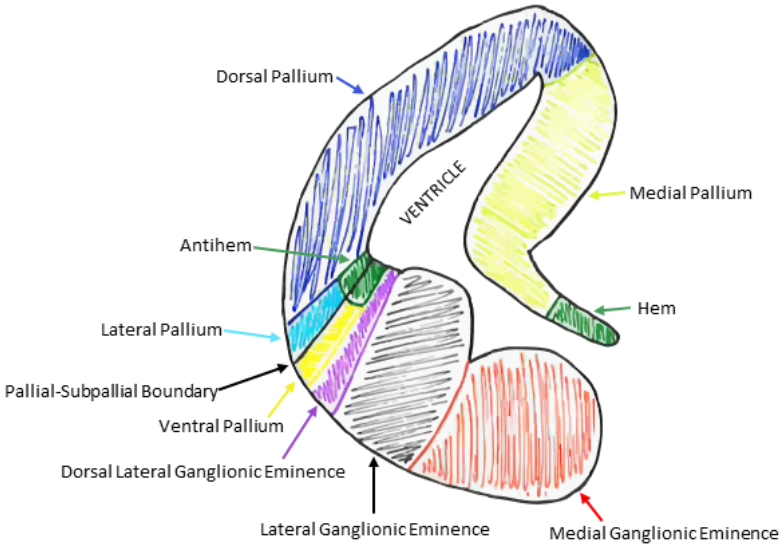

Figure 5: Subdivisions of the early telencephalon. *Coronal section indicating the position of various domains.*

Dorsoventral patterning at the cranial end of the neural tube, within the telencephalon, is, however, considerably more complicated (Figure 5). This secondary vesicle is subdivided into two domains, the dorsal pallium and ventral subpallium, separated by the pallial-subpallial boundary (PSB). The dorsal pallium is then further divided into four domains, the medial, dorsal, lateral and ventral pallia. The subpallium is divided into two domains, the lateral ganglionic eminence and the medial ganglionic eminence. Both these latter structures produce inhibitory interneurons, which migrate tangentially to populate the neocortex (Molnar *et al.*, 2006).

The dorsal pallium, the largest pallial domain, expresses the LIM-homeodomain transcription factor LHX2 and contains the neocortical primordium (Porter *et al.*, 1997). The neocortical primordium is flanked within the pallium by two signalling centres, the hem and antihem. Neither contributes directly to the formation of the neocortex, however, in the absence of LHX2, both regions expand at the expense of the neocortical primordium demonstrating the importance of regional specification within the developing forebrain (Bulchand *et al.*, 2001; Mangale *et al.*, 2008).

III. Neurogenesis

The cerebral hemispheres, arising from the telencephalon, are composed of the outermost cortex, containing neuronal cell bodies and known as the grey matter, and the innermost white matter layer formed principally of myelinated axons (G.C. Schoenwolf *et al.*, 2014). The cortex has a well characterised six-layered organisation, first described over a hundred years ago by Retzius and Cajal. Although, much progress has been made since these first observations, the complex processes

required for the formation of neurons and glia and their organisation in the mature cerebral cortex remain only partially understood.

a. Neocortical Progenitors

The neural tube is initially formed of a single layer of columnar neuroepithelial cells (NECs) (Hinds *et al.*, 1971). NECs are multipotent progenitors, and extensive rounds of self-proliferative mitoses are required to generate a sufficient progenitor pool to give rise to the cells of the nervous system (Alvarez-Buylla *et al.*, 2001; Gotz *et al.*, 2005). As development proceeds, NECs of the neocortical primordium gain glial characteristics, expressing SLC1A3 and BLBP, and become apical radial glial cells (aRGCs) (Hartfuss *et al.*, 2001). These cells initially undergo a proliferative self-renewal phase, but subsequently switch to asymmetrical, neurogenic divisions (Haydar *et al.*, 2003). Neurogenesis can occur directly, when mitosis results in the formation of a post-mitotic neuron, or indirectly when a more restricted intermediary progenitor is generated (Figure 6). The generation of specialised, terminally differentiated neural and glial cells is a highly coordinated, multi-step process (Tan *et al.*, 2013). While neuron production is believed to begin around E33 and be completed before birth (Bystron *et al.*, 2006), the formation of glia continues throughout at least the first two years of life.

In addition to the layers of the mature cortex, transient embryonic layers, or zones, have been characterised to define various stages of neurogenesis during development. Each zone has a distinct composition of progenitor and differentiated cell types undergoing different processes ("Embryonic vertebrate central nervous system: revised terminology. The Boulder Committee," 1970; Bystron *et al.*, 2008).

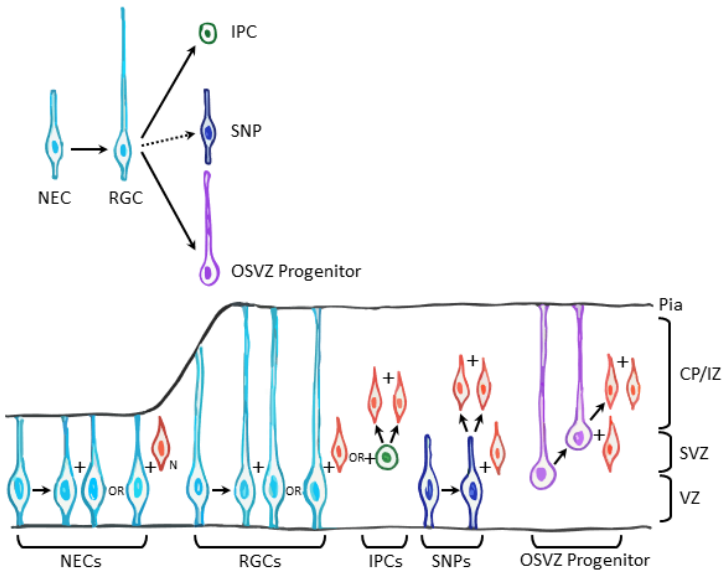

Figure 6. Neocortical Progenitors. *Neocortical progenitor (NEC), radial glial cell (RGC), intermediate progenitor cell (IPC), short neuron precursor (SNP), outer subventricular zone progenitor (OSVZ), neuron (N), ventricular zone (VZ), subventricular zone (SVZ), cortical plate (CP), intermediate zone (IZ). Inspired by Tan et al. (2013).*

i. Neuroepithelial Cells

As in the neural tube, NECs of the primitive cortex possess apicobasal polarity and connect to both the inner, ventricular, and outer, pial, surfaces. Initially these cells result in a pseudostratified appearance, with the position of each nucleus depending upon the current stage within unsynchronised cell cycles. During S-phase, nuclei are present at the pial surface, with mitosis occurring exclusively at the ventricular surface. The movement of nuclei within the cytoplasm during the cell cycle is termed Interkinetic Nuclear Migration [INM; (Sauer, 1935; Taverna *et al.*, 2010)]. The term 'ventricular zone' was coined to describe this layer of mitotic nuclei and is present as early as E30 (Bystron *et al.*, 2008). By undergoing mitosis at the luminal surface, it has been proposed that the mitotic cells are exposed to various secreted factors whose concentrations differ along the anteroposterior axis of the developing brain (Lehtinen *et al.*, 2011).

NECs are highly polarised, expressing specific apical makers, such as prominin-1, and tight junction and adherens junction proteins laterally at the apical surface (Aaku-Saraste *et al.*, 1996; Zhadanov *et al.*, 1999; Fargeas *et al.*, 2003), and basal markers such as integrin α_6 (Wodarz *et al.*, 2003). Centrosomes are located at the apical surface, with the mother centriole nucleating a primary cilium (Guemez-Gamboa *et al.*, 2014). During early development they undergo self-renewing mitosis to amplify the progenitor population. However, the onset of neurogenesis is marked by the expression of various transcription factors, including FOXG1, LHX2, PAX6 and EMX2 (Molyneaux *et al.*, 2007). NECs can subsequently produce either early neurons, or become more restricted aRGCs.

ii. Apical Radial Glial Cells

aRGCs are progenitor cells, possessing both radial and apical processes and formed from NECs. aRGCs express radial markers such as GLAST and GFAP (Campbell *et al.*, 2002). They were first thought to act as structural support cells, aiding in the migration of neurons from the VZ to the pial surface. However, they have subsequently been identified as progenitors of both neurons and glia (Noctor *et al.*, 2001). aRGCs are known to express PAX6, which is believed to repress cell cycle exit, thus maintaining a progenitor state (Gotz *et al.*, 1998).

aRGCs, as NECs, can divide to self-renew and amplify the progenitor population, but can also divide to produce more differentiated cell types (Huttner *et al.*, 2005). During neurogenesis, aRGCs can divide to give post-mitotic neurons, Intermediate Progenitor cells (IPCs) and Outer Subventricular Zone Radial Glial (oRG) progenitor cells (Tan *et al.*, 2013). This transition is thought to be related to a loss of PAX6 expression. During gliogenesis, aRGCs can generate astrocytes and oligodendrocytes (Kriegstein *et al.*, 2009).

iii. Outer Subventricular Radial Glial Cells

Contrary to aRGCs and NECs, oRGs migrate radially from the VZ and occupy an adjacent layer, known as the Outer Subventricular Zone (oSVZ). oRGs are unipolar, retaining a basal process in contact with the pial surface (Hansen *et al.*, 2010). In accordance with the loss of apical contact, oRGs do not express apical markers, such as Prominin-1, and PAR3 (Fietz *et al.*, 2010). While aRGCs and NECs undergo INM, whereby the nucleus migrates towards the ventricular surface prior to mitosis, the soma of oRGs ascends radially towards the pial surface in a process termed Mitotic Somal Translocation [MST; (Hansen *et al.*, 2010)]. Mitosis usually results in the inheritance of the radial process by one daughter cell, while the other becomes bipolar. Both daughter cells can undergo several rounds of self-renewing mitoses before generating post-mitotic neurons (Betizeau *et al.*, 2013).

iv. Intermediate Progenitor Cells

IPCs do not possess radial or apical processes, or, therefore, undergo INM. They also express higher levels of the transcription factors *EOMES*, *CUX1*, *CUX2* and *SAFB2* (Nieto *et al.*, 2004; Zimmer *et al.*, 2004; Britanova *et al.*, 2005; Englund *et al.*, 2005). IPCs deriving from aRGCs migrate radially to occupy the SVZ with IPCs from oRGs (Noctor *et al.*, 2004). While IPCs from aRGCs usually divide only once to give two post-mitotic neurons, those deriving from oRGs are known to be important amplifying cells which self-renew several times before producing neurons (Hansen *et al.*, 2010).

v. Short Neuron Precursors

Finally, short neuron precursors (SNPs) occupy the VZ with the aRGCs, but are a molecularly distinct progenitor subtype. They possess an apical process, in contact with the ventricular surface, but have a short, or absent, radial process, therefore failing to connect to the outer, pial surface. These cells contribute directly to neurogenesis by producing two neurons upon mitosis, termed a self-consuming division. Their cell cycle kinetics are believed to differ from those of the RGCs (Gal *et al.*, 2006; Stancik *et al.*, 2010).

b. Mitotic Symmetry

The self-renewal of progenitor cells or the generation of neurons or glia is thought to be highly related to the symmetry of cell division. Depending on the fate of the resulting cells from division of a progenitor, two different types of mitosis have been distinguished (Figure 7). Self-renewal of progenitors is considered symmetrical division, while the formation of a post-mitotic neuron along with the renewal of the mother progenitor is termed asymmetrical (Tan *et al.*, 2013). The mechanisms which regulate the symmetry of mitosis in progenitors are only partially understood, yet the correct functioning of these processes is known to be crucial for the formation of a mature and functional cortex.

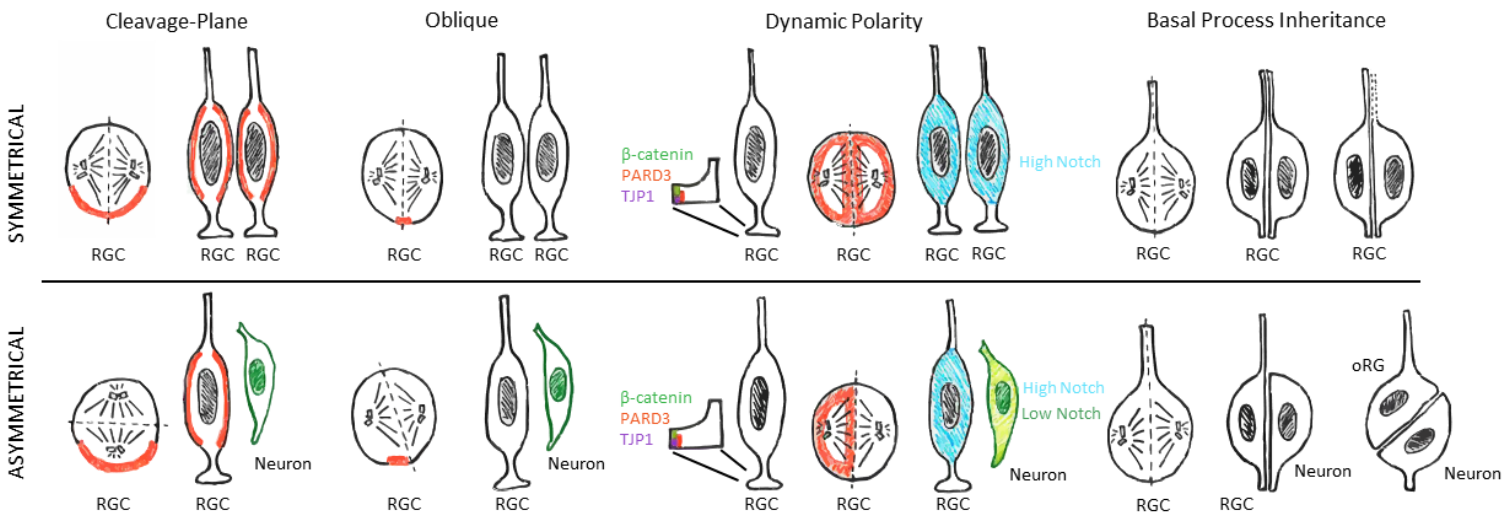

Figure 7. Models of the Orientation of Mitosis in Neocortical Progenitors. *Representation of cleavage-plane orientation, oblique division, dynamic polarity and basal process inheritance mechanisms.*

i. Cleavage-Plane Orientation

The orientation of the plane of mitosis has long been proposed to be an important, yet simple, mechanism to control the symmetry of cell division. When the spindles are oriented perpendicular to the ventricular surface, with both daughter cells sharing an apical membrane at this surface, mitosis is considered symmetrical (Chenn *et al.*, 1995). Although they largely remain to be identified, specific fate determinants are thought to be present at the ventricular surface. A cleavage plane which is perpendicular to this surface would ensure that these determinants are equally inherited by the two daughter cells (Zhong *et al.*, 1996). These divisions are, therefore, thought to be self-renewing, whereby the two daughter cells share the same progenitor state as the mother cell. However, when the spindles are oriented parallel to the ventricular surface, only one daughter cell remains in contact with the fate determinants present at this surface, thus maintaining a progenitor state. The remaining daughter cell, having lost an apical contact with the ventricular surface, becomes either a post-mitotic neuron, or a more restricted progenitor than the mother cell (Chenn *et al.*, 1995).

ii. Oblique Division

Although the cleavage-plane model was initially widely accepted, recent data have questioned the simplicity of this model (Huttner *et al.*, 2005). Apparently symmetrical divisions, where the cleavage-plane is perpendicular to the ventricular surface, have been shown to give rise to neurons (Noctor *et al.*, 2008; Postiglione *et al.*, 2011). In order to account for these discrepancies, the oblique division model was proposed. This model states that only a very small portion of the apical membrane is important for the inheritance of fate determinants. When the cleavage-plane is perpendicular to this patch of membrane, which is then divided equally between the two daughter cells, division is said to

be symmetrical. Both daughter cells inherit the fate determinants, and the progenitor cell is self-renewed (Kosodo *et al.*, 2004). However, given that the critical portion of membrane is so small, slight changes in the angle of cleavage would result in the loss of this membrane in one of the daughter cells. The daughter cell inheriting the membrane remains a progenitor, while the other becomes a neuron, or more restricted progenitor, and the division is considered asymmetrical. This mode of division has been shown to generate IPCs and oSVZ progenitors in the mouse (Shitamukai *et al.*, 2011). Thus far, only one marker of this small patch of membrane has been identified, Prominin-1 [CD133; (Corbeil *et al.*, 1999; Postiglione *et al.*, 2011)].

iii. Dynamic Polarity

Complementary to the models describing the orientation of the plane of cleavage, the distribution of certain polarity markers has also been identified as a possible mechanism to control the symmetry of division (X. Wang *et al.*, 2009). Interphasic progenitors have an established apicobasal polarity. At the apical surface, markers such as PARD3 and TJP1 are present on the lateral membranes (Bultje *et al.*, 2009). During mitosis, PARD3 becomes redistributed throughout the cell, yet remains perpendicular to the cleavage plane. When the distribution of PARD3 is symmetrical, both cells retain a progenitor state. However, asymmetrical inheritance of PARD3 results in differences in the activation of NOTCH signalling. An increased expression of PARD3 is correlated with a higher level of NOTCH signalling and maintenance of a progenitor state. However, daughter cells inheriting lower levels of PARD3 subsequently have lower levels of NOTCH signalling and become neurons or IPCs (Bultje *et al.*, 2009).

iv. Basal Process Inheritance

In addition to these models of polarity, inheritance of the basal process of the progenitor cell has been suggested to play a role in the symmetry of division (Kosodo *et al.*, 2009). Conflicting reports have implicated both the loss and inheritance of the basal process in the maintenance of a progenitor state. During the early self-renewing phase of mitoses, required for the amplification of progenitors, division has been shown to divide both the apical and basal processes symmetrically between the two daughter cells (Shitamukai *et al.*, 2011). However, at later stages the basal process may be inherited asymmetrically even in symmetrical mitoses (Miyata *et al.*, 2001; Noctor *et al.*, 2004). In asymmetrical cell division, both progenitor cells and neurons have been shown to preferentially retain the apical or basal process (Tamamaki *et al.*, 2001).

v. Centrosome Asymmetry

A further mechanism to differentiate dividing cells is centrosome inheritance. During cell division the centrioles of the mother cell are duplicated and separated to form the centrosomes of the two daughter cells. The mother and daughter centrioles of a cell are inherently different. The primary cilium

is a sensory organelle present on the surface of many quiescent cells which forms from the mother centriole. Inheritance of the centrosome possessing the original mother centriole, thus termed the mother centrosome, has been associated with maintenance of the progenitor state in RGCs (X. Wang *et al.*, 2009). The ciliary membrane is distinct from the plasma membrane and has been shown to be asymmetrically inherited by neural progenitors (Paridaen *et al.*, 2013). The ciliary membrane was endocytosed at the onset of mitosis and remained associated with one spindle pole. The cell having inherited the ciliary membrane assembled a cilium more rapidly than the remaining daughter cell, and also retained the progenitor state.

vi. Cell Cycle Kinetics

Finally, the length of the cell cycle has also been shown to influence the fate of the dividing cells. The length of the cell cycle of RGCs undergoing symmetrical, self-renewing mitoses is shorter than that of mitosis resulting in a differentiated, post-mitotic neuron. This observation is thought to be correlated with the length of time specific fate determinants have to act on the cell, rather than the polarity of their distribution (Calegari *et al.*, 2003; Calegari *et al.*, 2005).

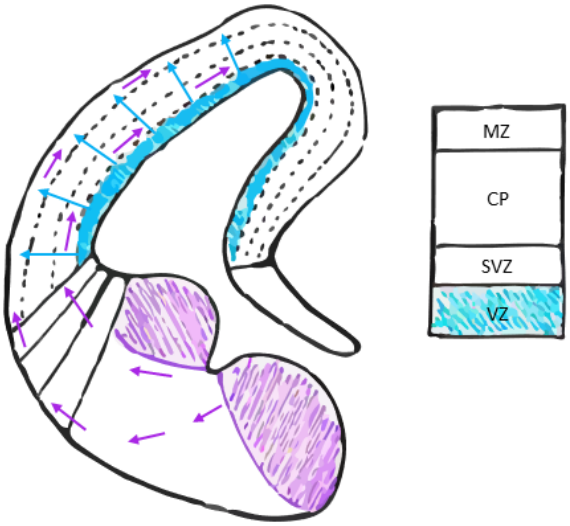

Figure 8. Migration of neurons within the developing telencephalon. *Most interneurons migrate radially from ganglionic eminences (purple), while excitatory projection neurons migrate radially from the ventricular zone (blue). Marginal zone (MZ), cortical plate (CP), subventricular zone (SVZ) and ventricular zone (VZ).*

c. Migration

Two major types of migration have been observed in the developing cortex, initially thought to depend on the type of cortical neuron [Figure 8; (Nadarajah *et al.*, 2002)]. Excitatory projection neurons originate from asymmetrical divisions of progenitor cells in ventricular and subventricular zones. These neurons migrate radially towards the pial surface to occupy their final laminar position within the mature cortex. On the other hand, most inhibitory interneurons originate in the ganglionic eminences

of the ventral telencephalon and migrate tangentially to the dorsally positioned cortex. However, in the development of the human brain a subpopulation of interneurons has also been shown to originate in the VZ and migrate radially (Letinic *et al.*, 2002). Additionally, projection neurons have been shown to migrate radially and tangentially simultaneously in occupying their final laminar position. Both radial and tangential migrations are crucial to the establishment of a mature, functional cortex.

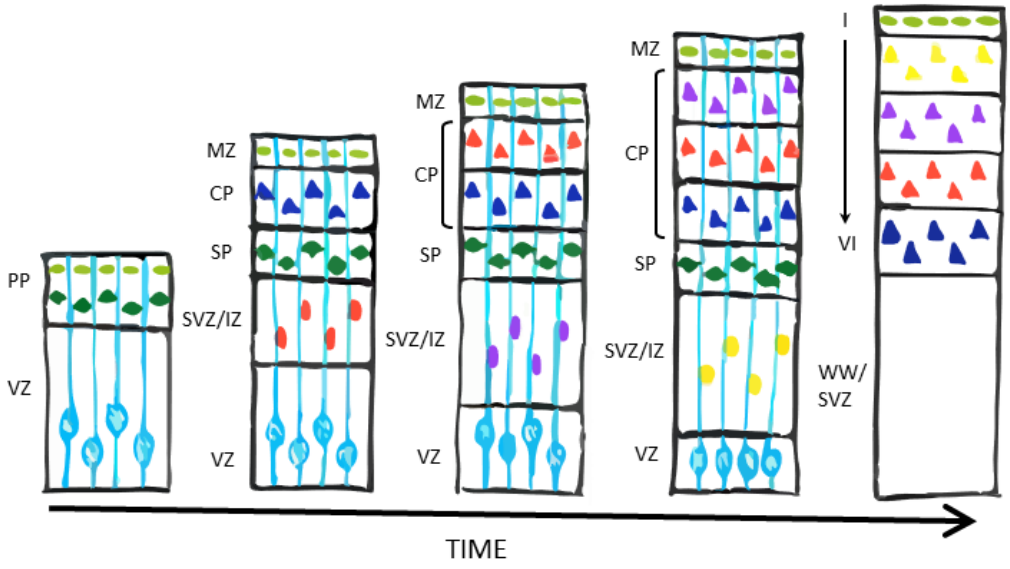

Figure 9. Organisation of Cortical Layers in the Developing Cortex. *Progressive formation and expansion of various cortical layers formed by inside-out migration over development. Ventricular zone (VZ), preplate (PP), subventricular zone (SVZ), intermediate zone (IZ), subplate (SP), cortical plate (CP), marginal zone (MZ), layers I-VI (I-VI) and white matter layer (WM). Inspired by Tan et al. (2013)*

During early development, the premature cortex consists of a single pseudo-stratified layer of progenitor cells. Early-born neurons undergo somal translocation, moving their nucleus through the cytoplasm of their radial process to 'migrate' towards the pial surface. As proliferation expands the size of the developing cortex, the distance between the ventricular and pial surfaces is greatly increased. Post-mitotic neurons subsequently use the radial processes of aRGCs as a scaffold to migrate away from the VZ [Figure 9; (Nadarajah *et al.*, 2001)].

The formation of Cajal-Retzius (CR) cells and early neurons, termed predecessor cells, marks the beginning of a highly proliferative phase after the closure of the neural tube. Predecessor cells are thought to originate in the VZ (Bystron *et al.*, 2006), while CR cells are known to derive from extra-cortical regions of the telencephalon, such as the hem, as well as the VZ (Meyer *et al.*, 1998; Lavdas *et al.*, 1999; Hevner *et al.*, 2003). The migration of these cells towards the pial surface of the neocortex generates the first cortical laminar division with the formation of the sub-pial preplate (PP) around E31 (Super *et al.*, 1998).

Asymmetrical mitosis of aRGCs in the VZ can generate oRGs and IPCs, which lack either radial processes, or both apical and radial processes, respectively. These cells migrate out of the VZ, forming a second proliferative layer, termed the Subventricular Zone (SVZ) by E45 (Bystron *et al.*, 2008). Both IPCs derived from oRGs, and oRGs themselves, can undergo several rounds of self-renewing, amplifying divisions before dividing asymmetrically to produce post-mitotic neurons (Betizeau *et al.*, 2013). Given the difference in the abundance of oRGs in the SVZ of gyrencephalic compared to lissencephalic species, this amplification process has been proposed to have been crucial during evolution. Interestingly, the expression of human-specific genes found to be upregulated in oRGs increases the oRG population and thickness of the SVZ resulting in cortical folding in lissencephalic species (Florio *et al.*, 2015).

The cortical plate (CP) is the zone of post-mitotic, post-migratory neurons which initially forms around E50 (Bystron *et al.*, 2008). The radial migration of neurons into the CP is closely associated with the formation of a sub-pial layer of CR cells, termed the marginal zone [MZ; (Meyer *et al.*, 2000)]. These cells express Reelin, a secreted factor which acts as a signal to halt neuronal migration. This process results in the formation of the mature cortical layers in an 'inside-out' manner, whereby later-born neurons will migrate past earlier-born neurons until they reach the sub-pial Reelin signal and form a more superficial layer (Rakic, 1974; Meyer *et al.*, 2000; Bystron *et al.*, 2006). Prior to the formation of the CP, an intermediate zone (IZ), populated by migrating neurons, emerges between the proliferative zones and the MZ. As development progresses, the uppermost layer of the IZ becomes the subplate (SP), containing both radially migrating excitatory neurons and tangentially migrating interneurons originating from the ganglionic eminences (Letinic *et al.*, 2002). The SP is initially important in the formation of early neuronal networks, although few neurons remain in the SP in later development. These neurons appear as interstitial cells present in the white matter, which forms from the IZ. The MZ becomes layer I of the mature cortex (Sidman *et al.*, 1973).

Within these global migration events, Noctor *et al.* (2004) described the four stages of radial neuronal migration from the VZ (Figure 10). Neurons generated following the asymmetrical mitosis of an aRGC in the VZ initially adopt a bipolar morphology and migrate radially to the SVZ. Within the SVZ, these newly-born neurons pause for at least 24 hours, whilst maintaining a multipolar morphology. Following this arrest, neurons become bipolar once more, and initially migrate back towards the VZ. After contacting the ventricular surface, neurons eventually migrate radially towards the CP. It is not currently known if neurons returning to the VZ interact with specific signals at the ventricular surface, but this remains a possibility to be explored.

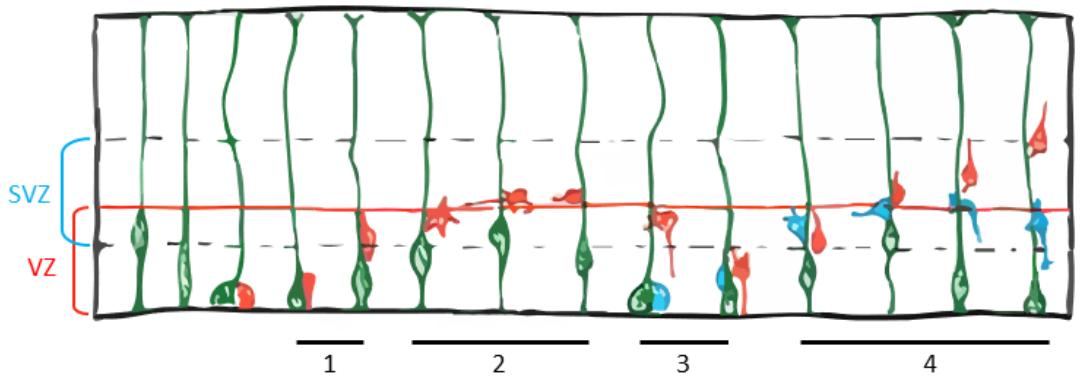

Figure 10. Four stages of radial neuronal migration. *Migration from the ventricular zone to the cortex occurs in four stages. Radial glial cell is represented in green and post-mitotic neurons in red and blue. Inspired by Noctor et al. (2004)*

IV. Malformations of Cortical Development

The complexity of the spatiotemporal events required for the development of a mature and functional brain generates a multitude of opportunities for problems to arise. Defects in the formation of the nervous system can occur very early, such as during the closure of the neural tube, or much later, in neuronal differentiation and synaptogenesis. Each of these defects can give rise to different human pathologies, affecting early foetal development, or later growth and learning. Since the term malformations of cortical development (MCD) was first introduced, (Barkovich *et al.*, 1996), the classification of these defects has been updated to reflect the advances in the understanding of the various mechanisms of pathogenesis [Figure 11; (Barkovich *et al.*, 2012)].

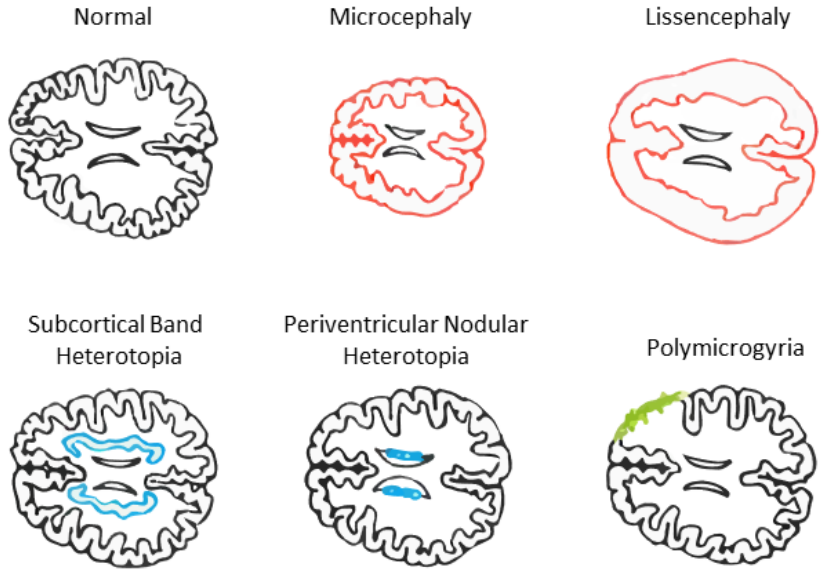

Figure 11. Schematic representations of the three classes of malformations of cortical development. *Class I: microcephaly, Class II: lissencephaly, subcortical band heterotopia and periventricular nodular heterotopia, and Class III: polymicrogyria. Inspired by Fernandez et al. (2016).*

MCDs are thus grouped into three classes. Class I are defects arising from the abnormal proliferation or apoptosis of neurons and glia. This class includes microcephaly, defined as a head circumference more than two standard deviations (SDs) below the mean, with many causative genes associated with ensuring sufficient mitosis of early progenitor cells. Megalencephaly is also included in class I, and is defined as a head circumference more than two SDs above the mean (DeMyer, 1972), with genes identified in signalling pathways involved in promoting cell proliferation and survival (Ghayda M. Mirzaa *et al.*, 2014). Finally, focal cortical dysplasias are a heterogeneous spectrum of disorders involving disorganisation of the cortical layers in a given region. The genes thus far identified show an overlap with the signalling pathways affected in megalencephaly (Marin-Valencia *et al.*, 2014).

Class II are malformations resulting from abnormal neuronal migration. Lissencephaly is another heterogeneous group of disorders, subdivided into two types. Type I lissencephaly encompasses a broad range of phenotypes, including the complete loss of gyri, resulting in a smooth brain, simplified gyri and a disorganised cortex. Many of the genes so far identified in lissencephaly are microtubule-associated proteins, including the kinesins KIF2A and KIF5C (Poirier *et al.*, 2013), highlighting the importance of the cytoskeleton in neuronal migration (Fry *et al.*, 2014). Type II lissencephaly, also called cobblestone lissencephaly, associates a disorganised cortex with a specific gyral pattern, and results from the overmigration of neurons beyond the pial surface. Genes found to cause type II lissencephaly include proteins important for the integrity of the cortical basement membrane (Devisme *et al.*, 2012). Finally, heterotopia is again a broad class of disorders characterised by an abnormal accumulation of neurons, often combined with defects in the ependymal layer at the ventricular surface. Heterotopia is, therefore, likely to be due to the failure of neurons to migrate out from the ventricular zone. Some of the causative genes so far identified have a role in maintaining the integrity of the ependymal layer, which appears to be important for efficient neuronal migration (Ferland *et al.*, 2009).

The last group of malformations, class III, are defects associated with postmigrational events and combine disorders with known genetic and environmental factors. Polymicrogyria is a highly heterogenous group of malformations characterised by an abnormal gyral pattern. Causative mutations have been found in a number of cases associating polymicrogyria with other MCDs, and it is highly likely that the aetiology is multifactorial (Squier *et al.*, 2014). Both schizencephaly, the presence of clefts within the cortex, and certain focal cortical dysplasias are also part of this final class of MCDs. Both appear to have mostly environmental origins (Jamuar *et al.*, 2015).

Although certain environmental factors have been identified, MCD is largely a spectrum of genetic diseases. While the three classifications separate clinically distinct phenotypes, their definitions are

partly based on the identification of causative mutations, and subsequent elucidation of the affected processes. Many genes have already been identified, and the clinical presentation well defined. In these cases, diagnosis can be confirmed by targeted sequencing of the gene suspected to be responsible. Where the clinical findings are less clear and a novel causative gene is likely, either Whole Exome- or Whole Genome- Sequencing (WES and WGS, respectively) can be employed. The identification of a novel MCD gene, as in many other genetic diseases, is often confirmed using an *in vivo* model, and these approaches have contributed to the understanding of the fundamental processes required for the formation of a mature, functional brain.

a. Microcephaly

Microcephaly is clinically defined as a head circumference more than two SDs below the mean, and is subdivided into primary and secondary microcephalies (Woods, 2004). Autosomal recessive primary microcephaly, (MCPH), is present at birth, reflecting a developmental defect. In contrast, secondary microcephaly is defined as a normal head circumference at birth but which then progresses postnatally to more than two SDs below the mean, and is therefore neurodegenerative. Another characteristic of microcephaly is that the neocortex does not usually show any organisational defects. The small brain size often results from a reduced number of neuronal progenitors, decreased neurogenesis or an increase in apoptosis. 23 MCPH genes have been identified to date, and many of the encoded proteins have been shown to have crucial roles at the centrosome during the cell cycle.

i. Spindle and Mitosis

Of the 23 genes so far identified, the encoded proteins of 10 are known to be important during mitosis. Mutations in *ASPM* are the most common cause of MCPH (Faheem *et al.*, 2015). *ASPM* encodes a protein which localises to the mitotic spindle and is highly expressed during the early, self-renewing phase of progenitor amplification. ASPM has been shown to play a role in maintaining the cleavage plane required for symmetrical mitosis, ensuring that the progenitor pool is sufficient before the onset of neurogenesis (Fish *et al.*, 2006). Similarly, WDR62 has been shown to localise to the spindle, with mutations also thought to lead to misorientation of the cleavage plane, and depletion of the progenitor pool (Nicholas *et al.*, 2010; Yu *et al.*, 2010).

Aside from the spindle, MCPH-causing mutations have been identified in genes encoding proteins localising to other mitotic structures. CASC5 is present at the kinetochore promoting microtubule docking and is implicated in cell cycle progression through control of the spindle assembly checkpoint. Mutations in *CASC5* were shown to result in micronuclei which was postulated to result from impaired DNA damage responses (Genin *et al.*, 2012; Szczepanski *et al.*, 2016). Similarly, CENPE also functions at the kinetochore, ensuring chromosome alignment and the binding of mitotic spindle microtubules.

Mutations in CENPE were shown to lead to chromosome lagging, multipolar spindles and binucleated cells (G. M. Mirzaa *et al.*, 2014).

Many MCPH-related proteins have been shown to localise to another equally important component of the cell, the centrosome. CDK6 has been shown to localise to the centrosome during mitosis and have an important role in cell cycle regulation, with mutations, again, thought to affect the proliferation of progenitors (Hussain *et al.*, 2013). CENPJ also localises to the centrosome and plays a role in centriole formation and length regulation. Mutations in *CENPJ* cause mitotic delay and lead to an increase in cell death (Bond *et al.*, 2005; Tang *et al.*, 2009; Insolera *et al.*, 2014). Similarly, STIL is also present at the centrosome, has a role in centriole amplification and STIL expression has been shown to be tightly regulated through the cell cycle. Mutations in *STIL* were found to cause an increase in centriole numbers due to a failure in degradation targeting (Kumar *et al.*, 2009; Arquint *et al.*, 2014). The expression level of SAS-6 is also controlled throughout the cell cycle in order to regulate centriole formation (Strnad *et al.*, 2007). Mutations identified in *SAS-6* affect centriole number and thus impact on spindle formation (Khan *et al.*, 2014).

Two MCPH-causing genes have been identified in proteins acting in the final steps of mitosis. Both CIT and KIF14 localise to the midbody during cytokinesis. Both have been shown to require the other for correct localisation and mutations in both have been shown to result in binucleated cells (Carleton *et al.*, 2006; Gruneberg *et al.*, 2006; Fujikura *et al.*, 2013; Watanabe *et al.*, 2013; Basit *et al.*, 2016; Harding *et al.*, 2016; Li *et al.*, 2016; Moawia *et al.*, 2017; Makrythanasis *et al.*, 2018).

ii. Centrosome

The centrosome is equally important for microtubule nucleation and organisation. CDK5RAP2 localises to the centrosome throughout the cell cycle, promoting γ-tubulin localisation and, therefore, microtubule nucleation. Mutations identified in *CDK5RAP2* affect the recruitment of γ-tubulin to the centriole and subsequently impact the microtubule networks during interphase and mitosis, both of which are important in neurogenesis (Bond *et al.*, 2005; Fong *et al.*, 2008). Both CEP152 and CEP135 localise to the centrosome and have been shown to play important roles in the formation and maintenance of mature centrioles. Mutations in both genes perturb their centriolar localisation and result in abnormal centriole numbers (Guernsey *et al.*, 2010; Hussain *et al.*, 2012).

Both the cell cycle and the formation and maturation of centrioles are tightly regulated and synchronised processes. MCPH1 localises to the centrosome and plays an important role in maintaining this synchronisation. Mutations in *MCPH1* result in premature entry into mitosis, affecting the cleavage plane during cell division and resulting in preferentially neurogenic divisions (Jackson *et al.*, 2002;

Gruber *et al.*, 2011). MCPH1 has also been implicated in DNA damage response (Z. W. Zhou *et al.*, 2013).

iii. Other

In addition to the cell cycle and centrosome, mutations have been identified in genes involved in several other processes. ZNF335 has a role in methylation of important neural progenitor genes (Y. J. Yang *et al.*, 2012), while PHC1 is involved in chromatin modification and the ubiquitination of proteins implicated in cell cycle control (Awad *et al.*, 2013). MFSD2A is expressed in the endothelium of the blood-brain barrier and is required for the transport of essential fatty acids into the developing brain (Nguyen *et al.*, 2014; Guemez-Gamboa *et al.*, 2015). WDFY3, identified in a case of autosomal dominant microcephaly, is an autophagy scaffold protein involved in the regulation of Wnt signalling (Kadir *et al.*, 2016). COPB2 is required for Golgi to endoplasmic reticulum trafficking (DiStasio *et al.*, 2017), while ANKLE2 has been implicated in nuclear envelope reassembly (Asencio *et al.*, 2012; Yamamoto *et al.*, 2014). Finally, mutations were identified in *NCAPD2*, *NCAPD3* and *NCAPDH*, components of the condensin complexes required for efficient chromosome segregation (Martin *et al.*, 2016).

Chapter Two - Development of the Kidney

The kidney, not unlike the brain, is a highly complex organ, whose proper function depends on a precise structural organisation. The kidneys are present as a pair, each connected to a ureter, and function to filter the blood from the renal arteries. The filtrate exits the kidney via the ureter, connected to the bladder, in the form of urine. Kidney function is important for the removal of toxins from the blood, as well as the synthesis of certain hormones (McMahon, 2016).

The kidney is divided into two regions, the outer, termed the cortex, and the inner, or medulla (Figure 12). The medulla is composed of multiple renal pyramids oriented such that the narrowest portion faces inwards, ending with the papillae. The papillae connect to the minor calyces, which join together, forming major calyces, and eventually merge with the renal pelvis. The renal pelvis narrows, becoming continuous with the ureter. Through this layered organisation, blood is filtered in the outer cortex and the filtrate flows inwards towards the renal pelvis. The functional unit of the kidney is the nephron, each mature kidney composed of up to approximately 2 million nephrons (Bertram *et al.*, 2011). Each nephron can itself be divided into distinct functional units (Figure 12). The blood-filtering glomerulus is present in the renal cortex and is connected to a continuous series of tubules composed of differentiated cells with discrete functions.

Three renal structures are generated over the course of mammalian renal development. Both the pronephros and mesonephros are temporary, with the pronephros being the simplest and most primitive in evolutionary terms, followed by the mesonephros and finally the mature metanephros. During human development, the pronephros is present from approximately embryonic day 20 (E20), and degenerates shortly after. Around this time, E25, the mesonephros begins to develop, becoming functional between 6-10 gestational weeks (GW). The mesonephros is eventually replaced by the final, mature kidney, the metanephros, which begins to form around GW4-5. Interestingly, the kidney continues to develop postnatally, with some nephron maturation and differentiation occurring 2-3 weeks after birth.

Much of the understanding of human kidney development was first established by Edith Potter in the 1960s. Her work in describing renal development preceded current studies of the causes of foetal kidney disease. To date, many essential genes and pathways have been described, often through the identification of affected foetuses and subsequent genetic analyses. The study of gene function is often complicated by the failure of mouse models to recapitulate human renal diseases, although the zebrafish has recently become an attractive alternative *in vivo* model.

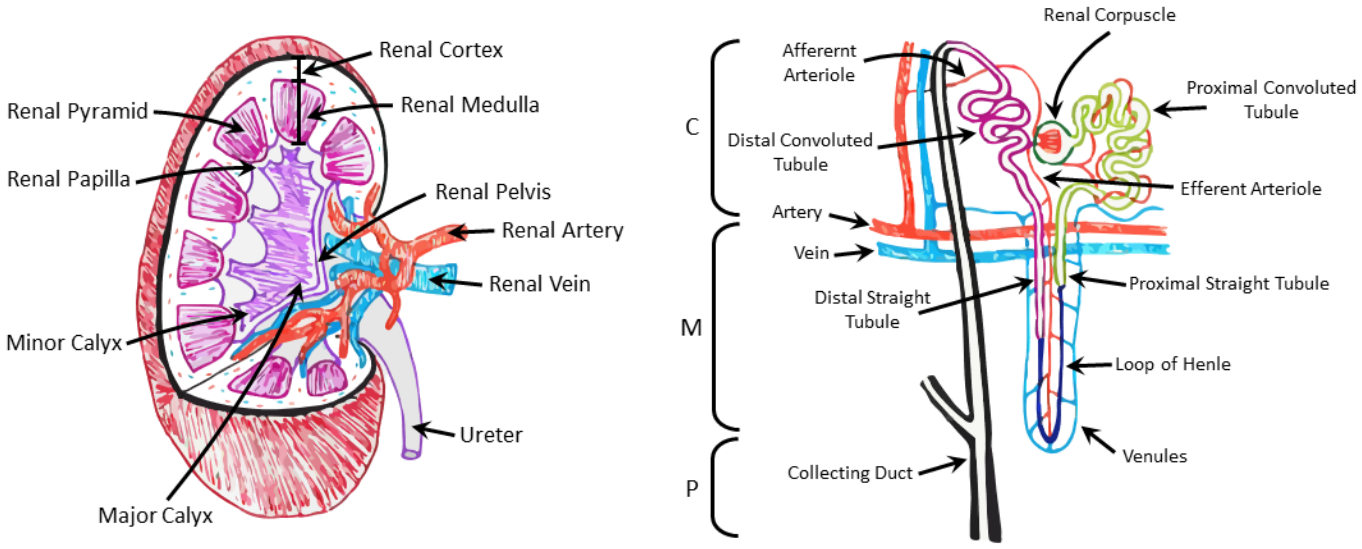

Figure 12. Structural organisation of the kidney and nephron. *Architecture of the mature metanephros, and the various distinct segments of the nephron, the functional unit of the kidney. Inspired by Marsh (1983) and McMahon (2016)*

I. Early Development of the Mammalian Kidney

Much of the research which has elucidated the pathways and mechanisms involved in mammalian renal development have been performed using the mouse as an *in vivo* model. Although recent work has begun to establish the parallels between these processes in the mouse and human (Lindstrom, Guo*, et al.*, 2018; Lindstrom, McMahon*, et al.*, 2018; Lindstrom, Tran*, et al.*, 2018), the following sections will focus on murine development unless indicated otherwise. As in the development of the nervous system, the cells of the future mammalian kidney are induced early, during gastrulation. The kidney develops from the cells of the intermediate mesoderm, in the caudal portion of the early embryo. A number of transcription factors are known to have a role in the specification of the intermediate mesoderm, including *Osr1*, *Lhx1*, and *Pax2/8*, and are activated by low concentrations of Bmp2 (Tsang *et al.*, 2000; Bouchard *et al.*, 2002; James *et al.*, 2005; James *et al.*, 2006). Epithelialisation of the anterior-most region of the intermediate mesoderm on either side of the midline results in the formation of bilateral nephric ducts (Obara-Ishihara *et al.*, 1999). Each nephric duct consists of an epithelial tube formed of a single layer of cells. The epithelial-to-mesenchymal transition of intermediate mesoderm cells at the caudal end of the developing nephric duct results in growth in a caudal direction towards the cloaca (Figure 13).

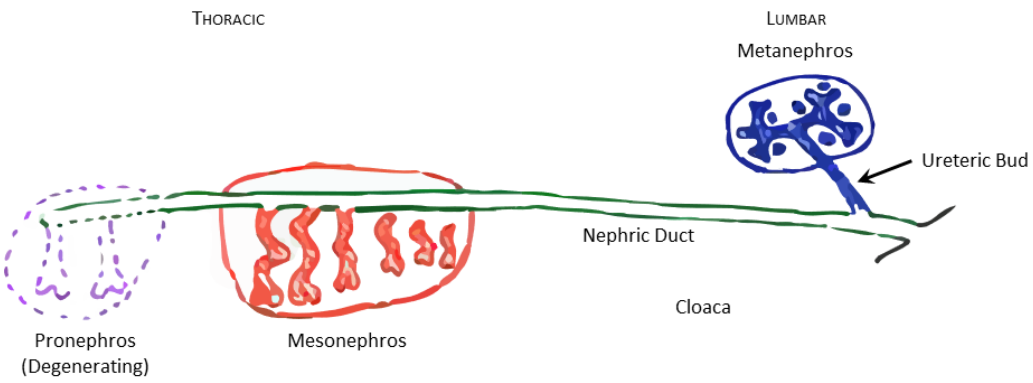

Figure 13. Development of mammalian kidneys. *Formation and degeneration of pronephroi and mesonephroi prior to, or during development of the metanephros. Inspired by Davies (2002)*

As the nephric duct extends, the adjacent medioventral mesoderm condenses to form a number of epithelialised structures. These structures, which develop around E20-22 in humans, form a lumen and are open both proximally and distally, with the distal end connected to the nephric duct (Oliver *et al.*, 1968). Together, these primitive tubules form the pronephroi of the developing embryo. The number of tubules formed over the course of human embryonic development is variable, although none are functional (Vize *et al.*, 2003). The pronephroi form at the cranial end of the nephric duct, but quickly regress and by E25 have completely degenerated (Figure 13). The development of the mesonephros occurs concomitantly with the loss of the pronephros and the fusion of the nephric ducts with the cloaca. The mesoderm, in a region between the lumbar and thoracic vertebrae, is again induced to condense into tubules. This induction occurs in a cranial to caudal direction, with around 40 mesonephric tubules formed over the course of embryonic development. The induction and formation of the mesonephric tubules is followed by a craniocaudal regression, whereby the cranial-most tubules regress as the caudal-most tubules develop (Ludwig *et al.*, 2005). The cranial mesonephric tubules differentiate to form mesonephric nephrons, connecting the nephric duct to a blood-filtering glomerulus. However, the caudal tubules are not functional and do not attach to the nephric duct. During human development the mesonephric nephrons form the earliest filtration and secretion system, functioning between 6-10GW (Figure 13).

a. Metanephros Formation

The formation of the final, mature kidney, the metanephros, begins prior to the establishment of the functioning mesonephros. At around 4-5GW, a caudal outgrowth of the nephric duct, termed the ureteric bud (UB), extends towards a specialised, caudal region of intermediate mesoderm, known as the metanephric mesoderm (MM; Figure 14). *Eyes absent 1*, *Eya1*, is one of few factors so far shown to be essential for the specification of the MM (Xu *et al.*, 1999). The induced MM subsequently secretes

glial cell-derived neurotrophic factor, Gdnf, the receptor of which is expressed by the caudal nephric duct (Sainio *et al.*, 1997). This signalling is believed to be crucial to the outgrowth of the UB, while Bmp-4 has been shown to suppress ectopic UB formation (Miyazaki *et al.*, 2000). In the absence of invasion by the UB, the MM undergoes apoptosis (Koseki, 1993), however the UB has been shown to secrete several factors which promote MM survival, including Fgf2 and Fgf8 (Barasch *et al.*, 1997; Grieshammer *et al.*, 2005). Two elements of the invading UB can be distinguished, the cells of the tip and those of the remaining tubule. The tip can either advance into the MM, or divide, in a process known as branching. The first division of the UB tip is symmetrical, resulting in the formation of two branches, the tips of which will continue to advance in opposite directions (Osathanondh *et al.*, 1963a; Saxen *et al.*, 1987). Subsequent branching can be either symmetrical or asymmetrical, whereby the latter generates branches of differing lengths to be directed to different areas (Figure 14). These events result in the complex patterning of the final mature kidney.

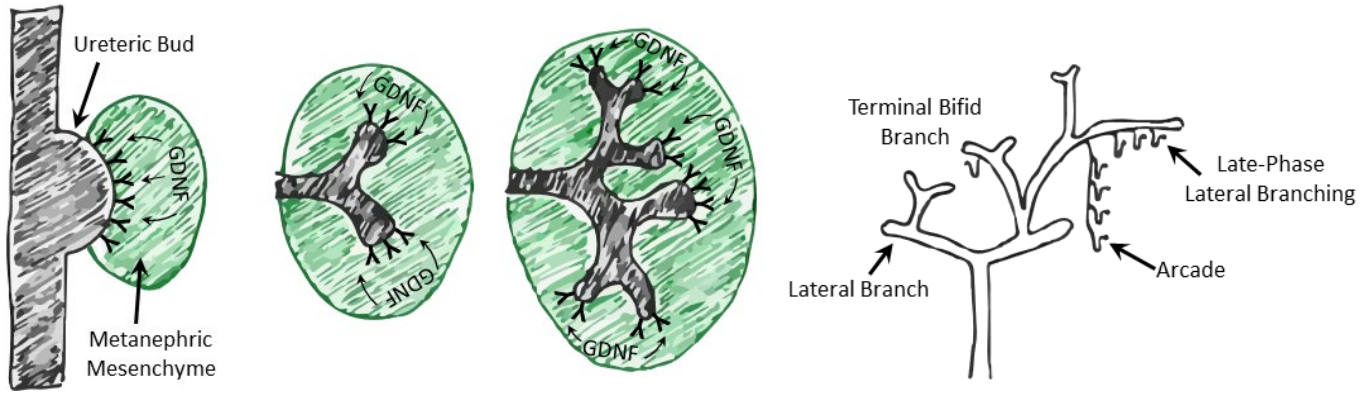

Figure 14. Branching of the ureteric bud. *Invasion of the metanephric mesenchyme (green) by the ureteric bud (black) and reciprocal GDNF/Ret signaling. Inspired by Walker et al. (2011). Schematic representation of the branching and arcade formation, inspired by Shah et al. (2004).*

Four periods have been described in the development of the human metanephros (Osathanondh *et al.*, 1963b). The first period includes the invasion of the MM by the UB, the initial branch formation and ends at 14-15GW. The predominant event during this period is branching, with little nephrogenesis, although this begins around 8-9GW (Vize *et al.*, 2003). Nephrons produced during this time are induced in an area adjacent to the tip, termed the growth zone, and progress with the tip. Although the tips undergo successive rounds of branching, these nephrons always remain associated with the growth zone, and therefore the most peripheral branches. The first 3-5 branching events are remodelled to form the renal pelvis and major calyces of the collecting duct system by 10-12GW. The following rounds of branching generate the minor calyces (Figure 12). The second period, between 14-15GW and 20-22GW, is characterised by increased nephrogenesis, with reduced branching. During this period, series of nephrons are produced successively within the growth zone of a single advancing tip.

These nephrons connect together to form arcades, with the most peripheral nephrons being the last to be produced. In the third period, ending around 32-36GW, branching events are rare, the tips degenerate and nephrons are produced outside of the growth zone. Finally, the fourth period, continuing postnatally, is characterised by growth and differentiation of the nephrons and interstitium (Little, 2015).

i. Branching

The process of branching in the metanephros is crucial to the formation of a mature and functional kidney. The mechanisms behind this process are not fully understood, although reciprocal interactions between branch tips and the surrounding MM are known to be essential (Costantini *et al.*, 2010). A number of factors secreted by the MM to promote branching have been identified, including Gdnf, Fgf10, Fgf7, pleiotrophin and Hgf (Pepicelli *et al.*, 1997; Qiao, Uzzo*, et al.*, 1999; Ohuchi *et al.*, 2000; Sakurai *et al.*, 2001; Michos *et al.*, 2010). Additionally, signals which negatively regulate branching have also been identified including Sprouty and Bmp-4 (Basson *et al.*, 2005; Michos *et al.*, 2007). Branch tip cells have been found to express the corresponding receptors, including Ret, Fgfr2 and Met (Pachnis *et al.*, 1993; H. Zhao *et al.*, 2004; Ishibe *et al.*, 2009). These interactions combine to promote the proliferation and branching of the UB tips.

Growth and branching require proliferation and self-renewal of progenitors. Mapping of expression profiles within the developing kidney has revealed differences between various cell populations, such as those of the tip and CM (Brunskill *et al.*, 2008), but additional analyses have highlighted differences between cells of the ureteric tips, and those of the branches (Schmidt-Ott *et al.*, 2005; Shakya *et al.*, 2005). Lineage tracing and time lapse imaging have revealed that the division of tip cells results in daughters which contribute to both the tips and branches. However, a subset were shown to remain within the tip throughout the duration of the analysis (Riccio *et al.*, 2016). These cells were shown to express Ret and the ETS-related transcription factor 4 (Etv4), both downstream effectors of Gdnf. These results were compatible with earlier findings that tip cells express many targets of Gdnf signalling (Schmidt-Ott *et al.*, 2005), which is highly expressed in the MM (Hellmich *et al.*, 1996), and suggests that this signalling pathway is preferentially maintained in a subset of self-renewing tip cells. This result would support the suggestion that differences between tip and branch cells results from tip cells retaining the expression of certain factors which promote a progenitor state. The analysis of expression profiles of tip and branch cells shows that branch cells express many genes important for the later function of the collecting duct (Schmidt-Ott *et al.*, 2005). One factor shown to promote a progenitor state in tip cells is β-catenin, the loss of which results in premature differentiation into collecting duct cells (Marose *et al.*, 2008). The finding that branching can occur in culture, in the

absence of interactions with the MM (Qiao, Sakurai*, et al.*, 1999), also contributes to the idea that differentiation into branch cells may be intrinsically regulated by those of the tip.

Both the tips and the branches undergo mitosis and contribute to growth, however cell cycle dynamics are different, with shorter cycles in the tips than the branches (Michael *et al.*, 2004; Riccio *et al.*, 2016). Although the significance of these cell cycle rates has not been explored, it may parallel the kinetics seen during brain development. Early progenitor cells undergoing self-renewing mitoses display shorter cell cycles than later neurogenic divisions (Calegari *et al.*, 2005). This difference is proposed to be due to the length of time specific cell fate determinants can act on the progenitors, although this remains to be demonstrated experimentally. Mitosis in the early developing brain occurs predominantly within the ventricular zone, at the luminal surface (Figure 6). Interestingly, mitosis in branch tips during kidney development has been shown to occur within the lumen and proceeds via an unusual mechanism of delamination and cell dispersal (Figure 15). Prior to mitosis, cells extend apically towards the lumen whilst maintaining contact with the basal surface. Subsequently mitosis occurs within the lumen, with one daughter cell re-entering the epithelium at the site of origin, and the remaining daughter cell reinserting a short distance away (Packard *et al.*, 2013). The significance of these luminal mitoses and the regulation of cell cycle kinetics within branch tips remains to be determined.

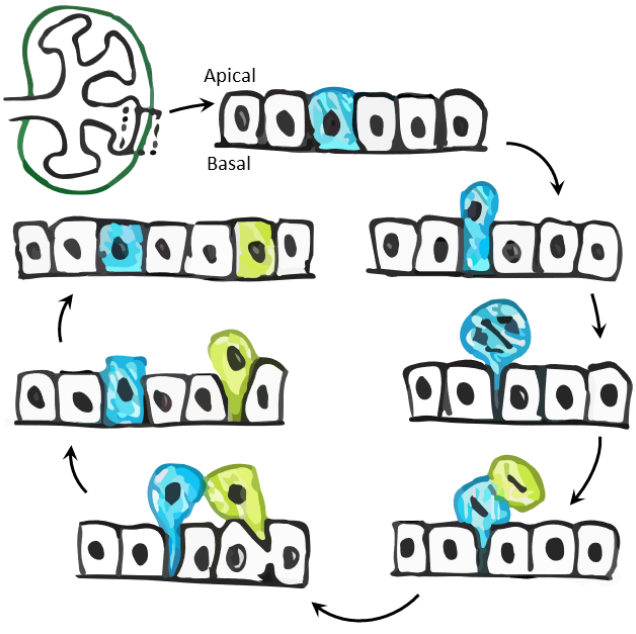

Figure 15. Mitosis and cell dispersion in the ureteric tips. *Mitotic cells of the ureteric tips divide at the apical surface within the lumen. Following mitosis, one daughter cell re-enters the epithelium a short distance from the original mother cells. Inspired by Packard et al. (2013)*

ii. Nephrogenesis

The processes of branching and nephron formation are intrinsically linked, with defects in branching associated with a reduction the final number of mature nephrons. Cells of the MM which condense around branch tips of the ureteric bud form the cap mesenchyme (CM) and give rise to the nephrons, while the remaining MM contributes interstitial cells. Analysis has highlighted differences in expression profiles and cell cycle kinetics of the various populations within the MM. *Forkhead box D1*, (*Foxd1*) is an early marker of interstitial cells (Hatini *et al.*, 1996), while Six2^{+} cells define early nephron progenitors (Self *et al.*, 2006). Lineage tracing has shown that these populations separate early during development (Mugford *et al.*, 2008). The CM can be further subdivided into two populations, one committed to differentiating, and the other containing progenitors. The expression of Six2 and Cited1, along with the absence of Wnt4, is found in progenitor cells (Boyle *et al.*, 2008; Mugford *et al.*, 2009). Cells expressing Six2 and Wnt4, and having lost the expression of Cited1, are considered to be induced and will undergo differentiation (A. Kobayashi *et al.*, 2008; Mugford *et al.*, 2009). Although both populations are Six2^{+}, differences in cell cycle kinetics have been identified. Short *et al.* (2014) identified a Six2^{HIGH} population at the periphery of the CM with a reduced rate of proliferation, proposed to represent the progenitor cells, and a less peripheral Six2^{LOW} population with a higher cell cycle rate, corresponding to those cells committed to differentiation. The progenitor population was shown to self-renew throughout development to generate a sufficient number of nephrons. The expression of Six2 was shown to be essential to these self-renewing mitoses (A. Kobayashi *et al.*, 2008).

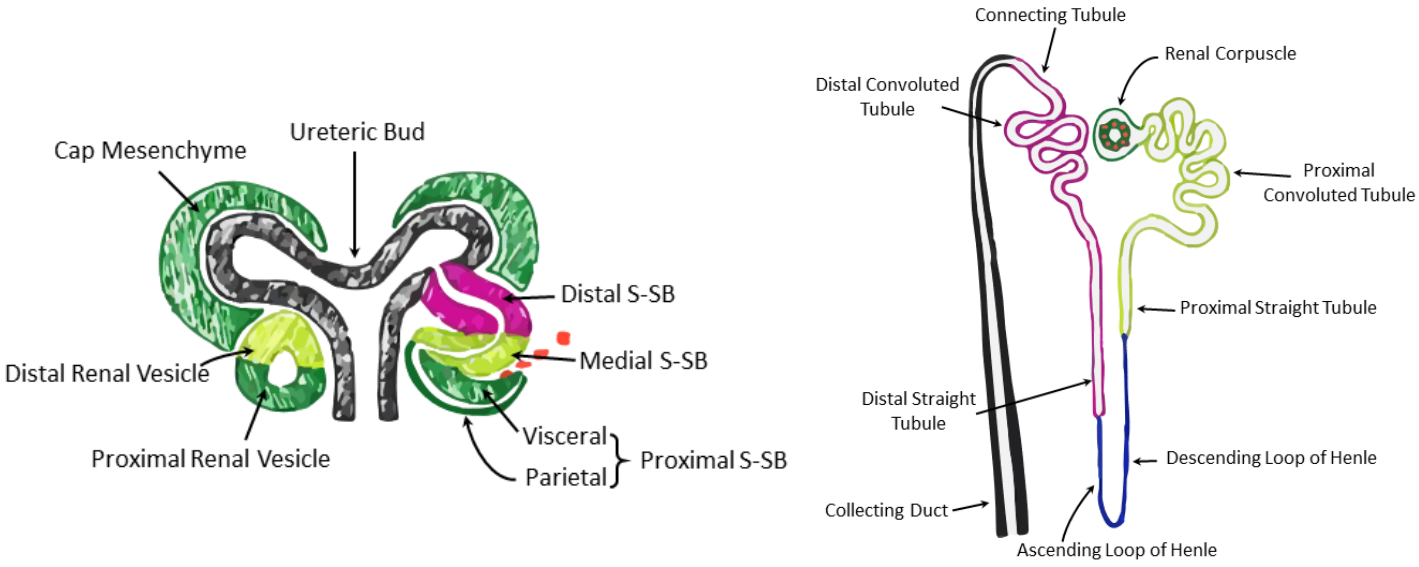

Figure 16. Developmental stages of nephrogenesis. *Formation of renal vesicle, followed by comma-shaped body, S-shaped body and developed nephron. Renal vesicle (RV), S-shaped body (S-SB). Inspired by McMahon (2016)*

Several stages have been described in the process of nephron formation (Figure 16), beginning with the pretubular aggregate, followed by the mesenchymal-to-epithelial transition to form the renal vesicle. The renal vesicle is polarised and these proximal and distal regions are maintained in the comma-shaped body. Mitosis accompanies the transition to the S-shaped body, the lumen of which connects to that of the ureteric tip, and from which the fully differentiated and segmented nephron forms. At the beginning of this process, a gradient of Wnt9b expression in the ureteric tips activates the canonical Wnt/β-catenin signalling pathway in a subset of cells, resulting in the formation of the pretubular aggregate beneath the branch tip (Carroll *et al.*, 2005). Subsequently, stabilised β-catenin induces the expression of Fgf8 and Wnt4, both of which are required for the progression of the pretubular aggregate into the renal vesicle (Carroll *et al.*, 2005; J. S. Park *et al.*, 2007). Fgf8 acts upstream of Wnt4, with Wnt4 required to maintain the expression of Fgf8, and both required to induce the expression of Lhx1 (Grieshammer *et al.*, 2005; A. Kobayashi *et al.*, 2005; Perantoni *et al.*, 2005). The initiation of the mesenchyme-to-epithelial transition of the pretubular aggregate appears to require canonical Wnt signalling, yet the progression to the renal vesicle is impaired upon constitutive activation of this pathway (J. S. Park *et al.*, 2007). Interestingly, non-canonical Wnt signalling has been implicated in the continuation of the mesenchyme-to-epithelial transition (Burn *et al.*, 2011; Tanigawa *et al.*, 2011).

The mechanisms which lead to the formation of the epithelialised renal vesicle remain to be fully elucidated, although both cadherin-6 and Tjp1 are expressed in the forming structure (Mah *et al.*, 2000). The establishment of cell polarity results in the formation of a lumen within the vesicle, which has been shown to require afadin, nonmuscle myosin IIA and IIB (Z. Yang *et al.*, 2013; Recuenco *et al.*, 2015). *In vitro*, afadin is required for the formation of adherens and tight junctions in canine renal cells [MDCK; (Ooshio *et al.*, 2007)]. *In vivo*, afadin was shown to be required for both the initial *de novo* lumen formation within the renal vesicle, as well as the expansion of the lumen as the renal vesicle differentiates into further elongated structures (Z. Yang *et al.*, 2013). At the S-shaped body stage a continuous lumen exists between the nascent nephron and the ureteric tip. This continuous lumen was shown to develop from the coalescence of multiple small lumens and required afadin expression. Interestingly, afadin has subsequently been implicated in the orientation of cell division within the renal vesicles. Mitosis was shown to occur perpendicular to the apico-basal axis, with the intercellular bridge and midbody positioned apically. Loss of afadin severely impairs lumen formation, which was proposed to impact the morphogenesis of the nascent nephron and likely affect function (Gao *et al.*, 2017).

In addition to apico-basal polarity, the expression of subsets of factors lead to the proximal-distal polarisation of the renal vesicle (Figure 17). While the distal portion of the renal vesicle will give rise to

the proximal and distal tubules, the proximal region will become the glomerulus. Notch2 signalling has been implicated proximally, while a gradient of canonical Wnt signalling is important for defining the medial and distal regions. Markers of the distal region include *Lhx1*, the Notch ligands *Dll1* and *Jag1*, *Bmp2* and factors involved in Wnt signalling, *Wnt4*, *Lef1* and *Dkk1*. Proximal markers include *Tmem100* and *Wt1* (Georgas *et al.*, 2009; Mugford *et al.*, 2009). Establishing the proximal-distal polarity has been shown to be crucial to the progression of nephron formation. Loss of *Lhx1* results in the absence of polarity in the renal vesicle which subsequently fails to develop into the S-shaped body (A. Kobayashi *et al.*, 2005). Although it remains to be shown experimentally, it has been proposed that signals from the ureteric tips, such as Wnt9b, may signal to the renal vesicle thus inducing polarity. Correctly patterned nephrons have been observed in the absence of ureteric tips, (Saxen *et al.*, 1987), and so it may be possible that additional factors, perhaps intrinsic to the renal vesicle, may also contribute to establishing proximal-distal polarity.

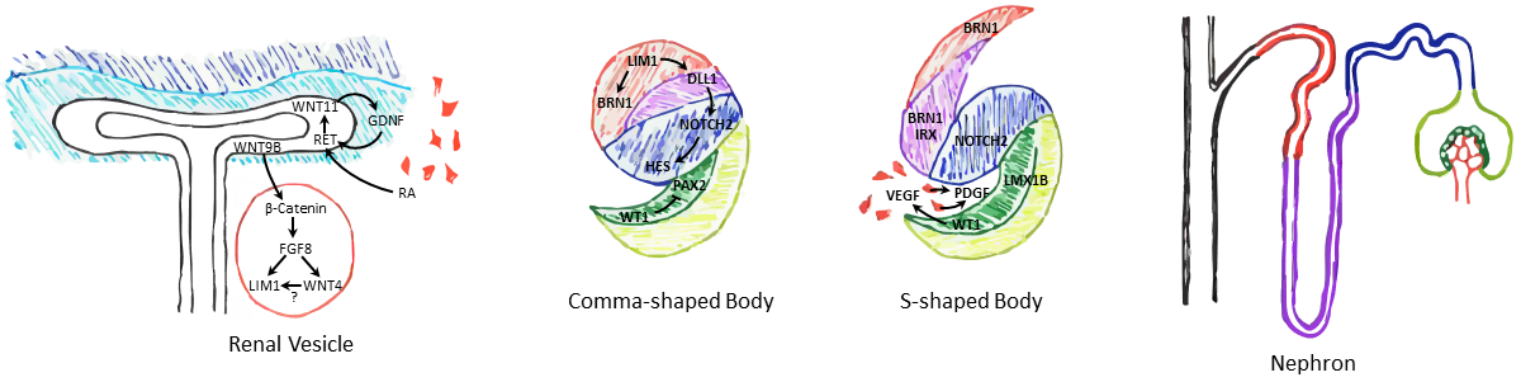

Figure 17. Stages of development of a functional nephron. *Schematic representation of the development and differentiation of a nephron beginning at the renal vesicle stage, followed by the comma-shaped body and S-shaped body. Inspired by Schedl (2007)*

The events following polarisation of the renal vesicle and the progression to the comma- and then S-shaped bodies are poorly understood. A higher number of proliferative cells were observed in the distal portion of the renal vesicle, which was proposed to reflect a higher rate of proliferation and subsequent distal elongation (Georgas *et al.*, 2009). Comma-shaped bodies are also distinguished from the renal vesicle by the presence of a slit at the proximal end. Further proliferation is proposed to result in the formation of the S-shaped body, which maintains a proximal, medial and distal polarity, and finally the mature nephron. Distal markers of the S-shaped body include *Lef1*, *Sox9* and *Lhx1*, of which *Sox9* and *Lhx1* have been implicated in the development of the distal nephron segments. Notch signalling has been identified in the medial S-shaped body with the expression of the ligands *Jag1* and *Dll1*, suggesting a role in the specification of the proximal nephron. Proximally expressed markers within the S-shaped body include *Mafb*, *Wt1* and *Lmxb1* which define the podocyte precursors

(Georgas *et al.*, 2009; Mugford *et al.*, 2009). The development of the functional nephron from the S-shaped body has not been well characterised but is believed to require further proliferation and differentiation. Interestingly, oriented cell division has again been implicated in the elongation of the nephrons and collecting ducts during a period of maturation (Fischer *et al.*, 2006). The various proximal and distal segments of the nephron express different solute carriers, reflecting the range of spatially restricted functions across the mature nephron. The signals expressed to establish the proximal-distal polarity during development are implicated in the differentiation of these various segments, intricately linking the structure and function of the mature nephron.

iii. Glomeruli Formation

The blood-filtering glomeruli develop at the proximal-most end of the nephron, and are composed of four cell types, the glomerular endothelial cells, podocytes, mesangial cells and the parietal epithelial cells. Initially, podocyte precursors in the slit formed during the comma-shaped body stage secrete VEGF to attract endothelial cell precursors. These cells likely originate from angioblasts present in the metanephric mesenchyme. Concomitantly with the formation of the capillaries, the apical domains of podocyte precursors expand and cell-junction proteins translocate to the basal surface. One stage of podocyte maturation involves complex morphological changes, which may be active or inactive, and result in the formation of primary and secondary processes. The primary, or major, processes are principally formed of microtubules and intermediate filaments, while the secondary, or foot, processes are actin-based. The foot processes of neighbouring podocytes interdigitate to envelope the forming capillaries. Unique cell-cell junctions, termed slit diaphragms, form between foot processes. These porous junctions are composed of distinct proteins, including nephrin and podocyin, and are crucial to the function of the mature nephron (Quaggin *et al.*, 2008; Scott *et al.*, 2015).

Glomerular endothelial cells share an extra cellular matrix with the mature podocytes, the glomerular basement membrane, and function together as the glomerular filtration barrier. This barrier serves to filter the blood, allowing the passage of water and small solutes, while preventing large, charged proteins from entering the tubules. The glomerular endothelial cells form the lumen of the capillaries through apoptosis, while interactions with the mesangial cells generate the complex looping of the mature capillary tuft. The capillaries are also porous to maximise the filtration rate, and lined with a lattice of negatively charged glycoproteins which, again, prevent the passage of proteins out of the blood. These structures are all encompassed by the Bowman's capsule, formed from the parietal epithelial cells. The filtrate which passes through the glomerular filtration barrier is contained within the Bowman's space, before entering the proximal tubule (Dressler, 2006; Quaggin *et al.*, 2008; Scott *et al.*, 2015)

iv. Intersitium

Cell fate and lineage tracing has suggested that the nephron and interstitial progenitors separate early during development. Both derive from $Osr1^+$ cells of the intermediate mesoderm. $Six2^+$ cells give rise to the nephron, and Six2 expression has been shown to be crucial for the maintenance of these cells. In contrast, $Foxd1^+$ cells give rise to the interstitium, however, Foxd1 is not essential in this process. Certain markers of the progenitor state of interstitial cells have been identified and include Pbx1. Differentiated interstitial cells include components of the glomeruli, such as the mesangial cells, and other cells associated with vascularisation of the kidney, including pericytes, and smooth muscle cells. It is not yet known whether the differentiation of the various interstitial cell types is due to responses to local environmental signals, or intrinsic patterning (Fanni *et al.*, 2016; McMahon, 2016).

II. Hereditary Kidney Disease

The complexity of the structure of the mature kidney and the intricate links between architecture and function, both during and following development, provide numerous opportunities for defects to occur. Many different types of kidney disease have been described, some of which are developmental and others degenerative leading to end-stage renal disease. Certain conditions are considered polygenic and influenced by various environmental factors, while others are monogenic. Recent work has identified many genes implicated in kidney disease and their roles in normal kidney development or function.

a. Congenital Abnormalities of the Kidney and Urinary Tract

Congenital abnormalities of the kidney and urinary tract (CAKUT) comprise a broad range of phenotypes affecting 3-6 per 1000 live births, and representing around one fifth of all congenital anomalies detected prenatally (Loane *et al.*, 2011). CAKUT is the leading cause of end stage renal disease during childhood (Ardissino *et al.*, 2003), and arises due to defects during renal development (Schedl, 2007). The severity of CAKUT phenotypes is variable but the most severe defects are associated with foetal or perinatal death and can affect the kidneys and/or ureters. CAKUT phenotypes affecting the kidney include renal agenesis, renal hypodysplasia and multicystic dysplastic kidney (Rodriguez, 2014). These phenotypes can occur in isolation or when present in conjugation with other, extra-renal conditions are termed syndromic (F. Hildebrandt, 2010). Although certain environmental factors have been found to cause CAKUT, including obesity and diabetes (Groen In 't Woud *et al.*, 2016; Macumber *et al.*, 2017), the identification of many familial cases has revealed the importance of genetic factors (Winyard *et al.*, 2008; Bulum *et al.*, 2013). Analysis of the modes of inheritance in these familial cases has revealed both autosomal recessive mutations and autosomal dominant with incomplete penetrance (Heidet *et al.*, 2017). In addition, the same mutations in the same genes often

result in different phenotypes, a phenomenon known as variable expressivity (van der Ven *et al.*, 2018). A large genetic heterogeneity is also seen in CAKUT, with mutations thus far identified in over 50 genes, many of which encode transcription factors or actors in signalling pathways with known roles during kidney development (Heidet *et al.*, 2017; Sanna-Cherchi *et al.*, 2018). A number of different approaches are currently used to identify novel candidate genes, including targeted- and whole-exome sequencing, and whole genome sequencing (Renkema *et al.*, 2014; Heidet *et al.*, 2017)

i. Renal Hypodysplasia

Of the spectrum of phenotypes in CAKUT, those malformations affecting the kidney are termed renal hypodysplasia (RHD; Figure 18). These defects, along with those affecting the ureters, can occur either unilaterally or bilaterally. In cases of bilateral anomalies, each kidney can present a different phenotype of varying severity.

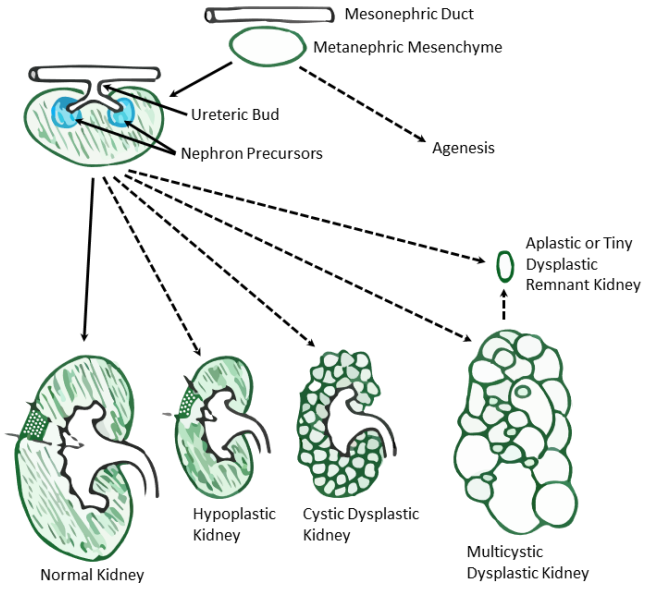

Figure 18. Spectrum of phenotypes observed in renal hypodysplasia. *Schematic representation of renal agenesis, hypoplasia and dysplasia. Inspired by Kerecuk et al. (2008)*

The absence of one kidney, or unilateral renal agenesis, is a relatively common form of RHD, with a prevalence of 1 in 5000 births. Unilateral renal agenesis can be asymptomatic when development of the remaining kidney proceeds normally, or can lead to perinatal lethality when combined with additional defects in the contralateral kidney. Bilateral renal agenesis is less frequent, affecting 1 in 30,000 births, and is associated with a number of phenotypes, collectively termed Potter's syndrome, and includes a receding chin, low-set ears, pulmonary hypoplasia and rocker-bottom feet (Rodriguez, 2014). The absence of kidney function reduces the volume of amniotic fluid, subsequently affecting pulmonary development and resulting in perinatal lethality. Renal agenesis is thought to be associated with early developmental defects, such as a failure of ureteric bud outgrowth or metanephric

mesenchyme specification (Schedl, 2007). Two genes have so far been identified in isolated autosomal recessive bilateral renal agenesis, *ITGA3* (Humbert *et al.*, 2014) and *FGF20* (Barak *et al.*, 2012). Recently mutations were identified in *GREB1L* in several cases of bilateral renal agenesis with an autosomal dominant mode of inheritance displaying incomplete penetrance and variable expressivity (De Tomasi *et al.*, 2017).

The development of a smaller but histologically normal kidney is termed renal hypoplasia. Hypoplastic kidneys are formed of fewer nephrons and are subsequently associated with poor renal function. Several studies have demonstrated the correlation between reduced nephron number and hypertension (Keller *et al.*, 2003), although unilateral renal hypoplasia may be asymptomatic (Goodyer, 2009). As ureteric branching and nephrogenesis are intricately linked, genes controlling either process have been identified in cases of renal hypoplasia. Additionally, the failure to maintain the self-renewing progenitor state of nephron precursors has also been linked to premature nephrogenesis and reduced nephron number. Several transcription factors implicated in these processes have been identified in cases of syndromic and isolated renal hypoplasia and one of the most frequent is *PAX2* (Sanyanusin *et al.*, 1995; Bower *et al.*, 2012)

Renal dysplasia refers to the formation of structurally disorganised and poorly differentiated kidneys. One study found that renal dysplasia most frequently arises due to an obstruction of urinary flow (Rubenstein *et al.*, 1961), although cases where no obstruction can be identified are also seen (Rodriguez, 2014). Histology of dysplastic kidneys reveals poorly differentiated collecting ducts, and regions of metaplastic cartilage and undifferentiated metanephric mesenchyme (Gilbert-Barness *et al.*, 2007). Cysts can also be identified in renal dysplasia and is often associated with renal hypoplasia, subsequently termed renal hypodysplasia (Schedl, 2007). *FRAS1* (McGregor *et al.*, 2003) and *FREM1* (Alazami *et al.*, 2009) both encode extracellular matrix proteins and have been associated with syndromic renal dysplasia.

The formation of enlarged kidneys consisting of multiple variably sized cysts is termed multicystic dysplastic kidney (MCDK). Cysts usually arise from the collecting ducts, are frequently present at the periphery of the kidney, and distort renal architecture, preventing function. Histology also reveals regions of undifferentiated metanephric mesenchyme, along with fibrosis and a reduced number of nephrons. MCDK is also often associated with uretral atresia (Gilbert-Barness *et al.*, 2007). Bilateral MCDK causes perinatal death, while unilateral MCDK can be isolated or appear in conjunction with other CAKUT defects affecting the contralateral kidney (Goodyer, 2009). One of the genes most frequently associated with MCDK is *HNF1β*, which is often found in cases combining renal cysts and

diabetes (Horikawa *et al.*, 1997; Heidet *et al.*, 2010). Of the CAKUT cases identified so far, mutations in either *PAX2 or HNF1β* account for up to 15% (Madariaga *et al.*, 2013)

Other renal defects within the CAKUT spectrum include horseshoe kidney, whereby the caudal-most regions of the kidneys cross the midline and fuse together. Horseshoe kidney is considered a common defect and is associated with a predisposition for renal infections and kidney stone formation (Gilbert-Barness *et al.*, 2007). Finally, ectopic kidneys are also included within the CAKUT spectrum and can relate to incorrectly positioned kidneys or the formation of an additional kidney. Ectopic kidneys may be hypoplastic and/or dysplastic with a reduced vasculature and be associated with a predisposition for renal infection (Gilbert-Barness *et al.*, 2007).

b. Renal Ciliopathies

Ciliopathies are a heterogenous group of disorders relating to defects in the formation and function of the primary cilium, a sensory organelle present on the surface of many cell types (Reiter *et al.*, 2017). Ciliopathies are monogenic diseases with a largely autosomal recessive mode of inheritance. Many ciliopathies are syndromic affecting multiple organs, including the kidney, and resulting phenotypes with variable severity.

One of the most severe renal ciliopathies is Meckel-Gruber syndrome, leading to foetal or perinatal death. Meckel-Gruber syndrome is characterised by the presence of occipital encephalocele, multicystic dysplastic kidneys and hepatic fibrosis. Additional phenotypes have also been reported including cleft lip and/or palate, corpus callosum agenesis, microphthalmia, polydactyly and heart defects. Many of the genes so far identified localise to the transition zone of cilia and have been implicated in the regulation of ciliary protein trafficking (Logan *et al.*, 2011).

Joubert syndrome affects around 1 in 100,000 births and is characterised by hypoplasia of the cerebellar vermis, visible on MRI and known as the molar tooth sign. Additional phenotypes include hepatic fibrosis, intellectual disability, retinal dystrophy and polydactyly. Kidney defects in Joubert syndrome include cystic renal dysplasia, while around 20-30% of patients develop another renal ciliopathy, nephronophthisis (Wolf, 2015). Nephronophthisis is a tubulointerstitial nephropathy characterised by interstitial fibrosis, corticomedullary cysts and leading to end-stage renal disease. Interestingly, a number of genes identified in Meckel-Gruber syndrome have also been identified in Joubert syndrome and a number of Joubert syndrome genes have been implicated in nephronophthisis, a phenomenon known as allelism. Many of the genes mutated in Joubert have also been shown to localise to the transition zone and have a role in ciliary protein trafficking (Romani *et al.*, 2013).

Short rib-polydactyly is a group of disorders characterised by a narrow thorax due to short ribs, with polydactyly observed in certain syndromes. Additional phenotypes include cleft lip and/or palate, hepatic fibrosis and pancreatic cysts, while kidneys are often multicystic and dysplastic. Genes identified in short-rib polydactyly include members of the intraflagellar transport complexes and the motor protein dynein (Huber *et al.*, 2012).

Bardet-Biedl syndrome is a rare and heterogeneous condition with phenotypes including retinitis pigmentosa, obesity, polydactyly and learning disabilities. Kidneys can be multicystic and dysplastic. Many of the genes associated with Bardet-Biedl syndrome function together in a complex termed the BBSome, which has been implicated in trafficking proteins to the cilium (Forsythe *et al.*, 2013).

Autosomal dominant polycystic kidney disease is most frequently caused by mutations in *polycystin 1* (*PKD1*) and *2* (*PKD2*), while autosomal recessive polycystic kidney disease is caused by mutations in *polycystic kidney and hepatic disease 1* (*PKHD1*). These genes all encode proteins which localise to the membrane of the primary cilium or basal body. Recessively inherited polycystic kidney disease is more severe than the dominant form, with the onset of disease occurring during development and frequently leading to perinatal death. Both forms are characterised by the formation of cystic kidneys which develop from the collecting ducts, along with hepatic and pancreatic cysts, chronic hypertension, and a higher risk of intercranial aneurysms (Paul *et al.*, 2014).

Chapter Three - Zebrafish as a Model Organism

The zebrafish, *Danio rerio*, first described by the Scottish physician Francis Hamilton in 1822, has become an important model organism in many areas of research (Hamilton, 1822; Pickart *et al.*, 2014). Their large clutch sizes, external development, and embryonic transparency lend them to many widely used techniques. Zebrafish development occurs rapidly and has been extensively studied with forward genetics, such as the use of mutagenic screens. The injection of Morpholinos into zebrafish embryos has subsequently become an important approach in reverse genetics to study the function of a given gene by reducing expression (knockdown, KD). More recently, CRISPR and TALEN technologies have been employed to generate targeted knockout (KO) and knock-in (KI) lines of specific genes or mutations, as well as to introduce fluorescent tags to genes of interest. The combination of these approaches, along with evolving microscopy techniques and the transparency of early embryos, has made the zebrafish a commonly used model organism in many fields (Bradbury, 2004).

The use of zebrafish as *in vivo* models is of particular interest in the study of human diseases. Many commonalities in early organ development have been described between humans and zebrafish. In addition, the KD or KO of genes in which potentially damaging mutations have been identified in humans often recapitulates the disease phenotype in zebrafish. Taken together, zebrafish are highly complementary to *in vitro* approaches in validating the pathogenicity of identified mutations in disease modelling (D. Ma *et al.*, 2015).

Figure 19. Representation of zebrafish egg. *First cleavage cycle, showing blastodisc at the animal pole. Second cleavage cycle, showing division restricted to the blastodisc. Sixth cleavage cycle, showing blastoderm formed from successive mitoses of the blastodisc. Inspired by Beams et al. (1976).*

I. Early Embryonic Development in Zebrafish

The cytoplasm of the egg cell of the zebrafish consists largely of the yolk, atop which, at the animal pole, sits the blastodisc, which will give rise to the embryo (Figure 19). The first mitoses are synchronised and rapid, dividing only the blastodisc to form the blastoderm. At the 10th cleavage cycle cell divisions begin to lose synchrony and cell cycle length starts to increase, this marks the start of the midblastula transition [MBT; (Kane *et al.*, 1993)]. These first mitoses rely on maternal gene transcripts, but the MBT marks the beginning of zygotic gene transcription. At this stage, three cell populations can be distinguished, of which the deep cells will give rise to the embryo. Of the remaining two, the

yolk syncytial layer (YSL) forms from the fusion of the blastoderm cells at the lower, vegetal edge with the yolk cell, while the enveloping layer (EVL) is formed from a single layer of the outermost cells of the blastoderm (Bruce, 2016).

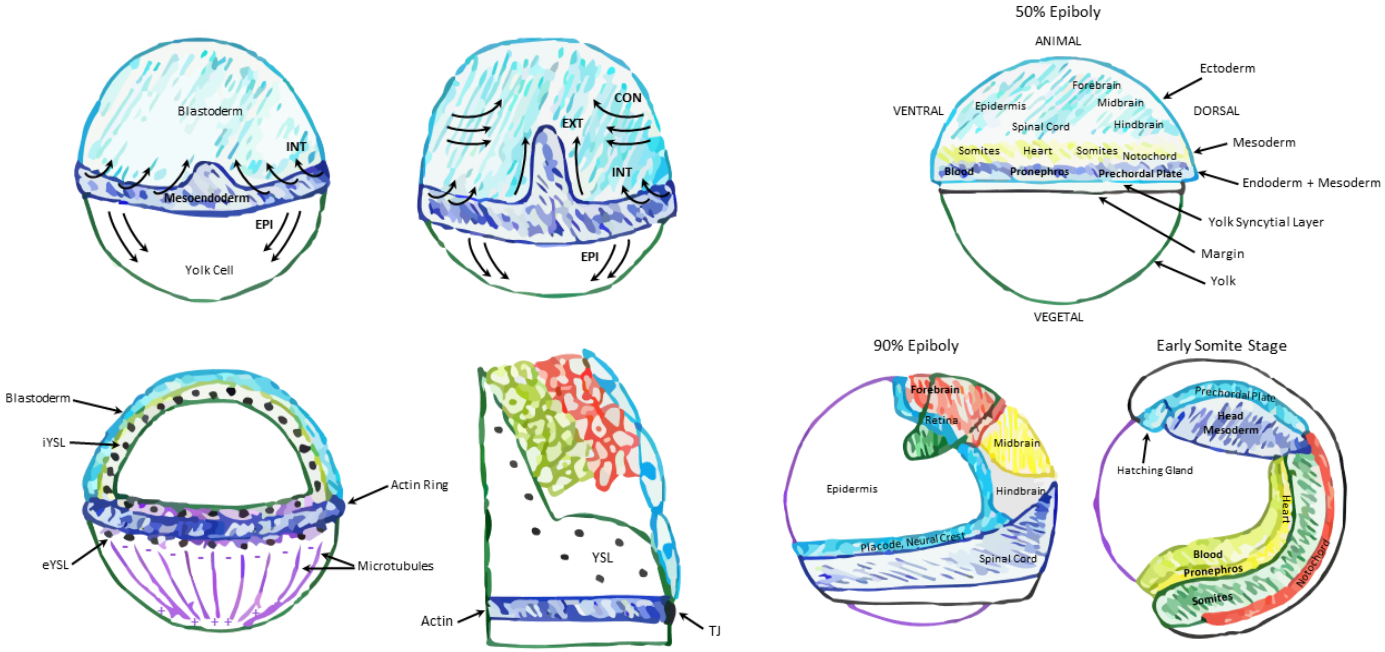

Figure 20. Gastrulation movements and fate mapping of early embryo. *Cell movements during gastrulation and formation of the epiblast (red) and hypoblast (green) layers. Internalising (INT), epiboly (EPI), convergence (CON), extension (EXT), yolk syncytial layer (YSL). Inspired by Carvalho et al. (2010). Fate map of zebrafish embryo at 50% epiboly, 90% epiboly and the early somite stage, inspired by Schier et al. (2005)*

Gastrulation in zebrafish begins with the migration of the blastoderm cells over the yolk, in a process termed epiboly [Figure 20; (Rohde *et al.*, 2007; Bruce, 2016)]. At the end of gastrulation the blastoderm has covered the entire yolk. Embryos can be staged according to the progress of the blastoderm over the yolk, termed percentage epiboly. Initially, the deep cells move outwards, intercalating with more superficially positioned cells, while the yolk cell moves upwards (Warga *et al.*, 1990). When around half of the yolk cell has been covered, 50% epiboly, a thickening of deep cells at the margin of the blastoderm forms the germ ring. The internalisation of deep cells at this margin forms two germ layers within the germ ring, the outermost epiblast and the innermost hypoblast. The epiblast layer will give rise to the ectoderm, while the earlier internalising cells will become the ectoderm, and the later internalising cells the mesoderm (Pezeron *et al.*, 2008).

Following the formation of the hypoblast and epiblast layers, cells of both layers begin to move towards the dorsal side of the embryo. This convergence results in a thickening, known as the shield, which acts to establish the dorsoventral axis of the embryo. Continuing cell movements result in the narrowing of the embryo at the dorsal midline and extension of the primary embryonic axis (Schier *et al.*, 2005). The first internalising cells at the shield will give rise to the prechordal plate, while those

following will form the precursor of the notochord (Rohde *et al.*, 2007). Both of these structures play a role in the neural induction of the overlying ectoderm by inhibiting Wnt and BMP signalling, resulting in the formation of the neural plate (Kudoh *et al.*, 2004; Tucker *et al.*, 2008; Garnett *et al.*, 2012). Both IGF and FGF signalling have been shown to be important in the formation of the rostral and caudal neural plate, respectively (Eivers *et al.*, 2004; Kudoh *et al.*, 2004). A fate map of zebrafish cell lineages has been described beginning at the onset of gastrulation (Schier *et al.*, 2005). The animal dorsal region will form the nervous system, while cells at the margin, ventrally from the shield, give rise to the blood and kidneys.

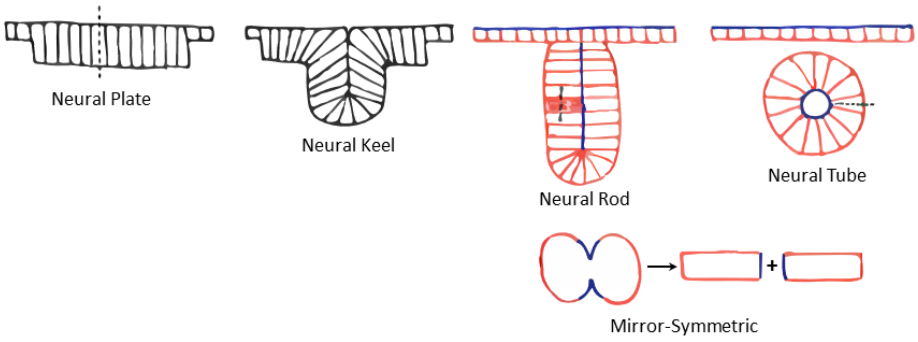

Figure 21. Neurulation and midline crossing mitosis. *Cell movements resulting in the formation of the neural tube from the neural plate. Basolateral domains are indicated in red and apical domains in blue. Inspired by Knust et al. (2007)*

II. Early Brain Development

In contrast to mammalian development, the neural plate of the zebrafish embryo does not appear to be formed of a uniform pseudostratified single-cell layer. Although the presumptive spinal cord region of the neural plate does adopt this organisation, the more anterior region which will give rise to the mesencephalon and the rhombencephalon is multi-layered and between 3-6 cells in depth (Hong *et al.*, 2006; Tawk *et al.*, 2007). These cells are thought to possess both mesenchymal and epithelial characteristics. The formation of the neural tube also differs between zebrafish and mammalian development (Figure 21). Beginning around 10hpf, the lateral neural plate cells converge towards the dorsal midline. At 12hpf, the cells at the midline internalise to form the neural keel, becoming the neural rod around 15-17hpf (Araya *et al.*, 2016). The formation of the neural rod and subsequent neural tube requires a process known as midline crossing, or C-division (Tawk *et al.*, 2007; Buckley *et al.*, 2013). In these mitoses, neural progenitors divide at the midline, with each daughter cell then being positioned on opposing sides of the neural rod. This process requires the accumulation of apical markers, including Pard3 and TJP1, towards the midline prior to mitosis. The mother progenitor cell retains a basal contact with the outer edge of the neural rod, while the daughter cell connects to the opposite side before the onset of cytokinesis. These midline crossing divisions are thought to be

important for lumen formation by establishing a mirror-symmetry of apical-basal polarity (Tawk *et al.*, 2007; Buckley *et al.*, 2013). The lumen of the neural tube begins to open around 17hpf with the coalescing of small midline lumens throughout the anterior-posterior axis of the developing embryo. Interestingly, when mitosis is blocked, therefore preventing midline crossing divisions, lumen formation is only partially affected, as cells traversing the midline form so called 'tissue-bridges' which interrupt the usually continuous neural tube lumen (Lowery *et al.*, 2005).

As in mammalian development, a combination of signalling factors in the neural plate determine the territories of the mature brain. The anterior neural border (ANB) is composed of the most anteriorly positioned cells and is adjacent to the presumptive telencephalon. The ANB, equivalent to the ANR in mammals, expresses Tlc, an important Wnt suppressor which acts to ensure a rostral identity (Houart *et al.*, 2002). The eye field is positioned adjacent to the telencephalon, while the presumptive hypothalamus appears more caudally at the midline (S. W. Wilson *et al.*, 2004). Early during development, between 5- to 12-somite stages, the hypothalamus moves rostrally, dividing the eye field in two (Varga *et al.*, 1999) and forming the ventral diencephalon.

Whereas the mammalian neural tube undergoes morphogenetic changes before closure, the zebrafish neural tube is initially straight. The presumptive forebrain, midbrain and hindbrain regions become visible around 18hpf (Kimmel *et al.*, 1995), while the ventricles are formed between 18hpf and 22hpf (Lowery *et al.*, 2005). Analysis of mitosis at 17hpf reveals no distinct regions of proliferation along the anterior-posterior axis. However, at 21hpf fewer mitoses are visible in a distinct area, marking the future hinge points of the midbrain-hindbrain boundary. Interestingly, the brain vesicles and boundaries form even in the absence of mitosis. The opening of the vesicles begins caudally, with the hindbrain, and proceeds rostrally with the midbrain and finally forebrain by 22hpf. At 24hpf the heart beat and circulation begin and subsequently contribute to the expansion of the ventricle size (Lowery *et al.*, 2005).

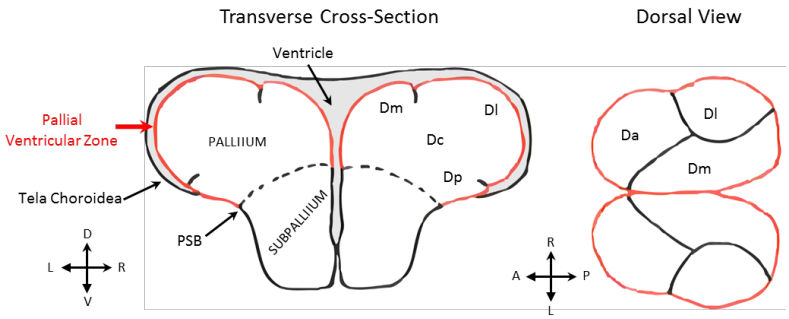

Figure 22. Schematic representation of the morphology of the everted zebrafish telencephalon. *Transverse cross-sectional and dorsal views of the zebrafish telencephalon indicating the pallial and subpallial regions, and subdivisions of the pallium. Dorsal medial (Dm), dorsal lateral (Dl), dorsal posterior (Dp), dorsal centre (Dc), dorsal anterior (Da), pallial-subpallial boundary (PSB). Dorsoventral and anteroposterior views as indicated.*

The zebrafish telencephalon is described as everted, in contrast to the evaginated mammalian telencephalon (Figure 22). The formation of the two telencephalic lobes of the zebrafish, which are solid, separated by a T-shaped ventricle and covered by a thin layer of non-neuronal cells, the tela choroidea, remains only partially understood. However, recent work has begun to shed light on the mechanism of eversion (Folgueira *et al.*, 2012). Beginning around 18hpf with the formation of the ventricles, the caudal-most part of the presumptive telencephalon folds outwards, forming the anterior intraencephalic sulcus (AIS). The formation of the AIS begins in the ventral telencephalon, before progressing dorsally and ultimately demarcating the boundary with the diencephalon. By 24hpf the two telencephalic lobes are separated at the midline by a narrow ventricle and have a posterior ventricular surface at the AIS. The everted morphology of the telencephalon is then formed through expansion along the anteroposterior axis (Folgueira *et al.*, 2012).

a. Neurogenesis

The development of the nervous system in zebrafish undergoes two waves of neuron formation. The first wave, termed primary neurogenesis, begins around 16hpf forming simple neural networks for basic movement (Kimmel *et al.*, 1991). This is followed by a second wave, secondary neurogenesis, starting around 2dpf and required for the establishment and organisation of the mature neural networks. Although secondary neurogenesis in the embryonic zebrafish telencephalon remains only partially understood, certain parallels have been drawn with neurogenesis in the mammalian telencephalon (Wullimann, 2009).

The primary proliferative, neurogenic zone of the evaginated mammalian telencephalon, the VZ, is positioned internally, with the cortical layers of postmitotic neurons formed inside-out (Figures 8 and 9). A consequence of the eversion of the zebrafish telencephalon is the positioning of the VZ at the surface (Figure 22). Although morphologically very different, the telencephalon of both mammals and zebrafish is divided into pallial and subpallial regions, separated by the PSB. The zebrafish pallium is composed of the medial pallium (Dm), lateral pallium (Dl), posterior pallium (Dp), and central pallium (Dc). As in the mammalian VZ, radial glial cells expressing GFAP have been identified in the zebrafish VZ (Marcus *et al.*, 1995), and shown to generate neurons (Johnson *et al.*, 2016). Recent work has demonstrated that neurogenesis in the VZ of the expanding zebrafish pallium proceeds outside-in [Figure 23; (Furlan *et al.*, 2017)]. A core of early-born neurons is positioned within the Dc by 5dpf, with later-born neurons continuing to be deposited more superficially until around 1.5mpf. These findings would appear to negate a role for radial and tangential neuronal migration, contrasting with the formation of mammalian cortical layers. Interestingly, whereas Reelin signalling has been shown to be highly ordered in mammalian radial migration, the complex expression pattern during zebrafish

development may help to explain these differences (Imai *et al.*, 2012). Additionally, clonal analyses revealed an absence of SVZ with very few intermediate progenitors in the pallium, and showed that the RGCs in the VZ were neurogenic throughout development (Furlan *et al.*, 2017).

Despite the many differences between the development and morphology of the telencephalon, the zebrafish has recently become an important model for human brain diseases.

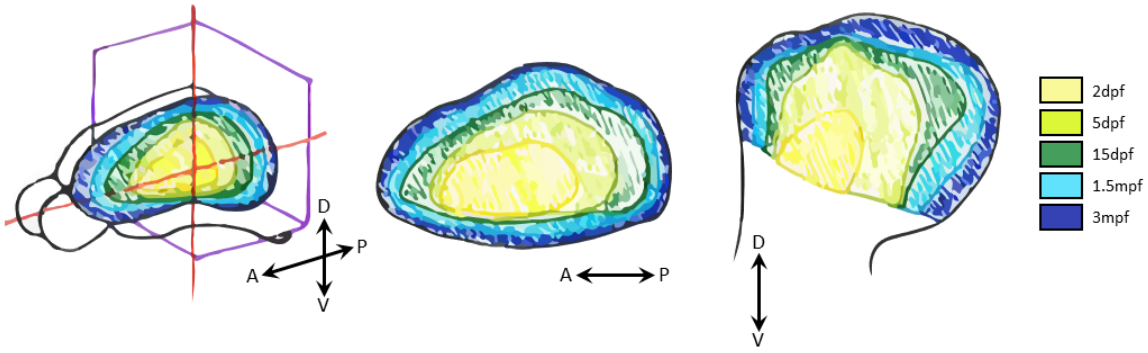

Figure 23. Neurogenesis in the zebrafish pallium. *Views of the expansion of the zebrafish telencephalon from 2dpf to 3mpf. Dorsoventral and anteroposterior axes as indicated. Inspired by Furlan et al. (2017)*

III. Early Kidney Development

The formation of the pronephros, mesonephros and metanephros in mammals not only defines the temporal development of the kidney, but also reflects an evolutionary complexity. Zebrafish, as many lower vertebrates, form a functional pronephros which is maintained throughout the embryonic period (Kimmel *et al.*, 1995). The mesonephros forms during the juvenile period, and is the mature kidney of the adult (Davidson, 2011). Despite the differences zebrafish have recently become a valuable organism to model human kidney disease, particularly glomerulopathies (Outtandy *et al.*, 2018). One distinct advantage of zebrafish research is the regenerative capacity of the adults, which allows the detailed characterisation of a complex kidney system (W. Zhou *et al.*, 2010).

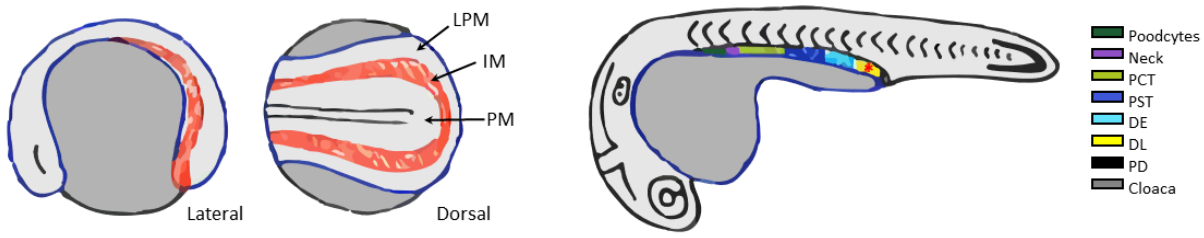

Figure 24. Specification and patterning of zebrafish pronephros. *Lateral and dorsal views of the early specification of the intermediate mesoderm at the tail bud stage (IM; red), lateral plate mesoderm (LPM), paraxial mesoderm (PM). Inspired by Gerlach et al. (2013). Lateral view of zebrafish embryo at 28 somite stage (SS) with specified pronephric segments. Proximal straight tubule (PST), proximal convoluted tubule (PCT), distal early (DE) and distal late (DL), pronephric duct (PD). Asterisk denotes corpuscle of Stannius.*

a. Formation of the Pronephros

As during the development of the mammalian kidney, the zebrafish kidney derives from the intermediate mesoderm following gastrulation (Kimmel *et al.*, 1990). At the tail-bud stage, the intermediate mesoderm is positioned ventrally, formed of two parallel lines of cells which join together caudally, and are located between the lateral plate mesoderm and the paraxial mesoderm [Figure 24; (Serluca *et al.*, 2001)]. BMP signalling has been implicated in maintaining the ventral position of the intermediate mesoderm, with reduced expression of *bmp2b* or *bmp7a* leading to a decrease in the number of renal progenitors, as defined by *pax2a* expression (Kishimoto *et al.*, 1997; Schmid *et al.*, 2000). As the convergence extension movements during early development elongate the embryo along the anterior-posterior axis, the bilateral lines of cells demarcating the renal progenitor cell field approach the midline (Lam *et al.*, 2009). These progenitors, expressing *pax2a*, *pax8* and *lhx1a*, are present more laterally but intermixed with primitive blood cells (Drummond *et al.*, 1998; Pfeffer *et al.*, 1998). The loss of function of transcription factors involved in these early patterning events affect pronephros formation, as well as other mesodermal cell fates, as in the case of the combined loss of *ntla* (Brachyury/T) and *tbx16* (Amacher *et al.*, 2002). The caudal type homeobox (*cdx*) transcription factors are important for the elongation of the body axis, and subsequently impact the position of the pronephros. The loss of function of *cdx4* with *cdx1a* together results in a severely shortened body length and multiple pronephric defects (Shimizu *et al.*, 2005; Davidson *et al.*, 2006).

Osr1 is expressed during early kidney development in both mammals and zebrafish, however, in zebrafish *osr1* is specifically required for the proximal-most pronephric fates (James *et al.*, 2006; Mudumana *et al.*, 2008). Depletion of *osr1* causes defects which become evident at the 14-somite stage, with a decrease in the expression levels of *pax2a* and *lhx1a* at the rostral end of the renal progenitor field and an increase in the angioblast lineage (Mudumana *et al.*, 2008). Subsequently, depletion of *osr1* results in the loss of podocytes and part of the proximal convoluted tubule. Interestingly, these defects can be rescued by re-expression of *pax2a* or the depletion of endoderm-specific transcription factors. These results suggest that *osr1* may have a role in regulating the expression of *pax2a* in order to maintain the pronephric fate of the renal progenitor field (Mudumana *et al.*, 2008). Wnt signalling has also been implicated in both mammalian and zebrafish kidney development (Schmidt-Ott *et al.*, 2008). The inhibition of β-catenin signalling results in similar proximal pronephros defects to the loss of *osr1* expression (Lyons *et al.*, 2009). However, it remains to be seen whether both *osr1* and Wnt signalling maintain the renal progenitor field by ensuring the expression of *pax2a*.

Following specification, the mesenchymal cells of the renal progenitor field undergo a mesenchyme-to-epithelial transition to form the tubule of the pronephros (Drummond *et al.*, 1998). The expression

of various proteins, such as protein kinase C, iota (prkci) and pard3, establishes an apicobasal polarity and precedes the opening of the lumen (Drummond *et al.*, 1998; Horne-Badovinac *et al.*, 2001). Claudin-b is a tight junction protein expressed in the pronephros and known to play a role in controlling membrane permeability. The knockdown of *claudin-b* leads to cardiac oedema and is thought to be due to defects in sodium uptake (Kwong *et al.*, 2013). Lumen formation occurs around 20SS and has been shown to occur even in the absence of various apical or basal factors (Panizzi *et al.*, 2007). As lumen formation is crucial for pronephros function it is possible that many of these factors act redundantly to ensure the fidelity of this process.

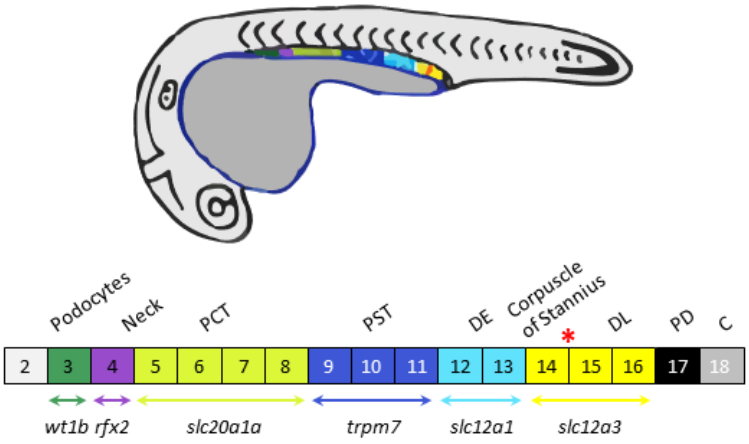

Figure 25. Segmentation pattern of pronephros at 28 somite stage. *Representation of somites and markers observable within each distinct pronephric segment. Proximal convoluted tubule (PCT), proximal straight tubule (PST), distal early (DE), distal late (DL), pronephric duct (PD), cloaca (C). Asterisk denotes position of the corpuscle of Stannius.*

The pronephros, as the mature mammalian nephron, consists of discrete functional regions which can be identified by the specific, non-overlapping expression of different solute transporters [Figure 25; (Desgrange *et al.*, 2015)]. The definition of these segments begins early during development, although gene expression profiles within the renal progenitor cell field have been shown to vary during the early somite stages (Wingert *et al.*, 2011). The specific expression of a number of transcription factors has been established in the initial definition of the broad rostral and caudal domains during nephron formation. Notch signalling is implicated in the rostral domain, with the expression of the ligands *dlc* and *jag2*, while the caudal domain is defined by the transcription factor *MDS1 and EVI1 complex locus* (*mecom*) (Wingert *et al.*, 2011). The podocyte lineage diverges early during development, with the localised expression of *wt1a* from 5SS (Serluca *et al.*, 2001). As development proceeds, further markers are expressed and define progressively smaller and more differentiated pronephric segments (Wingert *et al.*, 2011). While the precise mechanisms behind the differentiation of these discrete regions and the role of the various identified transcription factors remains to be elucidated, the establishment of

the appropriate pronephric patterning is known to be crucial to the subsequent function. One well-characterised factor which has been shown to influence this process is retinoic acid (Wingert *et al.*, 2007). Retinoic acid is expressed early during development by the anterior paraxial mesoderm and is important for the rostral-most pronephric segments (Wingert *et al.*, 2007). Inhibition of retinoic acid signalling results in a reduction of the proximal pronephric domains and the expansion of more distal domains. Similarly, endogenous retinoic acid signalling expands the proximal domains at the expense of distal regions, and suggest that retinoic acid promotes proximal pronephric fates (Wingert *et al.*, 2007). Other factors have been found to be essential for the development of other regions, such as the importance of *pax2a* inhibition for podocyte differentiation (Drummond *et al.*, 1998; Majumdar, Lun*, et al.*, 2000), and *irx3b* expression for distal pronephric fates (Wingert *et al.*, 2011). The range of factors so far identified, and the critical interplay of each in the differentiation of discrete nephric segments parallels mammalian development and highlights the complexity of this, at first, simplistic structure.

In addition to the importance of patterning during development, ciliogenesis has also been shown to be crucial for the formation of a functional pronephros (Sun *et al.*, 2004). The distribution of mono- and multiciliated cells within the pronephros has been shown to be dependent on lateral inhibition upon Notch signalling (Liu *et al.*, 2007; M. Ma *et al.*, 2007). The expression of *rfx2*, which is associated with multiciliated cells, is inhibited by Notch and promoted by jagged2a. Constitutive activation of Notch signalling severely reduces the number of multiciliated cells and consequently increases the number of cells presenting a single cilium. Similarly, inhibition of Notch signalling increases the number of multiciliated cells at the expense of mono-ciliated cells (M. Ma *et al.*, 2007). Cilia in the pronephros are crucial to generate fluid flow, with defects in either the formation or function of cilia shown to lead to the formation of pronephric cysts and tubule dilations (Drummond *et al.*, 1998; Sun *et al.*, 2004). The opening of the pronephric duct to the external environment, or cloaca, is additionally important for pronephric function and with defects similarly resulting in cysts and dilations (Pyati *et al.*, 2006; Burckle *et al.*, 2011). The cloaca is formed through the apoptosis of a large, ventrally positioned epidermal cell and the concomitant migration of pronephric cells to this site, and is thought to open around 25SS (Pyati *et al.*, 2006). Defects in pronephric function, whether relating to cloaca opening or cilia function, are invariably lethal, with embryos often dying by 5dpf.

Following the definition of the different pronephric segments, the distal cells have been shown to migrate collectively in an anterior direction towards the glomerular region (Vasilyev *et al.*, 2009; Vasilyev *et al.*, 2012). This migration results in the complex morphology of the proximal convoluted tubule, and the expansion of the proximal straight tubule. While mitosis occurs in both proximally, in the neck region, and distally, in the distal late segments, this does not seem to be the principle driving

force behind this migration (Vasilyev *et al.*, 2012). In contrast, glomerular function and subsequently filtrate flow within the pronephros were shown to be essential (Vasilyev *et al.*, 2009).

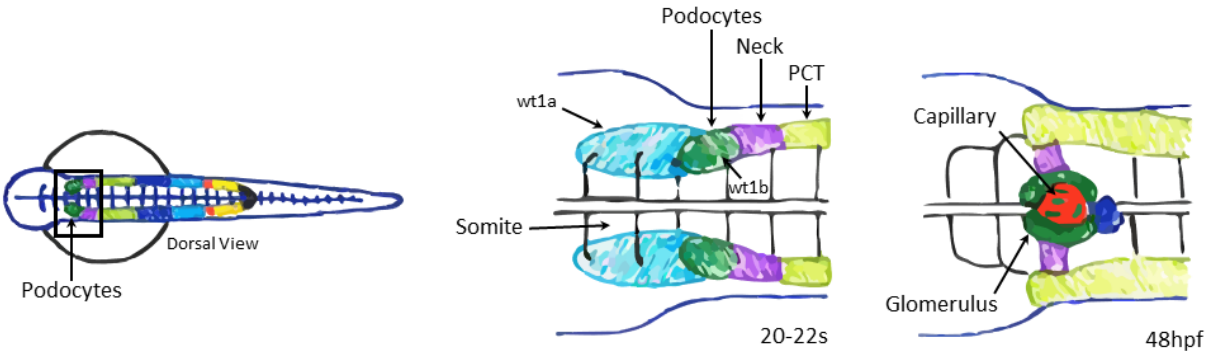

Figure 26. Glomerular specification and formation. *Dorsal representation of the early specification of the glomerular region and the subsequent differentiation to form the functional glomerulus. Inspired by Gerlach et al. (2013).*

b. Glomerulus Formation

The specification of podocyte precursors occurs early during zebrafish development, with *pax2a*, *wt1a*, and *wt1b* all found to be important [Figure 26; (Serluca *et al.*, 2001; Perner *et al.*, 2007)]. While the expression of *wt1a* is broader than that of *wt1b*, those cells expressing both are thought to be podocyte precursors (Perner *et al.*, 2007). Additional transcription factors are also expressed by these cells later during development, including *foxc1a*, *lhx1a*, *mafba*, and *hey1 (O'Brien et al., 2011)*, while markers of podocyte differentiation, such as *nephrin* and *podocin*, are visible between 24-26hpf (Kramer-Zucker *et al.*, 2005). Interestingly, these different transcription factors are thought to function together in a complex which can be modified throughout development. At later stages, higher levels of *wt1a* have been found to drive the expression of markers of podocyte differentiation (O'Brien *et al.*, 2011). It remains to be seen whether these mechanisms are specific to zebrafish development, or are also conserved in mammalian podocyte differentiation.

The formation of the blood-filtering glomerulus at the proximal end of the pronephros begins with the migration and subsequent fusion of podocyte precursors at the midline and is thought to be in response to signals from the overlying notochord (Drummond *et al.*, 1998; Majumdar & Drummond, 2000). Subsequently, differentiating podocytes express VEGF, attracting endothelial precursors and contributing to the formation of the glomerular basement membrane (Serluca *et al.*, 2002). As in mammalian glomeruli, the podocyte foot processes interdigitate and rearrangement of cell-cell junctions results in the formation of the highly specialised slit diaphragms required for efficient blood filtration, which begins around 48hpf (Majumdar *et al.*, 1999). Development of the zebrafish pronephric glomerulus, therefore, parallels in many ways the development of mammalian glomeruli.

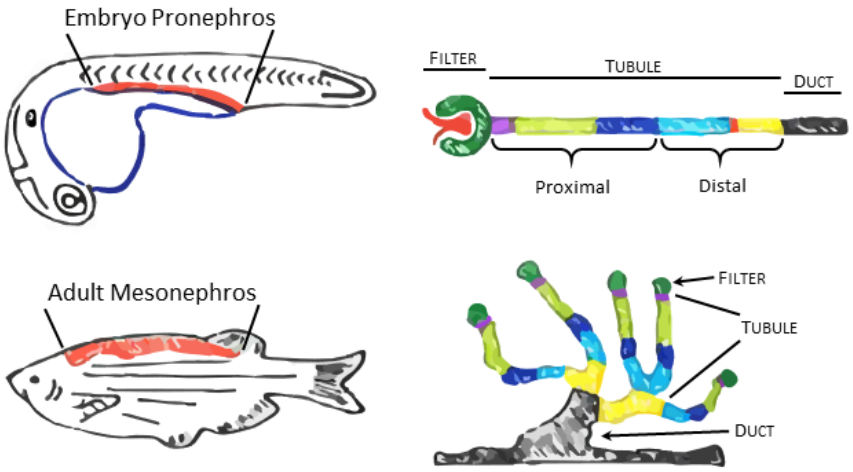

Figure 27. Comparison the pronephros and mesonephros. *Representation of nephrons from embryonic pronephros and adult mesonephros. Inspired by McCampbell et al. (2014)*

c. Formation of the Mesonephros

The pronephros is the functional kidney of the zebrafish embryo, however, at the juvenile stage the mesonephros begins to develop [Figure 27; (Diep *et al.*, 2015)]. Cells expressing the early developmental marker *lhx1a* have been shown to aggregate close to the pronephros where they expand and elongate to form a new nephron (Diep *et al.*, 2011). These nephrons express many of the markers of the developing pronephros, such as *wt1b* at the proximal end. Initially these nephrons are initially formed in a restricted distal region of the pronephros, however, nephrogenesis subsequently occurs in both proximal and further distal regions (W. Zhou *et al.*, 2010; Diep *et al.*, 2011).

The adult mesonephros consists of three domains, the head, saddle and tail, positioned in the dorsally (W. Zhou *et al.*, 2010). Interestingly, the collecting ducts appear as two parallel tracts suggestive of the pronephros. Considering the positioning of the initial mesonephros nephrogenesis it is possible that the pronephros is remodelled to form the adult collecting ducts, although this remains to be demonstrated experimentally. One advantage of zebrafish kidney research is that the adults retains the ability to generate new nephrons. Renal progenitor cells have been identified in the stroma of the adult mesonephros, and are capable of neonephrogenesis in response to growth or injury. Remarkably, transplantation experiments of renal progenitors into renal compromised fish have shown that the formation of new nephrons requires a permissive environment, and is not cell intrinsic (Diep *et al.*, 2011). The factors present in the adult stroma which allow neonephrogenesis remain to be elucidated.

Chapter Four - Kinesins

Intracellular transport, or the movement of components within the cell, is a conserved process occurring in many different organisms and with a range of functions depending on the cell type. Intracellular transport in eukaryotic cells relies on both an active network within the cell, called the cytoskeleton, and a number of motor proteins. The cytoskeleton is composed of actin, intermediate filaments and microtubules. Each of these components has a different molecular composition, and each contributes to various cellular functions. Numerous motor proteins have been described, with differing affinities for microtubules or actin and distinct roles within the cell cycle. Myosins, kinesins and dyneins are superfamilies of motor proteins, of which myosin binds to actin, and kinesins and dyneins bind to microtubules. Many motor proteins bind to distinct sets of cargoes and proceed unidirectionally along the filaments of the cytoskeletal network. This processivity requires the hydrolysis of ATP within a conserved protein region, termed the motor domain. The motor domain is also the site of microtubule or actin binding. The remaining protein sequences are highly divergent, reflecting the ability to interact with a wide range of cargoes.

Microtubules are polarised hollow filaments formed from the addition of heterodimers of α- and β-tubulin onto a growing plus-end and arranged as 13 protofilaments. The opposite, minus, end is usually, but not always, anchored to a microtubule organising centre [MTOC; (Luders *et al.*, 2007)], such as the centrosome in mammalian cells. While dyneins have been found to proceed towards the minus ends of microtubules, many kinesins function in the opposite direction, and transport cargo towards the plus ends. However, within the kinesin superfamily (KIF) proteins with minus-end directed cargo transport and microtubule depolymerising function have additionally been described.

Both microtubules and kinesins are crucial for many different processes, including mitosis and ciliogenesis. Kinesins have been shown to function at various stages of mitosis, such as spindle assembly, chromosome congression, and cytokinesis. Additionally, a number of kinesins have been implicated in the formation and function of the cilium, a microtubule-based sensory organelle present on the surface of many cell types. Despite much progress, the precise role of many of kinesins within these processes remains to be elucidated.

I. Kinesin Superfamily (KIF)

The first member of the kinesin superfamily was identified through the observation of organelle transport in the axons of giant squid in 1985 by Ronald Vale, following 20 years after the identification of dynein within cilia (Gibbons *et al.*, 1965). This kinesin, initially termed Kinesin-I or conventional kinesin, was shown to bind microtubules and proceed along them in an ATP-dependent manner. Subsequent work revealed the similarities between the molecular structures of kinesin and myosin, with a motor domain, a coiled-coil-containing linker and cargo-binding tail (Hirokawa *et al.*, 1989; Scholey *et al.*, 1989; J. T. Yang *et al.*, 1989). Initially, a single homologous kinesin was observed in each species studied, however, the identification of kinesin-like proteins involved in diverse cellular functions, including mitosis and nuclear transport, raised the possibility of the existence of a kinesin superfamily. These proteins shared a conserved region of around 350 amino acids, corresponding to the motor domain, while the remaining sequences were considerably more divergent (Enos *et al.*, 1990; Meluh *et al.*, 1990).

Initial analyses characterised kinesins based upon the position of the motor domain within the sequence and determined 3 subgroups. While kinesins with N-terminally positioned motor domains proceeded towards the plus ends of microtubules, C-terminal motor domain kinesins moved in the opposite direction (Vale *et al.*, 1985; McDonald *et al.*, 1990). Those kinesins with an internal motor domain (M) were suggested to play a role in regulating the microtubule network (Walczak *et al.*, 1996). Eventually the advent of whole genome analysis confirmed the presence of 45 separate kinesin superfamily members in mammals [Figure 28; (Miki *et al.*, 2001)]. Phylogenetic analysis using the protein sequences of each member led to the classification of these 45 kinesins into 14 subfamilies (Miki *et al.*, 2001; Lawrence *et al.*, 2004). Every kinesin possesses a motor domain, the sequence of which is highly conserved throughout the superfamily. The kinesin proteins are also comprised of a variable combination of functional modules including a neck linker, a coiled-coil-containing stalk, and a cargo-binding domain. The differences in the sequences of the cargo-binding domains may reflecting the wide range of interactants and functions (Miki *et al.*, 2005), although functions are often similar between members of the same subfamily. Of the 14 identified subfamilies, members of kinesin-8 and kinesin-13 have been shown to have microtubule-depolymerising activity (Walczak *et al.*, 2013), while members of the kinesin-4 and kinesin-11 families demonstrate microtubule-stabilising and remodelling activities (R. Zhou *et al.*, 2009; van der Vaart *et al.*, 2013). The remaining families show plus-end directed movement along microtubules except the kinesin-14 subfamily, which have minus-end directed processivity (Friel *et al.*, 2012).

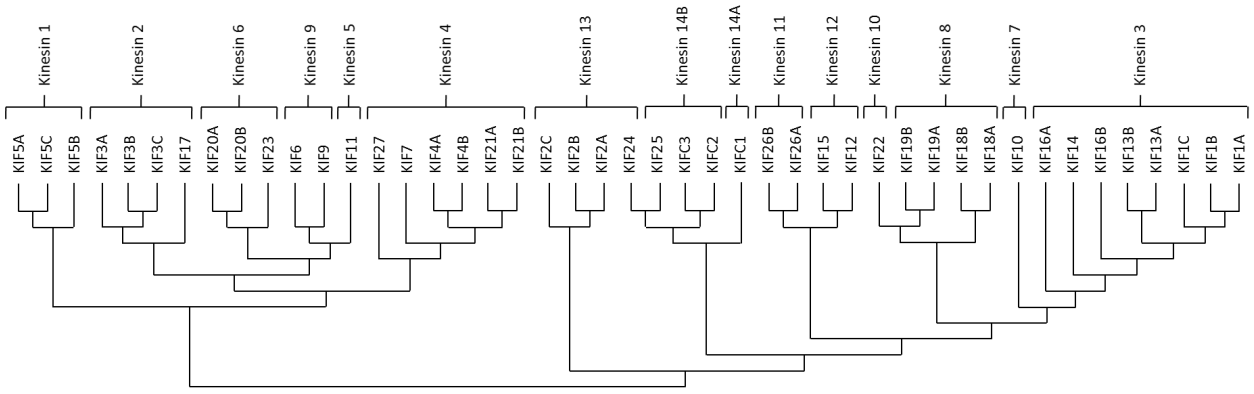

Figure 28. Phylogeny of the kinesin superfamily. *Inspired by Miki et al. (2001)*

a. Functional Domains

Different members of the superfamily function via different mechanisms, which may be inherent to their role within the cell (Verhey *et al.*, 2011). Initial electron microscopy analyses of kinesin suggested a protein resembling myosin. The N- and C-terminal domains bound microtubules and cargoes respectively, with the intervening sequence promoting dimerisation (Amos, 1987). This kinesin was subsequently shown to act as a heterotetramer composed of dimers of kinesin heavy-chain, encoded by *KIF5A*, *KIF5B* and *KIF5C*, and kinesin light-chain, encoded by the *KLC1-KLC4* genes (Kuznetsov *et al.*, 1988; Verhey *et al.*, 2011). The motor domain is present within the kinesin heavy-chain sequences, along with a neck domain, the coiled-coil-containing stalk and a C-terminal cargo-binding tail region (Jeppesen *et al.*, 2012). The neck domain is composed of the linker, required for movement of the motor, and the neck coil, required for homodimerisation. The stalk allows conformational changes within the protein switching between an active or autoinhibitory structure. In the kinesin-2 family, the stalk has been proposed to play an alternative role. The most N-terminal regions of the stalk sequences are composed of contrastingly charged amino acids in the KIF3A protein compared to KIF3B, and so are thought to promote heterodimerisation over homodimerisation (Chana *et al.*, 2002; Chana *et al.*, 2005). Coiled-coil domains are also known to be involved in protein-protein interactions, and so can be involved in regulating the activation state of the kinesin through cargo binding and the relief of autoinhibition, as has been shown for KIF17 (Hammond *et al.*, 2010; Truebestein *et al.*, 2016). Finally, the kinesin-3 family encode an FHA domain (Verhey *et al.*, 2011), a regulatory region which interacts specifically with phosphorylated threonine residues (Almawi *et al.*, 2017). However, non-phosphorylation dependent functions have been identified for the FHA domains in kinesins, which have been associated with autoregulation. In KIF1A, interactions between the FHA and a coiled-coil domain were shown to inhibit prevent to microtubules, therefore inhibiting processive movement (Hammond *et al.*, 2009).

b. Motor Processivity

The tertiary and quaternary structures of the various members of the kinesin superfamily is of particular interest when considering the mechanisms behind their movements along microtubules. In this regard the identification of monomeric compared to dimeric kinesins is particularly interesting as they appear to contradict the classical 'hand-over-hand' model of processivity (Hackney, 1994; Yildiz *et al.*, 2004). This model states that the cyclic binding and release of alternating motor domains within a protein dimer drives directed movement. Much research into the precise mechanics of kinesin processivity has been performed using KIF5B, originally designated conventional kinesin, and has built on the initial observations of the requirement for ATP- and microtubule-binding (Vale *et al.*, 1985; W. Wang *et al.*, 2015). The cycle of ATP hydrolysis by the motor domain, releasing ADP and phosphate, occurs concomitantly with the binding to and unbinding from microtubules (Coy *et al.*, 1999; Rosenfeld *et al.*, 2003). The ATP-binding site of the motor domain contains three elements, Switch 1, Switch 2 and the P-loop, which together compose a conserved catalytic core (Figure 29). The motor domain can be considered in terms of three subunits, the Switch 1/2, P-loop and tubulin-binding subdomains, which are rearranged upon ATP-binding. These structural rearrangements cause a cavity outside of the ATP-binding site and surrounded by conserved residues within the P-loop and tubulin-binding subdomains to open. This cavity is filled by a conserved isoleucine of the neck linker following additional rearrangements. When the motor domain is not bound to ATP the cavity is filled and thus the neck linker is prevented from docking (Rice *et al.*, 1999). With each step the kinesin moves a distance of 8nm along the length of the microtubule, corresponding to the distance between consecutive heterodimers of tubulin (Ray *et al.*, 1993; Coy *et al.*, 1999). Each step requires the hydrolysis of a single ATP molecule, which is coupled to variations in the microtubule-binding affinity of the motor domain (Hua *et al.*, 1997; Woehlke *et al.*, 1997). The coupling of ATP hydrolysis and microtubule-binding with the structural rearrangements allows both motor domains of the dimer to be in different states. The coordination of these events, along with the variable conformations of the neck linker, drive the processive motility of the kinesin. Although many of these processes have been elucidated based on KIF5B, they are likely to be broadly applicable to many of the other processive kinesin motors.

c. Microtubule Depolymerisation

In contrast to the processive kinesins with an N- or C-terminal motor domain, the kinesin-13 family encode the motor domain within the middle of the sequence. These kinesins are not processive, but possess microtubule depolymerising activity, requiring the ATP-hydrolysis and microtubule-binding functions of the motor domains. Members of the kinesin-8 and -13 families are thought to depolymerise microtubules using different mechanisms. The kinesin-13 families have been shown to

cause the bending of microtubule protofilaments. Upon binding, ATP-hydrolysis promotes the removal of tubulin heterodimers from the protofilaments. In contrast, members of the kinesin-8 family are processive and are thought to regulate tubulin dynamics less directly. Some members may bind to microtubule plus-ends and prevent the addition of tubulin heterodimers, while others bind microtubules and force the removal of already present kinesin motors along with the heterodimers to which they were bound (Walczak *et al.*, 2013).

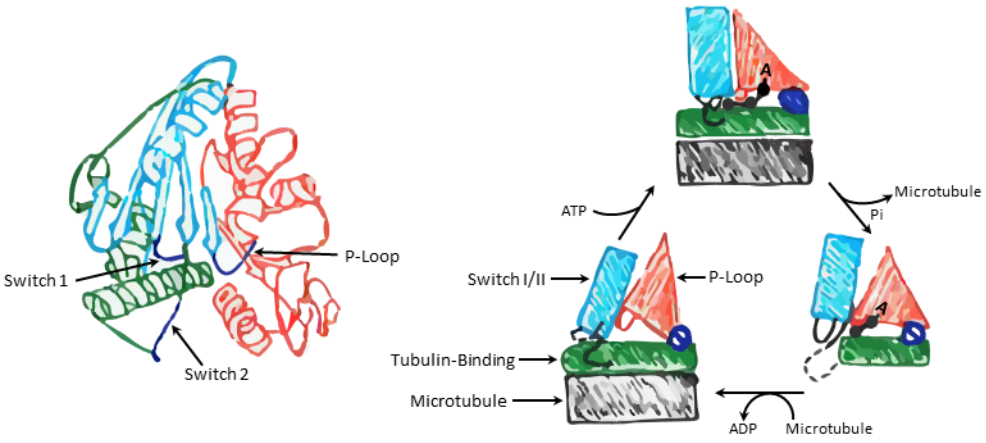

Figure 29. Interactions between different subdomains of the kinesin motor drive processivity. *3D model of the Switch 1/2 and P-loop domains of a kinesin motor domain. Schematic representation of the subdomain interactions over the ATP-hydrolysis cycle. Tubulin-binding domain (green), the P-loop (red), the Switch 1/2 domains (blue) and a microtubule (black). Inspired by W. Wang et al. (2015)*

II. Kinesin Functions

The kinesin superfamily has been implicated in a wide range of functions within different organisms. Many of these functions are conserved between species, such as the role of kinesin-2 motors in axonemal transport within cilia and flagella (Scholey, 2013), and the role of KIF11 (Eg5) at mitotic spindle (Ferenz *et al.*, 2010). Interestingly, kinesins are the only family of motor proteins conserved across all eukaryotes thus far analysed, and it has been suggested that many kinesin members were already present in the last common eukaryotic ancestor (Wickstead *et al.*, 2010). Gene duplications have no doubt increased the number of kinesins encoded within the genome of higher organisms, likely reflecting the increasing complexity required (Wickstead *et al.*, 2006). Certain members of the kinesin superfamily are, therefore, absent from the genome of model organisms, complicating their functional analysis *in vivo*. Despite these challenges, research continues to identify novel roles for kinesins in various contexts.

a. Ciliary Functions

Cilia are conserved microtubule-based structures present in most eukaryotes. In mammals, many cells possess a single, immotile primary cilium, which has been shown to have critical roles during development (Wheway *et al.*, 2018). Alternatively, multiciliated cells form many motile cilia, which have diverse roles including generating flow in the brain ventricles and clearing mucus in the airways (Meunier *et al.*, 2016). Transverse electron microscopy has been used to demonstrate differences in both the structural composition and formation of these cilia (Sorokin, 1968; Satir *et al.*, 2007). The cilium is composed of a microtubule-based axoneme which extends from the basal body, formed from the mother centriole of the centrosome in primary cilia, or the amplification of centrioles in motile cilia (Figure 30). The axoneme of the cilium is surrounded by a highly specialised ciliary membrane. The mother centriole is distinguished from the daughter centriole by the presence of additional proteins, forming the distal and subdistal appendages. The proximal end the mother centriole is formed of nine symmetrically arranged triplets of microtubules, termed A-, B-, and C-tubules. The distal end is composed of doublets of A- and B-tublules. Only the A-tubule is formed of 13 protofilaments of α- and β-tubulin heterodimers, while the B- and C-tubules are composed of 10 protofilaments and share 3 with the adjoining tubule (Winey *et al.*, 2014). The ciliary axoneme is formed from the extension of the A- and B-tubules, with the plus-ends at the growing tip of the cilium (Ishikawa *et al.*, 2011). Two ciliary architectures can then be distinguished, '9+0' and '9+2'. In addition to the 9 doublets of microtubules, 9+2 cilia also contain two inner singlet microtubules, as well as a number of structures thought to be required for motility, such as the dynein arms and radial spokes. 9+2 cilia are, therefore, generally classed as motile, and the 9+0 cilia as immotile. However, cilia in the node are 9+0 but possess dynein arms and are motile, while 9+2 kinocilia of the inner ear are immotile (Satir *et al.*, 2007).

In mammalian cells centrosomes are important for a number of different processes, including the formation of a cilium, or ciliogenesis, as well as the assembly of the mitotic spindle during mitosis. Consequently, ciliogenesis is tightly coupled to the cell cycle, with cilia present on the surface of cells in G0 and being disassembled before cells begin mitosis (Ishikawa *et al.*, 2011). In mammalian cells, ciliogenesis begins with the docking of the mother centriole onto intracellular, primary ciliary vesicles through the distal appendages. The fusion of these vesicles results in the capping of the distal end of the mother centriole in a ciliary vesicle (Sorokin, 1968; T. J. Park *et al.*, 2008; Ishikawa *et al.*, 2012). CP110, an important ciliary regulator, is also present at the distal end of the mother centriole and prevents the elongation of centriolar microtubules. Following the formation of the ciliary vesicle, the removal of CP110 is, therefore, conducive with axonemal elongation (Sanchez *et al.*, 2016). The distal appendages become the transition fibres, with the transition zone formed at the proximal end of the axoneme. The protein composition of the cilium has been shown to be distinct from the cytoplasm, as

has the ciliary membrane, despite being continuous with the plasma membrane of the cell (Ishikawa *et al.*, 2012). The transition zone has been implicated in forming a restrictive barrier preventing diffusion of soluble proteins directly into the cilium (Q. Hu *et al.*, 2010). Due to the absence of protein synthesis within the cilium, a specialised form of transport is required for ciliogenesis and ciliary function. The transition fibres have been proposed to participate in the formation and function of the selective barrier, as well as in forming a loading zone for the entry of these cargoes into the cilium. Potentially, a ciliary localisation signal directs transport to this region prior to and allowing entry into the cilium.

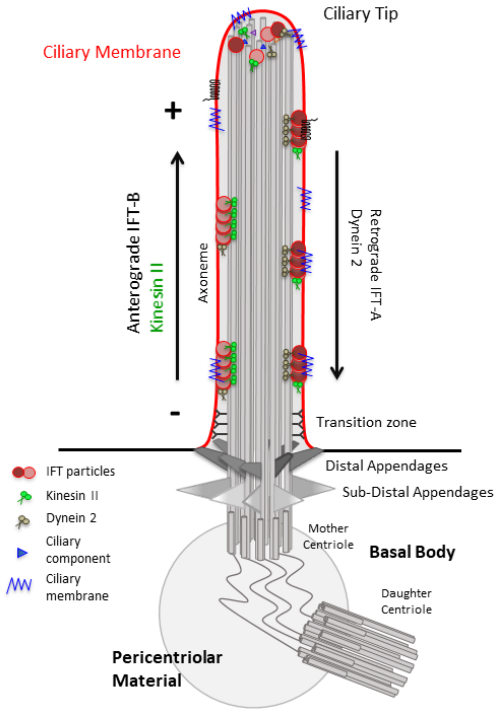

Figure 30. Schematic representation of a cilium. *Plus and minus-ends of microtubules within the cilium are indicated, along with the direction of kinesin and IFT-B-mediated anterograde transport and dynein and IFT-A-mediated retrograde transport.*

Intraflagellar transport (IFT) is a highly conserved process in which cargo bound to a complex of numerous proteins, termed IFT trains, move bidirectionally along the axonemal doublet microtubules from the base of the cilium to the tip (Figure 30). Anterograde transport is the movement of cargoes from the base to the tip and requires IFT-B proteins, as well as the kinesin-2 family of molecular motors. At the tip of the cilium, complex remodelling of the IFT trains permits retrograde transport back to the base of the cilium, requiring IFT-A proteins and cytoplasmic dynein 2 [DYNC2H1, (Ishikawa *et al.*, 2011)].

Much research has been done to characterise the proteins required for ciliogenesis, ciliary function and, more recently, disassembly. Along with the IFT trains, another complex of proteins, termed the BBSome, has been identified as crucial to the formation and function of cilia. Many of the proteins identified so far are essential for both primary and motile cilia, however, certain, such as the proteins of the dynein arms and radial spokes, are specific to motile cilia. Ciliogenesis in multiciliated cells requires the formation of 30 to 300 centrioles, this centriolar amplification relies on structures known as deuterosomes (Spassky *et al.*, 2017). Many of the genes encoding components of these motile cilia-specific structures are under the control of the transcription factor FOXJ1. In contrast, many of the genes encoding proteins required for the formation of a primary cilium are under the control of the RFX family of transcription factors (Thomas *et al.*, 2010).

Cilia act as signalling platforms required for both development and tissue homeostasis and, unsurprisingly therefore, mutations in ciliary genes have been identified in a number of complex diseases, collectively termed ciliopathies (Reiter *et al.*, 2017). Recently, mutations have been identified in several genes encoding members of the kinesin superfamily in cases of ciliopathy phenotypes (van Dam *et al.*, 2013). This work has revealed the wide range of cilia-related functions performed by different kinesin proteins.

i. Intraflagellar Transport

The essential role of the kinesin-2 family in IFT was first demonstrated in *Chlamydomonas reinhardtii* (Huang *et al.*, 1977; Cole *et al.*, 1998). A temperature-sensitive mutation in *FLA-10* resulted in flagellar disassembly and prevented flagellar re-growth at the restrictive temperature. The loss of *FLA-8* was also shown to result in flagellar defects (Adams *et al.*, 1982). *FLA-10* was identified as the homologue of *KIF3A* (Walther *et al.*, 1994), while *FLA-8* is the homologue of *KIF3B* (Miller *et al.*, 2005). KIF3A and KIF3B form a heterotrimer with the non-motor, kinesin associated protein (KAP) and are responsible for anterograde IFT. The knockout of any of the components of this heterotrimer in the mouse leads to embryonic lethality, an absence of cilia in the embryonic organiser, the node, and ciliopathy-related defects, such as *situs inversus* (Nonaka *et al.*, 1998; Marszalek *et al.*, 1999).

In contrast to the well-established role for KIF3A/3B, the role of the homodimeric KIF17 in IFT is more controversial. In *Caenorhabditis elegans* the KIF17 homologue, *OSM-3*, has been shown to be required for IFT along the singlet microtubules present at the distal end of the cilium, while KIF3A/KIF3B-mediated IFT is restricted to the proximal end, along doublet microtubules (Snow *et al.*, 2004; Prevo *et al.*, 2015). However, the requirement for KIF17-mediated IFT in vertebrate cilia is unclear. Morpholino-mediated knockdown of *kif17* in the zebrafish was shown to result in retinal degeneration, while knockout was shown to cause a delay in retinal development which recovers by 6dpf (Insinna *et*

al., 2008; Lewis *et al.*, 2017). Prior knockout studies in zebrafish had failed to find ciliary defects (C. Zhao *et al.*, 2012). Similarly, no ciliary defects could be identified in *Kif17* knockout mice (Jiang *et al.*, 2015). Singlet microtubules are present in the outer segment of photoreceptors and cilia of olfactory neurons (Falk *et al.*, 2015), however, KIF17-mediated IFT was not found to be restricted to these singlet microtubule regions (Williams *et al.*, 2014). The importance of KIF17 in vertebrate IFT, therefore, remains to be clarified.

ii. Microtubule Dynamics

IFT is a well-established function of members of the kinesin-2 subfamily, however, more recently, additional ciliary functions have been ascribed to other members of the kinesin superfamily. Both KIF24 and KIF2A are part of the kinesin-13 subfamily, possess microtubule-depolymerising activity and have been implicated in ciliary disassembly. The microtubule-depolymerising activity of KIF2A has been shown to be activated by the cell cycle-regulated kinase Polo-like kinase 1, PLK1. Knockout of KIF2A in retinal pigmented epithelial (RPE1) cells resulted in a delay in ciliary disassembly (Miyamoto *et al.*, 2015). Similarly, phosphorylation by the cell cycle-regulated NIMA-related kinase 2 (NEK2) was suggested to induce the centriolar-specific microtubule-depolymerising activity of KIF24 (S. Kim *et al.*, 2015). Knockdown of KIF24 was shown to lead to aberrant ciliogenesis in cycling cells, thought to be due to the loss of the distal centriolar capping protein, CP110 (T. Kobayashi *et al.*, 2011). Another kinesin with microtubule-depolymerising activity is KIF7, which has been implicated in SHH signalling (Cheung *et al.*, 2009; Endoh-Yamagami *et al.*, 2009). KIF7 localises to the tips of cilia, where remodelling of the plus-ends of microtubules was suggested to create a signalling platform for SHH (He *et al.*, 2014). KIF19A, again, possesses microtubule-depolymerising activity and is required for the regulation of ciliary length specifically in motile cilia. Loss of KIF19A results in longer cilia, which impairs beating and fluid flow in affected tissues (Niwa *et al.*, 2012; D. Wang *et al.*, 2016). Somewhat surprisingly, the loss of KIF18B in zebrafish, which had previously been shown to promote microtubule catastrophe (McHugh *et al.*, 2018), decreased the length of cilia in the pronephros (Choksi *et al.*, 2014). The mechanism behind this ciliary length regulation is, as yet, unknown.

iii. Other Ciliary Functions

In addition to roles in microtubule dynamics and ciliary length regulation, a number of kinesins have also been implicated in diverse functions at cilia. KIF13B has been implicated in SHH signalling through interactions with NPHP4 at the transition zone (Schou *et al.*, 2017). KIF5B indirectly affects ciliary length through the negative regulation of CCDC28, which in turn interacts with components of the BBSome to positively regulate cilia length (Cardenas-Rodriguez *et al.*, 2013). The loss of KIF5B, therefore, results in the overactivation of CCDC28 and increases ciliary length (Novas *et al.*, 2018). KIFC1 may play a role in the early steps of ciliogenesis during the fusion of ciliary vesicles to the distal end of the mother

centriole. It has been proposed that interactions with ASAP1 promote the transport of these vesicles from the Golgi, although loss of Kifc1 in the mouse did not result in ciliary defects (Hirokawa *et al.*, 2010; S. H. Lee *et al.*, 2018). KIF27 was found to be important for ciliogenesis in multiciliated cells, with loss of Kif27 in the mouse resulting in a number of motile ciliary defects, including hydrocephalus (Vogel *et al.*, 2012). In *Drosophila melanogaster*, KIF27 interacts with Fused, which was shown to be required for the formation of the central pair of singlet microtubules generally found in motile cilia (C. W. Wilson *et al.*, 2009). It remains to be seen whether this interaction is conserved in mammals. Both KIF9 and KIF6 have been implicated in ciliary motility in *Chlamydomonas reinhardtii* and *Trypanosoma brucei* respectively (Bernstein *et al.*, 1994; Demonchy *et al.*, 2009). In the mouse, the expression of KIF9 is regulated by Foxj1 (Jacquet *et al.*, 2009), and is found in multiciliated cells in the lungs in man (Ross *et al.*, 2007). Loss of *kif6* in the zebrafish leads to body axis curvature (Buchan *et al.*, 2014), which has recently been suggested to result from impaired ciliary motility affecting cerebrospinal fluid flow (Grimes *et al.*, 2016). The precise functions of both KIF6 and KIF9 in mammals remain to be elucidated.

b. Mitotic Functions

Ciliogenesis, is intricately coupled to the cell cycle. The ciliary axoneme extends from the microtubules of the mother centriole, however, in mammalian cells, centrosomes are also required to form the mitotic spindle. A number of ciliary kinesins have additional or complementary roles during mitosis, likewise IFT proteins have been implicated in mitosis (Taulet *et al.*, 2017). Mitosis is divided into different stages in eukaryotes, namely prophase, prometaphase, metaphase, anaphase and telophase (Figure 31). During prophase, the duplicated centrosomes move to opposite sides of the nucleus, the chromosomes condense and the nuclear envelope breaks down. The bipolar mitotic spindle forms during prometaphase, during which time the movement of the chromosomes to form the metaphase plate also begins. At metaphase, all the chromosomes are aligned at the spindle equator. Anaphase can be subdivided into anaphase A, where the sister chromatids are pulled towards the spindle pole, and anaphase B, where the central spindle elongates, the cleavage furrow forms and begins to ingress. During telophase the compacted central spindle has formed the midbody, and the intercellular bridge is cleaved, resulting in two daughter cells. Many of these processes require the tight control of microtubule dynamics, as well as the movement of various components, both of which have been shown to rely on several members of the kinesin superfamily (Glotzer, 2009; Cross *et al.*, 2014; D'Avino *et al.*, 2015).

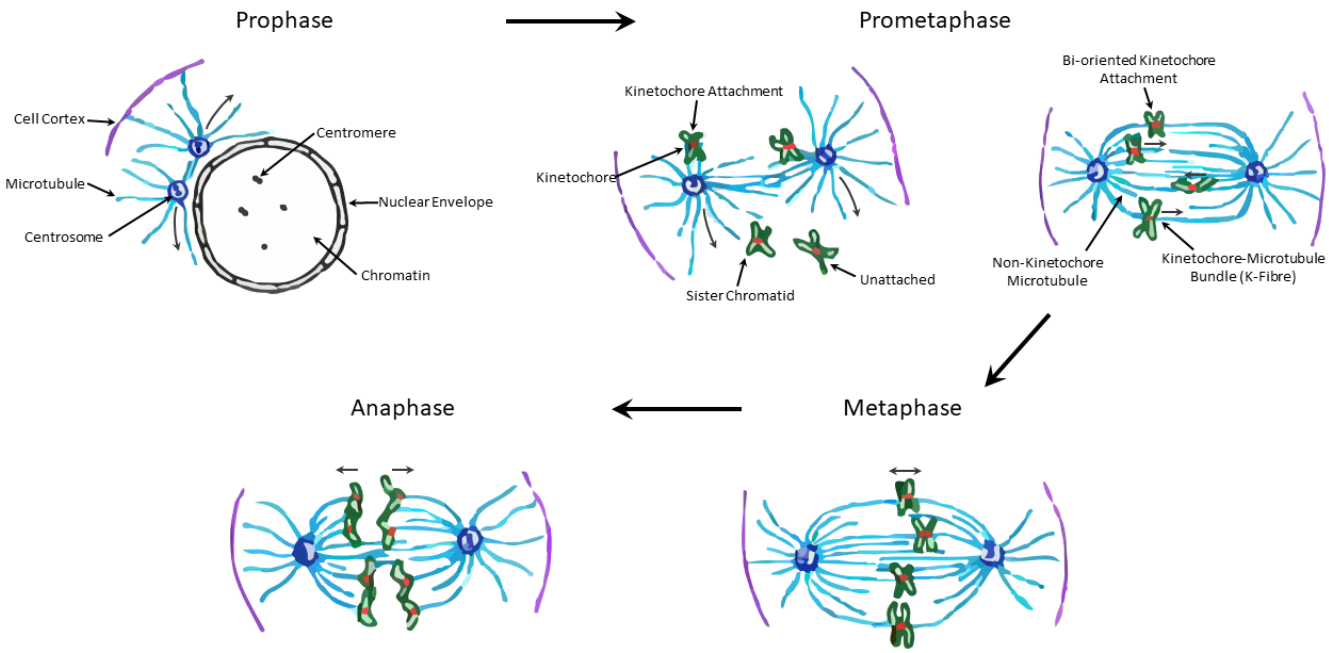

Figure 31. Schematic representation of the stages of mitosis. Inspired by Cross et al. (2014)

During prophase, the duplicated centrosomes migrate to opposite sides of the nucleus before the onset of nuclear envelope breakdown. Microtubule nucleation at the centrosomes increases during migration along the nuclear envelope. Being intrinsically polarised, the plus-ends of microtubules extend away from the centrosomes, some of which reach the cortex of the cell, while others overlap those of the opposing centrosome (Glotzer, 2009). One of the factors required for centrosomal separation is the plus-end directed motor, KIF11 [Eg5; (Tanenbaum *et al.*, 2010)]. KIF11 functions as a tetramer, formed as two anti-parallel homodimers. This arrangement leads to paired microtubule-binding motor domains at opposing ends of the tetramer, and allows KF11 to slide anti-parallel microtubules from opposing centrosomes apart, generating a force to drive separation (Kashina *et al.*, 1996; Kapitein *et al.*, 2005; E. R. Hildebrandt *et al.*, 2006; Acar *et al.*, 2013). The formation of the mitotic spindle during prometaphase, involving substantial microtubule rearrangements, also requires the function of KIF11, along with KIF15, KIFC1, KIF1B, KIF18B and KIF2A. Overlapping anti-parallel microtubules from opposing centrosomes, termed interpolar microtubules, are stabilised by KIF11 (Kapoor *et al.*, 2000). In the absence of KIF11, it has been shown that KIF15 can act redundantly to promote bipolar spindle assembly (Tanenbaum *et al.*, 2009). In contrast to KIF11, KIF15 functions as a homodimer with paired motor domains at the N-terminal end. It has been suggested that by interacting with the microtubule-binding targeting protein for xklp2 (TPX2) at the C-terminal tail, KIF15 can crosslink anti-parallel microtubules (Wittmann *et al.*, 1998).

Remodelling of the astral microtubules is also important, both during spindle assembly and later in mitosis. KIF1B was shown to interact with DLC2 at the cell cortex and to destabilise astral microtubules.

Loss of either KIF1B or DLC2 led to an increase in astral microtubule stability, which subsequently affected chromosome alignment and segregation (Vitiello *et al.*, 2014). The mechanism behind this destabilisation of astral microtubules remains to be elucidated, although it was suggested that KIF1B may possess microtubule-depolymerising activity. Similarly, KIF18B was shown to affect astral microtubule dynamics. KIF18B is a plus-end directed motor and was shown to promote astral microtubule catastrophe, depending upon the phosphorylation state. Procession towards the plus-ends of the astral microtubules was suggested to coincide with a cytoplasmic dephosphorylation, promoting KIF18B activity and aiding spindle positioning (Stout *et al.*, 2011; Walczak *et al.*, 2016; McHugh *et al.*, 2018). KIF2A is a microtubule-depolymerising kinesin with a centriolar localisation, being present at the basal body of cilia and spindle poles during mitosis (Miyamoto *et al.*, 2015). In the absence of KIF2A the centrosomes initially separate and form a bipolar spindle. However, this organisation is eventually lost, resulting in the formation of monopolar or asymmetric bipolar spindles, and is thought to be due to a process termed microtubule flux (Ganem *et al.*, 2004; C. Zhu *et al.*, 2005; Ganem *et al.*, 2005). Correct spindle positioning also requires KIFC1, a C-terminal motor domain kinesin with minus-end directed motility. KIFC1 motility functions to counteract the actions of KIF11 and KIF15, regulating the length of the mitotic spindle (Cai *et al.*, 2009).

The alignment of chromosomes at the spindle equator requires binding of the kinetochores, complex protein structures formed at the centromere of each chromosome, onto spindle microtubules. KIF10 is a plus-end directed motor protein required for the binding of kinetochores to microtubules and their subsequent repositioning at the metaphase plate (Wood *et al.*, 1997). Kinetochores bound to microtubules nucleated at both spindle poles are termed bioriented. The movement of kinetochores either towards or away from a given spindle pole requires highly dynamic microtubules. Both KIF2B and KIF2C of the kinesin-13 family, as well as KIF18A have been implicated in these processes. KIF2B localises to both the centrosomes and kinetochores and has been to shown to be essential for chromosome alignment. PLK1-mediated phosphorylation of KIF2C at the kinetochores induces the microtubule-depolymerising activity of this kinesin, and is required for chromosome segregation (Kline-Smith *et al.*, 2004; Manning *et al.*, 2007). KIF18A also localises to the kinetochores and has been proposed to play a role in regulating microtubule polymerisation. Overexpression of KIF18A led to an increase in the number of cells forming multipolar spindles, purportedly due to effects on microtubule dynamics (Mayr *et al.*, 2007; Du *et al.*, 2010). Both KIF22 and KIF4A are chromokinesins, a subclass of kinesins which localise to the chromosomes and contribute to bipolar spindle assembly. KIF22, also known as Kid, contributes to the polar ejection force, the mechanism through which the chromosome arms are oriented towards the spindle equator and away from the poles. Loss of this plus-end directed motor affects chromosome orientation and segregation (Levesque *et al.*, 2001; Yajima *et al.*, 2003). In

contrast, KIF4A was suggested to function antagonistically, repressing the polar ejection force by preventing microtubule polymerisation and reducing the spindle length (Stumpff *et al.*, 2012).

During anaphase the microtubules connected to the kinetochores shorten, pulling the sister chromatids towards the opposing spindle poles. This movement has been suggested to result from the microtubule depolymerising activity of members of the kinesin-13 subfamily (Gorbsky *et al.*, 1987; Rogers *et al.*, 2004). Concomitantly, the astral microtubules lengthen and the central spindle is assembled. The central spindle requires the bundling of anti-parallel microtubules in a region equidistant from opposing poles, termed the midzone. The minus-ends of the microtubules forming the midzone are no longer anchored at the poles. A number of kinesins localise to the central spindle, including KIF20A, KIF20B, KIF23 and KIF4A. KIF4A is required for the recruitment of protein regulating cytokinesis 1 (PRC1), which is in turn required for bundling of the anti-parallel microtubules of the midzone (Mollinari *et al.*, 2002; Zhu *et al.*, 2005; Janson *et al.*, 2007). In addition, the microtubule-regulating functions of KIF4A control the size of the central spindle (C. K. Hu *et al.*, 2011; Nunes Bastos *et al.*, 2013). KIF20A has been shown to promote the recruitment of the mitotic kinases Aurora B and PLK1 to the central spindle (Gruneberg *et al.*, 2004; Neef *et al.*, 2007). Aurora B forms part of the chromosome passenger complex which has roles in phosphorylating components of the central spindle during anaphase. Homodimeric KIF23 forms a tetramer with a dimer of CYK4 to form the centralspindlin complex, again localising to the central spindle. This localisation is dependent upon both KIF23 and CYK4 and promotes microtubule bundling as well as RhoA activity and the recruitment of factors required for cytokinesis (Mishima *et al.*, 2002; Pavicic-Kaltenbrunner *et al.*, 2007).

The central spindle plays a role in promoting the final stage of mitosis, cytokinesis, through the positioning and assembly of the contractile ring. This structure, formed from myosin motors and actin filaments on the inner surface of the plasma membrane, contracts, eventually forming the midbody and contributing to abscission (D'Avino *et al.*, 2015). A key actor in contractile ring formation and function is the GTPase RhoA, which indirectly stimulates actin polymerisation and myosin contractility (Y. L. Wang, 2005; Jordan *et al.*, 2012). The KIF23-containing centralspindlin complex interacts with a RhoA activator, ECT2, and is required for the localisation of ECT2 at the membrane, activation of RhoA and stimulation of ring contraction (Yuce *et al.*, 2005; Hutterer *et al.*, 2009).

The formation of the contractile ring and the contacts between the central spindle and the cell cortex are mediated, in part, by anillin and citron kinase [CIT; (D'Avino, 2009; Bassi *et al.*, 2011)]. CIT, along with anillin, can interact with actin and myosin and has been implicated in the correct localisation of a number of factors essential for the progression of telophase, including RhoA, KIF14 and PRC1 (Bassi *et al.*, 2013). Along with KIF23, these are all components of the midbody, a structure which forms from

the bundling and constriction of the microtubules of the central spindle by the contractile ring. Despite the high microtubule composition, immunofluorescence staining for tubulin fails to stain the midbody itself, which appears as an extremely dense region on electron microscopy (Byers *et al.*, 1968; D'Avino *et al.*, 2015). Following ingression, the membranes on either side of the midbody constrict and the microtubules are depolymerised. Subsequently, abscission can occur either symmetrically, on both sides of the midbody, or asymmetrically, on one side (Pohl *et al.*, 2009; Elia *et al.*, 2011). Symmetrical abscission results in the release of the midbody, whereas in asymmetrical abscission the midbody is usually inherited by one of the two daughter cells (Crowell *et al.*, 2014). KIF23 has a role in cytokinesis through interactions with CEP55, which in turn has been shown to interact with a component of the ESCRT complex (Fabbro *et al.*, 2005; W. M. Zhao *et al.*, 2006). This complex is required for abscission, likely through remodelling of the cell membrane to promote fission.

III. KIF14

KIF14 is part of the kinesin-3 family and has an unusual protein sequence (Figure 32). Despite being classified as an N-terminal kinesin, the motor domain follows around 350 amino acids after the N-terminal-most domain, which interacts with PRC1 (Gruneberg *et al.*, 2006). *KIF14* also encodes a forkhead homology-associated domain, important for phosphorylation-regulated protein-protein interactions, as well as intramolecular interactions in the case of KIF1A. However, the functional importance of the FHA domain in KIF14 remains to be addressed. *KIF14* also encodes four C-terminal coiled-coil domains, again known to be important for protein-protein interactions, such as the interaction with citron kinase [CIT; (Gruneberg *et al.*, 2006; Watanabe *et al.*, 2013)]. The role of these coiled-coil domains in homodimerisation has not yet been investigated, and whether KIF14 functions as a dimer is currently unknown. Finally, a PDZ motif was identified in KIF14 which was shown to interact with Radil, and binding occurred through the two most C-terminal amino acid residues. KIF14 recruited Radil onto microtubules, which prevented binding to Rap1, a GTPase implicated in cell adhesion and migration (Ahmed *et al.*, 2012).

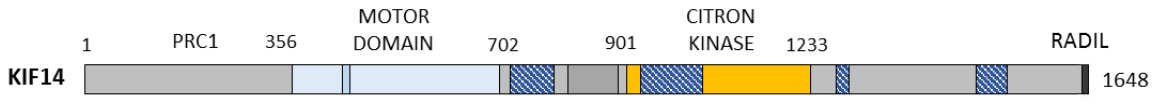

Figure 32. Schematic representation of the protein domains encoded within the* KIF14 *sequence*. Protein regulating cytokinesis 1 (PRC1), motor domain (light blue), citron kinase (CIT; yellow), FHA domain (grey), Radil (dark grey), coiled-coil domains (dark blue stripes).*

Initially the role of KIF14 in the cell cycle was somewhat controversial. *In vivo* analyses using *Drosophila melanogaster* carrying a mutation in *Klp38B*, the orthologue of *KIF14*, revealed an increase in the percentage of polyploid cells, with a significant increase observed in tissues of the nervous system. The authors proposed that the absence of an increase in the number of cycling cells demonstrated that Klp38B functioned in cytokinesis (Ohkura *et al.*, 1997). In contrast, Molina *et al.* (1997) suggested that Klp38B acted as a chromokinesin, colocalising with chromosomes during mitosis and being required for alignment and segregation. An increased number of mitotic cells was observed in mutant flies, and suggested to be due to a failure in metaphase and anaphase progression. These authors suggested that the discrepancies were due to the types of mutants analysed, with hypomorphic mutations in the first publication, and null mutations in the second. Subsequently an siRNA screen performed in *Drosophila melanogaster* S2 cells failed to identify a mitotic role for Klp38B (Goshima *et al.*, 2003).

Analyses of KIF14 in HeLa cells were also initially contradictory. C. Zhu *et al.* (2005) used 3'UTR-targeting siRNA and demonstrated that the knockdown of KIF14 resulted in defects in chromosome congression. Knockdown did not affect bipolar spindle formation and the chromosomes were shown to align at the metaphase plate. However, congression was unstable with chromosomes moving continuously between the spindle equator and poles, subsequently delaying the metaphase-to-anaphase transition. These results were suggested to demonstrate that KIF14 functioned at kinetochores to generate a poleward force. Subsequently, Carleton *et al.* (2006) determined that the expression of KIF14 was regulated throughout the cell cycle, with an increase in G2/M phase. KIF14 was shown to localise in the cytoplasm during interphase, to enter the nucleus at the onset of mitosis and accumulate at the spindle poles and along microtubules during prophase and metaphase. KIF14 was present at the midzone during anaphase and at the midbody during telophase. The authors tested 11 different siRNAs and determined that the resultant phenotypes varied depending on the efficacy of the knockdown. Four of the siRNA sequences, engendering a moderate decrease in protein levels to around 50%, resulted in hypoploidy and apoptosis. In contrast, the remaining sequences, decreasing protein levels by around 80%, were associated with polyploidy. In these cells, mitosis proceeded normally until abscission of the two daughter cells. A midbody was formed, which collapsed following the failure to complete cytokinesis and generated a binucleated cell. The difference between the phenotypes between these siRNA sequences was suggested to reflect a requirement for varying concentrations of KIF14 throughout mitosis.

In agreement with this study, Gruneberg *et al.* (2006) showed that the central spindle localisation of KIF14 was mediated by an interaction with PRC1. This binding domain was mapped to the N-terminal region adjacent to the motor domain (1-356 aa). The localisation of KIF14 to the central spindle and midbody were again lost upon siRNA-mediated knockdown. The localisation of various proteins

implicated in furrow ingression and cytokinesis, including KIF23, KIF4, ECT2 and RhoA, were unaffected by the loss of KIF14. The level of CIT at the central spindle and midbody was reduced and the percentage of binucleated cells was increased. CIT was shown to bind to the C-terminal tail of KIF14 (901-1648 aa), and interestingly, the localisation of KIF14 at the central spindle and midbody was lost upon siRNA-mediated knockdown of CIT, demonstrating a co-dependency (Gruneberg *et al.*, 2006). This interaction was further explored by Watanabe *et al.* (2013), who mapped the CIT-binding region of KIF14 more precisely to a smaller C-terminal region encoding two coiled-coil domains. Knockdown of CIT affected the localisation of RhoA, anillin and septins to the midbody, as well as that of KIF14. KIF14 was proposed to function in the translocation of CIT from the cleavage furrow to the midbody. It was suggested that CIT binding to the C-terminal tail led to the activation of KIF14 in a mechanism reminiscent of KIF17, whereby cargo binding relieves autoinhibition of the motor domain (Hammond *et al.*, 2010). Interestingly, the motor activity of KIF14 was recently shown by Arora *et al.* (2014) to differ from previously characterised kinesins. As opposed to KIF5B, which hydrolyses one molecule of ATP for each step, KIF14 is a highly inefficient motor, with very slow processive movement towards the plus-ends of microtubules and hydrolyses around 7 molecules of ATP per step. In addition, KIF14 was shown to have a high affinity for microtubules and a high basal ATPase activity, which was less sensitive to the addition of microtubules than another processive member of the kinesin-3 family, KIF1A.

Following the description of several mutant fly models of KIF14, a knockout mouse was more recently reported. The mutation in *Kif14* caused exon skipping within the motor domain and various transcripts could be identified at the cDNA level. A robust decrease in the level of protein expression was seen in mutant mice, which had severe microcephaly, cerebellar dysplasia and died by 21 days (Fujikura *et al.*, 2013). Interestingly, rodent models carrying mutations in the partner of KIF14, *Cit*, were also shown to cause severe, isolated microcephaly (Sarkisian *et al.*, 2002).

Recently, mutations in both *KIF14* and *CIT* have been identified in cases of mild to severe microcephaly in humans (Filges *et al.*, 2014; Harding *et al.*, 2016; Li *et al.*, 2016; Shaheen *et al.*, 2016; Moawia *et al.*, 2017; Makrythanasis *et al.*, 2018). Initially, mutations in *KIF14* were shown to lead to a severe lethal syndrome affecting both brain and kidney development (Filges *et al.*, 2014). Affected foetuses presented with corpus callosum agenesis and cerebellar hypoplasia, both of which are commonly identified in ciliopathies. The combination of severe brain and kidney phenotypes was reminiscent of Meckel-Gruber syndrome and so *KIF14* was designated as *MKS12* (MIM: 616258). Subsequently, several cases of isolated and milder microcephaly have been reported, with only a single case additionally presenting with renal defects (Moawia *et al.*, 2017; Makrythanasis *et al.*, 2018). Mutations in *CIT* were also shown to result in microcephaly with varying severity, with several individuals also presenting corpus callosum agenesis and cerebellar hypoplasia (Harding *et al.*, 2016; Li *et al.*, 2016;

Shaheen *et al.*, 2016). Of these cases, two affected individuals from the same family also presented renal aplasia or agenesis, resulting in neonatal lethality (Harding *et al.*, 2016). Unilateral renal agenesis was identified in an additional individual (Shaheen *et al.*, 2016). The genotype-phenotype analysis of these mutations, in both *KIF14* and *CIT*, was not performed. Differences in phenotypic severity, as well as the involvement of multiple organs, are often seen in ciliopathies. The potential role of KIF14 at cilia has not yet been examined, but will be explored herein.

Results

Congenital abnormalities of the kidney and urinary tract (CAKUT) are a heterogeneous group of disorders, ranging in severity and representing the leading cause of end-stage renal disease in children. CAKUT can result from environmental factors, such as obesity and maternal diabetes, as well as genetic factors. To date, more than 50 genes have been associated with CAKUT, many of which encode transcription factors known to be important for renal or urinary tract development. Analysis of familial cases of CAKUT has revealed both autosomal dominant and autosomal recessive modes of inheritance. However, the identification of novel CAKUT genes is complicated by the variable expressivity and incomplete penetrance. Previously, autosomal recessive mutations were identified in *KIF14*, in foetuses presenting with a severe syndrome affecting brain and kidney development. *KIF14* encodes a member of the kinesin superfamily, shown to have an essential role in cytokinesis. The identified phenotypes were reminiscent of the severe ciliopathy Meckel-Gruber syndrome, and so *KIF14* was subsequently designated *MKS12*. Using whole- and targeted-exome sequencing, we identified mutations in individuals from an additional four families. Tissue sections from the brain and kidneys of affected individuals revealed the presence of binucleated cells, demonstrating a failure in cytokinesis. We demonstrated that the identified mutations affected the activity of KIF14 and impaired cytokinesis, highlighting parallels between brain and kidney development. In order to explore whether *KIF14* was a novel ciliopathy gene, we used the zebrafish as an *in vivo* model. Initial observations of mutant zebrafish embryos revealed, in addition to recapitulating the severe syndrome of the affected individuals, a number of ciliopathy-related phenotypes. However, further analysis showed that these effects resulted from an accumulation of cells arrested in mitosis. Taken together, our results confirm that mutations in *KIF14* result in a severe, lethal syndrome affecting both brain and kidney development, and which phenocopies a ciliopathy.

Loss of function mutations in *KIF14* cause severe microcephaly and kidney development defects in humans and zebrafish.

Madeline Louise Reilly[1,2,3], Marijn F. Stokman[4], Virginie Magry[1,2], Cecile Jeanpierre[1,2], Marine Alves[1,2], Mohammadjavad Paydar[5], Jacqueline Hellinga[6], Marion Delous[1,2], Daniel Pouly[1,2], Marion Failler[1,2], Jelena Martinovic[7,8], Laurence Loeuillet[9], Brigitte Leroy[10], Julia Tantau[10], Joelle Roume[11], Cheryl Gregory Evans[12], Xianghong Shan[12], Isabel Filges[13,14,15,], John S. Allingham[6], Benjamin H. Kwok[5], Sophie Saunier[1,2], Rachel H. Giles[15] and Alexandre Benmerah[1,2,#]

[1]INSERM UMR 1163, Laboratory of Hereditary Kidney Diseases, 75015 Paris, France

[2]Paris Descartes – Paris University, Imagine Institute, 75015 Paris, France

[3]Paris Diderot University, Paris, France

[4]Department of Genetics, University Medical Center Utrecht, Utrecht University, Utrecht, Netherlands.

[5]Institute for Research in Immunology and Cancer (IRIC), Département de médecine, Université de Montréal, P.O. Box 6128, Station Centre-Ville, Montréal, QC H3C 3J7, Canada.

[6]Dept. of Biomedical and Molecular Sciences, Queen's University, Kingston, ON K7L 3N6, Canada.

[7]Unit of Fetal Pathology, Antoine Béclère Hospital, AP-HP, Paris, France

[8]INSERM U-788, Génétique/ Neurogénétique, Kremlin-Bicêtre, France

[9]Service d'Histologie-Embryologie-Cytogénétique, Hôpital Necker-Enfants Malades, AP-HP, 75015 Paris, France

[10]Service d'Anatomie et de Cytologie Pathologiques, CHI Poissy, 78100 Saint Germain en Laye, France

[11]Service de Génétique, CHI Poissy, 78100 Saint Germain en Laye, France

[12]Department of Ophtalmology, University of British Columbia, Vancouver, Canada

[13]Medical Genetics, Institute of Medical Genetics and Pathology, University Hospital and University of Basel, Basel, Switzerland

[14]Department of Clinical Research, University Hospital and University of Basel, Basel, Switzerland.

[15]Department of Genetics, University of British Columbia, Vancouver, Canada

[16]Department of Nephrology and Hypertension, University Medical Center Utrecht, Utrecht University, Utrecht, Netherlands.

Abstract

Mutations in *KIF14* have previously been associated with either severe isolated or syndromic microcephaly with renal hypodysplasia (RHD). Syndromic microcephaly-RHD was strongly reminiscent of clinical ciliopathies, relating to defects of the primary cilium, a signalling organelle present on the surface of many quiescent cells. *KIF14* encodes a mitotic kinesin which plays a key role at the midbody during cytokinesis and has not previously been shown to be involved in cilia-related functions. Here, we analysed four families with foetuses presenting with the syndromic form and harbouring bi-allelic variants in *KIF14*. Our functional analyses show that the identified variants severely impact the activity of KIF14 and likely correspond to loss-of-function (LOF) mutations. Analysis in human foetal tissues further revealed the accumulation of KIF14-positive midbody remnants in the lumen of ureteric bud tips indicating a shared function of KIF14 during brain and kidney development. Subsequently, analysis of a *kif14* mutant zebrafish line showed a conserved role for this mitotic kinesin. Interestingly, ciliopathy-associated phenotypes were also present in mutant embryos, supporting a potential direct or indirect role for KIF14 at cilia. However, our *in vitro* and *in vivo* analyses did not provide evidence of a direct role for KIF14 in ciliogenesis and suggested that *kif14* LOF phenocopies ciliopathies through an accumulation of mitotic cells in ciliated tissues. Altogether, our results demonstrate that *KIF14* mutations result in a severe syndrome associating microcephaly and RHD through its conserved function in cytokinesis during kidney and brain development.

Introduction

Congenital Anomalies of the Kidney and Urinary Tract (CAKUT) comprise a broad spectrum of renal and urinary tract malformations of varying severity. Kidney defects can range from unilateral or bilateral renal agenesis (BRA) to renal hypodysplasia (RHD), or can include multicystic kidney dysplasia (MCKD) (Nicolaou *et al.*, 2015). MCKD can also be part of the phenotypic spectrum of foetal forms of ciliopathies (Meckel-Gruber syndrome, MKS), linked to mutations in genes encoding key components of primary cilia (PC) (Braun *et al.*, 2017). RHD results from defects during differentiation of the metanephros, initiated by a reciprocal induction between the ureteric bud (UB) and the metanephric mesenchyme (MM). The UB invades the MM and, in response to signals from the MM, undergoes several rounds of branching, expanding through the proliferation of UB tip epithelial cells to form the collecting ducts. Inductive signals from the UB drive the condensation of MM cells at the tips of the UB branches to form the CAP mesenchyme. These cells undergo a mesenchyme-to-epithelial transition to form the renal vesicle, which will differentiate into several intermediate structures (comma body, then S-shaped body) to finally form the nephron, the functional unit of the kidney. The proximal region of the S-shaped body will differentiate to give rise to the blood-filtering glomerulus, while the distal region will connect to the collecting ducts. Nephrogenesis takes place in the cortex of the developing kidneys and ends before birth (35-36 weeks) in humans (McMahon, 2016; Seely, 2017).

The mouse has been a widely used model to decipher the mechanisms controlling nephrogenesis, as many of the processes involved in metanephric kidney development are well conserved (McMahon, 2016; Seely, 2017). However, zebrafish have recently become a powerful alternative model for both kidney development and disease modelling (Drummond *et al.*, 2016; Poureetezadi *et al.*, 2016). The pronephros of zebrafish larvae is functional and consists of two nephrons with a fused glomerulus. Early development of the zebrafish pronephros requires the condensation of progenitors into two epithelial tubes, which retain a pattern of segmentation similar to that of mammalian nephrons. A functional kidney is formed by 48 hours post-fertilisation (hpf) through the frontward migration of cells towards the glomerulus, along with spatially and temporally controlled waves of mitosis (Drummond *et al.*, 2016; Poureetezadi *et al.*, 2016).

To date, mutations resulting in RHD in humans have been identified in more than 50 genes with a role in kidney development, revealing a great genetic heterogeneity (Nicolaou *et al.*, 2015; Uy *et al.*, 2016). Most of these genes encode transcription factors (PAX2, SIX1, EYA1, HNF1B) and actors in key signalling pathways (RET-GDNF, FGF, NOTCH). Few of these genes were associated with BRA (Barak *et al.*, 2012; Humbert *et al.*, 2014; De Tomasi *et al.*, 2017). Interestingly, biallelic loss-of-function mutations in *KIF14*, encoding a mitotic kinesin required for cytokinesis, were recently reported in foetuses presenting with

BRA or RHD associated with complex brain malformations including very severe microcephaly (Filges *et al.*, 2014; Heidet *et al.*, 2017).

Microcephaly is a condition in which foetuses or infants present with a very small head and brain, and is part of a family of highly heterogeneous disorders grouped under the term of malformations of cortical development (MCD). The initial phase of brain development depends on an intense phase of progenitor proliferation within the ventricular zone (VZ). Symmetrical mitosis of these progenitor cells occurs at the apical face of the neuroepithelium, lining the lumen of the neural tube. Following this initial amplification phase, cells begin to divide asymmetrically and waves of committed, post-mitotic cells undergo an active phase of migration (Paridaen *et al.*, 2014). Defects in any of these complex events lead to MCD or microcephaly. Microcephaly, like CAKUT, is genetically heterogeneous, with mutations identified in genes regulating signalling pathways, microtubule dynamics and mitotic spindle orientation, including several kinesin family members (Romero *et al.*, 2018).

Kinesins are molecular motors known to bind their respective cargos through their C-terminal domain and microtubules through their motor domain. Following these interactions, the kinesin then moves along microtubules (MTs), usually in a plus-end directed manner, through the hydrolysis of ATP (Verhey *et al.*, 2011). KIF14 is a member of the Kinesin 3 family, which is highly conserved during evolution and possesses a slow processive activity (Arora *et al.*, 2014). It was identified as a key actor in cytokinesis (Carleton *et al.*, 2006; Gruneberg *et al.*, 2006; D'Avino *et al.*, 2015), through its interaction with PRC1 and citron kinase (CIT) (Gruneberg *et al.*, 2006; Bassi *et al.*, 2013). KIF14 accumulates at the spindle midzone and the midbody, where it is recruited by CIT (Gruneberg *et al.*, 2006). KIF14 also acts reciprocally to ensure the correct distribution of CIT within this latter structure (Bassi *et al.*, 2013; Watanabe *et al.*, 2013). Although initially considered an artefact, the formation of the midbody, or Flemming body, is known to be crucial for the completion of mitosis (Dionne *et al.*, 2015). Proteins involved in cleavage furrow ingression accumulate between the two parts of the intercellular bridges and then recruit components of the ESCRT machinery to ensure scission of the plasma membrane at one or both sides of this central structure which is then either inherited by one daughter cell or "secreted" into the extracellular milieu (Dionne *et al.*, 2015). Unsurprisingly, depletion of KIF14 in HeLa cells therefore leads to cytokinesis defects and binucleated cells (Carleton *et al.*, 2006; Gruneberg *et al.*, 2006). Besides its role during cytokinesis, KIF14 regulates migration in cancer cells via C-terminal interactions with RADIL (Ahmed *et al.*, 2012).

In vivo, loss of KIF14 in *Drosophila* leads to cytokinesis and developmental defects (Alphey *et al.*, 1997; Molina *et al.*, 1997; Ohkura *et al.*, 1997; Ruden *et al.*, 1997) and in mice to microcephaly and growth retardation (Fujikura *et al.*, 2013). In humans, in addition to the syndromic cases including severe

microcephaly and RHD (Filges *et al.*, 2014; Heidet *et al.*, 2017), mutations in *KIF14* were recently identified in isolated, mild- to severe- microcephaly (Moawia *et al.*, 2017; Makrythanasis *et al.*, 2018), with a phenotypic spectrum similar to the one observed in cases with mutations in *CIT* (Basit *et al*., 2016; Harding *et al*., 2016; Li *et al*., 2016; Shaheen *et al*., 2016). In these reports, microcephaly was not associated with major kidney malformations in any of the individuals harbouring mutations in either *KIF14* or *CIT*. In addition, as the clinical features of syndromic cases showed partial overlap with the phenotypic spectrum of MKS (intrauterine growth restriction, cystic kidneys and brain developmental defects, including cerebellar hypoplasia and vermis agenesis), *KIF14* was then subsequently suggested as *MKS12* (OMIM 616258). All proteins encoded by MKS genes identified thus far are present at the primary cilium and so KIF14 was proposed to have a ciliary function.

The main objective of this study was to better characterise the phenotypic spectrum associated with mutations in *KIF14* and to better understand its role during kidney development. We describe novel biallelic *KIF14* mutations in foetuses presenting with RHD and MCPH. We analyse the functional effects of the mutations identified in four families and their consequences on cytokinesis and the potential role of KIF14 in ciliogenesis. We also use the zebrafish model to investigate the consequences of the loss of KIF14 *in vivo*, demonstrating a conserved function during both kidney and brain development. Finally, we provide direct evidence for similarities and distinctions between mitotic events occurring during proliferation in both brain and kidney development.

Results

I. Identification of mutations in *KIF14*

In addition to the initial family that we described several years ago (Filges *et al.*, 2014), we identified a further four families (Families 1 to 4) with foetuses presenting with highly reminiscent phenotypes, MCPH and cystic RHD or BRA (Table S1), linked to biallelic mutations in *KIF14*. Mutations identified in family 1 and 2 have been reported recently (Heidet *et al.*, 2017), while those in family 3 and 4 have never been described.

Whole- or targeted-exome sequencing approaches enabled the identification of biallelic pathogenic variants in *KIF14* in all these families (Fig. 1A,B; Table S1). The affected foetus in family 1 harboured a homozygous out-of-frame deletion of exons 23, 24 and 25 (c.[3567-?_4072+?del]) leading to a frameshift (p.Arg1189Argfs*9). Compound heterozygous variations associating a predicted damaging missense variation in the motor domain (c.1090C>T [p.Arg364Cys] or c.1367C>T [p.Thr456Met]) with a nonsense mutation predicted to lead to a loss of the C-terminal region of the protein (c.3910C>T [p.Gln1304*] or c.4138C>T [p.Gln1380*]) were identified in family 2 and 3 respectively. Finally, the affected foetus in family 4 harboured a homozygous nonsense mutation predicted to lead to an early truncation in the motor domain (c.1792C>T [p.Arg598*]). All variations were absent from in-house and public databases (gnomAD) and missense variants were predicted damaging by Polyphen and Sift (0.787/0.01 for Thr456Met; (Heidet *et al.*, 2017)). Segregation of the identified mutations with the developmental defects was confirmed for all the families by Sanger sequencing. The parents were heterozygous, while affected foetuses, where DNA was available, harboured the corresponding biallelic variations in *KIF14* (Table S1, Fig. S1; (Heidet *et al.*, 2017)).

Despite the heterogeneity of the variations identified in these families, all the affected foetuses presented with strikingly similar severe brain and kidney phenotypes (Table S1). All affected foetuses presented with microcephaly with a flattened forehead (Figs. 1C-E, S1). Autopsy revealed a strong delay in the development of the telencephalon leading to agenesis of the occipital lobes and corpus callosum. Additionally, all affected foetuses presented a hypoplasia of the cerebellum with foliation delay (Figs. 1C-E, S1; Table S1). The kidney phenotype was equally severe, with either BRA (3/11 cases), severe non cystic (2/11) or cystic RHD (6/11). Histochemistry of the cystic kidneys revealed, in addition to large cortical cysts, a lack of nephrogenic zone and absence of corticomedullary differentiation (Fig. 1C-E). Few glomeruli could be observed, some were cystic (in families 1, 2 and 4), and tubules were rare (Figs. 1C,E, S1 and S2) and surrounded by undifferentiated mesenchymal tissue. Immunohistochemistry confirmed the lack of nephrogenic zone (PAX2/SIX2 stainings) in foetuses from families 1 and 3 and the presence of few remaining glomeruli in foetus 1 from family 1 (Fig. S2A-B).

Altogether these results clearly ascertain that biallelic mutations in *KIF14* lead to a syndrome characterised by severe developmental defects in both brain and kidney leading to arhinencephaly/atelencephaly and RHD.

II. Impact of mutations on KIF14 activity

Kinesins bind MTs through their motor domain, which in many cases is negatively regulated through intramolecular interactions with the C-terminal cargo-binding domain (Verhey *et al.*, 2011). In the case of KIF14, this negative regulation of the motor domain is released upon interaction with CIT, which binds to the C-terminal region of KIF14 (aa 901-1233) through its N-terminal coiled-coil domain (CCf domain; (Watanabe *et al.*, 2013)). As the mutations identified affect the two key domains of KIF14, we predicted that they would have dramatic functional effects.

We first tested the consequences of the missense and truncation mutations on the steady state localisation of KIF14. Indeed, depending on its activation state, KIF14 could either be found diffusely distributed in the cytoplasm or on microtubules when transiently expressed in non-mitotic cells (Watanabe *et al.*, 2013). Expression of a GFP-fusion encoding wild-type (WT) KIF14 revealed a diffuse cytoplasmic localisation (Fig. 2A) which was unaffected by the missense variations, T456M and R364C (Fig. 2B,C). In contrast, the C-terminal truncations (Q1380*, Q1304* and R1189*) all affected KIF14 localisation and impacted upon cell morphology (Fig. 2D-F). The Q1380* mutant strongly accumulated at the tips of transfected cells, which became highly elongated, and where it colocalised with acetylated α-tubulin (AcTub; Fig. 2D). Both Q1304* (Fig. 2E) and R1189* (Fig. 2F) were present on MTs, colocalised with AcTub, and could occasionally be observed accumulated at the extremities of microtubules at the cell periphery. These observations suggest that the C-terminal truncations lead to constitutively active forms of KIF14 which are capable of binding MTs. The procession of these active forms, particularly Q1380*, towards the plus-end of MTs appears to cause distension of the cell into protrusions, as was previously characterised for other Kinesin family members (Verhey *et al.*, 2011).

As CIT is one of the main partners of KIF14 and regulates its activity (Watanabe *et al.*, 2013), we next investigated the impact of the identified mutations on this interaction. We performed co-immunoprecipitation assays from lysates of cells co-expressing WT or variant forms of KIF14 and the KIF14-binding domain of CIT (CCf; Fig. 2G). As expected, the CIT CCf domain was efficiently co-immunoprecipitated with WT KIF14 but not with the N-terminal PRC1 binding domain (1-356). This interaction was unaffected by the missense mutations in the motor domain (R364C, T456M) and by the two more C-terminal truncation mutations (Q1304*, Q1380*), which are localised after the previously mapped CIT binding site (aa 901-1233; Fig. 2H). Surprisingly, the most N-terminal truncation variation, R1189*, also retained the interaction (Fig. 2G) despite being expected to result in the partial

truncation of the CIT binding domain (Fig. 2H). This result indicates that the CIT interaction domain of KIF14 in fact lies between amino acids 901 and 1189 (Fig. 2H).

As the nonsense mutation in the motor domain (family 4) was very similar to that previously described (Filges *et al.*, 2014) and those of the mouse model (Fujikura *et al.*, 2013), their negative impact was not investigated here. In contrast, the functional consequence of the missense variations identified in families 2 and 3 remained to be demonstrated. Site-directed mutagenesis has identified amino acids crucial to the activity of the motor domain, usually relating to ATP-binding and hydrolysis. Arg364 (Fig. 3A), which is replaced by Cys in family 2, is analogous to Arg14 in conventional Kinesin, which, when mutated, was shown to result in a severe reduction of MT-gliding velocity (Kapoor *et al.*, 1999). The p.Arg364Cys variation is therefore expected to result in loss-of-function of the KIF14 motor domain. Based on the resolved structure of the murine Kif14 motor domain (Arora *et al.*, 2014), the Thr456 residue (Thr491 in mouse), replaced by Met in family 3, is part of the ATP-binding pocket of KIF14 where it faces Arg364 (Fig. 3A). This variation was therefore also expected to severely impact the function of the motor domain, which was investigated using a MT sedimentation assay. As previously demonstrated for the murine Kif14 motor domain (Arora *et al.*, 2014), the human KIF14 motor domain efficiently co-pelleted with MTs (Fig. 3B). The introduction of the p.Thr456Met variation (T456M) severely impaired MT binding, and the mutant motor domain remained within the supernatant (Fig. 3B). In addition, measurement of the ATPase activity of the motor domains revealed that ATP hydrolysis remained unchanged after the addition of MTs to the T456M mutant (Fig. 3C). Similar results were obtained with the murine motor domain, where the equivalent human variant was introduced and compared to the WT (T491M; Fig. S3).

As indicated above, the CIT interaction activates KIF14 and allows binding to MTs. In contrast to WT KIF14 (Fig. 3D), R364C and T456M variants failed to translocate onto MTs when co-expressed with the CCf domain of CIT (Fig. 3E,F). As the missense variants retain the ability to bind CIT (Fig. 2), these data show that both variations severely impair the ability of the motor domain to bind MTs, thus rendering these variant kinesins non-functional.

In conclusion, all identified variants could thus be considered as strongly damaging mutations.

III. KIF14 mutations lead to cytokinesis defects

Previous *in vitro* work has focused on the impact of a transient loss of KIF14 in HeLa cells (Carleton *et al.*, 2006; Gruneberg *et al.*, 2006). In order to better characterise the effect *KIF14*-loss in stable conditions in kidney cells, we performed a knockout of the gene in murine inner medullary collecting duct cells (mIMCD3). We used CRISPR/Cas9 (nickase) with guides targeting exon 5 encoding part of the motor domain (Fig. S4A). Clones were isolated and sequenced to identify homozygous mutational

events. Two clones (KO1 and KO2), both with partial deletions of the 3' region of exon 5 and 5' region of intron 5-6 (Fig. S4B), were selected for further analysis. Sequencing of RT-PCR products revealed that the exon/intron deletions resulted in exon skipping in both clones, which could lead to an in-frame deletion in KO1 (exon5+6) and/or to a frameshift and early stop codon in exon 6 in both KO1 and KO2 (Fig. S4C-E). These events likely result in non-functional proteins since they generate short truncated forms and/or proteins lacking a stretch of 28 aa within the motor domain (Fig. S4F). Two clones in which no mutational events in *Kif14* could be identified (WT1 and WT2) and which expressed similar levels of Kif14 to the parental cell line (Fig. S4F) were maintained as controls.

While Kif14 (green) was detected at the midbody in parental IMCD3 cells (not shown) and control clones, it was absent from the intercellular bridges (AcTub staining, red) of KO clones (Fig. 4A), which were elongated compared to those of controls (Fig. 4B). In addition, CIT localisation at the midbody was affected in KO clones, showing either a diffuse distribution along bridges or being present as two rings instead of a unique one (Fig. 4C,D), as previously described (Watanabe *et al.*, 2013). Consequently, the loss of Kif14 in KO clones led to an increase in the proportion of binucleated cells (Fig. 4E,F). Interestingly, similar defects were observed in fibroblasts obtained from the affected foetus 21 from family 4 (Fig. 4G,H) with longer intercellular bridges and increased proportion of binucleated cells compared to control (7.8% (29/372) vs. 0% (0/215), respectively).

Human kidney development is severely impaired in cases where KIF14 function is lost, with affected foetuses presenting with either BRA or cystic RHD (Figs. 1 and S1). To explore the role of this mitotic kinesin in development, we analysed the protein localisation in tissue sections from normal human foetal kidneys. Sections were stained for both KIF14 and PAX2, a marker of epithelial and mesenchymal components of the developing kidney (McMahon, 2016; Seely, 2017). Strikingly, the lumen of some PAX2-positive epithelial structures were filled with KIF14-positive dots which, when observed at a higher magnification, appeared as rings (Fig. 5A), indicative of the presence of KIF14-positive midbodies in UB tips. In agreement with this observation, CIT showed a similar ring-shaped pattern in the lumen of PAX2-positive structures surrounded by SIX2-positive cells (Fig. 5B), a marker of the cap mesenchyme. Finally, we observed a colocalisation of both KIF14 and CIT in ring-shaped structures within clearly identifiable PAX2-positive UB branch tips (Fig. 5C).

These results were suggestive of a luminal accumulation of midbodies or midbody remnants following mitosis. Interestingly, mitosis of the epithelial cells of the UB tips was shown to occur in the lumen, with the daughter cell bodies subsequently reinserting into the epithelium (Packard *et al.*, 2013). In this context, it was expected that the cytokinesis failure induced upon loss of KIF14 would generate binucleated cells, which should then be found in the lumen or epithelium layer. Careful analysis of

kidney sections from affected foetuses revealed the presence of binucleated cells protruding from the surface of the epithelium along the lumen of large cysts (Fig. 5D,E) or inside the lumen of smaller cystic structures (Fig. 5F,G). In contrast to controls (H-K), numerous binucleated cells were also found in the cortex of the older affected foetus (pyramidal cells, Fig. 5L,M) and to a lesser extent, in Purkinje cells in the cerebellum (Fig. 5N,O).

In conclusion, KIF14 plays a crucial function in cytokinesis during kidney and brain development.

IV. Ciliopathy-related phenotypes in *kif14*$^{-/-}$ zebrafish embryos

A previous *in vivo* study in the mouse demonstrated that the loss of Kif14 resulted in microcephaly and growth restriction but failed to replicate the kidney phenotype observed in humans (Fujikura *et al.*, 2013). We therefore chose to use the zebrafish as an alternative *in vivo* model in order to explore a potential conserved kidney specific role for KIF14.

A mutant line was acquired from the Zebrafish Mutation Project [Sanger Institute; sa24165 (Kettleborough *et al.*, 2013)], in which a single nucleotide substitution resulted in a nonsense mutation and an early truncation just after the motor domain (c.1870C>T[p.Gln624*]; Fig. 6A), a mutation similar to those identified in affected foetuses. The presence of the mutation was confirmed by Sanger sequencing (Fig. 6B). Macroscopically visible phenotypes were observed in ¼ of the embryos from crosses of heterozygous (Htz) individuals and Sanger sequencing confirmed that the affected larvae were homozygous for the mutation, hereafter *kif14*$^{-/-}$. These phenotypes were 100% penetrant in *kif14*$^{-/-}$ embryos, while heterozygous embryos were indistinguishable from WT siblings. *kif14*$^{-/-}$ embryos were not viable and died by 5 days post fertilisation (dpf). By 48 hours post fertilisation (hpf), they demonstrated microcephaly, eye defects, body curvature, which could be dorsal, ventral or lateral, and cardiac oedema (Fig. 6C,D). Similar phenotypes were also observed in *kif14* morphants (Fig. S5).

Data from zebrafish models of brain development have demonstrated that morphogenesis occurs first through the establishment of the forebrain, midbrain and hindbrain ventricles between 17 and 21 hpf, followed by expansion of the ventricles between 21 and 36 hpf (Lowery *et al.*, 2005). Microcephaly in mutant *kif14*$^{-/-}$ embryos was evident around 22 hpf, with an absence of clear ventricular definition on both lateral and dorsal views (Fig. 6C). As shown in many microcephaly models *kif14*$^{-/-}$ mutant embryos also present microphthalmia (Fig. 6C; Fig. S6A,B), with occasional coloboma (Fig. 6C; Fig. S6A,B, blue asterisk). In addition, the *kif14*$^{-/-}$ embryos presented with cardiac oedema, often an indication of pronephric cysts (Drummond *et al.*, 2016; Marra *et al.*, 2016). In order to examine the potential kidney defects, we used the *Tg(wt1b:GFP)* transgenic line expressing GFP under the control of *wt1b* promoter (Perner *et al.*, 2007). GFP expression in the proximal pronephros allowed us to confirm the presence of glomerular cysts in *73%* of *kif14*$^{-/-}$ mutant embryos at 48hpf (n=47, 4 separate clutches; Fig. 6E).

Defects in pronephric development can be coupled to a failure in patterning. *In situ* hybridisation using *slc20a1a*, a marker of the proximal convoluted tubule, revealed a deficiency in cell migration and subsequent absence of convolutions (Fig. S6C). Altogether, these data show that the loss of *kif14* in zebrafish recapitulates both the brain and kidney developmental phenotypes observed in the affected foetuses.

V. Phenocopy of ciliopathy in *kif14*$^{-/-}$ embryos

Interestingly, pronephric cysts and body curvature, along with otolith defects, are among the phenotypes widely seen in zebrafish models of known ciliopathy genes (Drummond *et al.*, 2016; Marra *et al.*, 2016). Otoliths are structures present within the lumen of the otic vesicle and composed of biominerals. Their formation at the tips of tether cilia of sensory neurons has been shown to rely, at least partially, on the presence of motile cilia at the luminal surface of the neuroepithelium (Lundberg *et al.*, 2015). We observed a variety of otolith defects at 72hpf in *kif14*$^{-/-}$ embryos (Fig. 7A,B). Most otoliths were smaller, with many incorrectly positioned within the vesicle (misplaced). Occasionally, otoliths were fused, or present as a single structure, whilst extranumerary otoliths were rare. To directly explore whether these defects were related to cilia dysfunction within the otic vesicle, we used a transgenic (Tg) line in which the ciliary membrane marker Arl13b is fused to GFP and ubiquitously expressed (Tg(*act2b:Arl13b-GFP*); (Borovina *et al.*, 2010)). Confocal imaging of WT larvae (24hpf) showed that the Arl13b fusion stained cilia present on most neuroepithelial cells lining the lumen of the otic vesicle. Analysis in mutant embryos revealed a strong decrease in the number of cilia compared to WT siblings (Fig. 7C). Taken together with the other phenotypes, these observations indicated that the loss of kif14 was impacting ciliogenesis.

To elucidate whether KIF14 plays a direct role in ciliogenesis, we initially tested two widely used *in vitro* models, IMCD3 and RPE1 cells, in which primary cilia formation can be easily monitored. Loss of *KIF14* by either transient siRNA-mediated knockdown in RPE1 cells (Fig. S7A-D) or stable KO in IMCD3 (Fig. S7E-G) did not have a significant effect on the percentage of ciliated cells and cilia length compared to controls. We subsequently investigated the impact of the loss of *kif14* on cilia *in vivo* using the *Tg(cldnB:lynGFP)* zebrafish line, in which GFP is expressed in the distal pronephros. Cilia in the cloaca are often affected in ciliopathy models (Burckle *et al.*, 2011; Bizet *et al.*, 2015), however, neither the length of cilia nor the percentage of ciliated cells were affected in *kif14*$^{-/-}$ embryos (Fig. S7H-J). Together these results indicate that KIF14 does not have a general role in ciliogenesis.

Cilia are present on the surface of quiescent cells and resorbed when cells enter mitosis. Mitotic cells are therefore not ciliated (Basten *et al.*, 2013). Interestingly, AcTub stainings in the distal pronephros revealed the presence of numerous cells with mitotic spindle and condensed chromosomes (Fig. S7H,

arrows). As kif14 is a mitotic kinesin, we reasoned that defects in ciliogenesis in *kif14*$^{-/-}$ embryos could be due to differences in the cell cycle, leading to an accumulation of non-ciliated mitotic cells. Immunofluorescence staining for phospho-histone H3 (PH3), a marker of cells in G2/M, revealed a significant increase in the number of mitotic cells in *kif14*$^{-/-}$ embryos, notably in the brain and along the spine (Fig. 7D), as has been shown in many microcephaly models (Novorol *et al.*, 2013). In order to test the effect of this increased mitosis on ciliogenesis, we again used the *Tg(cldnB:lynGFP)* line in which the neuroepithelial cells lining the otic vesicle express GFP (Haas *et al.*, 2006). Confocal imaging of 24hpf embryos revealed a drastic increase in the number of mitotic cells in *kif14*$^{-/-}$ mutant embryos compared to siblings (Fig. 7E,F), which mirrored ciliogenesis in the organ (Fig. 7C). We also analysed mitosis in the pronephros. As expected (Vasilyev *et al.*, 2012), very few PH3-positive cells could be observed in proximal (*Tg(wt1b:GFP)*; Fig. 7G,H) and distal (*Tg(cldnB:lynGFP)*; Fig. S8) tubules at 48hpf, in both WT and kif14$^{+/-}$ embryos. However, the number of mitotic cells was drastically increased in *kif14*$^{-/-}$ embryos in both regions (Fig. 7G,H; Fig. S8). Taken together, these data show that the loss of *kif14* in zebrafish causes ciliopathy-like phenotypes, including in the otic vesicle and pronephros, which are likely linked to an accumulation of mitotic, and therefore non-ciliated cells in those tissues.

VI. Mitotic spindle defects in *kif14*$^{-/-}$ embryos

The accumulation of mitotic PH3+ cells in most tissues of *kif14*$^{-/-}$ mutant embryos was unexpected given the established function of KIF14 in cytokinesis in mammalian cells [(Carleton *et al.*, 2006; Gruneberg *et al.*, 2006) and Fig.4]. Indeed, expected binucleated cells are not positive for PH3 until they re-enter mitosis. The increased number of PH3+ cells could then be due to either an increased proliferation rate, or a block/delay in mitosis, as shown in other zebrafish microcephaly models (Pfaff *et al.*, 2007; H. T. Kim *et al.*, 2011). By staining embryos with both AcTub and α-tubulin we could visualise the mitotic spindles, and therefore analyse the different stages of mitosis of the PH3+ neuroepithelium cells of the otic vesicle in Tg(*cldnB:lynGFP*) embryos. Confocal imaging revealed that PH3+ cells in both WT/Htz and *kif14*$^{-/-}$ fish were either in the G2 phase (absence of assembled spindle) or in metaphase (assembled bipolar spindles with condensed chromosomes; Fig. 8A,B). However, in *kif14*$^{-/-}$ embryos we observed a lower proportion of PH3+ cells without an assembled spindle and a drastic increase in the number of PH3+ cells with condensed chromosomes and aberrant spindles. Most of these cells had monopolar spindles (Fig. 8B,C), although multipolar spindles could occasionally be observed (Fig. 8B,C). In addition to the otic vesicle, PH3+ cells with monopolar spindles were observed in many other tissues, including the spine, posterior lateral line and retina (see Fig. S9 for examples).

The observation of a higher proportion of cells with an assembled mitotic spindle indicates that the increase in PH3+ cells is linked to either a delay or block in mitosis. This also suggests that kif14 likely plays a role at an early stage of mitosis in zebrafish, possibly in the organisation of the mitotic spindle.

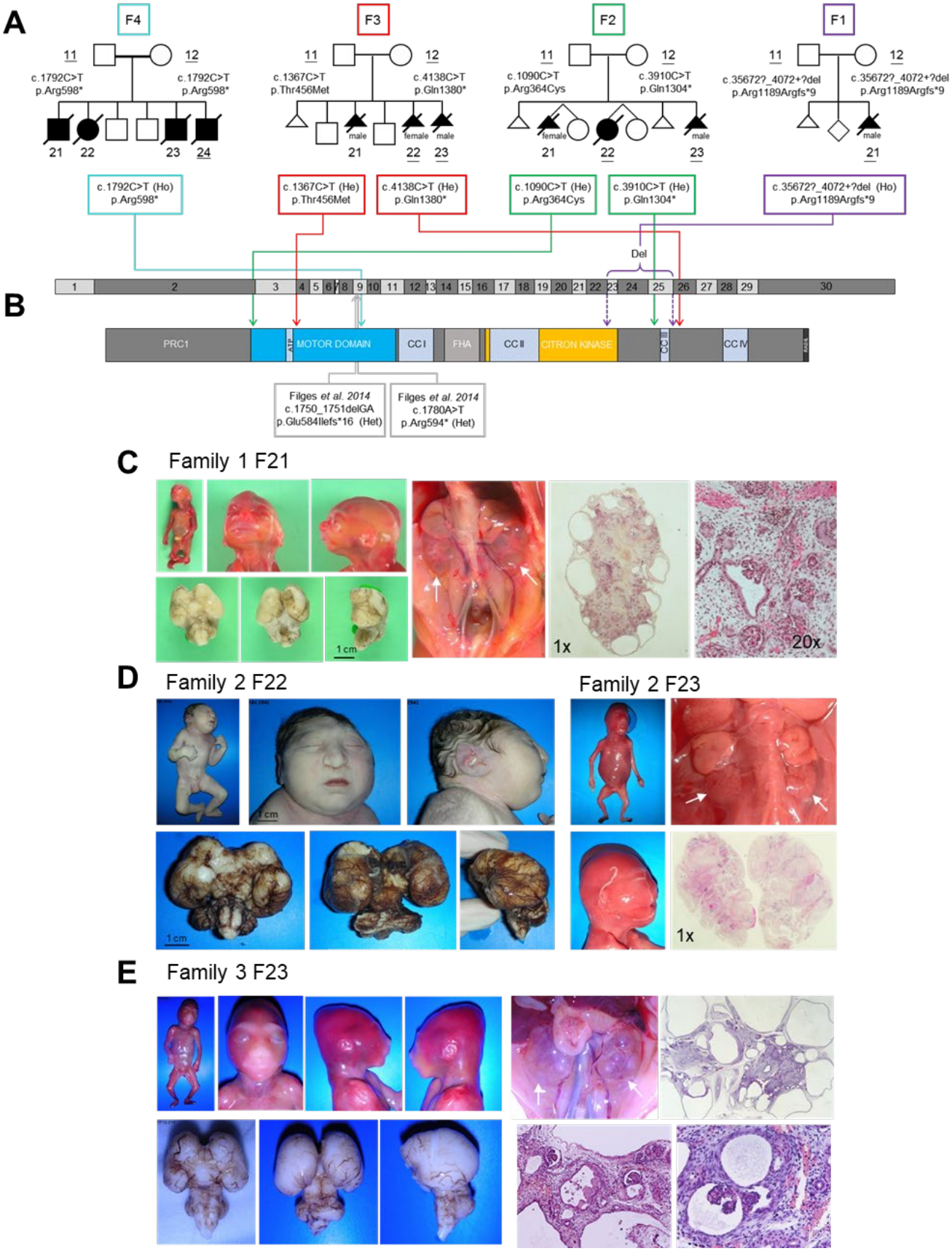
A
F4
F3
F2
F1
11
12
c.1792C>T
p.Arg598*
c.1792C>T
p.Arg598*
c.1367C>T
p.Thr456Met
c.4138C>T
p.Gln1380*
c.1090C>T
p.Arg364Cys
c.3910C>T
p.Gln1304*
c.35672?_4072+?del
p.Arg1189Argfs*9
c.35672?_4072+?del
p.Arg1189Argfs*9
21
22
23
24
male
female
c.1792C>T (Ho)
p.Arg598*
c.1367C>T (He)
p.Thr456Met
c.4138C>T (He)
p.Gln1380*
c.1090C>T (He)
p.Arg364Cys
c.3910C>T (He)
p.Gln1304*
c.35672?_4072+?del (Ho)
p.Arg1189Argfs*9
Del
B
PRC1
ATP
MOTOR DOMAIN
CC I
FHA
CC II
CITRON KINASE
CC III
CC IV
Filges et al. 2014
c.1750_1751delGA
p.Glu584Ilefs*16 (Het)
Filges et al. 2014
c.1780A>T
p.Arg594* (Het)
C
Family 1 F21
1 cm
1x
20x
D
Family 2 F22
Family 2 F23
1 cm
1x
E
Family 3 F23

Figure 1. Identification of mutations in* KIF14 *in a lethal, foetal syndrome associating severe microcephaly with bilateral renal agenesis, or renal hypodysplasia. *(A) Pedigrees of the identified families (F1-4) with homozygous or compound heterozygous mutations in* KIF14*. (B) Schematic representation of* KIF14 *cDNA (exons) and protein showing the position of the identified mutations. The PRC1 and Citron Kinase (CIT) binding domains are shown, along with the motor, Forkhead Associated (FHA) and the four coiled-coil (CC I-IV) domains. The compound heterozygous mutations of the previously identified family are also shown (Filges et al., 2014). Abbreviations: heterozygous (he), homozygous (ho). (C) Foetus 21 of family 1 (18 weeks gestation), pictures of brains and kidneys with representative histological sections from one kidney. (D) Foetus 22 (37 weeks gestation), and foetus 23 (18 weeks) from family 2, pictures of brains and kidneys along with histology of F23 kidneys. (E) Foetus F23 of family 3 (18 weeks gestation), pictures of brain and kidneys along with kidney histology.*

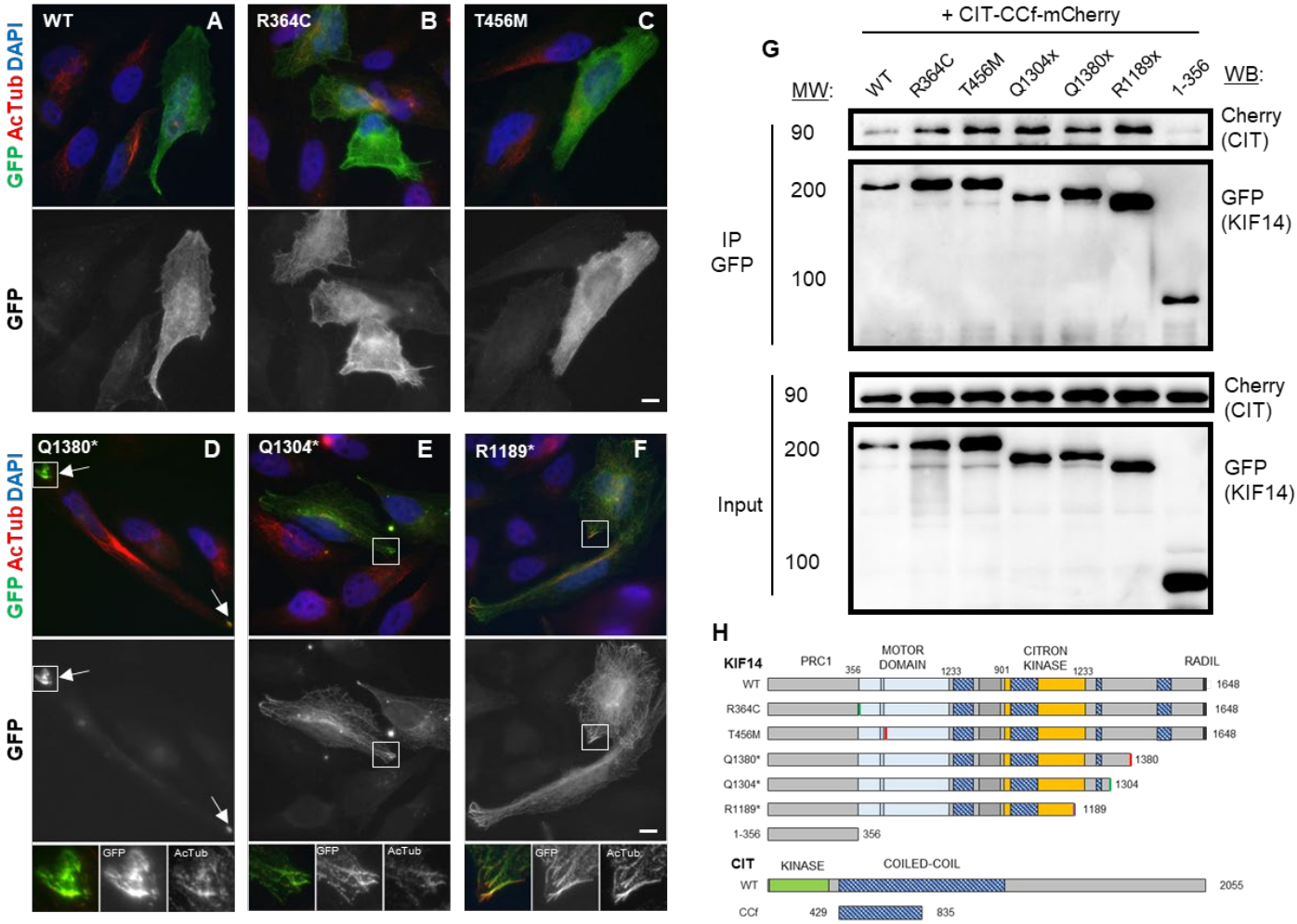

Figure 2. C-terminally truncated variant KIF14 proteins are constitutively targeted to microtubules without impairing CIT binding. *(A-F) Immunofluorescence of HeLa cells transfected with a GFP-fusion encoding wild-type or mutant KIF14 GFP fusions. Microtubules were stained using an antibody against acetylated-α-tubulin (AcTub; red), and nuclei using Hoechst (blue). Merge colour pictures (top panels) and black and white pictures corresponding to GFP fusions (KIF14; bottom panels) are shown. Scale bars: 5 µm. (G) Lysates from HEK293 cells co-transfected with plasmids encoding GFP-fusions of WT or mutant KIF14 and with an mCherry-fusion of the KIF14 binding domain of CIT (CCf) were immunoprecipitated using an anti-GFP antibody. Lysates and immunoprecipitated proteins were analysed through Western blotting, using antibodies against GFP (KIF14) or mCherry (CIT-CCf). (H) Schematic representation of the constructs used in immunofluorescence and co-immunoprecipitation experiments.*

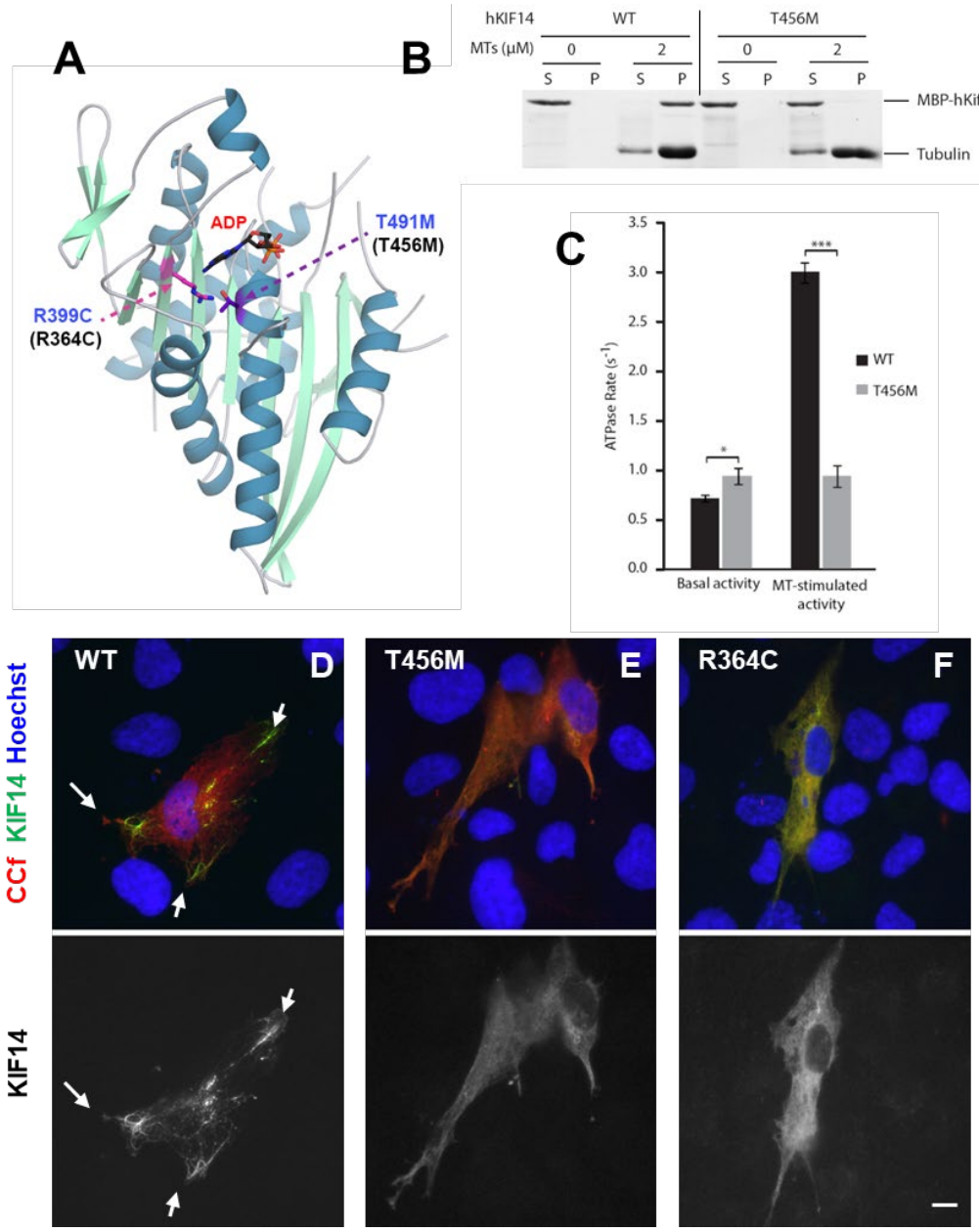

Figure 3. Identified motor domain mutations affect KIF14 activity and impair microtubule binding. *(A) Structure of mouse KIF14-MD is shown (PDB ID:* ***4OZQ ; (Arora et al., 2014)*** *with the mutated residues labelled (mouse residues in blue and the corresponding human residues in black). This image was produced in PyMol (The PyMOL Molecular Graphics System, Version 2.0 Schrödinger, LLC.) (B) The microtubule-binding activity of human KIF14 motor construct (MBP-hKIF14) was assessed in an ultracentrifugation-based co-sedimentation assay. A representative coomassie blue-stained gel, from four independent experiments, is shown. KIF14 motor constructs and tubulin are indicated. S, supernatant; P, pellet; MT, microtubules. (C) Basal and MT-stimulated ATPase activities of a KIF14 motor construct (MBP-hKIF14) were shown. Data from 4 independent experiments. Error bars, S.D.. Statistics: * p ≤ 0.05 ; *** p ≤ 0.001; by Student's T-test. (D-F) Immunofluorescence of RPE1 cells co-transfected with plasmids encoding GFP-fusion (D) of WT or (E,F) mutant KIF14 [(E) T456M or (F) R364C], along with an mCherry-fusion of the KIF14 binding domain of CIT (CCf, red). Nuclei were stained using Hoechst (blue). Scale bars: 5 µm.*

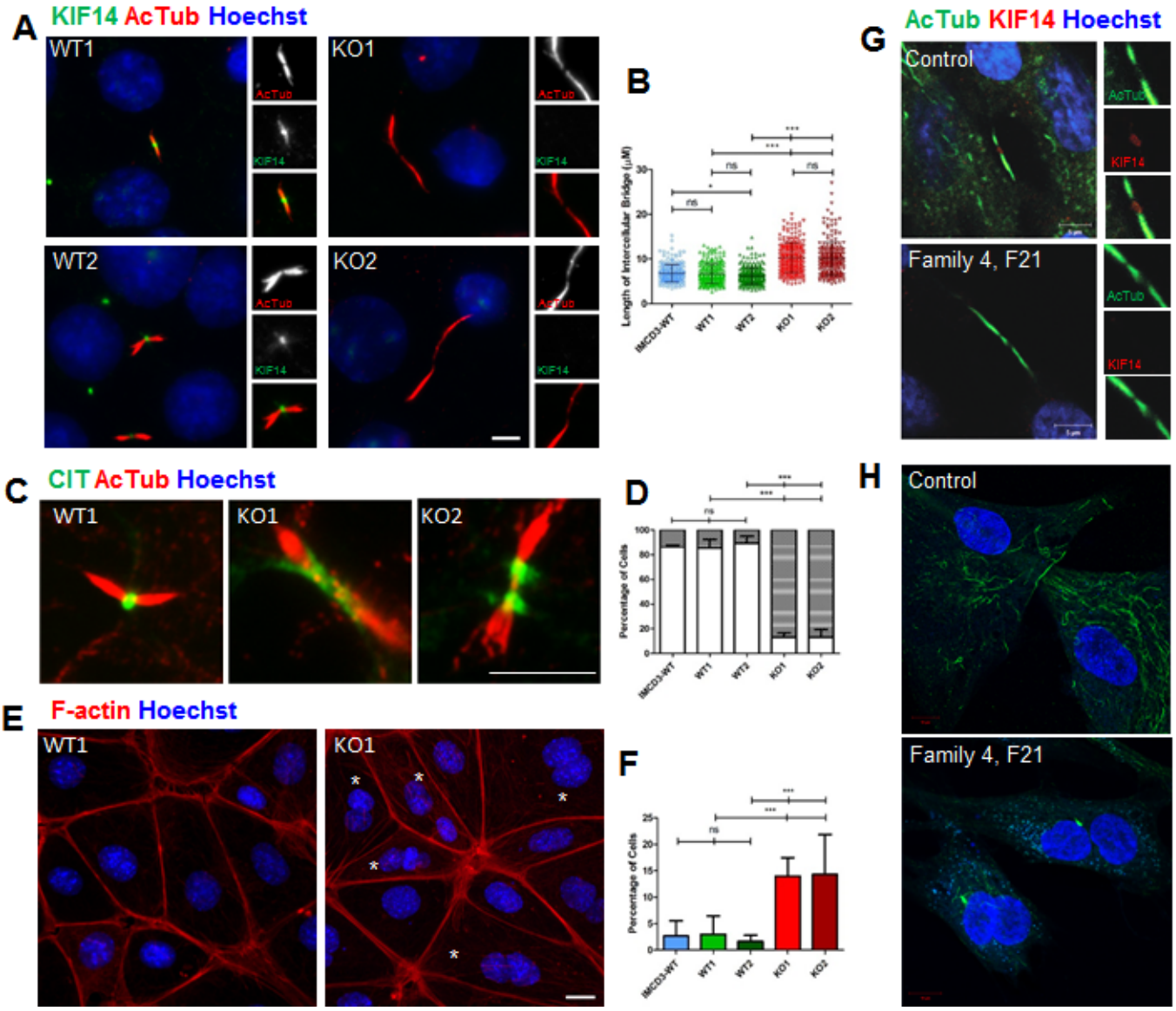

Figure 4. Loss of Kif14 leads to cytokinesis defects in mIMCD3 cells and in cells from the affected foetuses. *(A,B) Cycling Kif14 wild-type (WT1, WT2) and knockout (KO1, KO2) mIMCD3 clones were stained for KIF14 (green), acetylated-α-tubulin (AcTub, red) and DNA (Hoechst, blue). Insets show higher magnification of intercellular bridges stained with AcTub. Length of intercellular bridges in parental IMCD3 cells (IMCD3 WT) and WT and KO clones were quantified using imageJ (B), as described in materials and methods. (C,D) WT and KO clones were immunostained for CIT (green) and AcTub (red) to quantify the localisation of CIT to the midbody (C) expressed as the percentage of cells with "normal" single ring CIT staining (D). (E,F) WT and KO clones were stained for F-actin using phalloidin (red), and nuclei using Hoechst (blue)(E) in order to identify binucleated cells (Asterisks). (F) Quantification of the percentage of binucleated cells in control and knockout cells. ns = not significant, **P< 0.001 ***P< 0.0001 from n=3 independent experiments, Dunn's Multiple Comparison Test following the Kruskal-Wallis ANOVA test for length of intercellular bridges (B), and Fischer's exact test for CIT localisation and binucleated cells (D, F). (G, H) Fibroblasts derived from control and foetus 21 from family 4 were stained for either acetylated α-tubulin (green) and KIF14 (red) (G) or acetylated α-tubulin (green) only (H), as well as for DNA (Hoechst, blue). Scale bars: 5 µm (A, C, E and F), 10 µm (H).*

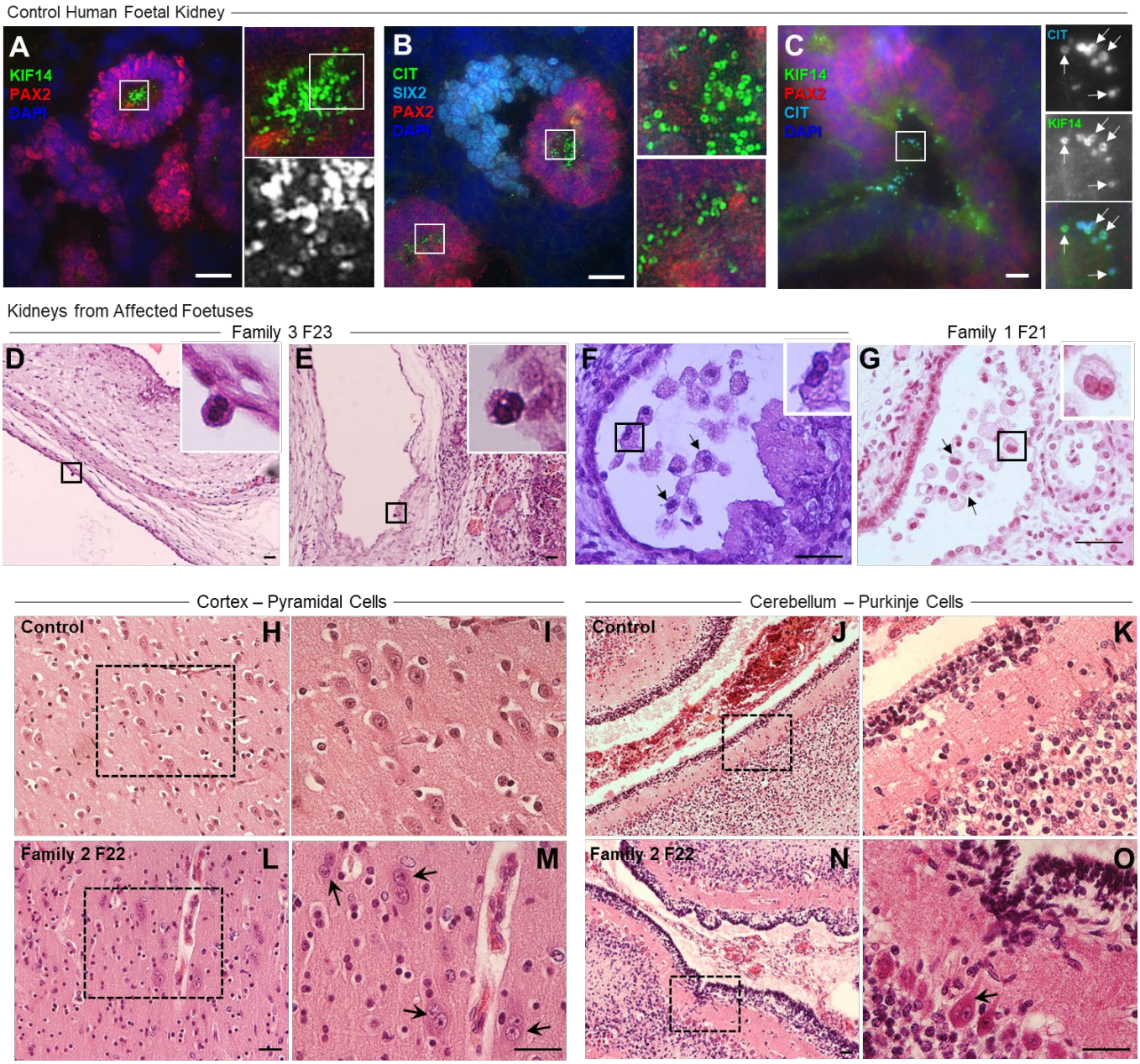

Figure 5. KIF14 is required for cytokinesis in developing human kidney. *Sections of control human foetal kidneys (23 weeks) were stained for: (A) KIF14 (green), PAX2 (red) and Hoechst (blue), (B) CIT (green), SIX2 (red), PAX2 (cyan), and Hoechst (blue), and (C) KIF14 (green), PAX2 (red), CIT (cyan), and Hoechst (blue). Insets show higher magnification of regions of interest, denoted by the white outline, and arrows point to ring-like structures corresponding to midbody remnants. Similar results were obtained in 3 other control foetuses. (D-G). Haematoxylin-eosin staining of kidney sections from foetus 3 from family 3 (D-F) and from foetus 1 from family 1 (G) showed the presence of binucleated cells (black boxes) which were enlarged in the corresponding insets. (H-K) Haematoxylin-eosin staining of pyramidal cells in the brain cortex (H, I) and Purkinje cells from the cerebellum (J, K) of control foetuses. (L-O) Haematoxylin-eosin staining of pyramidal cells in the brain cortex (L, M) and Purkinje cells from the cerebellum (N, O) of foetus 2 from family 2 showed the presence of binucleated neurons (black arrows). Boxed areas (H, J, L, N) are enlarged (I, K, M, O). Scale bars xxμm.*

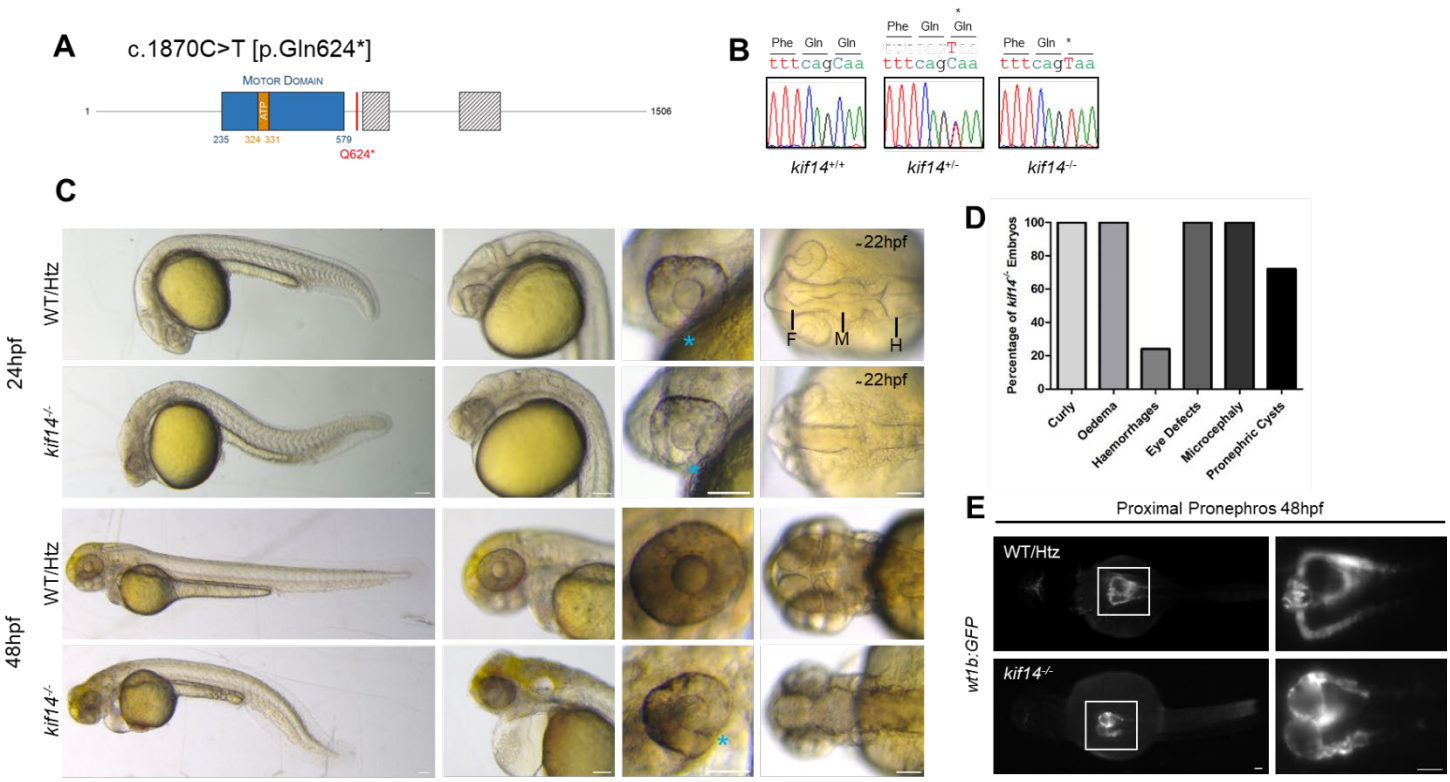

Figure 6. **In vivo *zebrafish model reveals loss of kif14 causes severe developmental defects of brain and kidneys.*** *(A) Schematic representation of zebrafish* kif14 *showing the position of the nonsense mutation. The motor and coiled-coil domains are also shown. (B) DNA trace from Sanger sequencing of exon 11 of* kif14 *in WT, heterozygous and homozygous embryos showing the nucleotide, and subsequent amino acid, change. (C) Representative images of the phenotypes observed in WT/Htz and* kif14$^{-/-}$ *embryos at 24hpf (top row) and 48hpf (bottom row). Coloboma, blue asterisk. Scale bar: 100 µm. F, forebrain; M, midbrain; H, hindbrain. (D) Quantification of macroscopic phenotypes. (E) Live imaging of* Tg(wt1b:GFP) *WT/Htz and* kif14$^{-/-}$ *embryos at 48hpf, dorsal view, with anterior to the left. Inset shows a higher magnification of proximal pronephros. Scale bars: 200 µm.*

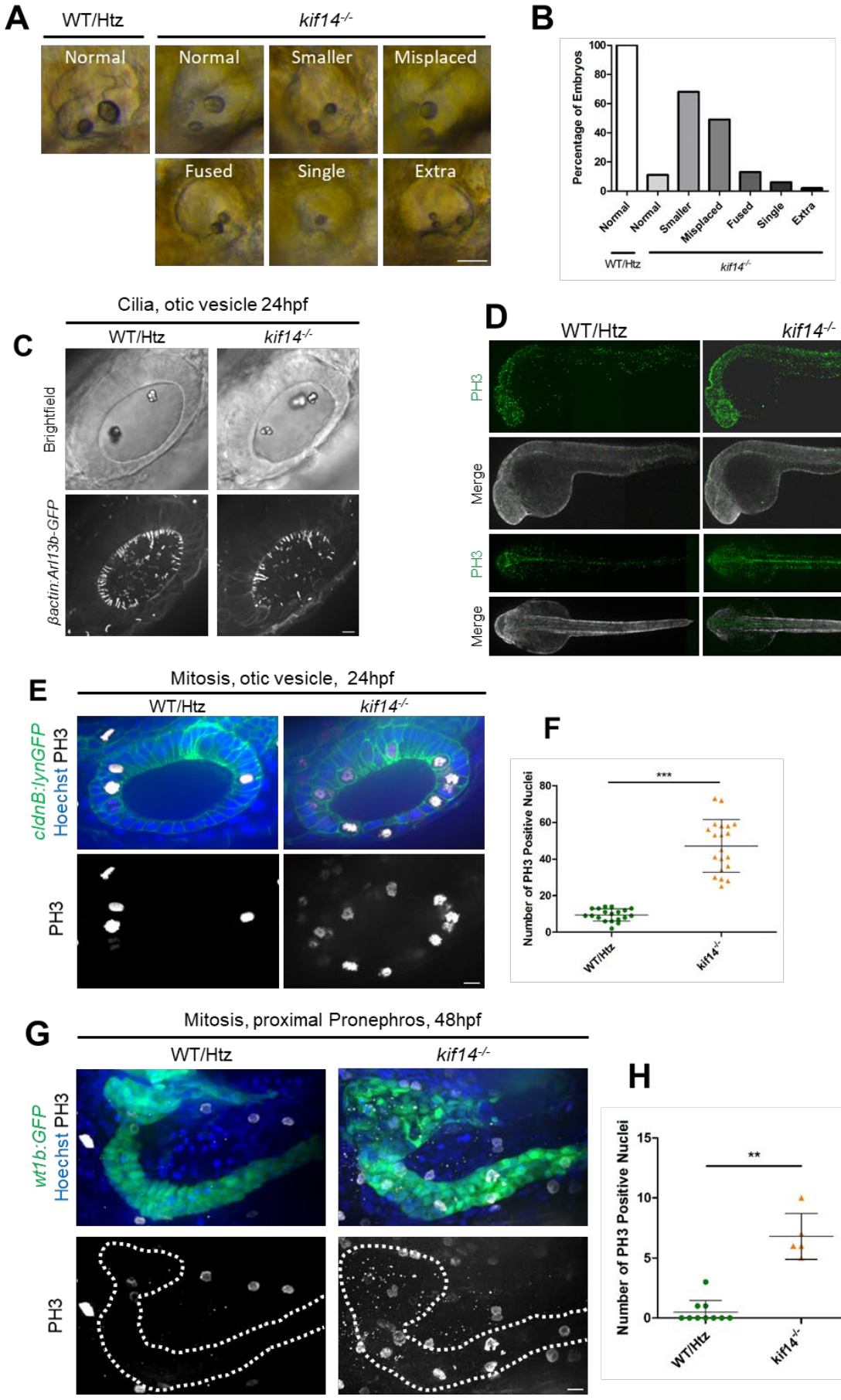
A
WT/Htz
kif14-/-
Normal
Normal
Smaller
Misplaced
Fused
Single
Extra
B
Percentage of Embryos
100
80
60
40
20
0
Normal
Normal
Smaller
Misplaced
Fused
Single
Extra
WT/Htz
kif14-/-
C
Cilia, otic vesicle 24hpf
WT/Htz
kif14-/-
Brightfield
βactin:Arl13b-GFP
D
WT/Htz
kif14-/-
PH3
Merge
PH3
Merge
E
Mitosis, otic vesicle, 24hpf
WT/Htz
kif14-/-
cldnB:lynGFP Hoechst PH3
PH3
F
***
Number of PH3 Positive Nuclei
80
60
40
20
0
WT/Htz
kif14-/-
G
Mitosis, proximal Pronephros, 48hpf
WT/Htz
kif14-/-
wt1b:GFP Hoechst PH3
PH3
H
**
Number of PH3 Positive Nuclei
15
10
5
0
WT/Htz
kif14-/-

Figure 7. In vivo zebrafish model presents ciliopathy-like phenotypes due to an accumulation of mitosis-blocked cells. *(A,B) Representative images (A), and quantification (B; n=61; 3 separate clutches), of otolith phenotypes observed at 72hpf in WT/Htz and kif14$^{-/-}$ embryos. (C) Live confocal imaging in brightfield (top row) and for GFP (cilia, bottom row) of Tg(act2b:Arl13b-GFP) of a representative otic vesicle of WT/Htz and kif14$^{-/-}$ embryos at 24hpf. (D) Immunofluorescence of WT/Htz and* kif14$^{-/-}$ *embryos at 24hpf immunostained for Phospho-Histone H3 (PH3, green) and AcTub (grey) shown in lateral (top row) and dorsal (bottom row) views, anterior to the left. Scale bars: 200 µm. (E,F) Immunofluorescence of PH3 (white), and Hoechst (blue) stained Tg(cldnB:GFP) otic vesicles at 24hpf. (F) Quantification of PH3+ nuclei in the otic vesicle. (G,H) Immunofluorescence of PH3 (white), and Hoechst (blue) stained Tg(wt1b:GFP) proximal pronephros at 48hpf (G). Quantification of PH3+ nuclei within these GFP positive cells (H). **P< 0.001, ***P< 0.0001 from n=2 independent experiments, t-test for PH3 quantifications (F,H). Scale bars: 10 µm.*

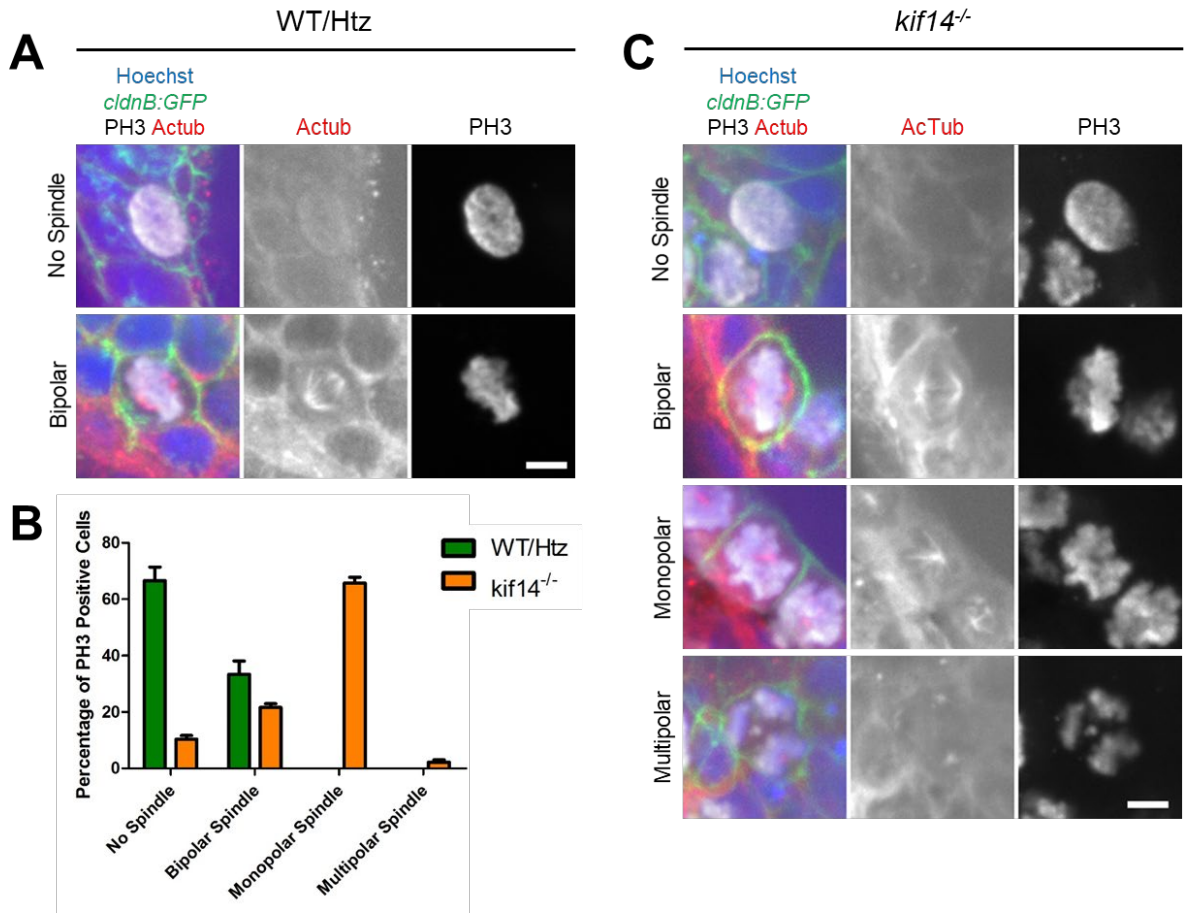

Figure 8. Loss of kif14 in vivo in zebrafish results in mitotic spindle defects. *(A-C) Different stages of mitosis in otic vesicles of WT/Htz and* kif14$^{-/-}$ *Tg(cldnB:lynGFP) embryos at 24hpf visualised through immunostaining for PH3 (white), AcTub/αTub (red), Hoechst (blue). (B) Quantification of the various visible mitoses. Scale bars: 5µm*

Discussion

The present study, in accordance with our previous one, describes a novel syndrome linked to mutations in *KIF14* and associated with severe developmental defects of both the brain (microcephaly/atelencephaly) and kidney (RHD). Here, we provide functional evidence that the mutations in the syndromic form cause a loss-of-function of *KIF14*. In addition, we used the zebrafish model to provide strong evidence that kif14 plays a crucial and conserved role during both brain and kidney development.

Two other groups recently identified mutations in *KIF14* in eight families with individuals presenting mild to severe microcephaly without major renal malformation (except one case out of 18; Fig. S8). Comparing the effect of these mutations provides some clues to explain the broad phenotypic spectrum associated with KIF14 mutations. Among the syndromic forms, two families harbour mutations leading to an early stop codon within the motor domain. These mutations are likely to correspond to a knock-out of KIF14 as even if alternative splicing were induced, any exon skipping in this region would lead to disruption of the motor domain. In addition, our functional studies clearly show that the mutations identified in the 3 other syndromic cases are also LOF mutations leading either to variant proteins unable to bind microtubules (motor domain), or to active non-functional forms which lack the C-terminal domain. Interestingly, our results show that a similar kif14 truncation mutation in the zebrafish mimics the human syndromic form.

On the contrary, analysis of the mutations described in the 8 families with isolated microcephaly (Makrythanasis et al., 2018; Moawia et al., 2017) indicates that they are likely to be less severe. Three missense mutations and a single amino acid deletion are located in the FHA domain, a domain which has regulatory functions in some kinesin family members (Verhey et al., 2011) but its function was not yet characterised in KIF14. One missense mutation leads to a deletion of a smaller part of the C-terminal tail and missense or silent mutations affecting splice sites, lead to coexpression of C-terminal truncated proteins and missense variant or WT protein, respectively. Interestingly, one mutation was also found in the motor domain (p.Gly459Arg); however, unlike both the Arg364 and Thr456 residues, the G459 residue is not present within the nucleotide binding pocket. It is likely, therefore, that the functional consequences of the p.Gly459Arg mutation would be far less severe than the p.Arg364Cys and p.Thr456Met mutations described here. Finally, the c.246delT/p.Asn83Ilefs*3 homozygous mutation described in a family with microcephaly but without kidney defects, would be expected to be even more severe than the ones in our syndromic families. Interestingly, it is in the same region as the c.263T>A/p.Leu88* mutation which was shown to activate a cryptic splice site and to lead to an in-frame deletion within exon 2, resulting in a deletion of 124 aa (p.G58_L181del) within the PRC1-binding domain. The potential consequences on splicing of the c.246del/p.Asn83Ilefs*

mutation remain to be tested in order to conclude on the lack of genotype/phenotype correlation for this specific case.

Therefore, we can conclude that LOF mutations in KIF14 lead to syndromic forms associating microcephaly and brain malformations with RHD, whereas hypomorphic mutations cause mild to severe microcephaly with no developmental kidney defects. The observation of small echogenic kidneys in one affected individual (out of 18), however, indicates the potential for kidney manifestations in individuals harbouring hypomorphic *KIF14* mutations.

Altogether, these results suggest that KIF14 likely has an important and similar function during the early steps of both kidney and brain development. There are very few reports of monogenic mutations identified in syndromes associating MCD or microcephaly with kidney phenotypes (Galloway-Mowat (Cooperstone et al., 1993) and DREAM-PL (Shaheen et al., 2016) syndromes). However, the kidney phenotypes in these syndromes, including glomerulopathy or occasional unilateral agenesis, are much less severe than those observed in the case of *KIF14* mutations. It is worth noting that associations of RA/RHD and MCD/microcephaly similar to those observed in individuals with *KIF14* mutations were described in cases with copy number variations (CNV) of varying sizes and at various loci, suggesting the involvement of one or several genes which were not characterised further (Sanna-Cherchi et al., 2018). Finally, while mutations in genes involved in microtubule dynamics, mitosis and/or orientation of the mitotic spindle represent a major cause of microcephaly (Romero et al., 2018), it is not the case for RA and RHD with none of the mutations identified thus far affecting genes from these functional families (see (Heidet et al., 2017; Sanna-Cherchi et al., 2018) for a recent list of CAKUT genes).

Ciliary defects were a plausible pathophysiological explanation for the two distinct phenotypes in foetuses harbouring LOF *KIF14* mutations as suggested earlier (Filges et al., 2014). Indeed, central nervous system manifestations are observed in patients also presenting with renal ciliopathies, such as cerebellar hypoplasia or agenesis of the corpus callosum, two defects that are present in all the affected foetuses. A plethora of brain developmental disorders are recognised clinical signs in many ciliopathy phenotypes (Braun and Hildebrandt, 2017), but the direct role of mutations in ciliary genes particularly for microcephaly has not been frequently explored. Interestingly, dominant mutations in *KIF2A* , a kinesin involved in both mitotic spindle dynamics and ciliogenesis, were shown to cause MCD through their impact on both cilia and cell cycle (Broix et al., 2018). In addition, bilateral agenesis and non-cystic RHD were very rarely reported among the renal phenotypic spectrum of ciliopathies (Grampa et al., 2016). However, a recent report identified that a homozygous LOF mutation in IFT27, encoding a component of the intraflagellar transport complex, causes BRA (Quélin et al., 2018), suggesting that defects in ciliary genes can indeed lead to RHD.

We investigated a potential role for KIF14 in ciliogenesis. We found that, upon overexpression, KIF14 localises to cilia (not shown), but failed to find any evidence for a direct role in ciliogenesis *in vitro*. Intriguingly, the zebrafish embryos harbouring LOF mutations in *kif14* demonstrate ciliopathy phenotypes, but, once again, our analyses failed to identify a direct impact on ciliogenesis *in vivo*. However, we cannot formally exclude its potential role in the transport of cargo into the cilium, which remains to be explored. Based on these results, it is therefore unlikely that a disruption of ciliary function can account for a shared mechanism at the origin of renal and brain developmental defects.

The localisation of KIF14 at midbodies accumulating within the lumen of UB tips in human foetal kidneys provided a key clue to better understand the mechanism by which the loss of KIF14 affects both brain and kidney development in humans. Indeed, it was shown that midbody remnants are released or 'secreted' into the cerebrospinal fluid in mice. This accumulation, during the early stages of brain development, corresponds to the amplification of neural progenitors. During the symmetrical divisions of these cells, cytokinesis occurs at the apical membrane of the progenitors and midbodies are formed within the lumen, where they are released following abscission (Dubreuil et al., 2007). In the UB tips, mitosis of proliferating UB epithelial cells occurs in the lumen of the expanding/branching tubular structures by a more complex process (Packard et al., 2013). Dividing cells protrude at the surface of the epithelium, within the lumen, and while one of the daughter cells remains attached to the basal membrane and retracts after mitosis, the other one intercalates between adjacent cells to integrate into the epithelium layer. Subsequently, midbodies are likely formed in the lumen of UB tips, where they could be released and accumulate, as occurs in the brain. To our knowledge there is no other organ where a similar process resulting in the massive release of midbody remnants has been reported. The fact that both organs are dramatically affected by *KIF14* LOF mutations strongly indicates that it plays a key role *in vivo* during these 'symmetric' divisions, whereby abscission occurs on both sides of the midbody and leads to their release into the extracellular milieu.

Intriguingly, LOF mutations in CIT lead to microcephaly but are not associated with kidney defects, neither in humans (Basit et al., 2016; Harding et al., 2016; Li et al., 2016; Shaheen et al., 2016) nor in rodents (Di Cunto et al., 2000; Sarkisian et al., 2002). These observations suggest that KIF14 might play a specific function in the kidney. Recent transcriptomic and single cell transcriptomic analyses revealed expression of mitosis-related genes during the early development of the human kidney (Lindström et al., 2018a, 2018b), including both CIT and KIF14, as well as other genes known to play crucial roles at the midbody (KIF23, KIF20A, ANLN, etc…). These data suggest that other proteins required for abscission would similarly play a crucial role during kidney development and may compensate for each other except in the case of KIF14.

The key question for future investigations is: do 'secreted' midbodies play a role or not? Recent work has changed the view of midbodies and midbody remnants as passive structures to be eliminated after mitosis. Several groups identified possible post-mitotic functions of midbodies when inherited or captured by daughter or neighbouring cells, including cell fate (stemness), polarity or ciliogenesis (Bernabé-Rubio et al., 2016; Dionne et al., 2015). In the brain, midbody remnants were purified from the ventricular fluid, indicating that most of them are not immediately recaptured by one of the daughter cells. Their function within the developing brain remains, however, to be determined. The images that we obtained clearly show the accumulation of midbodies in the lumen of UB tips. We cannot exclude that they may remain associated with the apical membrane of the UB tips cells where they could be involved in local signalling events and/or ciliogenesis. However, their localisation in the central part of the lumen in most UB tip profiles suggests that they are released within the lumen, as in the developing brain. In this case, it is tempting to speculate that the connection of these midbody-filled UB tips to a newly functional nephron would result in the expulsion of those midbodies by the incoming urine flow, leading, either, to signalling in the collecting duct, or to elimination in the urine. All these exciting issues remain open and a source of future investigations.

Acknowledgements

We are grateful to the families for their participation. We greatly acknowledge N. Goudin and M Garfa-Traoré (Necker cell imaging facility) for providing expert knowledge on confocal microscopy and C. Arrondelle and F. Legendre for their help on tissue sections and immnunohistochemistry. We acknowledge E.D. Peters for immunofluorescence experiments. We would like to thank F. Barr, U. Gruneberg, S. Angers and S. Narumiya for their generous gifts of KIF14 and Citron Kinase encoding plasmids. This work was supported by the Fondation pour la Recherche Médicale (DEQ20130326532 to SS); the European Union's Seventh Framework Programme (FP7/2007–2013) grant 305608 (EURenOmics; CJ); the GIS-Institut des Maladies Rares (AMA11025KSA; CJ and SS); the Canadian Cancer Society Research Institute (CCSRI : 703405 ; BHK) ; Natural Sciences and Engineering Research Council of Canada (BHK); Canadian Institutes of Health Research (CIHR: MOP-97928 & Project Grants 201604, 201610; BHK); the Swiss National Science Foundation (SNSF; IF); the Dutch Kidney Foundation KOUNCIL consortium (CP11.18); the Natural Sciences and Engineering Research Council of Canada (NSERC) discovery grant (RGPIN 2013-356025 ; JSA) ; the Canadian Cancer Society Research Institute (CCSRI) Innovation Grant (JSA). JSA holds a Canada Research Chair in Structural Biology. BHK is a recipient of the Fonds de Recherche du Québec–Santé (FRSQ). The Imagine Institute is supported by an ANR grant (ANR A0-IAHU-01). We acknowledge the Imagine Institute for the purchase of Leica SP8 STED and Zeiss Spinning Disk microscopes, and the Fondation ARC (EML20110602384) for the purchase of the LEICA SP8 confocal microscope.

Material and Methods

Genetics analyses, WES and Sanger sequencing

Family 3: Foetuses with severe kidney development defects, possibly associated with extrarenal defects, were collected though MARHEA (Centre de référence des Maladies Rénales Héréditaires de l'enfant et de l'adulte). Written informed consent was obtained from parents and the study was approved by the "Comité de Protection des Personnes pour la Recherche Biomédicale Ile de France II". DNA was extracted from frozen lung biopsies of the two affected foetuses of family 3 and whole exome sequencing was performed using the 50 Mb Agilent SureSelect all exon V3 and a HiSeq2500 (Illumina) sequencer. Sequence data were aligned to the human genome reference sequence (hg19 build) using BWA aligner. Downstream processing was carried out with the Genome Analysis Toolkit (GATK), SAMtools, and Picard (http://www.broadinstitute.org/gatk/guide/topic?name=best-practices). The average coverage was 50, with 93.5% of the targeted regions covered > 15X. Variants were annotated using a software system developed by the Paris Descartes University Bioinformatics Platform, based on the Ensembl (GRCh37/hg19), dbSNP, EVS, 1000 genome, ExAC and GnomAD databases. Variants were then prioritised according to their damaging effect (nonsense, frameshift, acceptor/donor splice site mutations, missense variants predicted to be damaging, and their absence or low frequency in GnomAD and in our in-house database (> 10,000 exomes). For missense variants, prediction of damaging effect was based on PolyPhen2, Sift, Grantham and CADD scores. According to a suspected autosomal recessive inheritance model, only one gene, *KIF14*, was identified as carrying 2 mutations common to both foetuses. Sanger sequencing in foetuses and parents confirmed compound heterozygosity. In order to look for additional mutations in *KIF14* probes covering the 30 exons of the gene were designed and added to a previously described SureSelect panel of 330 genes used for molecular diagnosis of CAKUT cases. *KIF14* mutations identified in foetuses from families 1 and 2 have been briefly described in (Heidet *et al.*, 2017).

Family 4: Patients were included via the AGORA (Aetiologic Research into Genetic and Occupational/environmental Risk factors for Anomalies in children) biobank project. The study protocol was approved by the regional Committee on Research involving Human Subjects (CMO Arnhem/Nijmegen 2006/048). DNA from fibroblasts and (umbilical cord) blood was obtained from foetus 1, 2 and 4 and from blood from both parents. Written informed consent was obtained from both parents for whole genome SNP-array analysis and whole-exome sequencing of DNA from foetus 4 and analysis of skin fibroblasts obtained from foetus 1. Because parents were consanguineous and autosomal recessive inheritance was suspected based on the phenotype, single nucleotide polymorphism (SNP)-array analysis was performed to investigate genes located inside regions of homozygosity. Genomic DNA was extracted from fibroblasts obtained from a skin biopsy from foetus

4 according to standard protocols. Analysis of regions of homozygosity and copy number profiling were performed using the CytoSNP-850K BeadChip SNP-array (Illumina, San Diego, CA, USA) according to standard procedures. SNP-array results were visualised and data analysis was performed using Nexus software version 7 (BioDiscovery, Los Angeles, CA, USA) and the reference Human genome build Feb. 2009 GRCh37/hg19. Results were classified with Cartagenia BENCH software (Cartagenia, Leuven, Belgium).

Whole-exome sequencing (WES) was performed on DNA from foetus 4. Protein coding genes and flanking (splice-site consensus) sequences were captured and enriched using the SureSelectXT Human All Exon V5 capture library (Agilent, Santa Clara, CA, USA) and sequenced in rapid run mode on the HiSeq 2500 Sequencing system (Illumina, San Diego, CA, USA) at a mean target depth of 100X. The target is defined as all coding exons of UCSC (Kent *et al.*, 2002) and Ensembl (Aken *et al.*, 2017) +/- 20bp intron flanks. At this depth ~95% of the target is covered at least 15X. Reads were aligned to the reference Human genome build Feb. 2009 GRCh37/hg19 using BWA (BWA-MEM v0.7.5a) and variants were called using the GATK haplotype caller (v2.7-2). Results were imported into Cartagenia BENCH Lab NGS Module (Cartagenia, Leuven, Belgium) for variant annotation, filtering and prioritisation. Filtering was performed for variants in genes associated with neurodevelopmental abnormalities (for a full list of genes, see Supplementary Methods S1). Identified variants were validated and segregation analysis was performed using standard Sanger sequencing.

Plasmids: Plasmids encoding wild-type KIF14 GFP-fusion and the CCf domain of CIT (429-835aa) fused to mCherry- were kind gifts from F. Barr and S. Narumiya, respectively (Gruneberg *et al.*, 2006; Watanabe *et al.*, 2013). Variants from the affected foetuses were introduced in the GFP-KIF14 construct using Pfu turbo site-directed mutagenesis as previously described (Bizet *et al.*, 2015). The GST-mKif14 construct (pGex6P1) was described previously (Arora *et al.*, 2014). Mutant mKIF14-MD-T491M DNA was generated by gene synthesis (Genscript, NJ, USA) and cloned into pGex6P1.

Antibodies: The primary antibodies used were; mouse anti-acetylated α-tubulin (1:10,000, Sigma, T6793), rabbit anti-KIF14 (1:300, Bethyl, A300-233A and A300-912A; 1:1,000, Abcam ab3746), mouse anti-α-Tubulin (1:5000, Sigma, T5168), mouse anti-CRIK (1:500, BD Biosciences, 611376), rabbit anti-SIX2 (1:200, Proteintech, 11562-I-AP), goat anti-PAX2 (1:200, RD System, AF3364), rabbit anti-phospho-histone H3 (1:200, Cell Signalling, #3377S) rabbit anti-GFP (Life Technologies, A-11122), rabbit anti-dsRed (ClonTech, 632496), mouse anti-GAPDH (Millipore, MAB374) and Phalloidin-TRITC (1:300, Sigma, P1951). Cells were incubated with secondary antibodies (Donkey) conjugated to Alexa Fluor® 488, 555 or 647 (Molecular Probes, Invitrogen). Sheep horseradish peroxidase-coupled antibodies were from GE Healthcare (anti-mouse: NA931V; anti-rabbit: NA934V).

Cell Culture: Foetal control- and foetus-derived fibroblasts, human Embryonic Kidney 293 (HEK293) and HeLa cells (ATCC) were cultured in Dulbecco's Modified Eagle Medium, DMEM (Gibco®, Life Technologies) supplemented with 10% Foetal Bovine Serum (FBS, Invitrogen), glutamine and penicillin/streptomycin. Inner Medullary Collective Duct 3 (IMCD3) and hTERT-Retinal Pigment Epithelial (RPE1) cells were cultured in Dulbecco's Modified Eagle Medium, DMEM F:12, (Gibco®, Life Technologies) also supplemented with 10% FBS, glutamine and penicillin/streptomycin. Hela, HEK293 and IMCD3 cells were transfected using Lipofectamine 2000 (Life Technologies, 11668-019) and RPE1 using FuGENE® (Promega, E2311) and maintained in culture for 24 hours.

Biochemistry: Transfected cells were lysed in 0.5% triton, 150mM NaCl and 50mM pH7.5 Tris HCl. For immunoprecipitations, cleared lysates were incubated with mouse isotypic control antibodies and G-protein beads (Sigma, P7700) for 2 hours at 4°C. 1mg of precleared proteins were incubated with mouse monoclonal anti-GFP antibodies (Roche, 11814460001) coupled to G-protein beads for 3 hours at 4°C. Beads were washed three times with increasing amounts of NaCl (150nM, 300nM and 600nM NaCl in 50mM Tris-HCl pH7.5), resuspended in 2x sample buffer (Sigma, S3401) and boiled at 95°C for 5 minutes. For immunoblotting, lysates and immunoprecipitates were separated by polyacrylamide gel electrophoresis (SDS-PAGE) and transferred onto polyvinylidene fluoride transfer membranes (PVDF, GE Healthcare). Immunoblotting was performed using the indicated primary antibodies and revealed using the ECL+ Detection Kit (GE Healthcare).

Microtubule co-sedimentation assay: Recombinant WT and mutant MBP-hKIF14-MD and GST-mKIF14-MD proteins were expressed and purified in the same manner as previously described (Arora *et al.*, 2014). Microtubule preparation and co-sedimentation assays were performed as previously described (Solinet *et al.*, 2013), with some modifications. Briefly, taxol-stabilised MTs were prepared by polymerising tubulin at 50µM in 1×BRB80 (80 mM Pipes pH 6.8, 1 mM EGTA, and 1 mM $MgCl_2$), 1 mM GTP, and 1 mM DTT in the presence of 10% DMSO at 37 °C for 25-30 min, then diluted to 10µM working stocks in 1× BRB80 containing 20µM taxol. Binding reactions were performed by mixing 500nM of the indicated KIF14 constructs with 2µM taxol-stabilised MTs in 1×BRB80 supplemented with 25mM KCl, 1 mM DTT, 0.01% Tween-20, and 20µM taxol. After a 20-minute incubation, mixtures were spun at 240,000×*g* for 5 minutes at 25°C. The supernatant and pellet fractions were recovered and resuspended in Laemmli buffer. Samples were resolved by SDS-PAGE. Gels were stained with Coomassie blue R250 dye, destained, and scanned with a digital scanner.

ATPase activity assay: KIF14 ATPase activity was monitor by a malachite green-based phosphate detection method, as previously described (Arora *et al.*, 2014). Briefly, reactions were carried out in BRB80-based buffer (80 mM PIPES pH 6.8, 1mM MgCl2, 1mM EGTA, 20µM taxol, 25mM KCl, 0.25mg/mL BSA, 1mM DTT, 0.02% Tween), supplemented with 1mM ATP, with 2µM taxol-stabilised MTs, and 50nM KIF14 protein constructs. Basal activity of the Kif14 constructs was determined using the same reaction condition without MTs. Reactions were allowed to proceed for 10 minutes, quenched with perchloric acid and malachite green reagent. The signal was quantified by measuring the absorbance at 620nm in a Genios Plus plate reader (Tecan).

CRISPR: Guides couples were designed using CRISPOR and MIT against exon 5 of *Kif14* and cloned into modified Cas9 Nickase plasmids expressing either GFP or mCherry (PX458, Addgene 48138 (Ran *et al.*, 2013)). Sequences of the guides used were; #4-GFP: AGTGTCCACTCGCCAGCGTGAGG and #17-mCherry: ATTGACAGGCCTTCAACATACGG. Transfected cells were sorted by flow cytometry for green and red fluorescence and clones were isolated. Nuclear DNA was extracted using QuickExtract™ DNA Extraction Solution (Tebu-bio, QE09050), and Sanger sequenced using the following primers; forward $^{5'}$gcacatctcgtgagaac$^{3'}$ and reverse $^{5'}$gaacaaagaactaagagccc$^{3'}$.

Immunofluorescence: Cells were cultured on cover slips and fixed in 4% paraformaldehyde. Primary antibody incubation was performed in Dulbecco's phosphate buffered saline (PBS, Sigma), 0.1% Triton-X-100 (Sigma) and 1mg/ml or 3% bovine serum albumin (BSA, Sigma). After 3 washes with the incubation buffer, cells were incubated with secondary antibodies (1:300) in PBS-BSA (1mg/ml) and after 3 washes in PBS, nuclei stained using Hoechst (#33342, Sigma). Coverslips were mounted onto glass slides using Mowiol® 4-88 (Sigma).

Frozen tissues from control and affected kidneys were sectioned (8µm) using a Leica microtome. Melted sections were postfixed in acetone (10 minutes, room temperature). The slides were washed twice in PBS and then blocked for 45 minutes at 4°C in 10% normal donkey serum diluted in PBT (PBS, 0.1% Tween) and then incubated with the primary antibodies diluted in PBT (overnight, 4°C). After 3 washes in PBT, sections were incubated with secondary antibodies diluted in PBT and, after two washes in PBS, nuclei stained using Hoechst (#33342, Sigma) and finally mounted onto glass slides using Mowiol® 4-88 (Sigma) or Fluormount G (Cell Lab, Beckman Coulter, Brea, CA, US).

Stained cells and tissues were imaged using an epi-illumination microscope (DMR, Leica) with a cooled charge-coupled device (CCD) camera (Leica DFC3000G). Images were acquired with LAS (Leica V4.6) and processed with ImageJ and Photoshop CS2 (Adobe Systems Inc., San Jose, CA, USA). Confocal imaging was performed for imaging stainings of fibroblasts using a Zeiss Confocal laser microscope LSM700 and images were processed with ZEN 2011 software.

Zebrafish Experiments: The zebrafish *kif14* mutant line sa24165 was acquired from ZIRC and maintained at 28.5°C under standard conditions and according to European Law. *Kif14*$^{+/-}$ zebrafish were crossed with *Tg(βactin:arl13bGFP)*, *Tg(wt1b:GFP)* and *Tg(cldnB:lynGFP)* to allow analysis of cilia (Borovina *et al.*, 2010), proximal (Perner *et al.*, 2007) and distal pronephros (Haas *et al.*, 2006), respectively. Genotyping was performed by placing embryos in 10mM Tris pH8.0, 1mM EDTA and 1.2mg/ml at 55°C overnight, and the reaction was stopped by incubating at 95°C for 5 minutes. DNA from exon 11 was Sanger sequenced using the following primers: forward $^{5'}$gtgtgagattcgagtgttttc$^{3'}$ and reverse $^{5'}$gttgcatatttaaacggaatg$^{3'}$.

Live embryos were analysed using a Leica M165FC stereoscope. For immunofluorescence, embryos were fixed in 4% PFA, washed in PBS and blocked in PBS, 0.3% Triton and 4% BSA. Both primary and secondary antibody incubations were performed overnight at 4°C. Fixed and stained embryos were stored in Mowiol and mounted in 1% low gelling temperature agarose (Sigma, A9414) and imaged using a Zeiss Axio Observer Z1 inverted microscope equipped with a Yokogawa CSU-X1 spinning disk. Images were acquired with a 40x water immersion objective (1.46) through a Hamamatsu Orca Flash 4.0 sCMOS Camera. Images were processed using ImageJ and Photoshop CS2 (Adobe Systems Inc., San Jose, CA, USA).

Supplementary Data

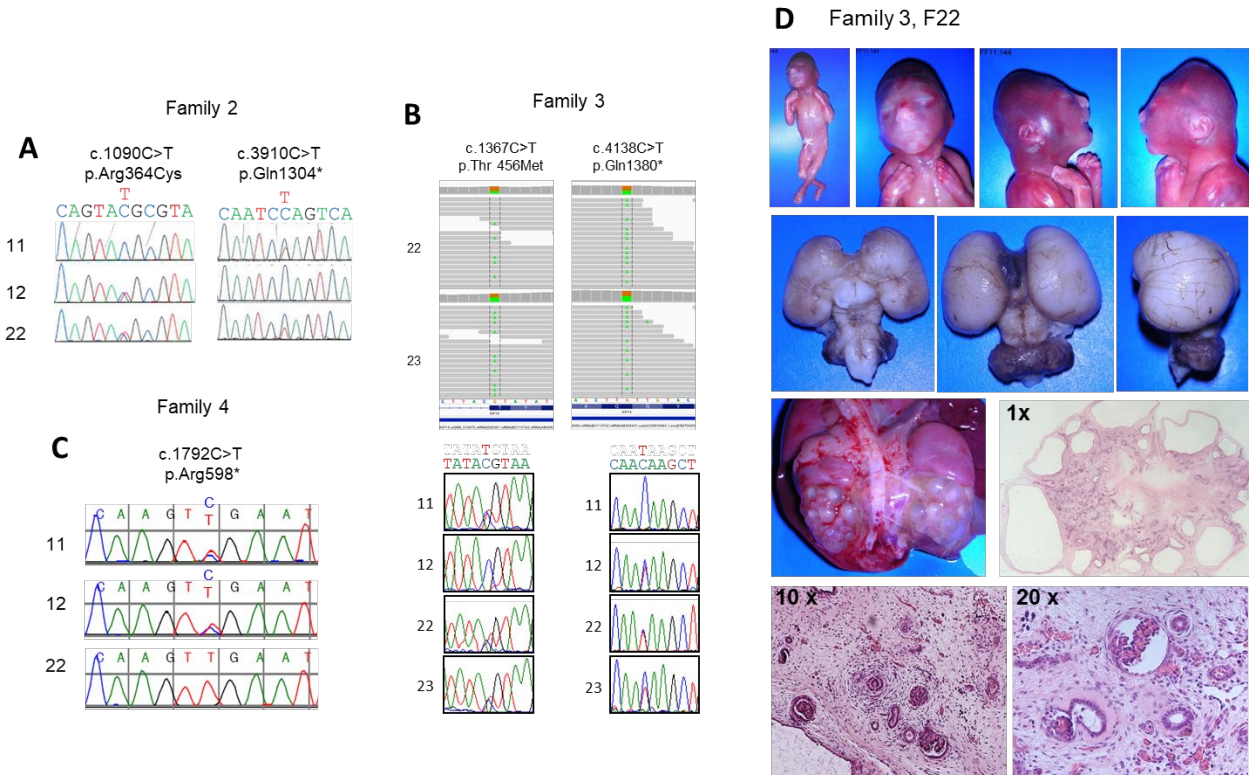

Figure S1. *(A-C) Segregation for families 2, 3 and 4. (D) Foetus 22 of family 3, with representative histological sections from one kidney.*

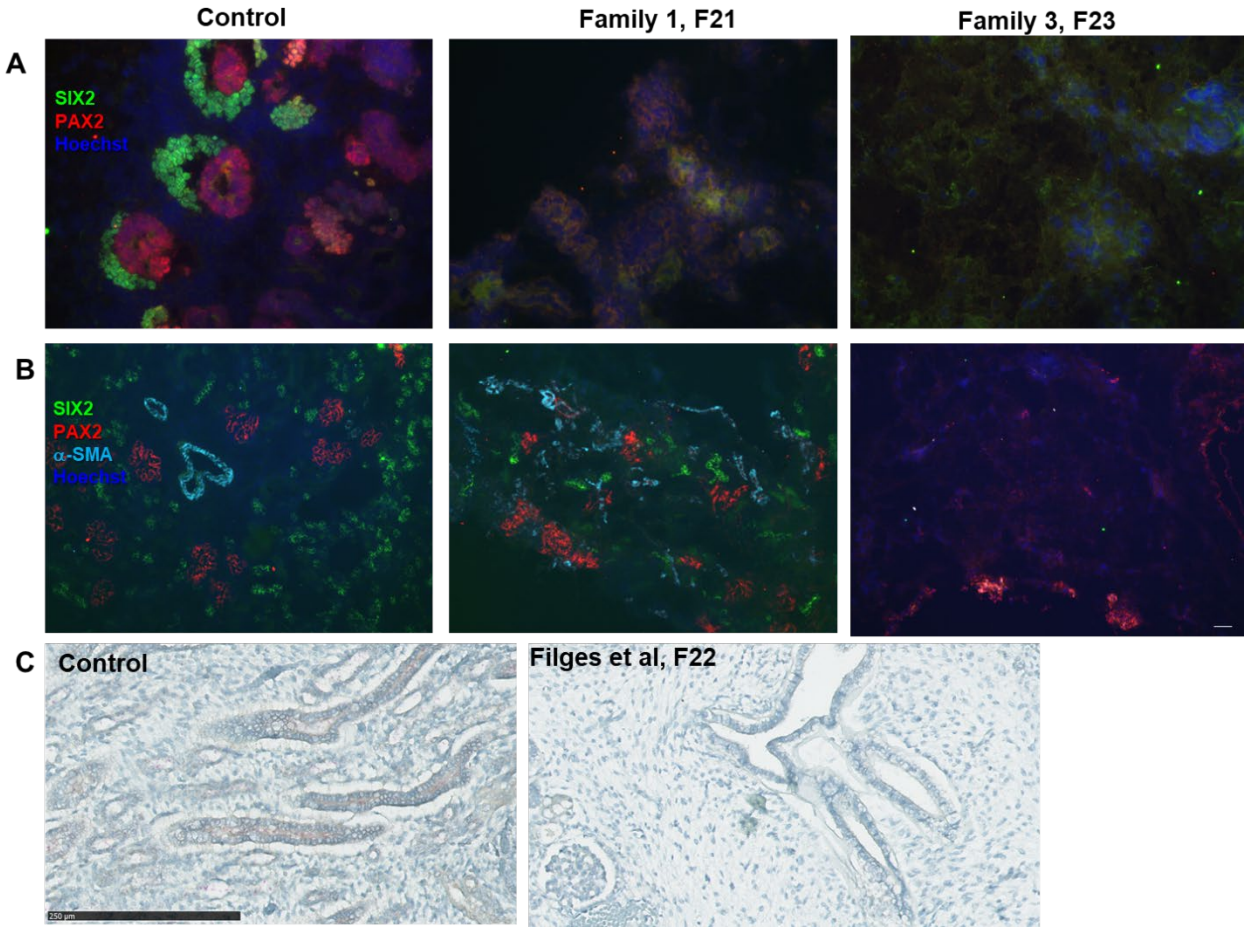

Figure S2. Immunohistochemistry of kidney biopsies from affected individuals. *(A,B) Cryosections of kidneys from control (25GW) or affected foetuses (Foetus 21, family 1; Foetus 23 family 3) were stained for either PAX2 (red, UB) and SIX2 (green, MM) (A) or Synaptopodin (red, glomeruli), E-cadherin (green, tubules) and α-SMA (cyan, vessels/fibrosis) in (B). (C) Sections of kidneys from control and affected foetuses described in Filges et al. (2014) were stained for KIF14 revealed with the OptiView DAB Detection Kitthen (brown) and for AcTub revealed with the UltraView Universal AP Red Detection Kit (red).*

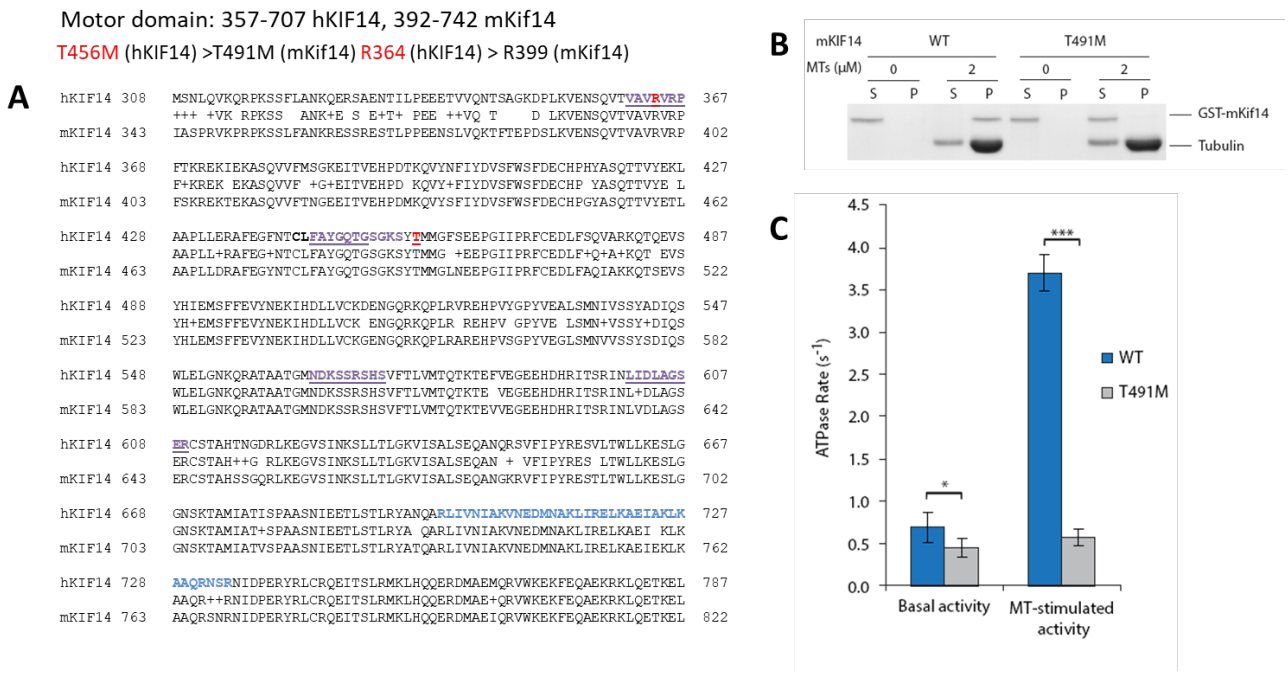

Figure S3. Defective microtubule binding and ATPase activity of murine Kif14 harbouring equivalent T456M mutation. (A) *Sequence alignment of motor domain of murine and human KIF14 where important functional subdomains are indicated in purple and blue and identified mutations in red. (B) The microtubule binding activity of the murine KIF14 motor constructs (GST-mKif14) was assessed as in Fig. 4. KIF14 motor constructs and tubulin are indicated. S, supernatant; P, pellet; MT, microtubules. (C) Basal and MT-stimulated ATPase activities of a KIF14 motor construct (GST-mKif14) is shown. Data from 4 independent experiments. Error bars, S.D.. Statistics: * $p \leq 0.05$; *** $p \leq 0.001$; by Student's T-test.*

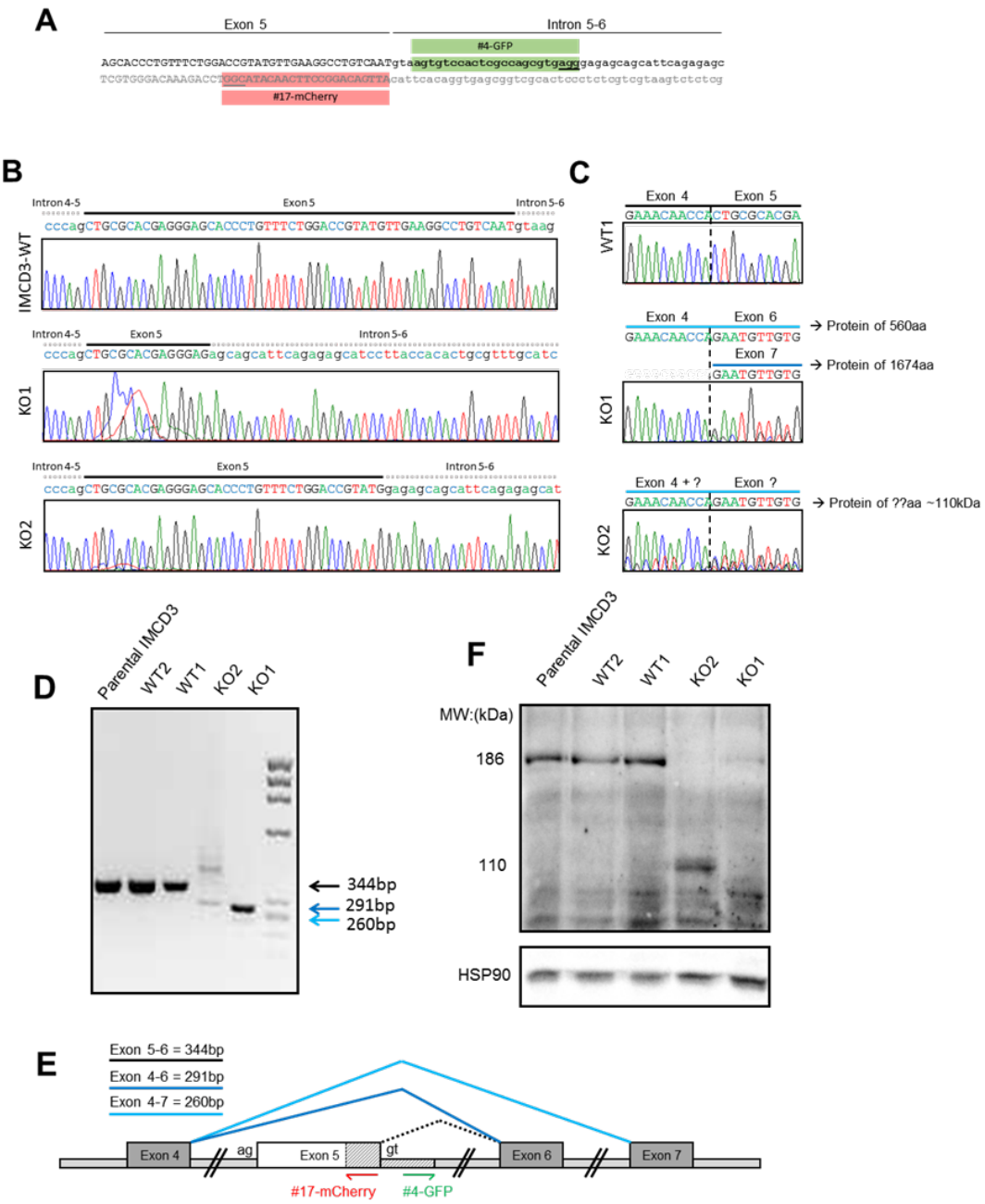

Figure S4. Characterisation of mutation events in CRISPR KO clones. *(A) Genomic DNA sequence of exon 5 of murine Kif14, showing the position and sequence of CRISPR guides used. (B) Sanger sequencing of genomic DNA extracted from Exon 5 of parental mIMCD3-WT cells and isolated KO clones, showing position of introns (grey) and exon 5 (black). (C) Sanger sequencing of cDNA transcribed from RNA extracted from parental mIMCD3-WT cells and isolated KO clones. Dotted line denotes end of exon 4, followed by exon 5 (black), exon 6 (light blue) and exon 7 (dark blue) sequences. Predicted size of protein, depending on exon splicing, is shown. (D) Agarose gel of RT-PCR products from mIMCD3-WT, CRISPR WT and KO clones. Size of bands is indicated, highlighted by arrows, colours corresponding to alternative splicing possibilities. (E) Schematic representation of alternative splicing demonstrated in CRISPR KO clones, showing the position of exons 4-7 and the guides used. (F) Lysates of mIMCD3, CRISPR WT and KO clones were analysed by Western Blot using antibodies against KIF14 (186kDa), and HSP90 as a loading control. Smaller fragment seen at 110kDa in CRISPR KO2 is indicated.*

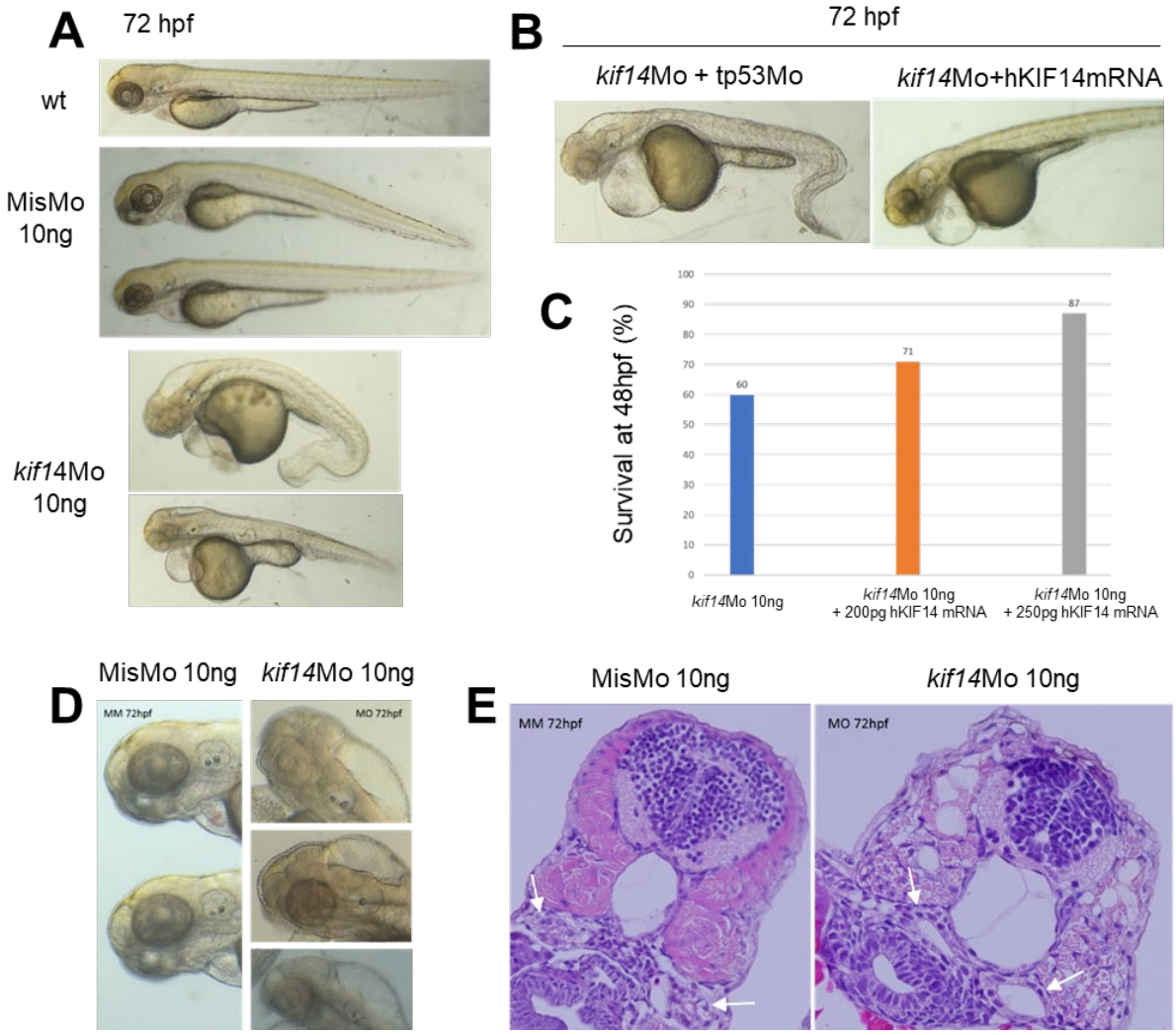

Figure S5. Morpholino-mediated knockdown of kif14 results in severe development defects, rescued by kif14 re-expression. *(A) Representative pictures of wild-type (WT) zebrafish or of zebrafish embryos (72hpf) injected with control (MisMo) and kif14 targeting morpholinos (kif14Mo). (B) Representative pictures of zebrafish embryos (72hpf) injected with kif14 targeting morpholinos (kif14Mo) together with morpholino targeting tp53 (tp53MO) or with human KIF14 mRNA. (C) Survival at 48hpf of kif14 morphants not injected (blue bar) or injected with 200 (orange bar) or 250 pg (grey bar) of human KIF14 mRNA. (D) Comparison of head size and otoliths in control and kif14 morphants, the latter showing smaller head size, hydrocephalus and variety of otoliths defects (additional, fused, single, misplaced). (E) Hematoxylin eosin sections of control and kif14 morphants (72hpf). Arrows show pronephric tubes which are dilated in kif14 morphants.*

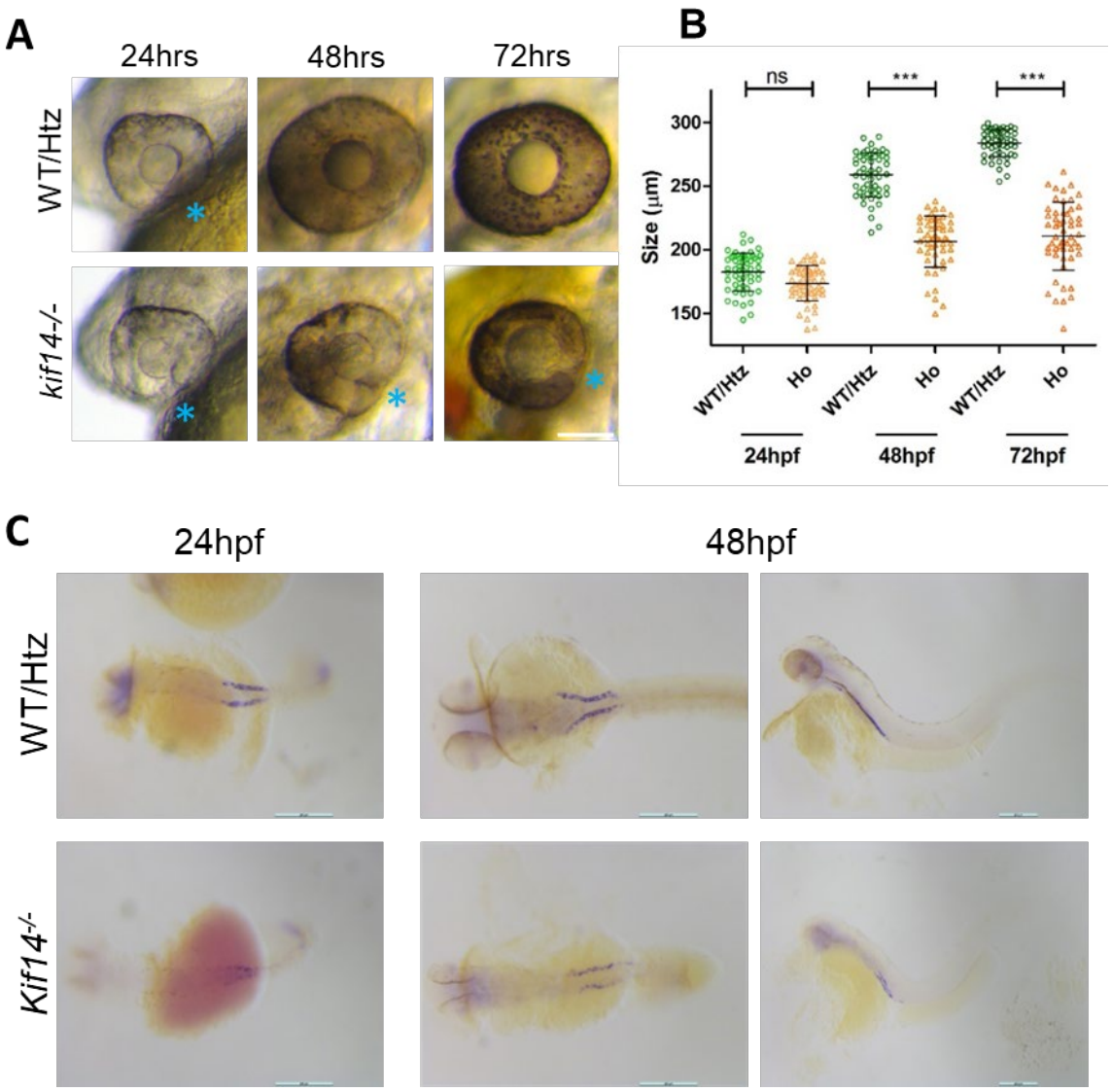

Figure S6. *(A) Representative images of the eyes of WT/Htz and* kif14$^{-/-}$ *embryos at 24hpf, 48hpf and 72hpf. Asterisks denote observed coloboma. Scale bars: 100 µm. (B) Quantification of eye size (diameter). ns = not significant, ***P< 0.0001 from n=3 independent experiments, t-test. (C)* In situ *hybridisation using probe against* slc20a1a *in WT/Htz (top row) and* kif14$^{-/-}$ *(bottom row) embryos at 24hpf (dorsal view, anterior to the left) and 48hpf (dorsal and lateral views, anterior to the left).*

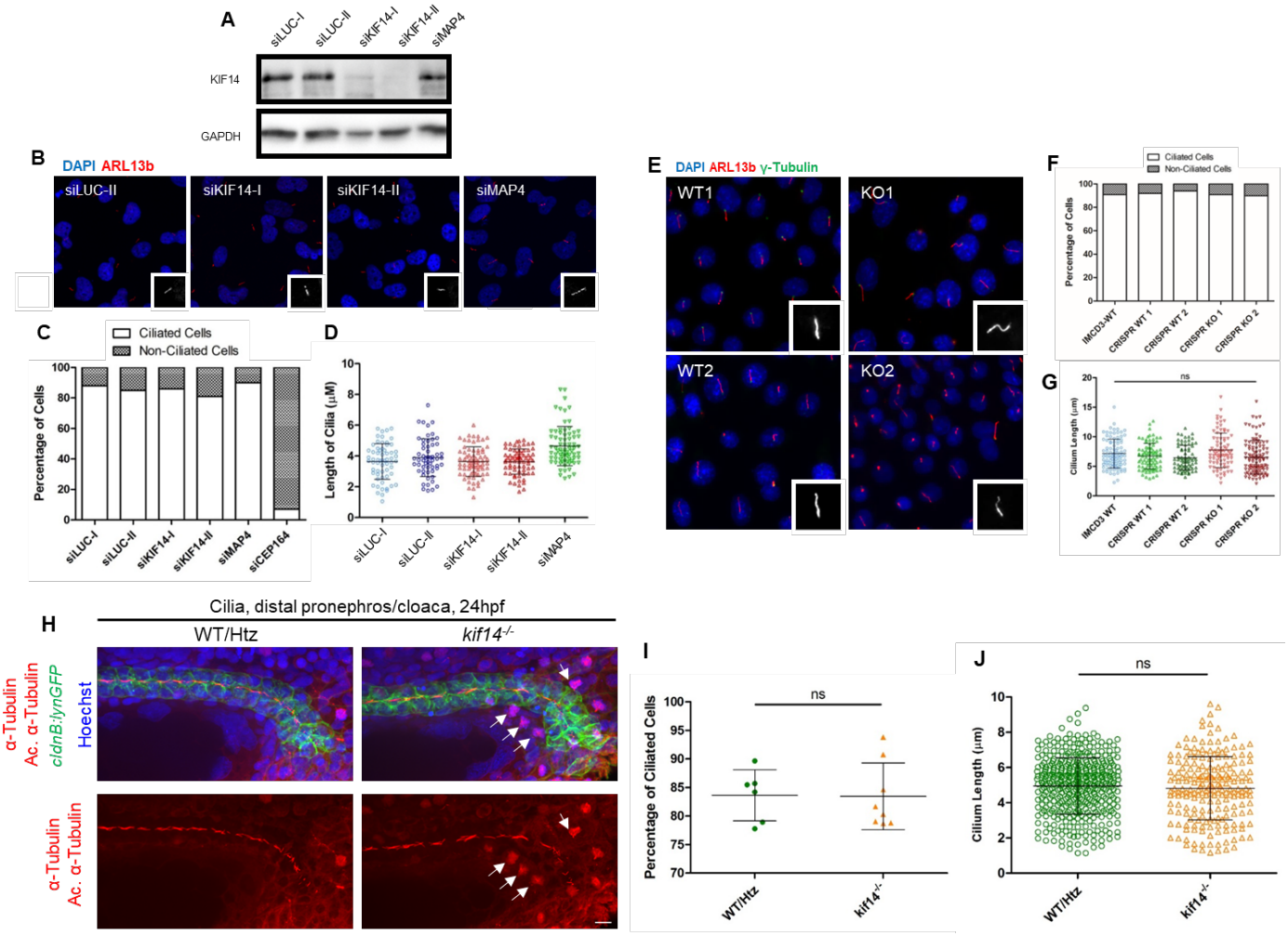

Figure S7 Ciliogenesis is unaffected by the loss of KIF14. *(A-D) RPE1 cells were transfected with siRNA targeting two different sequences of KIF14. Two sequences of siLUC were used as negative controls, and siMAP4 as a positive control for cilium elongation (Ghossoub et al., 2013). (A) Efficiency of transient knockdown was confirmed in lysates of transfected cells analysed by Western Blot using antibodies against KIF14 and GAPDH as a loading control. (B) Representative images from RPE1 cells transfected with corresponding siRNA, including siCEP164 as a positive control for ciliogenesis defects, and immunostained for ciliary membrane marker, ARL13b (red), and Hoechst (blue). Insets show higher magnification of cilia. The percentage of ciliated cells (C), and length of cilia (D) were quantified. (E) Immunofluorescence of CRISPR WT and KO mIMCD3 cells immunostained for ARL13b (red), γ-tubulin (green) and Hoechst (blue). Insets show higher magnification of representative cilia, ARL13b staining. The percentage of ciliated cells (F), and length of cilia (G) were quantified. ns = not significant, from n=3 independent experiments, Dunn's Multiple Comparison Test following the Kruskal-Wallis ANOVA test for length of cilia (D,G), and Fischer's exact test for percentage of ciliated cells (C,F). (G) Immunofluorescence of the distal pronephros of WT/Htz and kif14-/- Tg(cldnB:GFP) embryos at 24hpf immunostained for Hoechst (blue) and α-tubulin/acetylated-α-tubulin (red), used to quantify the percentage of ciliated cells (H) in at least 7 embryos. Quantification of length of cilia (I) performed based on ARL13b in WT/Htz or kif14-/- Tg(act2b:Arl13b-GFP) embryos at 24hpf (WT/Htz, n=7; kif14-/-, n=3) . ns = not significant. T-test for length of cilia (J), and percentage of ciliated cells (I).*

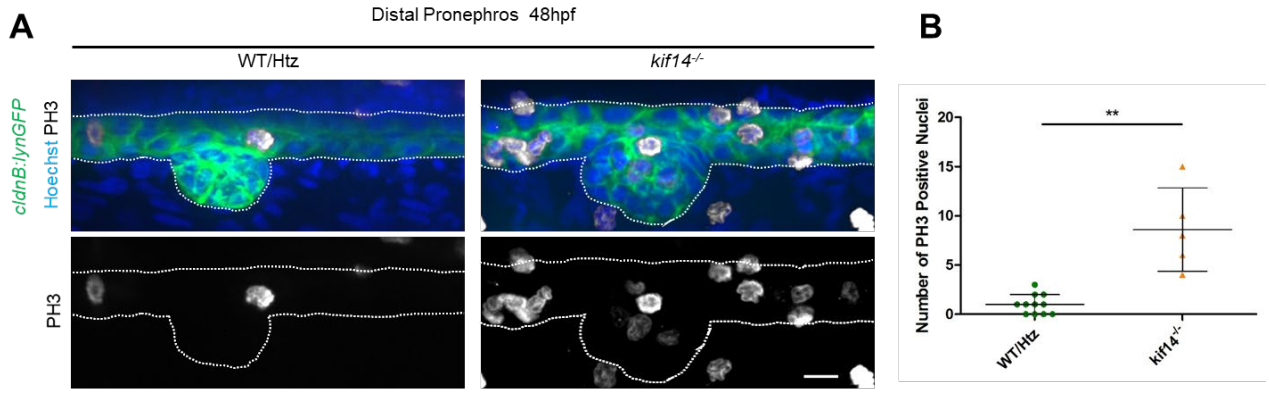

Figure S8. Increase in mitotic cells in distal pronephros at 48hpf of* kif14$^{-/-}$ *embryos. *(A) Immunofluorescence of the distal pronephros of WT/Htz and kif14$^{-/-}$ Tg(cldnB:GFP) embryos at 48hpf immunostained for Hoechst (blue) and PH3 (grey). Representative images of the Corpuscle of Stannius region. (B) Quantification of the total number of PH3+ cells in the distal pronephros. **P< 0.001 from n=1, T-test for PH3 quantifications.*

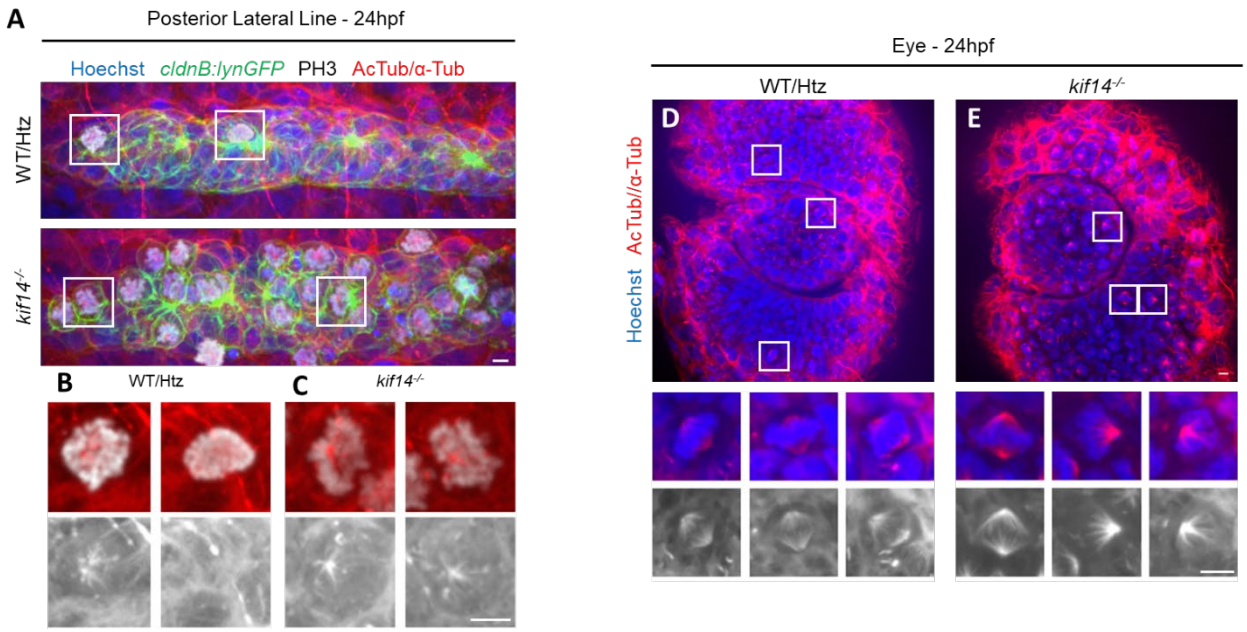

Figure S9. Loss of kif14 in vivo in zebrafish results in mitotic spindle defects. *(A-C) Different mitoses in lateral line of WT/Htz and* kif14$^{-/-}$ *Tg(cldnB:GFP) (B and C respectively) embryos at 24hpf visualised through immunostaining for PH3 (white), AcTub/αTub (red), Hoechst (blue). (D,E) Different mitoses in eye of WT/Htz and* kif14$^{-/-}$ *Tg(act2b:Arl13b-GFP) (D and E respectively) embryos at 24hpf visualised through immunostaining for AcTub/αTub (red) and Hoechst (blue). Insets show higher magnifications of representative mitoses.*

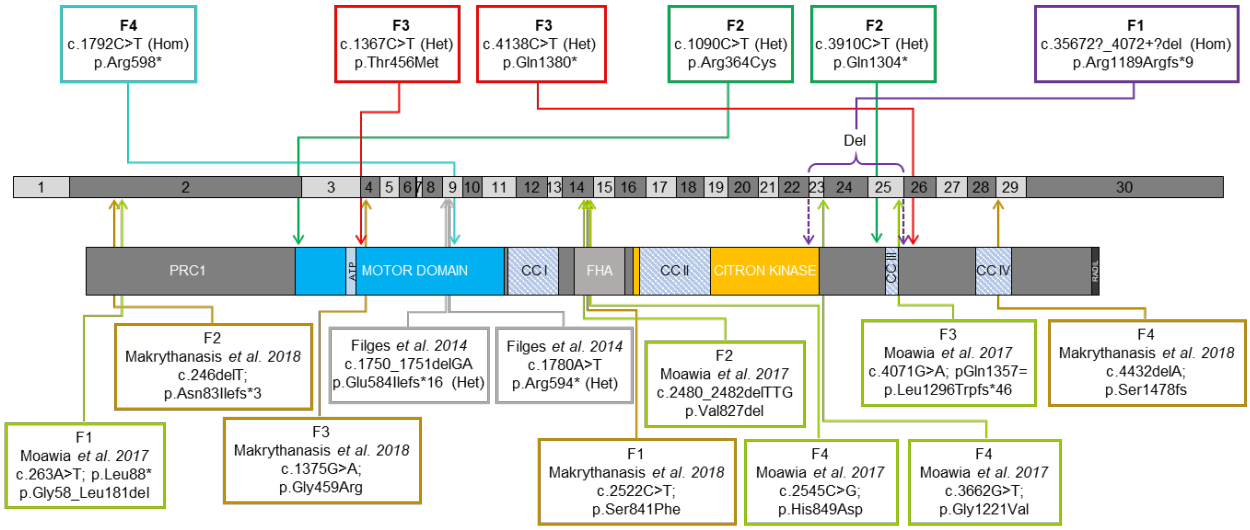

Individuals	Variation	Functional domain	Phenotypes
Family 1 Fetus (1)	p.Arg1189Argfs*9	C-terminal tail	**cRHD** Micrencephaly
Family 2 Fetuses (3)	p.Gln1304* p.Arg364Cys	C-terminal tail Motor domain	**cRHD (3)** Micrencephaly
Family 3 Fetuses (3)	p.Gln1380* p.Thr456Met	C-terminal tail Motor domain	**BRA (2) or RHD (1)** Micrencephaly
Family 4 Fetuses (4)	p.R598*	Motor domain	**cRHD (2) RHD (1) BRA (2)** Micrencephaly
Filges I. et al Fetuses (2)	p.R594* p.E584Ifs*46	Motor domain	**cRHD (1) BRA (1)** Micrencephaly
Moawia et al Family 1 (3)	**p.L88*/** **p.G58_L181del**	PRC1 binding early stop*	Microcephaly
Moawia et al Family 2 (2)	p.V827del	FHA	Microcephaly
Moawia et al Family 3 (3)	**p.Q1357=/** **p.L1296Wfs*46**	C-terminal tail	Microcephaly
Moawia et al Family 4 (2)	p.H847D **p.G1221V/p.G1221** **_K1296delInsVal**	FHA C-terminal tail	**Echogenic kidneys (1/2)** Microcephaly
Makrythanasis et al. Family 1 (2)	p.Ser841Phe	FHA	Mental retardation
Makrythanasis et al. Family 2 (2)	p.Asn83Ilefs*3	PRC1 binding early stop	Microlissencephaly
Makrythanasis et al. Family 3 (2)	p.Gly459Arg	Motor domain	Microlissencephaly
Makrythanasis et al. Family 4 (2)	p.Ser1478fs*	C-terminal tail	Microcephaly

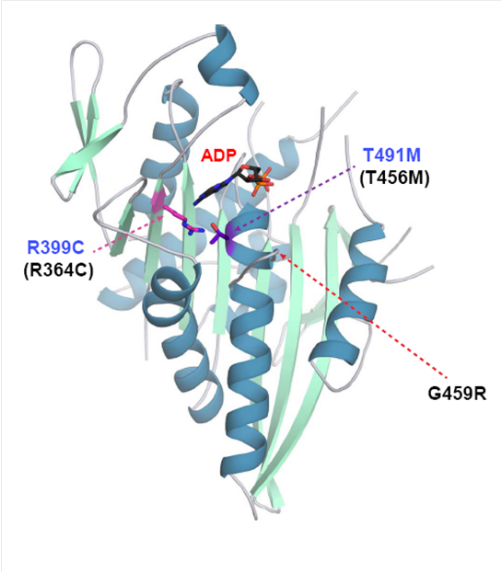

Figure S10. Genotype/phenotype correlation for KIF14 mutations in syndromic/isolated forms. *Table and scheme with all described KIF14 mutations, the functional domain of KIF14 affected and the brain and kidney phenotypes of the individuals. Number of affected cases per family is indicated in the first column. Mutations indicated in bold are to stress cases of with exon skipping leading to the expression of two different mRNA. Structure of mouse Kif14 motor domain is shown with the mutated residues labelled (mouse residues in blue and the corresponding human residues in black), including the G459R identified in an individual with isolated microcephaly.*

Supplementary Material and Methods

siRNA: Transfections of siRNA (Eurogentec) were performed using Lipofectamine RNAi MAX (Invitrogen, Life Technologies) with 80nM of siRNA. The following previously validated siRNA sequences, (Ghossoub *et al.*, 2013), were used; siLUC-I: $^{5'}$GCC-ATT-CTA-TCC-TCT-AGA-GGA-TG$^{3'}$, siLUC-II: $^{5'}$CGT-ACG-CGG-AAT-ACT-TCG-A$^{3'}$, siMAP4: $^{5'}$CTG-GCC-AGA-AGA-TAC-CAA-C$^{3'}$, siCEP164: $^{5'}$CAG-GTG-ACA-TTT-ACT-ATT-TCA$^{3'}$. siKIF14-I: $^{5'}$TTC-CCG-ATC-TCA-TTC-AGT-TTT$^{3'}$ (Gruneberg *et al.*, 2006) and siKIF14-II: $^{5'}$GTT-GGC-TAG-AAT-TGG-GAA-A$^{3'}$ (Carleton *et al.*, 2006).

Cell Culture: For siRNA in RPE1, cells were plated at ~40% confluence and cultured for 48hrs post-transfection in DMEM F:12 supplemented with 10% FBS alone. The medium was then replaced with OptiMEM (Gibco®, Life Technologies) and cells cultured for 48hrs to induce ciliogenesis before fixation and immunofluorescence as previously. For siRNA in HeLa, cells were plated at 40% confluence and cultured for 48hrs post-transfection in DMEM supplemented with 10% FBS alone before being processed for immunoblotting. CRISPR KO IMCD3 cells were similarly plated at ~40% confluence and subsequently cultured in OptiMEM to induce ciliogenesis, before being processed for either immunofluorescence or immunoblotting as before. Length of cilia and percentage of ciliated cells were measured as described elsewhere (Ryan *et al.*, 2018).

Antibodies: For immunofluorescence, cilia were stained using rabbit anti-Arl13b (1:400, Proteintech, 17711-1-AP), and centrosomes using goat anti-γ-tubulin (1:200, Santa Cruz, sc-7396). Nuclei were stained using Hoechst as before. For immunoblotting, primary antibodies used were rabbit anti-KIF14 (1:300, Bethyl, A300-233A [siRNA], or A300-912A [mIMCD3]) and mouse anti-GAPDH (Millipore, MAB374).

RNA extraction and RT-PCR: mRNA from CRISPR clones was isolated using Qiagen Extraction Kit and treated with DNase I. 2µg of mRNA was reverse-transcribed using Superscript II (Life Technologies, 18064) and amplified and Sanger sequenced using the following primers: forward $^{5'}$ACGATGATGGGGCTTAATGA$^{3'}$ and reverse $^{5'}$GACCGGGAGCTTTTATCGTT$^{3'}$ present within exon 3 and 7 of *Kif14* respectively.

Immunohistochemistry: Kidney sections were cut at a thickness of 4µm, put on positively charged glass slides and stained using the VENTANA BenchMark ULTRA automated slide stainer (Ventana Medical Systems, Inc.). Briefly, deparaffinisation, rehydration, and antigen retrieval were performed by CC1 (prediluted; pH 8.0) antigen retrieval solution. Slides were incubated with anti-KIF14 antibody 936

(rabbit polyclonal, 1:50; Abcam ab3746), followed by visualization with the OptiView DAB Detection Kit. Next, slides were incubated with anti-α-tubulin antibody (mouse monoclonal, 1:15,000; Sigma T6793), followed by visualization with the UltraView Universal AP Red Detection Kit. Slides were then counterstained with haematoxylin II and bluing reagent and coverslipped.

Morpholino and in situ *in Zebrafish*

For *kif14* knockdown carboxyfluorescein-modified antisense ATG morpholino oligonucleotides (*kif14*MO) were designed and obtained from GeneTools ($^{5'}$CTCCATGAGGTGTGCTGGAGCTCAT$^{3'}$) and injected into embryos at 1-2 cell stages at 10ng. For controls a mismatch oligo (MisMo) ($^{5'}$CTCGATCAGCTGTCCTGCAGCTCAT$^{3'}$) was injected into wild-type embryos. We performed concurrent p53 knockdown to exclude an off-target effect. We raised embryos and observed live and whole mount embryo phenotypes according to phenotypic assays previously described (Zaghloul *et al.*, 2011) for lethality, defective convergent extension including shortening of the body axis and body curvature, reduced head size. For rescue experiments, full-length human KIF14 plasmids were linearised with *Not*1 and *BamH*I, and mRNA synthesised using Ambion mMessage mMachine T7 Ultra transcription kit. Wild-type kif14 mRNA (200-250pg) was injected into the cytosol of 1-2 cell-stage embryos with *kif14* MO. For whole mount studies embryos were fixed with Dent's fixative (80% MeOH and 20% DMSO), stained with standard HE for pronephros phenotyping.

In situ hybridisation was performed in embryos at 24 and 48hpf as previously described, (Ryan *et al.*, 2018). Probe for *slc20a1a* was amplified from cDNA of 24hpf embryos using the sequences described previously (Nichane *et al.*, 2006).

Discussion

Congenital abnormalities of the kidney and urinary tract (CAKUT) are a heterogeneous group of disorders. CAKUT ranges in severity and can result from environmental factors, such as obesity and maternal diabetes, as well as genetic factors. To date, more than 50 genes have been associated with CAKUT, many of which encode transcription factors known to be important for renal or urinary tract development. Both autosomal dominant and autosomal recessive modes of inheritance have been described, although the identification of novel CAKUT genes is complicated by variable expressivity and incomplete penetrance. Previously, autosomal recessive mutations were identified in *KIF14*, in a single family with two affected foetuses. *KIF14* encodes a member of the kinesin superfamily, whose expression was shown to be highly regulated throughout the cell cycle, and to have an essential role in cytokinesis. The identified individuals presented with a severe, lethal syndrome affecting both brain and kidney development, and reminiscent of the severe ciliopathy Meckel-Gruber syndrome. *KIF14* was subsequently designated *MKS12*. Using whole- and targeted-exome sequencing, we identified mutations in individuals from an additional four families. We demonstrated that these mutations affected the activity of KIF14 and tissue sections from the brain and kidneys of affected individuals revealed the presence of binucleated cells. These results showed that the mutations impaired cytokinesis and highlighted parallels between brain and kidney development. To explore this further we used the zebrafish as an *in vivo* model. Initial observations of mutant zebrafish embryos revealed a number of ciliopathy-related phenotypes, in addition to recapitulating the severe syndrome of the affected individuals. However, further analysis showed that these effects resulted from an accumulation of cells arrested in mitosis. Taken together, our results confirm that mutations in *KIF14* result in a severe, lethal syndrome affecting both brain and kidney development, and which phenocopies a ciliopathy.

Identification of Mutations in *KIF14*

In order to identify novel mutations affecting kidney development we performed targeted-exome sequencing on a cohort of 204 unrelated individuals. 330 known or candidate CAKUT genes were sequenced, including *KIF14* (Heidet *et al*., 2017). Two individuals were identified harbouring mutations in *KIF14* which were predicted to be damaging. The affected foetus in family 1 harboured a homozygous deletion of exons 23, 24 and 25 (c.[3567-?_4072+?del]) leading to a frameshift (p.Arg1189Argfs*9). The affected foetuses in family two harboured compound heterozygous mutations associating a missense mutation in the motor domain (c.1090C>T [p.Arg364Cys]) with a nonsense mutation predicted to lead to a loss of the C-terminal region of the protein (c.3910C>T [p.Gln1304*]; (Heidet *et al.*, 2017)). In addition, in a third family three affected foetuses harboured

similar compound heterozygous mutations to those of the second family. A missense mutation in the motor domain (c.1367C>T [p.Thr456Met]) was associated with a nonsense mutation in the C-terminal region (c.4138C>T [p.Gln1380*]). Finally, our collaborators identified a family with four affected foetuses harbouring early homozygous nonsense mutations within the motor domain, (c.1792C>T [p.Arg598*]) similar to those of the first identified family (Filges *et al.*, 2014).

Incomplete penetrance, whereby unaffected individuals harbour heterozygous mutations predicted to be damaging, is often seen in familial cases of CAKUT. Interestingly, an autosomal recessive mode of inheritance with a complete penetrance was observed in the families we identified. Of these 11 foetuses, 8 presented with bilateral renal hypodysplasia, which were predominantly cystic (6/8), and 3 with bilateral renal agenesis. The aetiology of CAKUT phenotypes is complex, although bilateral renal agenesis is largely due to defects either in ureteric bud outgrowth, failure to invade the metanephric mesenchyme or defects in nephrogenesis. Renal hypoplasia, as well as renal agenesis, refers to an absence of differentiation, and is often due to defects in ureteric bud branching, or a premature exhaustion of progenitors in the metanephric mesenchyme. Renal dysplasia is a disorganised and poorly differentiated structure, which may form cysts. Histological sections of kidneys from affected foetuses revealed a highly disorganised architecture. Immunostaining of these sections for SIX2, a marker of the metanephric mesenchyme, and PAX2, an epithelial and mesenchymal marker, confirmed the absence of recognisable differentiating structures (Fig. 5D-G and Fig. S2A,B). The identification of individuals harbouring the same mutations but presenting with different phenotypes, as in the families herein, is frequently observed in CAKUT and is known as variable expressivity (van der Ven *et al.*, 2018). The characterisation of novel CAKUT genes and an understanding of the aetiology of the disease is, therefore, complicated by this phenomenon.

Recently, two other groups identified mutations in *KIF14* in eight families with individuals presenting mild to severe microcephaly but, mostly, without renal defects (Moawia *et al.*, 2017; Makrythanasis *et al.*, 2018). Moawia *et al.* (2017) described 10 affected individuals from 4 different families, while Makrythanasis *et al.* (2018) described 8 cases, again from 4 families (Fig. S10). In one of these families, the mutations were compound heterozygous, while the affected individuals of the 7 remaining families harboured homozygous mutations. Of these, 2 missense mutations and one single amino acid deletion were present in the forkhead homology-associated (FHA) domain (c.2522C>T [p.Ser841Phe]; c.2545C>G [p.His849Asp] and c.2480_2482delTTG [p.Val827del]). Of these mutations, c.2545C>G [p.His849Asp] was compound heterozygous and associated with a missense mutation in the C-terminal region (c.3662G>T [p.Gly1221Val]). The deletion of a single nucleotide was identified in another family, leading to a frameshift and predicted to introduce a stop codon 27aa downstream (c.4432delA [p.Ser1478fs27*]). Another single nucleotide variation appeared to be synonymous c.4071G>A

[p.Gln1357=]. A missense mutation in the motor domain was also identified c.1375G>A [p.Gly459Arg]. Finally, two families harboured mutations in the PRC1-binding domain predicted to lead to early stop codons (c.246delT [p.Asn83Ilefs*3] and c.263A>T [p.Leu88*]). Of these 18 individuals, renal defects were detected in one case via ultrasound. This individual, harbouring compound heterozygous missense mutations in the FHA domain and C-terminal region, presented with small echogenic kidneys, along with severe microcephaly. Interestingly, the brain malformations were more complex in this individual, as he also presented with cerebellar hypoplasia and corpus callosum agenesis. This complex phenotype, therefore, more closely resembles those described in our study. In order to delineate the differences between the individuals of the various families presenting either with isolated microcephaly or syndromic CAKUT, it is important to understand the functional consequences of the identified mutations.

Effect of Missense Mutations in the Motor Domain

A previous study by our collaborators established that Kif14 functions as a processive, plus-end directed motor and generated a 3D model of the protein (Arora *et al.*, 2014). Analysis of this model suggested that the identified missense mutations within the motor domain affected residues contacting ATP, and so would be expected to impact on hydrolysis. The ability of the KIF14 motor domains to bind microtubules and hydrolyse ATP was subsequently tested *in vitro*. The p.Arg364 variation identified here is equivalent to the Arg14 within KIF5B, which, when mutated, was shown to cause a significant decrease in microtubule-gliding velocity (Woehlke *et al.*, 1997). We demonstrated that the second missense variation, p.Thr456Met, is damaging, affecting the ability of the motor domain to bind microtubules and hydrolyse ATP (Fig. 3B,C). When co-expressed with CIT these variant forms of KIF14 failed to translocate onto microtubules, further demonstrating that these mutations render the kinesin inactive (Fig. 3D-F). In addition, we introduced these identified mutations into a ‘rigor mutant’ construct (Fig. A1G). Site-directed mutagenesis of the motor domain of KIF5B has identified a residue which when mutated prevents ATP hydrolysis, promoting tight microtubule binding, independently of the ATP-cycle. This mutated protein has, therefore, been described as a rigor mutant (Rice *et al.*, 1999). Mutagenesis of the equivalent residue in the KIF14 motor domain, p.Gly606Ala, led to an accumulation of KIF14 on microtubules upon overexpression in RPE1 cells (Fig. A1.A,B). When combined with either of the identified missense motor domain mutations, p.Thr456Met or p.Arg364Cys, the constitutive microtubule binding of the rigor mutant was impaired (Fig. A1C-F). Taken together these results demonstrated the pathogenicity of these mutations.

Effect of C-Terminal Truncation Mutations

Previous studies established a role for KIF14 during cytokinesis through interactions with citron kinase [CIT; (Gruneberg *et al.*, 2006)]. CIT binding was shown to require the coiled-coil domains within the C-terminal region of KIF14 (Watanabe *et al.*, 2013). Coiled-coils are tertiary protein structures known to be important for many different protein-protein interactions. Our co-immunoprecipitation assays revealed that the mutations we identified did not affect the ability of KIF14 to bind to CIT (Fig. 2G), including the R1189* nonsense mutation present within the previously mapped CIT-binding domain. This result allowed us to refine the CIT-binding domain of KIF14 to the second coiled-coil (CCII) from 922-1079aa. As binding to CIT was previously shown to activate KIF14 (Watanabe *et al.*, 2013), we investigated the impact of our mutations on this effect. While overexpression of the wild-type (WT) GFP-tagged KIF14 resulted in a diffuse cytoplasmic distribution within the cell (Fig. 2A), the co-expression with CIT caused KIF14 to translocate onto microtubules and accumulate at the cell periphery, likely at the plus-ends of microtubules (Fig. 3D). Upon overexpression, the C-terminally truncated forms of KIF14 translocated onto microtubules and accumulated at the periphery of the cell, even in the absence of CIT (Fig. 2D-F). This result suggested that these truncated forms of KIF14 were not responding to CIT-binding and existed in a constitutively processive state. The cargo-binding domains of kinesins are usually present in the C-terminal regions, and in addition to CIT binding, KIF14 is known to interact with Radil through the last amino acid (Ahmed *et al.*, 2012). Radil was recruited onto microtubules by KIF14, which prevented interactions with the GTPase Rap1, affecting integrin activation. The loss of KIF14 was shown to release Radil and to lead to impaired cell migration and focal adhesion disassembly through overactivated integrin signalling (Ahmed *et al*., 2012). The nonsense mutations resulting in C-terminally truncated proteins would also, therefore, lack the Radil-binding domain, which would likely impact upon cell migration and adhesion in the affected foetuses. As well as important roles in cell migration and adhesion, Rap1 has also been implicated in mitosis (Dao *et al.*, 2009). The impaired focal adhesion disassembly induced by the loss of interaction between KIF14 and Radil could also affect entry into mitosis. The nonsense mutations would, therefore, likely be highly deleterious and could affect various processes, such as adhesion and migration, known to be important in development.

Comparison of the effects of these C-terminal mutations with the rigor mutant also suggests that the accumulation of KIF14 at the cell periphery is due to procession of the kinesin towards the plus-ends of microtubules, providing insights into potential autoregulatory sequences within the protein. The activity of kinesins is known to be tightly regulated, and cargo binding through the C-terminal tail has been shown to be directly involved in this regulation. Homodimerisation of KIF17 leads to the auto-inhibition of one motor domain through the C-terminal, cargo-binding tail of the other. Cargo binding

to KIF17 releases the auto-inhibition of the motor domain, allowing binding to microtubules and processivity of the kinesin motor (Hammond *et al.*, 2010). Our *in vitro* data could, therefore, suggest that a mechanism of auto-inhibition may also be present in KIF14. The sequence of KIF14 encodes four coiled-coil (CC) domains (CCI-CCIV). As the CCIV domain is lost in all of the truncation mutations identified, which then accumulate at the plus-ends of microtubules, this domain could be required to negatively regulate KIF14 activity. We propose a mechanism whereby CCIV interacts with CCII, the CIT-binding domain, in order to maintain a closed conformation. This intramolecular interaction would prevent binding to microtubules and processivity. By binding to CCII, CIT would interfere with the intramolecular interaction with CCIV, changing the conformation of the protein and relieving this auto-inhibition. It has not currently been tested whether KIF14 acts as a dimer, but this analysis would aid in the understanding of the mechanisms through which KIF14 is activated. Within a coiled-coil, specific residues are essential for the formation of the tertiary structure. Site-directed mutagenesis of these residues within CCIV and CCII would provide further evidence for our proposed model. In addition, if KIF14 was found to function as a dimer, the identification and mutation of residues required for dimerisation could provide insight into the control of KIF14 activation.

In our analysis of KIF14 function, we generated a *Kif14* knockout in murine inner medullary collecting duct (mIMCD3) cells using CRISPR. These cells demonstrated the expected cytokinesis defects, with longer intercellular bridges, an increase in the percentage of binucleated cells and a mislocalisation of CIT (Fig. 4A-F). In order to conclude on the pathogenicity of the patient mutations, we transduced these cells with constructs encoding WT KIF14 or the p.Thr456Met and p.Gln1380* variations (Annexe Fig. A2). As previously observed, overexpression of KIF14 was highly problematic and failed for p.Gln1380* (Maliga *et al.*, 2013; Cullati *et al.*, 2017). Western blotting and immunofluorescence confirmed the re-expression of WT KIF14 and the p.Thr456Met variants, along with the GFP control (Fig.A2A-D). However, the level of protein expression was markedly different between KIF14-WT and the p.Thr456Met, complicating the interpretation of rescue data. Interestingly, the intensity of GFP localised to the midbody was higher with the p.Thr456Met variant than in KIF14 WT (Fig.A2E). While CIT localised to the midbody in cells re-expressing WT KIF14, the variant form failed to rescue CIT localisation (Fig.A2F,G), further confirming the effect of this inactivating mutation. Both demonstrated a reduction in the length of intercellular bridges, with the variant form appearing to show a greater reduction in length than the WT (Fig.A2H). Watanabe *et al.* (2013) demonstrated that the activity of KIF14 was required for the translocation of CIT from the cleavage furrow to the midbody. The increase in the length of intercellular bridges in the absence of KIF14 could be due to the impaired CIT localisation, which in turn, affects the recruitment of a number of factors required for efficient abscission. In contrast, the shorter intercellular bridges seen upon expression of p.Thr456Met suggest

that the pathogenicity of the mutation is not as simple as a complete loss of function. Our *in vitro* analyses demonstrate that this mutation no longer binds microtubules, although this does not appear to affect localisation to the midbody. Previous *in vitro* and *in vivo* analyses on the function of KIF14 have suggested that varying phenotypes can be seen based on the level of expression (Molina *et al.*, 1997; Ohkura *et al.*, 1997; C. Zhu *et al.*, 2005; Carleton *et al.*, 2006; Gruneberg *et al.*, 2006). siRNA-mediated knockdown of KIF14 in HeLa cells was shown to cause hypoploidy and apoptosis at lower efficiencies, while higher efficiency knockdown caused polyploidy (Carleton, 2006). These results strongly suggest that the expression of KIF14 must be tightly regulated throughout the cell cycle. It is possible that the increased recruitment of the p.Thr456Met variant form of KIF14 has an additional deleterious effect, which also results in cytokinesis failure through an as yet undetermined mechanism.

In addition to the cytokinesis defects observed upon invalidation of Kif14 in IMCD3 cells, we could also identify binucleated cells in brain and kidney sections from affected foetuses (Fig. 5D-K). Combined with the *in vitro* data, these results suggest that both the missense and nonsense mutations impair KIF14 function and cause a failure in cytokinesis. Intriguingly, the affected foetuses from families two and three carry compound heterozygous variations, which, according to our *in vitro* analyses, would result in the simultaneous expression of constitutively processive and inactive forms of KIF14 from opposing alleles. The cellular impact of this simultaneous expression was not investigated, but would likely depend on whether KIF14 functions as a dimer.

Isolated and Syndromic Phenotypes

In their recent report of cases of isolated microcephaly, Moawia *et al.* (2017) investigated the impact of *KIF14* mutations on fibroblasts from affected individuals from three of their families. Immunostaining of mitotic cells revealed that neither KIF14, nor CIT were present at the midbody. They also demonstrated an increase in the percentage of binucleated and apoptotic fibroblasts. The differences in the severity of phenotypes observed in the affected individuals identified in these recent studies and our own could be explained most simply by the phenomenon of incomplete penetrance. Although more frequently associated with autosomal dominant inheritance, incomplete penetrance can also occur in cases of autosomal recessive conditions (van der Ven *et al.*, 2018). This phenomenon is particularly common in CAKUT, as environmental and epigenetic factors are thought to play a significant role in the development of the disease. Alternatively, these phenotypic variations may be due to the differences between the mutations themselves. We showed that mutations of at least one allele in three of the four families we identified caused a constitutively processive protein. In two of these families the second allele encoded an inactive form of the protein. In the absence of patient material, we were unable to test these mutations directly, however it is possible that the constitutively

processive kinesin leads to a dominant negative effect. *In vitro*, we have observed that the truncating mutations we identified have toxic effects on the cells. In accumulating at the plus-ends of microtubules toward the periphery, these variant proteins appear to affect cell morphology. However, these effects were seen upon overexpression, and it is likely that these effects would be less severe at a physiological level. In addition, segregation of the autosomal recessive mutations was confirmed in each family and the heterozygous parents were healthy in each case. This would suggest that these mutations are not dominant negative, however, it remains possible that epigenetic factors could affect expression of a damaging mutation during development (Feil *et al.*, 2012). Epigenetics is known to play an important role during kidney development (Nicolaou *et al.*, 2015), and the healthy heterozygous parents may suppress the deleterious allele. Studying the expression of one or both alleles in the parents of these affected individuals could help to rule out this possibility.

Finally, the mutations described recently in cases of isolated microcephaly may be hypomorphic. Of the 9 mutations identified (7 homozygous, 2 compound heterozygous), two were present in the PRC1 domain, one in the motor domain, three in the FHA domain and three in the C-terminal region. These mutations, therefore, largely affect different domains to those we identified. The consequence at the protein level of the mutations identified within the FHA domain are unknown. FHA domains are important for phosphorylation-regulated protein-protein interactions, and have also been shown to play a role in intramolecular interactions in the case of KIF1A (J. R. Lee *et al.*, 2004; Huo *et al.*, 2012). However, no function has thus far been established for the FHA domain of KIF14. Many of the mutations were shown to induce alternative splicing events, which may be sufficient to generate a partially functional protein. cDNA was synthesised from RNA extracted from the blood of the affected individual harbouring the c.4071G>A/p.Gln1357= variation. RT-PCR revealed the presence of an alternatively spliced transcript lacking exon 25 and causing a frameshift and premature stop codon (p.Leu1296Trpfs*46). This C-terminally truncated protein would be expected to lack the, herein, proposed auto-regulatory CCIV domain, as well as the Radil-binding domain. However, the transcript encoding the c.4071G>A/p.Gln1357= synonymous variant was also observed. This expression of WT KIF14 alongside a C-terminally truncated protein is, therefore, reminiscent of the healthy heterozygous parents. As the individuals with isolated microcephaly express both a WT transcript and a C-terminally truncated transcript, this is likely less damaging than the homozygous loss of KIF14 in the affected foetuses we identified.

Alternative splicing in the N-terminal region was also demonstrated for the c.263A>T/p.Leu88* mutation identified in an individual with isolated microcephaly. The activation of a cryptic splice site led to a transcript lacking 123aa within the PRC1-binding domain (p.Gly58_Leu181del), which again may be sufficient for residual protein function. Although KIF14 was shown to bind to PRC1 (Gruneberg

et al., 2006), the effect of this binding on the activity of KIF14 has not yet been examined. In addition, the PRC1-binding domain was mapped to the entire N-terminal region adjacent to the motor domain, although the minimal sequence required has not been reported. Moawia *et al.* (2017) did not investigate the impact of this p.Gly58_Leu181del mutation on PRC1 binding, and it is possible that the interaction is not entirely lost. It is likely that with a functional motor domain and in the presence of the CIT binding and C-terminal regulatory domains this protein retains some function.

The effects of the mutations identified in Makrythanasis *et al.* (2018) were not studied, however we used the model of the 3D structure of murine Kif14 to examine the position of the c.1375G>A; p.Gly459Arg missense mutation. Interestingly, the p.Gly459 residue is outside of the ATP-binding site and the Arginine substitution is, therefore, likely to be less damaging than the p.Thr456Met and p.Arg364Cys mutations described herein. Introducing the p.Gly459Arg mutation into the KIF14 constructs we have characterised and studying the impact on ATP-hydrolysis and microtubule-binding would provide further insights into the damaging effects of this mutation.

In order to conclude on the genotype/phenotype correlations, further *in vitro* and *in vivo* functional analyses of the mutations identified by Moawia *et al.* (2017) and Makrythanasis *et al.* (2018) would be required. However, mutations in *KIF14* appear to be highly penetrant and analysis suggests that severe mutations, such as those described here and originally, (Filges *et al.*, 2014), lead to a lethal syndrome affecting both brain and kidney development. In the reported cases of isolated microcephaly, the mutations are likely to be hypomorphic and result in either the expression of a residual level of protein, or a protein with residual function.

KIF14 as a Novel Ciliopathy Gene?

Initial analyses suggested that KIF14 may be a novel ciliopathy gene. In addition to kidney defects, the affected foetuses identified by Filges *et al.* (2014) presented with phenotypes commonly seen in ciliopathies, such as agenesis of the corpus callosum and cerebellar hypoplasia (Edwards *et al.*, 2014; De Luca *et al.*, 2016). A previously unpublished siRNA screen aiming to identify new cilia-related genes revealed that the loss of KIF14 increased the length of cilia (A. Benmerah, unpublished). In addition, KIF14 was identified as a target of members of a family of transcription factors, RFX, known to control ciliogenesis (B. Durand, unpublished). Taken together, these data suggested that KIF14 may represent a novel ciliary kinesin.

By overexpressing GFP-tagged WT KIF14 and inducing ciliogenesis we revealed that KIF14 did indeed localise to the cilium. KIF14 was present at the basal body, along the ciliary axoneme and at the tip (AFig.3A). As the plus-ends of microtubules are present at the tip of cilia and KIF14 has been shown to act as a plus-end directed motor, it was possible that this novel ciliary localisation could be an artefact

of overexpression. We subsequently examined the localisation of a number of different GFP-tagged kinesins in ciliated RPE1 cells (Fig.A3A-E). KIF23, KIF5B, KIF9 and KIF26B are all frequently identified in large-scale screens aiming to characterise novel ciliary proteins (Gupta *et al.*, 2015; Mick *et al.*, 2015). While KIF23, KIF5B and KIF26B all localised to cilia and were present at the tip (AFig.3B-D), no such localisation could be seen for KIF9 (Fig. A3E). These results suggested that the ciliary localisation of KIF14 observed upon overexpression was not an artefact. In addition, the strong axonemal staining was unique to KIF14, while the N-terminal processive kinesin KIF5B accumulated primarily at the tip.

To further examine this potential novel localisation, we immunostained endogenous KIF14 in ciliated cells but did not observe a ciliary localisation (Fig. A4B). To verify that this localisation was not related to the fluorescent tag, we used a construct in which both GFP and KIF14 were expressed, but were unfused. Immunostaining with a KIF14 antibody again revealed an axonemal staining (Fig. A4C). We also mapped the domains of KIF14 required for ciliary localisation. The PRC1-binding domain and C-terminal tail regions were not required for ciliary targeting, which was seemingly dependent upon the motor domain (Fig.A4D-E). The expression level of KIF14 has previously been shown to be highly regulated (Carleton *et al.*, 2006), and ciliogenesis is tightly coupled to the cell cycle. The lack of ciliary localisation upon staining of endogenous KIF14 reflects previous difficulties in detecting ciliary proteins which has been proposed to be due to the effects of fixation (Nachury *et al.*, 2007; Conkar *et al.*, 2017). The combination of a very low level of expression in ciliated conditions with the difficulties in detecting certain ciliary proteins may explain the absence of axonemal staining of KIF14 at the endogenous level.

In order to determine the impact of the identified mutations on the ciliary localisation of KIF14, we transfected RPE1 cells with the variant constructs. Overexpression of the mutated forms of KIF14 affected both the ciliary localisation and length of cilia (Fig. A4G,H). The C-terminal truncations p.Gln1304* and p.Gln1380* both resulted in significantly shorter cilia. Interestingly, all three C-terminal truncations appeared to accumulate in the tips of cilia, causing them to become spoon-shaped. This effect has previously been demonstrated upon loss of IFT-A components (Qin *et al.*, 2011; Liem *et al.*, 2012), as well as in mice lacking intestinal cell kinase [ICK; (Chaya *et al.*, 2014)]. IFT-A proteins are required for retrograde intraflagellar transport (IFT), the movement of cargoes from the tip of cilia to the base, in association with cytoplasmic dynein 2 (DYNC2H1). Loss of IFT-A is therefore thought to lead to an accumulation of IFT and cargoes at the ciliary tip, which consequently becomes bulbous. Cilia in *ICK*$^{-/-}$ mouse embryonic fibroblasts (MEFs) were also shown to become spoon-shaped and to contain an accumulation of IFT-A and IFT-B proteins. ICK was proposed to regulate the switch between IFT-B-mediated anterograde transport and IFT-A-mediated retrograde transport (Chaya *et al.*, 2014). We subsequently sought to establish whether the overexpression of the C-terminally truncated KIF14 constructs was impacting IFT dynamics. Immunostaining of IFT-A and IFT-B

components in RPE1 cells transfected with the p.Gln1380* variant revealed an accumulation of IFT proteins at the tips of cilia (Fig. A4I,J), and so suggested that KIF14 could be participating in the regulation of IFT dynamics. However, we performed live-cell imaging upon transfection of WT and variant forms of KIF14, but failed to identify IFT-like movements. This result, therefore, suggested that KIF14 was not participating in cargo transport or dynamics.

To determine the function of KIF14 at cilia we performed an siRNA-mediated knockdown in RPE1 cells (Fig. S7A,B). Initially, we confirmed the results of the previous siRNA screen performed by the lab (A. Benmerah, unpublished), and observed an increase in the length of cilia upon KIF14 knockdown. However, this effect could not be repeated, and we subsequently observed no impact on either the percentage of ciliated cells, or the length of cilia (Fig. S7C,D). We also examined the cilia in the *Kif14*$^{-/-}$ mIMCD3 cell lines we generated, and once again failed to observe a difference in the percentage of ciliated cells, or the length of cilia (Fig. S7E-G). Taken together, these data demonstrated that KIF14 localised to cilia upon overexpression and that mutant forms affected cilia structure, but failed to definitely confirm that KIF14 was a novel ciliary kinesin or identify a function at cilia.

Zebrafish as a Disease Model

In order to establish a ciliary function for KIF14 and to examine the role of this kinesin in brain and kidney development, we used the zebrafish as an *in vivo* model. The zebrafish has become a widely-used model for many human diseases, including ciliopathies, and a number of ciliopathy-related phenotypes have been well characterised in zebrafish larvae (Song *et al.*, 2016). These phenotypes include body axis curvature, hydrocephalus, *situs inversus*, otolith defects, photoreceptor degeneration and pronephric cysts. By 2 days post-fertilisation (2dpf) the *kif14*$^{-/-}$ embryos recapitulated the severe syndrome described in the affected foetuses we identified. We observed a severe microcephaly and pronephric cysts, demonstrating a conserved role for kif14 in brain and kidney development in the zebrafish (Fig. 6A-E). In addition, they also had many classical ciliopathy phenotypes, including body curvature and otolith defects (Fig. 6A and Fig. 7A,B). Otoliths are structures composed of biominerals, whose formation at the tips of tether cilia on the surface of sensory neurons has been suggested to rely, at least partially, on the presence of cilia within the otic vesicle (Stooke-Vaughan *et al.*, 2012). In the absence of tether cilia, otoliths are formed, but dock directly onto the apical surface of sensory neurons. In the absence of sensory neurons and tether cilia, otoliths again form, but fail to dock and form a single large aggregate within the vesicle. Analysis of otoliths in the *kif14*$^{-/-}$ embryos revealed that they were often smaller, fused or incorrectly positioned within the vesicle, all phenotypes which could be related to ciliary defects. Using a transgenic line in which the ciliary membrane protein Arl13b is fused to GFP, we observed a significant decrease in the number of

cilia in the otic vesicles of *kif14*$^{-/-}$embryos compared to siblings (Fig. 7C). These results indicated that KIF14 may indeed have a ciliary function. Pronephric cysts are another established ciliopathy phenotype. The pronephros is composed of a heterogeneous population of cells possessing a single primary or motile cilium, or multiple motile cilia. Defects in either the formation or function of cilia leads to the perturbation of flow within the tubule and subsequent cyst formation (Drummond *et al.*, 2016; Marra *et al.*, 2016). Analysis of the distal pronephros did not reveal differences in the percentage of ciliated cells or the length of cilia, suggesting that the pronephric cysts were not resulting from ciliary defects (Fig. S7H-J). In addition, we could not identify any defects in laterality, implying that the cilia of the Kuppfer's vesicle, the equivalent of the embryonic node, were unaffected. Taken together, these data suggested that the phenotypes observed in *kif14*$^{-/-}$ embryos may not be directly due to defects in the formation or function of cilia.

Cilia are present on the surface of many cell types and act as signalling platforms, but their formation and disassembly are highly regulated processes tightly coupled with the cell cycle. Cilia are formed in quiescent, or G0 cells and are nucleated from the basal body originating from the mother centriole in primary cilia, or amplified centrioles in multiciliated cells. As the centrioles of the centrosome form the mitotic spindle in mammalian cells, the cilium must be disassembled before the cell enters mitosis. Immunostaining of *kif14*$^{-/-}$ embryos revealed a significant number of cells arrested in mitosis. In the otic vesicle, this increase in the number of cycling cells corresponded with the decrease in ciliogenesis (Fig. 7E,F). Interestingly, despite this increase in cells blocked in mitosis we did not observe a difference in the size of the otic vesicle. The otic vesicle develops from the formation of a lumen in the otic primordium, derived from the otic placode (Hoijman *et al.*, 2015). The formation of a lumen, or lumenogenesis, is an important process throughout zebrafish development, from the formation of the neural tube to the pronephros. Different mechanisms are used to form lumen in different structures. Expansion of the lumen of the otic vesicle has been shown to rely, partly, on mitosis of the epithelial cells lining the vesicle. Nuclei migrate apically towards the surface of the lumen prior to the onset of mitosis. During mitosis cells become round and contribute to a mechanical stretching of the anteroposterior axis (Hoijman *et al.*, 2015). The increase in the number of larger, round mitotic cells contributing to lumen expansion of the otic vesicles of *kif14*$^{-/-}$ embryos likely explains the discrepancy in otic vesicle size.

Interestingly, the contribution of mechanical stretch to lumen formation in the pronephros has not been investigated. Lumenogenesis has been shown to occur around 20-22 somites, and to require the establishment of an apicobasal polarity in the renal precursors (Gerlach *et al.*, 2014). It is possible that increased cell rounding during mitosis may also contribute to the establishment of a lumen in the pronephros. We observed an increased number of mitotic cells in the glomerular and distal regions of

the pronephros of *kif14*$^{-/-}$ embryos (Fig. 77G,H and Fig. S8). Additionally, we also observed tubule dilations (data not shown) and pronephric cysts (Fig.6E). The individual contributions of ciliary functions, mitosis and apicobasal polarity to the development of the pronephros would be difficult to evaluate. However, the role of the mechanical forces of increased mitotic rounding on lumen, or even cyst formation, remain an interesting avenue to explore. Interestingly, the causes of glomerular cyst formation in the zebrafish are not completely understood. Cysts were proposed to occur primarily in response to defects in cilia-mediated flow within the pronephros (Kramer-Zucker *et al.*, 2005). As we did not observe obvious differences in ciliogenesis within the pronephros (Fig. S7H-J), and live imaging revealed that cilia were motile (data not shown), the mechanism behind cyst formation in the *kif14*$^{-/-}$ is unknown. However, we observed tubule dilations in the *kif14*$^{-/-}$ embryos prior to the onset of glomerular filtration (data not shown), and it is possible that these dilations are sufficient to impair the flow of filtrate, resulting in an accumulation of fluid at the glomerulus.

Previous reports have shown that mitosis in the pronephros occurs predominantly in the neck region and in the distal pronephros (Vasilyev *et al.*, 2012). Cell proliferation in the distal pronephros was proposed to occur in response to the mechanical stretch induced by collective cell migration towards the glomerulus, which begins at 29hpf (Vasilyev *et al.*, 2012). This migration is important for the formation of the convolutions of the developing proximal convoluted tubule (PCT) region of the pronephros and was suggested to require glomerular filtration. Despite mitosis being proposed to be induced by collective cell migration, mitotic inhibition failed to prevent migration (Vasilyev *et al.*, 2009). *In situ* hybridisation of *slc20a1a*, a well-characterised marker of the PCT, demonstrated a defect in migration in the *kif14*$^{-/-}$ embryos (Fig. S6C). Injection of fluorescent dextran into the cardiovascular system of zebrafish embryos is used to study defects in glomerular filtration. Injection of the *kif14*$^{-/-}$ embryos did not reveal obvious glomerular filtration defects (data not shown). In mammalian cells, KIF14 has been shown to interact with Radil, promoting cell migration and adhesion (Ahmed *et al.*, 2012). This interaction remains to be tested in the zebrafish, however, it is possible that this additional migratory phenotype in the *kif14*$^{-/-}$ embryos is due to a loss of Radil interaction.

In conclusion, the *kif14*$^{-/-}$ embryos recapitulated the syndromic brain and kidney phenotypes we observed in the affected foetuses. Although this syndrome was originally thought to correspond to a ciliopathy (Filges *et al.*, 2014), the observed phenotypes in the zebrafish were not directly related to ciliary defects, but to an increase in cells arrested in mitosis. The corpus callosum agenesis and cerebellar hypoplasia of the affected foetuses, which were considered ciliopathy phenotypes (Edwards *et al.*, 2014; De Luca *et al.*, 2016), are likely explained by impaired progenitor proliferation. The mitotic defects in the *kif14*$^{-/-}$ embryos were visible throughout, including the otic vesicle, pronephros and neural tissue (Fig. 7D). However, given that KIF14 was widely reported to have a role in cytokinesis and

that binucleated cells were observed in kidney and brain section of the affected foetuses, the absence of such defects was unexpected (Ohkura *et al.*, 1997; Carleton *et al.*, 2006; Gruneberg *et al.*, 2006). Further analysis of the PH3-positive nuclei in various organs, including the otic vesicle (Fig. 8), the posterior lateral line (Fig. S9A-C) and the eye (Fig. S9D,E) revealed a significant increase in the number of cells with condensed chromosomes associated with a monopolar spindle (Fig. 8B). This result revealed an earlier failure in mitosis than expected, and suggested that kif14 was functioning in the assembly of the mitotic spindle in zebrafish.

Interestingly, in contrast to the reports stating that KIF14 had a role in cytokinesis, two groups demonstrated a role as a chromokinesin (Molina *et al.*, 1997; C. Zhu *et al.*, 2005). These studies showed that KIF14 was required for the efficient segregation of chromosomes at the metaphase plate. Both Molina *et al.* (1997) and Ohkura *et al.* (1997) examined the impact of mutations in *Klp38B*, the paralogue of *KIF14* in *Drosophila melanogaster*. Molina *et al.* (1997) suggested that the mutations in their study were loss of function leading to chromosome segregation defects, while Ohkura *et al.* (1997) used hypomorphic mutations resulting in cytokinesis defects, and that this difference explained the discrepancies in the phenotypes observed. Carleton *et al.* (2006) showed that the most efficient siRNA-mediated knockdown of KIF14 in HeLa cells caused polyploidy and cytokinesis defects. This report suggested that the siRNA used by C. Zhu *et al.* (2005) was less efficient and so resulted in defects in chromosome segregation defects. These conflicting studies suggest that the expression of KIF14 is highly regulated throughout the cell cycle, and that the phenotypes observed will depend on the efficiency of the downregulation of expression. The zebrafish line that we have characterised harbours a nonsense mutation after the motor domain (Fig. 6A). This mutation is similar to that of the family identified by our collaborators, and likely leads to RNA decay and an absence of protein expression, however this was not directly tested. Given that the *kif14*$^{-/-}$ embryos present a chromosome segregation defect, rather than the expected cytokinesis defect, it will be important to examine the precise effect of the mutation on the expression of kif14. In addition, zebrafish zygotes initially rely on maternal transcripts and zygotic gene transcription does not begin until the midblastula transition. The stability of the maternal transcripts will impact the length of time during which WT kif14 may be expressed in the *kif14*$^{-/-}$ embryos. This maternal contribution could be significant as the presence of residual KIF14 protein appears to affect the phenotype observed. Further characterisation of the regulation of protein expression and localisation in cultured cell models and the zebrafish, as well as the stability of the maternal transcripts in zygotes, will be important to delineate the differences in the observed phenotypes. This analysis would also contribute to an understanding of the genotype/phenotype correlation in patient mutations.

Role of KIF14 in Development

The *kif14*$^{-/-}$ zebrafish embryos described herein recapitulate the syndromic brain and kidney defects observed in the affected foetuses we identified. Previously, a *Kif14*$^{-/-}$ mouse model was reported with isolated microcephaly, reflecting the phenotype recently reported by Moawia *et al.* (2017) and Makrythanasis *et al.* (2018). The common phenotype in every case is the presence of a primary microcephaly, which has frequently been associated with mutations in genes involved in mitosis. The development of the mammalian brain has been shown to be highly sensitive to disruptions of the cell cycle. The initial mitoses required for the amplification of neuroepithelial cells before the onset of neurogenesis have been shown to be symmetrical. A number of different mechanisms have been proposed for maintaining symmetry in mitosis. The orientation of the mitotic spindle perpendicular to the ventricular zone has been associated with the self-renewal of neuroepithelial cells. This may be related to the symmetrical division of a small patch of membrane at the ventricular surface, composed of, as yet, largely uncharacterised fate determinants. A failure to maintain the perpendicular position of the cleavage plane impacts the subsequent cell fates. The premature switch to asymmetric mitosis, and the resulting failure to sufficiently amplify neuroepithelial cells prior to the onset of neurogenesis has been shown to lead to microcephaly. Despite being ubiquitously expressed, loss of KIF14 leads to defects specifically in brain and kidney development. Binucleated cells could be observed in brain and kidney sections from the affected individuals, demonstrating that the loss of KIF14 causes cytokinesis failure. These mitotic defects are likely highly deleterious, significantly reducing the progenitor population during early development. An understanding of the parallels between the mechanisms of mitosis in the brain and kidney provides insights into the impact on these organs.

The development of the mammalian kidney has also been shown to be sensitive to changes in the orientation of cell division. Mitotic spindles are oriented perpendicular to the apical-basal polarity of the developing nephron, with the intercellular bridge positioned at the apical side (Yang *et al*., 2013; Gao *et al*., 2017). Interestingly, mitosis in the ureteric tips during branching has been shown to occur via an unusual mechanism of delamination and cell dispersal (Packard, *et al*., 2013). Cells divide within the lumen, with one daughter cell reinserting into the epithelium at the site of the original mother cell, while the remaining daughter cell enters the epithelium a short distance away. The significance of this luminal mitosis remains to be elucidated, however it highlights certain parallels with the development of the brain. Mitosis in the brain has been proposed to occur at the ventricular zone in order to facilitate the access to certain fate determinants present within the cerebrospinal fluid in the developing ventricles. These, as yet, uncharacterised factors are proposed to play a role in regulating the balance between self-renewing and neurogenic divisions. It is possible that similar mechanisms exist during kidney development and affect self-renewal or differentiation of progenitor cells.

During mitosis, proteins required for the abscission of daughter cells are recruited to the intercellular bridge to form the midbody ring. Initially this structure was believed to be an artefact but has recently been the subject of intense study. Abscission can occur asymmetrically, whereby one of the two daughter cells retains the midbody, or symmetrically, where neither cell inherits the midbody, which is instead released into the extracellular space (Crowell *et al.*, 2014; Dionne *et al.*, 2015). Interestingly, several groups have proposed that the midbody can act as a signalling platform and retention by one of the two cells is implicated in maintenance of a progenitor-state. During development of the murine brain, division of the neuroepithelial cells at the ventricular zone has been shown to lead to an accumulation of midbodies within the cerebrospinal fluid, suggestive of symmetrical abscission, with neither cell retaining the midbody (Dubreuil *et al.*, 2007). It follows, therefore, that this symmetry in cytokinesis is one of the mechanisms required for self-renewal of the progenitor population. Although, the release of midbodies into the cerebrospinal fluid may simply be a consequence of this requirement for symmetrical mitosis early in development. Midbody release may act as an efficient mechanism to control expression levels of mitotic proteins within the cell. Whereas the importance of various mitoses has been explored during brain development, less is known about the kidney. We demonstrate here the accumulation of midbody rings within the lumen of ureteric buds during early human foetal kidney development, likely due to the symmetrical abscission of the two daughter cells (Fig. 5). These midbodies are positive for KIF14, suggesting perhaps a distinct role in ensuring symmetrical abscission. If midbody retention has been linked to maintenance of a progenitor state, the physiological consequences of midbody release are not yet well understood. Midbodies released into the lumen of developing ureteric buds could be an artefact of symmetric abscission occurring at the luminal surface, or equally could act to transmit signals throughout the developing organ, potentially inducing ciliogenesis. It is possible that the regulation of symmetrical and asymmetrical mitoses could play an important role during development and patterning of the kidney and these possibilities warrant further investigation. The use of transgenic zebrafish lines, such as anillin-eGFP (Cepero Malo *et al.*, 2017), would reveal whether these mechanisms of midbody release are conserved. It would then be important to establish whether this midbody release is present in the brain and kidneys of the *kif14*$^{-/-}$ embryos, and also whether any loss of midbody release was specific to *kif14*$^{-/-}$ embryos and not all cytokinesis mutants. The importance of midbodies in kidney development would be difficult to establish as the development of pronephric cysts can occur in relation to many different defects, but the comparison of different zebrafish mutants may be informative. Removal of the cerebrospinal fluid from zebrafish embryos has been shown to lead to cell death in the developing brain, while the injection of certain cell survival promoting factors rescued these defects (Chang *et al.*, 2016). The injection of midbody-associated proteins or purified midbodies themselves, (Skop *et al.*, 2004), into

the brain ventricles of *kif14*$^{-/-}$ embryos could help to reveal the importance of these factors and their potential roles as signalling centres during brain development.

Interestingly, CIT is also present at the midbody, and colocalises with KIF14. Loss of CIT leads to cytokinesis defects *in vitro* and recently mutations in *CIT* have been identified in individuals with microcephaly (Basit *et al.*, 2016; Harding *et al.*, 2016; Li *et al.*, 2016). Two affected individuals within one family presented with renal aplasia or agenesis, resulting in neonatal lethality, and an additional individual presented with unilateral renal agenesis. Several of the affected individuals also had complex brain malformations, including corpus callosum agenesis and cerebellar hypoplasia. These phenotypes are similar to those observed with mutations in *KIF14*, which, given that they function together during cytokinesis, is perhaps unsurprising. The genotype/phenotype correlation in the cases of *CIT* mutations also appears to be complex, with kidney involvement revealing incomplete penetrance. The rodent models of the loss of *Cit* demonstrate microcephaly, but no renal defect, again resembling mutations in *Kif14* (Sarkisian *et al*., 2002). Further characterisation of the precise roles of both KIF14 and CIT at the midbody will be required to delineate these differences.

In conclusion, we provide further evidence that mutations in *KIF14* can lead to a novel, lethal syndrome of microcephaly and CAKUT. Contrary to the initial report, this syndrome phenocopies a ciliopathy, and represents a rare association of bilateral renal agenesis and microcephaly within the CAKUT spectrum. In addition, most of the known CAKUT genes encode transcription factors or actors in key signalling pathways. *KIF14*, as a molecular motor and part of the cytokinesis machinery, is an uncommon CAKUT gene. However, Lindstrom, De Sena Brandine*, et al.* (2018) recently demonstrated that mitotic genes are highly upregulated during early kidney development. The identification of mutations associated with CAKUT in additional cytokinesis genes would aid in the understanding of the molecular mechanisms behind the pathogenesis of *KIF14* mutations.

Conclusion

Congenital abnormalities of the kidney and urinary tract (CAKUT) comprise a large spectrum of developmental malformations and represent the leading cause of end-stage renal disease during childhood. The identification of novel candidate genes is often complicated by variable expressivity and incomplete penetrance. Despite these complexities, mutations in more than 50 genes have been associated with CAKUT, many of which encode transcription factors or actors in signalling pathways key to kidney development.

Previously, biallelic loss-of-function mutations were identified in *KIF14*, a mitotic kinesin required for cytokinesis, in foetuses presenting with bilateral renal agenesis or RHD and associated with severe microcephaly (Filges *et al.*, 2014). This phenotype was reminiscent of Meckel-Gruber syndrome, part of the spectrum of diseases related to defects in the structure or function of the primary cilium. We identified novel mutations in *KIF14* in foetuses presenting with similar phenotypes to this initial report. Through the functional characterisation of the role of KIF14, both *in vitro* and *in vivo*, we have shown that these mutations result in a phenocopy of a ciliopathy. Using the zebrafish as a model organism, we demonstrated that the loss of kif14 reduced ciliogenesis, however this was due to an accumulation of cells arrested in mitosis.

Interestingly, many of the genes currently known to be associated with microcephaly function during mitosis. However, KIF14, as a molecular motor and part of the cytokinesis machinery, represents an uncommon CAKUT gene. Recent reports have begun to demonstrate the importance of mitotic genes during specific phases of renal development. In addition, our analysis of foetal kidney sections has revealed parallels in the mechanisms of mitosis during the development of these two organs. Further characterisation will be required to elucidate the precise role of KIF14 during this process. The identification of candidate genes in individuals with severe syndromes resembling that described herein, would provide further insights into the similarities between brain and kidney development.

References

Aaku-Saraste, E., Hellwig, A., & Huttner, W. B. (1996). Loss of occludin and functional tight junctions, but not ZO-1, during neural tube closure--remodeling of the neuroepithelium prior to neurogenesis. *Dev Biol, 180*(2), 664-679. doi:10.1006/dbio.1996.0336

Acar, S., Carlson, D. B., Budamagunta, M. S., Yarov-Yarovoy, V., Correia, J. J., Ninonuevo, M. R.*, et al.* (2013). The bipolar assembly domain of the mitotic motor kinesin-5. *Nat Commun, 4*, 1343. doi:10.1038/ncomms2348

Adams, G. M., Huang, B., & Luck, D. J. (1982). Temperature-Sensitive, Assembly-Defective Flagella Mutants of CHLAMYDOMONAS REINHARDTII. *Genetics, 100*(4), 579-586.

Ahmed, S. M., Theriault, B. L., Uppalapati, M., Chiu, C. W., Gallie, B. L., Sidhu, S. S.*, et al.* (2012). KIF14 negatively regulates Rap1a-Radil signaling during breast cancer progression. *J Cell Biol, 199*(6), 951-967. doi:10.1083/jcb.201206051

Aken, B. L., Achuthan, P., Akanni, W., Amode, M. R., Bernsdorff, F., Bhai, J.*, et al.* (2017). Ensembl 2017. *Nucleic Acids Res, 45*(D1), D635-d642. doi:10.1093/nar/gkw1104

Alazami, A. M., Shaheen, R., Alzahrani, F., Snape, K., Saggar, A., Brinkmann, B.*, et al.* (2009). FREM1 mutations cause bifid nose, renal agenesis, and anorectal malformations syndrome. *Am J Hum Genet, 85*(3), 414-418. doi:10.1016/j.ajhg.2009.08.010

Almawi, A. W., Matthews, L. A., & Guarne, A. (2017). FHA domains: Phosphopeptide binding and beyond. *Prog Biophys Mol Biol, 127*, 105-110. doi:10.1016/j.pbiomolbio.2016.12.003

Alphey, L., Parker, L., Hawcroft, G., Guo, Y., Kaiser, K., & Morgan, G. (1997). KLP38B: a mitotic kinesin-related protein that binds PP1. *J Cell Biol, 138*(2), 395-409.

Alvarez-Buylla, A., Garcia-Verdugo, J. M., & Tramontin, A. D. (2001). A unified hypothesis on the lineage of neural stem cells. *Nat Rev Neurosci, 2*(4), 287-293. doi:10.1038/35067582

Amacher, S. L., Draper, B. W., Summers, B. R., & Kimmel, C. B. (2002). The zebrafish T-box genes no tail and spadetail are required for development of trunk and tail mesoderm and medial floor plate. *Development, 129*(14), 3311-3323.

Amos, L. A. (1987). Kinesin from pig brain studied by electron microscopy. *J Cell Sci, 87 (Pt 1)*, 105-111.

Araya, C., Ward, L. C., Girdler, G. C., & Miranda, M. (2016). Coordinating cell and tissue behavior during zebrafish neural tube morphogenesis. *Dev Dyn, 245*(3), 197-208. doi:10.1002/dvdy.24304

Ardissino, G., Dacco, V., Testa, S., Bonaudo, R., Claris-Appiani, A., Taioli, E.*, et al.* (2003). Epidemiology of chronic renal failure in children: data from the ItalKid project. *Pediatrics, 111*(4 Pt 1), e382-387.

Arora, K., Talje, L., Asenjo, A. B., Andersen, P., Atchia, K., Joshi, M.*, et al.* (2014). KIF14 binds tightly to microtubules and adopts a rigor-like conformation. *J Mol Biol, 426*(17), 2997-3015. doi:10.1016/j.jmb.2014.05.030

Arquint, C., & Nigg, E. A. (2014). STIL microcephaly mutations interfere with APC/C-mediated degradation and cause centriole amplification. *Curr Biol, 24*(4), 351-360. doi:10.1016/j.cub.2013.12.016

Asencio, C., Davidson, I. F., Santarella-Mellwig, R., Ly-Hartig, T. B., Mall, M., Wallenfang, M. R.*, et al.* (2012). Coordination of kinase and phosphatase activities by Lem4 enables nuclear envelope reassembly during mitosis. *Cell, 150*(1), 122-135. doi:10.1016/j.cell.2012.04.043

Awad, S., Al-Dosari, M. S., Al-Yacoub, N., Colak, D., Salih, M. A., Alkuraya, F. S.*, et al.* (2013). Mutation in PHC1 implicates chromatin remodeling in primary microcephaly pathogenesis. *Hum Mol Genet, 22*(11), 2200-2213. doi:10.1093/hmg/ddt072

Bangalore, L., & Chudler, E. H. (2009). *Brain Development*: Facts On File, Incorporated.

Barak, H., Huh, S. H., Chen, S., Jeanpierre, C., Martinovic, J., Parisot, M.*, et al.* (2012). FGF9 and FGF20 maintain the stemness of nephron progenitors in mice and man. *Dev Cell, 22*(6), 1191-1207. doi:10.1016/j.devcel.2012.04.018

Barasch, J., Qiao, J., McWilliams, G., Chen, D., Oliver, J. A., & Herzlinger, D. (1997). Ureteric bud cells secrete multiple factors, including bFGF, which rescue renal progenitors from apoptosis. *Am J Physiol, 273*(5 Pt 2), F757-767.

Barkovich, A. J., Guerrini, R., Kuzniecky, R. I., Jackson, G. D., & Dobyns, W. B. (2012). A developmental and genetic classification for malformations of cortical development: update 2012. *Brain, 135*(Pt 5), 1348-1369. doi:10.1093/brain/aws019

Barkovich, A. J., Kuzniecky, R. I., Dobyns, W. B., Jackson, G. D., Becker, L. E., & Evrard, P. (1996). A classification scheme for malformations of cortical development. *Neuropediatrics, 27*(2), 59-63. doi:10.1055/s-2007-973750

Basit, S., Al-Harbi, K. M., Alhijji, S. A., Albalawi, A. M., Alharby, E., Eldardear, A*., et al.* (2016). CIT, a gene involved in neurogenic cytokinesis, is mutated in human primary microcephaly. *Hum Genet, 135*(10), 1199-1207. doi:10.1007/s00439-016-1724-0

Bassi, Z. I., Audusseau, M., Riparbelli, M. G., Callaini, G., & D'Avino, P. P. (2013). Citron kinase controls a molecular network required for midbody formation in cytokinesis. *Proc Natl Acad Sci U S A, 110*(24), 9782-9787. doi:10.1073/pnas.1301328110

Bassi, Z. I., Verbrugghe, K. J., Capalbo, L., Gregory, S., Montembault, E., Glover, D. M*., et al.* (2011). Sticky/Citron kinase maintains proper RhoA localization at the cleavage site during cytokinesis. *J Cell Biol, 195*(4), 595-603. doi:10.1083/jcb.201105136

Basson, M. A., Akbulut, S., Watson-Johnson, J., Simon, R., Carroll, T. J., Shakya, R*., et al.* (2005). Sprouty1 is a critical regulator of GDNF/RET-mediated kidney induction. *Dev Cell, 8*(2), 229-239. doi:10.1016/j.devcel.2004.12.004

Basten, S. G., & Giles, R. H. (2013). Functional aspects of primary cilia in signaling, cell cycle and tumorigenesis. *Cilia, 2*(1), 6. doi:10.1186/2046-2530-2-6

Beams, H. W., & Kessel, R. G. (1976). Cytokinesis: A Comparative Study of Cytoplasmic Division in Animal Cells: Views regarding the mechanism of cytokinesis are presented together with scanning and transmission electron microscope studies on the contraction ring, cell cortex, and membrane specializations associated with the cleavage furrow. *American Scientist, 64*(3), 279-290.

Bernstein, M., Beech, P. L., Katz, S. G., & Rosenbaum, J. L. (1994). A new kinesin-like protein (Klp1) localized to a single microtubule of the Chlamydomonas flagellum. *J Cell Biol, 125*(6), 1313-1326.

Bertram, J. F., Douglas-Denton, R. N., Diouf, B., Hughson, M. D., & Hoy, W. E. (2011). Human nephron number: implications for health and disease. *Pediatr Nephrol, 26*(9), 1529-1533. doi:10.1007/s00467-011-1843-8

Betizeau, M., Cortay, V., Patti, D., Pfister, S., Gautier, E., Bellemin-Menard, A*., et al.* (2013). Precursor diversity and complexity of lineage relationships in the outer subventricular zone of the primate. *Neuron, 80*(2), 442-457. doi:10.1016/j.neuron.2013.09.032

Bizet, A. A., Becker-Heck, A., Ryan, R., Weber, K., Filhol, E., Krug, P*., et al.* (2015). Mutations in TRAF3IP1/IFT54 reveal a new role for IFT proteins in microtubule stabilization. *Nat Commun, 6*, 8666. doi:10.1038/ncomms9666

Bond, J., Roberts, E., Springell, K., Lizarraga, S. B., Scott, S., Higgins, J*., et al.* (2005). A centrosomal mechanism involving CDK5RAP2 and CENPJ controls brain size. *Nat Genet, 37*(4), 353-355. doi:10.1038/ng1539

Borovina, A., Superina, S., Voskas, D., & Ciruna, B. (2010). Vangl2 directs the posterior tilting and asymmetric localization of motile primary cilia. *Nat Cell Biol, 12*(4), 407-412. doi:10.1038/ncb2042

Bouchard, M., Souabni, A., Mandler, M., Neubuser, A., & Busslinger, M. (2002). Nephric lineage specification by Pax2 and Pax8. *Genes Dev, 16*(22), 2958-2970. doi:10.1101/gad.240102

Bower, M., Salomon, R., Allanson, J., Antignac, C., Benedicenti, F., Benetti, E*., et al.* (2012). Update of PAX2 mutations in renal coloboma syndrome and establishment of a locus-specific database. *Hum Mutat, 33*(3), 457-466. doi:10.1002/humu.22020

Boyle, S., Misfeldt, A., Chandler, K. J., Deal, K. K., Southard-Smith, E. M., Mortlock, D. P.*, et al.* (2008). Fate mapping using Cited1-CreERT2 mice demonstrates that the cap mesenchyme contains self-renewing progenitor cells and gives rise exclusively to nephronic epithelia. *Dev Biol, 313*(1), 234-245. doi:10.1016/j.ydbio.2007.10.014

Bradbury, J. (2004). Small fish, big science. *PLoS Biol, 2*(5), E148. doi:10.1371/journal.pbio.0020148

Braun, D. A., & Hildebrandt, F. (2017). Ciliopathies. *Cold Spring Harb Perspect Biol, 9*(3). doi:10.1101/cshperspect.a028191

Britanova, O., Akopov, S., Lukyanov, S., Gruss, P., & Tarabykin, V. (2005). Novel transcription factor Satb2 interacts with matrix attachment region DNA elements in a tissue-specific manner and demonstrates cell-type-dependent expression in the developing mouse CNS. *Eur J Neurosci, 21*(3), 658-668. doi:10.1111/j.1460-9568.2005.03897.x

Bruce, A. E. (2016). Zebrafish epiboly: Spreading thin over the yolk. *Dev Dyn, 245*(3), 244-258. doi:10.1002/dvdy.24353

Brunskill, E. W., Aronow, B. J., Georgas, K., Rumballe, B., Valerius, M. T., Aronow, J.*, et al.* (2008). Atlas of gene expression in the developing kidney at microanatomic resolution. *Dev Cell, 15*(5), 781-791. doi:10.1016/j.devcel.2008.09.007

Buchan, J. G., Gray, R. S., Gansner, J. M., Alvarado, D. M., Burgert, L., Gitlin, J. D.*, et al.* (2014). Kinesin family member 6 (kif6) is necessary for spine development in zebrafish. *Dev Dyn, 243*(12), 1646-1657. doi:10.1002/dvdy.24208

Buckley, C. E., Ren, X., Ward, L. C., Girdler, G. C., Araya, C., Green, M. J.*, et al.* (2013). Mirror-symmetric microtubule assembly and cell interactions drive lumen formation in the zebrafish neural rod. *EMBO J, 32*(1), 30-44. doi:10.1038/emboj.2012.305

Bulchand, S., Grove, E. A., Porter, F. D., & Tole, S. (2001). LIM-homeodomain gene Lhx2 regulates the formation of the cortical hem. *Mech Dev, 100*(2), 165-175.

Bultje, R. S., Castaneda-Castellanos, D. R., Jan, L. Y., Jan, Y. N., Kriegstein, A. R., & Shi, S. H. (2009). Mammalian Par3 regulates progenitor cell asymmetric division via notch signaling in the developing neocortex. *Neuron, 63*(2), 189-202. doi:10.1016/j.neuron.2009.07.004

Bulum, B., Ozcakar, Z. B., Ustuner, E., Dusunceli, E., Kavaz, A., Duman, D.*, et al.* (2013). High frequency of kidney and urinary tract anomalies in asymptomatic first-degree relatives of patients with CAKUT. *Pediatr Nephrol, 28*(11), 2143-2147. doi:10.1007/s00467-013-2530-8

Burckle, C., Gaude, H. M., Vesque, C., Silbermann, F., Salomon, R., Jeanpierre, C.*, et al.* (2011). Control of the Wnt pathways by nephrocystin-4 is required for morphogenesis of the zebrafish pronephros. *Hum Mol Genet, 20*(13), 2611-2627. doi:10.1093/hmg/ddr164

Burdsal, C. A., Damsky, C. H., & Pedersen, R. A. (1993). The role of E-cadherin and integrins in mesoderm differentiation and migration at the mammalian primitive streak. *Development, 118*(3), 829-844.

Burn, S. F., Webb, A., Berry, R. L., Davies, J. A., Ferrer-Vaquer, A., Hadjantonakis, A. K.*, et al.* (2011). Calcium/NFAT signalling promotes early nephrogenesis. *Dev Biol, 352*(2), 288-298. doi:10.1016/j.ydbio.2011.01.033

Byers, B., & Abramson, D. H. (1968). Cytokinesis in HeLa: post-telophase delay and microtubule-associated motility. *Protoplasma, 66*(4), 413-435.

Bystron, I., Blakemore, C., & Rakic, P. (2008). Development of the human cerebral cortex: Boulder Committee revisited. *Nat Rev Neurosci, 9*(2), 110-122. doi:10.1038/nrn2252

Bystron, I., Rakic, P., Molnar, Z., & Blakemore, C. (2006). The first neurons of the human cerebral cortex. *Nat Neurosci, 9*(7), 880-886. doi:10.1038/nn1726

C. Zhu, Zhao, J., Bibikova, M., Leverson, J. D., Bossy-Wetzel, E., Fan, J. B.*, et al.* (2005). Functional analysis of human microtubule-based motor proteins, the kinesins and dyneins, in mitosis/cytokinesis using RNA interference. *Mol Biol Cell, 16*(7), 3187-3199. doi:10.1091/mbc.e05-02-0167

Cai, S., Weaver, L. N., Ems-McClung, S. C., & Walczak, C. E. (2009). Kinesin-14 family proteins HSET/XCTK2 control spindle length by cross-linking and sliding microtubules. *Mol Biol Cell, 20*(5), 1348-1359. doi:10.1091/mbc.E08-09-0971

Calegari, F., Haubensak, W., Haffner, C., & Huttner, W. B. (2005). Selective lengthening of the cell cycle in the neurogenic subpopulation of neural progenitor cells during mouse brain development. *J Neurosci, 25*(28), 6533-6538. doi:10.1523/jneurosci.0778-05.2005

Calegari, F., & Huttner, W. B. (2003). An inhibition of cyclin-dependent kinases that lengthens, but does not arrest, neuroepithelial cell cycle induces premature neurogenesis. *J Cell Sci, 116*(Pt 24), 4947-4955. doi:10.1242/jcs.00825

Campbell, K., & Gotz, M. (2002). Radial glia: multi-purpose cells for vertebrate brain development. *Trends Neurosci, 25*(5), 235-238.

Cardenas-Rodriguez, M., Irigoin, F., Osborn, D. P., Gascue, C., Katsanis, N., Beales, P. L.*, et al.* (2013). The Bardet-Biedl syndrome-related protein CCDC28B modulates mTORC2 function and interacts with SIN1 to control cilia length independently of the mTOR complex. *Hum Mol Genet, 22*(20), 4031-4042. doi:10.1093/hmg/ddt253

Carleton, M., Mao, M., Biery, M., Warrener, P., Kim, S., Buser, C.*, et al.* (2006). RNA interference-mediated silencing of mitotic kinesin KIF14 disrupts cell cycle progression and induces cytokinesis failure. *Mol Cell Biol, 26*(10), 3853-3863. doi:10.1128/MCB.26.10.3853-3863.2006

Carroll, T. J., Park, J. S., Hayashi, S., Majumdar, A., & McMahon, A. P. (2005). Wnt9b plays a central role in the regulation of mesenchymal to epithelial transitions underlying organogenesis of the mammalian urogenital system. *Dev Cell, 9*(2), 283-292. doi:10.1016/j.devcel.2005.05.016

Carvalho, L., & Heisenberg, C. P. (2010). The yolk syncytial layer in early zebrafish development. *Trends Cell Biol, 20*(10), 586-592. doi:10.1016/j.tcb.2010.06.009

Cepero Malo, M., Duchemin, A. L., Guglielmi, L., Patzel, E., Sel, S., Auffarth, G. U.*, et al.* (2017). The Zebrafish Anillin-eGFP Reporter Marks Late Dividing Retinal Precursors and Stem Cells Entering Neuronal Lineages. *PLoS One, 12*(1), e0170356. doi:10.1371/journal.pone.0170356

Chana, M., Tripet, B. P., Mant, C. T., & Hodges, R. (2005). Stability and specificity of heterodimer formation for the coiled-coil neck regions of the motor proteins Kif3A and Kif3B: the role of unstructured oppositely charged regions. *J Pept Res, 65*(2), 209-220. doi:10.1111/j.1399-3011.2005.00210.x

Chana, M., Tripet, B. P., Mant, C. T., & Hodges, R. S. (2002). The role of unstructured highly charged regions on the stability and specificity of dimerization of two-stranded alpha-helical coiled-coils: analysis of the neck-hinge region of the kinesin-like motor protein Kif3A. *J Struct Biol, 137*(1-2), 206-219. doi:10.1006/jsbi.2002.4446

Chang, J. T., Lehtinen, M. K., & Sive, H. (2016). Zebrafish cerebrospinal fluid mediates cell survival through a retinoid signaling pathway. *Dev Neurobiol, 76*(1), 75-92. doi:10.1002/dneu.22300

Chaya, T., Omori, Y., Kuwahara, R., & Furukawa, T. (2014). ICK is essential for cell type-specific ciliogenesis and the regulation of ciliary transport. *EMBO J, 33*(11), 1227-1242. doi:10.1002/embj.201488175

Chenn, A., & McConnell, S. K. (1995). Cleavage orientation and the asymmetric inheritance of Notch1 immunoreactivity in mammalian neurogenesis. *Cell, 82*(4), 631-641.

Cheung, H. O., Zhang, X., Ribeiro, A., Mo, R., Makino, S., Puviindran, V.*, et al.* (2009). The kinesin protein Kif7 is a critical regulator of Gli transcription factors in mammalian hedgehog signaling. *Sci Signal, 2*(76), ra29. doi:10.1126/scisignal.2000405

Choksi, S. P., Babu, D., Lau, D., Yu, X., & Roy, S. (2014). Systematic discovery of novel ciliary genes through functional genomics in the zebrafish. *Development, 141*(17), 3410-3419. doi:10.1242/dev.108209

Cole, D. G., Diener, D. R., Himelblau, A. L., Beech, P. L., Fuster, J. C., & Rosenbaum, J. L. (1998). Chlamydomonas kinesin-II-dependent intraflagellar transport (IFT): IFT particles contain proteins required for ciliary assembly in Caenorhabditis elegans sensory neurons. *J Cell Biol, 141*(4), 993-1008.

Conkar, D., Culfa, E., Odabasi, E., Rauniyar, N., Yates, J. R., 3rd, & Firat-Karalar, E. N. (2017). The centriolar satellite protein CCDC66 interacts with CEP290 and functions in cilium formation and trafficking. *J Cell Sci, 130*(8), 1450-1462. doi:10.1242/jcs.196832

Copp, A. J., & Greene, N. D. (2013). Neural tube defects--disorders of neurulation and related embryonic processes. *Wiley Interdiscip Rev Dev Biol, 2*(2), 213-227. doi:10.1002/wdev.71

Corbeil, D., Roper, K., Hannah, M. J., Hellwig, A., & Huttner, W. B. (1999). Selective localization of the polytopic membrane protein prominin in microvilli of epithelial cells - a combination of apical sorting and retention in plasma membrane protrusions. *J Cell Sci, 112 (Pt 7)*, 1023-1033.

Costantini, F., & Kopan, R. (2010). Patterning a complex organ: branching morphogenesis and nephron segmentation in kidney development. *Dev Cell, 18*(5), 698-712. doi:10.1016/j.devcel.2010.04.008

Coy, D. L., Wagenbach, M., & Howard, J. (1999). Kinesin takes one 8-nm step for each ATP that it hydrolyzes. *J Biol Chem, 274*(6), 3667-3671.

Cross, R. A., & McAinsh, A. (2014). Prime movers: the mechanochemistry of mitotic kinesins. *Nat Rev Mol Cell Biol, 15*(4), 257-271. doi:10.1038/nrm3768

Crowell, E. F., Gaffuri, A. L., Gayraud-Morel, B., Tajbakhsh, S., & Echard, A. (2014). Engulfment of the midbody remnant after cytokinesis in mammalian cells. *J Cell Sci, 127*(Pt 17), 3840-3851. doi:10.1242/jcs.154732

Cullati, S. N., Kabeche, L., Kettenbach, A. N., & Gerber, S. A. (2017). A bifurcated signaling cascade of NIMA-related kinases controls distinct kinesins in anaphase. *J Cell Biol, 216*(8), 2339-2354. doi:10.1083/jcb.201512055

D'Avino, P. P. (2009). How to scaffold the contractile ring for a safe cytokinesis - lessons from Anillin-related proteins. *J Cell Sci, 122*(Pt 8), 1071-1079. doi:10.1242/jcs.034785

D'Avino, P. P., Giansanti, M. G., & Petronczki, M. (2015). Cytokinesis in animal cells. *Cold Spring Harb Perspect Biol, 7*(4), a015834. doi:10.1101/cshperspect.a015834

Dao, V. T., Dupuy, A. G., Gavet, O., Caron, E., & de Gunzburg, J. (2009). Dynamic changes in Rap1 activity are required for cell retraction and spreading during mitosis. *J Cell Sci, 122*(Pt 16), 2996-3004. doi:10.1242/jcs.041301

Davidson, A. J. (2011). Uncharted waters: nephrogenesis and renal regeneration in fish and mammals. *Pediatr Nephrol, 26*(9), 1435-1443. doi:10.1007/s00467-011-1795-z

Davidson, A. J., & Zon, L. I. (2006). The caudal-related homeobox genes cdx1a and cdx4 act redundantly to regulate hox gene expression and the formation of putative hematopoietic stem cells during zebrafish embryogenesis. *Dev Biol, 292*(2), 506-518. doi:10.1016/j.ydbio.2006.01.003

Davies, J. A. (2002). Morphogenesis of the metanephric kidney. *ScientificWorldJournal, 2*, 1937-1950. doi:10.1100/tsw.2002.854

De Luca, A., Cerrato, V., Fuca, E., Parmigiani, E., Buffo, A., & Leto, K. (2016). Sonic hedgehog patterning during cerebellar development. *Cell Mol Life Sci, 73*(2), 291-303. doi:10.1007/s00018-015-2065-1

De Tomasi, L., David, P., Humbert, C., Silbermann, F., Arrondel, C., Tores, F*., et al.* (2017). Mutations in GREB1L Cause Bilateral Kidney Agenesis in Humans and Mice. *Am J Hum Genet, 101*(5), 803-814. doi:10.1016/j.ajhg.2017.09.026

Demonchy, R., Blisnick, T., Deprez, C., Toutirais, G., Loussert, C., Marande, W*., et al.* (2009). Kinesin 9 family members perform separate functions in the trypanosome flagellum. *J Cell Biol, 187*(5), 615-622. doi:10.1083/jcb.200903139

DeMyer, W. (1972). Megalencephaly in children. *Clinical syndromes, genetic patterns, and differential diagnosis from other causes of megalocephaly, 22*(6), 634-634. doi:10.1212/wnl.22.6.634

Desgrange, A., & Cereghini, S. (2015). Nephron Patterning: Lessons from Xenopus, Zebrafish, and Mouse Studies. *Cells, 4*(3), 483-499. doi:10.3390/cells4030483

Devisme, L., Bouchet, C., Gonzalès, M., Alanio, E., Bazin, A., Bessières, B*., et al.* (2012). Cobblestone lissencephaly: neuropathological subtypes and correlations with genes of dystroglycanopathies. *Brain, 135*(2), 469-482. doi:10.1093/brain/awr357

Diep, C. Q., Ma, D., Deo, R. C., Holm, T. M., Naylor, R. W., Arora, N*., et al.* (2011). Identification of adult nephron progenitors capable of kidney regeneration in zebrafish. *Nature, 470*(7332), 95-100. doi:10.1038/nature09669

Diep, C. Q., Peng, Z., Ukah, T. K., Kelly, P. M., Daigle, R. V., & Davidson, A. J. (2015). Development of the zebrafish mesonephros. *Genesis, 53*(3-4), 257-269. doi:10.1002/dvg.22846

Dionne, L. K., Wang, X. J., & Prekeris, R. (2015). Midbody: from cellular junk to regulator of cell polarity and cell fate. *Curr Opin Cell Biol, 35*, 51-58. doi:10.1016/j.ceb.2015.04.010

DiStasio, A., Driver, A., Sund, K., Donlin, M., Muraleedharan, R. M., Pooya, S.*, et al.* (2017). Copb2 is essential for embryogenesis and hypomorphic mutations cause human microcephaly. *Hum Mol Genet, 26*(24), 4836-4848. doi:10.1093/hmg/ddx362

Dressler, G. R. (2006). The cellular basis of kidney development. *Annu Rev Cell Dev Biol, 22*, 509-529. doi:10.1146/annurev.cellbio.22.010305.104340

Drummond, I. A., & Davidson, A. J. (2016). Zebrafish kidney development. *Methods Cell Biol, 134*, 391-429. doi:10.1016/bs.mcb.2016.03.041

Drummond, I. A., Majumdar, A., Hentschel, H., Elger, M., Solnica-Krezel, L., Schier, A. F.*, et al.* (1998). Early development of the zebrafish pronephros and analysis of mutations affecting pronephric function. *Development, 125*(23), 4655-4667.

Du, Y., English, C. A., & Ohi, R. (2010). The kinesin-8 Kif18A dampens microtubule plus-end dynamics. *Curr Biol, 20*(4), 374-380. doi:10.1016/j.cub.2009.12.049

Dubreuil, V., Marzesco, A. M., Corbeil, D., Huttner, W. B., & Wilsch-Brauninger, M. (2007). Midbody and primary cilium of neural progenitors release extracellular membrane particles enriched in the stem cell marker prominin-1. *J Cell Biol, 176*(4), 483-495. doi:10.1083/jcb.200608137

Echelard, Y., Epstein, D. J., St-Jacques, B., Shen, L., Mohler, J., McMahon, J. A.*, et al.* (1993). Sonic hedgehog, a member of a family of putative signaling molecules, is implicated in the regulation of CNS polarity. *Cell, 75*(7), 1417-1430.

Edwards, T. J., Sherr, E. H., Barkovich, A. J., & Richards, L. J. (2014). Clinical, genetic and imaging findings identify new causes for corpus callosum development syndromes. *Brain, 137*(Pt 6), 1579-1613. doi:10.1093/brain/awt358

Eivers, E., McCarthy, K., Glynn, C., Nolan, C. M., & Byrnes, L. (2004). Insulin-like growth factor (IGF) signalling is required for early dorso-anterior development of the zebrafish embryo. *Int J Dev Biol, 48*(10), 1131-1140. doi:10.1387/ijdb.041913ee

Elia, N., Sougrat, R., Spurlin, T. A., Hurley, J. H., & Lippincott-Schwartz, J. (2011). Dynamics of endosomal sorting complex required for transport (ESCRT) machinery during cytokinesis and its role in abscission. *Proc Natl Acad Sci U S A, 108*(12), 4846-4851. doi:10.1073/pnas.1102714108

Embryonic vertebrate central nervous system: revised terminology. The Boulder Committee. (1970). *Anat Rec, 166*(2), 257-261. doi:10.1002/ar.1091660214

Endoh-Yamagami, S., Evangelista, M., Wilson, D., Wen, X., Theunissen, J. W., Phamluong, K.*, et al.* (2009). The mammalian Cos2 homolog Kif7 plays an essential role in modulating Hh signal transduction during development. *Curr Biol, 19*(15), 1320-1326. doi:10.1016/j.cub.2009.06.046

Englund, C., Fink, A., Lau, C., Pham, D., Daza, R. A., Bulfone, A.*, et al.* (2005). Pax6, Tbr2, and Tbr1 are expressed sequentially by radial glia, intermediate progenitor cells, and postmitotic neurons in developing neocortex. *J Neurosci, 25*(1), 247-251. doi:10.1523/jneurosci.2899-04.2005

Enos, A. P., & Morris, N. R. (1990). Mutation of a gene that encodes a kinesin-like protein blocks nuclear division in A. nidulans. *Cell, 60*(6), 1019-1027.

Fabbro, M., Zhou, B. B., Takahashi, M., Sarcevic, B., Lal, P., Graham, M. E.*, et al.* (2005). Cdk1/Erk2- and Plk1-dependent phosphorylation of a centrosome protein, Cep55, is required for its recruitment to midbody and cytokinesis. *Dev Cell, 9*(4), 477-488. doi:10.1016/j.devcel.2005.09.003

Faheem, M., Naseer, M. I., Rasool, M., Chaudhary, A. G., Kumosani, T. A., Ilyas, A. M.*, et al.* (2015). Molecular genetics of human primary microcephaly: an overview. *BMC Med Genomics, 8 Suppl 1*, S4. doi:10.1186/1755-8794-8-s1-s4

Falk, N., Losl, M., Schroder, N., & Giessl, A. (2015). Specialized Cilia in Mammalian Sensory Systems. *Cells, 4*(3), 500-519. doi:10.3390/cells4030500

Fanni, D., Gerosa, C., Vinci, L., Ambu, R., Dessi, A., Eyken, P. V.*, et al.* (2016). Interstitial stromal progenitors during kidney development: here, there and everywhere. *J Matern Fetal Neonatal Med, 29*(23), 3815-3820. doi:10.3109/14767058.2016.1147553

Fargeas, C. A., Florek, M., Huttner, W. B., & Corbeil, D. (2003). Characterization of prominin-2, a new member of the prominin family of pentaspan membrane glycoproteins. *J Biol Chem, 278*(10), 8586-8596. doi:10.1074/jbc.M210640200

Feil, R., & Fraga, M. F. (2012). Epigenetics and the environment: emerging patterns and implications. *Nat Rev Genet, 13*(2), 97-109. doi:10.1038/nrg3142

Ferenz, N. P., Gable, A., & Wadsworth, P. (2010). Mitotic functions of kinesin-5. *Semin Cell Dev Biol, 21*(3), 255-259. doi:10.1016/j.semcdb.2010.01.019

Ferland, R. J., Batiz, L. F., Neal, J., Lian, G., Bundock, E., Lu, J.*, et al.* (2009). Disruption of neural progenitors along the ventricular and subventricular zones in periventricular heterotopia. *Hum Mol Genet, 18*(3), 497-516. doi:10.1093/hmg/ddn377

Fernandez, V., Llinares-Benadero, C., & Borrell, V. (2016). Cerebral cortex expansion and folding: what have we learned? *EMBO J, 35*(10), 1021-1044. doi:10.15252/embj.201593701

Fietz, S. A., Kelava, I., Vogt, J., Wilsch-Brauninger, M., Stenzel, D., Fish, J. L.*, et al.* (2010). OSVZ progenitors of human and ferret neocortex are epithelial-like and expand by integrin signaling. *Nat Neurosci, 13*(6), 690-699. doi:10.1038/nn.2553

Filges, I., Nosova, E., Bruder, E., Tercanli, S., Townsend, K., Gibson, W. T.*, et al.* (2014). Exome sequencing identifies mutations in KIF14 as a novel cause of an autosomal recessive lethal fetal ciliopathy phenotype. *Clin Genet, 86*(3), 220-228. doi:10.1111/cge.12301

Fischer, E., Legue, E., Doyen, A., Nato, F., Nicolas, J. F., Torres, V.*, et al.* (2006). Defective planar cell polarity in polycystic kidney disease. *Nat Genet, 38*(1), 21-23. doi:10.1038/ng1701

Fish, J. L., Kosodo, Y., Enard, W., Pääbo, S., & Huttner, W. B. (2006). Aspm specifically maintains symmetric proliferative divisions of neuroepithelial cells. *Proceedings of the National Academy of Sciences, 103*(27), 10438-10443. doi:10.1073/pnas.0604066103

Florio, M., Albert, M., Taverna, E., Namba, T., Brandl, H., Lewitus, E.*, et al.* (2015). Human-specific gene ARHGAP11B promotes basal progenitor amplification and neocortex expansion. *Science, 347*(6229), 1465-1470. doi:10.1126/science.aaa1975

Folgueira, M., Bayley, P., Navratilova, P., Becker, T. S., Wilson, S. W., & Clarke, J. D. (2012). Morphogenesis underlying the development of the everted teleost telencephalon. *Neural Dev, 7*, 32. doi:10.1186/1749-8104-7-32

Fong, K. W., Choi, Y. K., Rattner, J. B., & Qi, R. Z. (2008). CDK5RAP2 is a pericentriolar protein that functions in centrosomal attachment of the gamma-tubulin ring complex. *Mol Biol Cell, 19*(1), 115-125. doi:10.1091/mbc.e07-04-0371

Forsythe, E., & Beales, P. L. (2013). Bardet-Biedl syndrome. *Eur J Hum Genet, 21*(1), 8-13. doi:10.1038/ejhg.2012.115

Friel, C. T., & Howard, J. (2012). Coupling of kinesin ATP turnover to translocation and microtubule regulation: one engine, many machines. *J Muscle Res Cell Motil, 33*(6), 377-383. doi:10.1007/s10974-012-9289-6

Fry, A. E., Cushion, T. D., & Pilz, D. T. (2014). The genetics of lissencephaly. *American Journal of Medical Genetics Part C: Seminars in Medical Genetics, 166*(2), 198-210. doi:10.1002/ajmg.c.31402

Fujikura, K., Setsu, T., Tanigaki, K., Abe, T., Kiyonari, H., Terashima, T.*, et al.* (2013). Kif14 mutation causes severe brain malformation and hypomyelination. *PLoS One, 8*(1), e53490. doi:10.1371/journal.pone.0053490

Furlan, G., Cuccioli, V., Vuillemin, N., Dirian, L., Muntasell, A. J., Coolen, M.*, et al.* (2017). Life-Long Neurogenic Activity of Individual Neural Stem Cells and Continuous Growth Establish an Outside-In Architecture in the Teleost Pallium. *Curr Biol, 27*(21), 3288-3301.e3283. doi:10.1016/j.cub.2017.09.052

Gal, J. S., Morozov, Y. M., Ayoub, A. E., Chatterjee, M., Rakic, P., & Haydar, T. F. (2006). Molecular and morphological heterogeneity of neural precursors in the mouse neocortical proliferative zones. *J Neurosci, 26*(3), 1045-1056. doi:10.1523/jneurosci.4499-05.2006

Ganem, N. J., & Compton, D. A. (2004). The KinI kinesin Kif2a is required for bipolar spindle assembly through a functional relationship with MCAK. *J Cell Biol, 166*(4), 473-478. doi:10.1083/jcb.200404012

Ganem, N. J., Upton, K., & Compton, D. A. (2005). Efficient mitosis in human cells lacking poleward microtubule flux. *Curr Biol, 15*(20), 1827-1832. doi:10.1016/j.cub.2005.08.065

Gao, L., Yang, Z., Hiremath, C., Zimmerman, S. E., Long, B., Brakeman, P. R.*, et al.* (2017). Afadin orients cell division to position the tubule lumen in developing renal tubules. *Development, 144*(19), 3511-3520. doi:10.1242/dev.148908

Garnett, A. T., Square, T. A., & Medeiros, D. M. (2012). BMP, Wnt and FGF signals are integrated through evolutionarily conserved enhancers to achieve robust expression of Pax3 and Zic genes at the zebrafish neural plate border. *Development, 139*(22), 4220-4231. doi:10.1242/dev.081497

Geng, X., Speirs, C., Lagutin, O., Inbal, A., Liu, W., Solnica-Krezel, L.*, et al.* (2008). Haploinsufficiency of Six3 fails to activate Sonic hedgehog expression in the ventral forebrain and causes holoprosencephaly. *Dev Cell, 15*(2), 236-247. doi:10.1016/j.devcel.2008.07.003

Genin, A., Desir, J., Lambert, N., Biervliet, M., Van Der Aa, N., Pierquin, G.*, et al.* (2012). Kinetochore KMN network gene CASC5 mutated in primary microcephaly. *Hum Mol Genet, 21*(24), 5306-5317. doi:10.1093/hmg/dds386

Georgas, K., Rumballe, B., Valerius, M. T., Chiu, H. S., Thiagarajan, R. D., Lesieur, E.*, et al.* (2009). Analysis of early nephron patterning reveals a role for distal RV proliferation in fusion to the ureteric tip via a cap mesenchyme-derived connecting segment. *Dev Biol, 332*(2), 273-286. doi:10.1016/j.ydbio.2009.05.578

Gerlach, G. F., & Wingert, R. A. (2013). Kidney organogenesis in the zebrafish: insights into vertebrate nephrogenesis and regeneration. *Wiley Interdiscip Rev Dev Biol, 2*(5), 559-585. doi:10.1002/wdev.92

Gerlach, G. F., & Wingert, R. A. (2014). Zebrafish pronephros tubulogenesis and epithelial identity maintenance are reliant on the polarity proteins Prkc iota and zeta. *Dev Biol, 396*(2), 183-200. doi:10.1016/j.ydbio.2014.08.038

Ghossoub, R., Hu, Q., Failler, M., Rouyez, M. C., Spitzbarth, B., Mostowy, S.*, et al.* (2013). Septins 2, 7 and 9 and MAP4 colocalize along the axoneme in the primary cilium and control ciliary length. *J Cell Sci, 126*(Pt 12), 2583-2594. doi:10.1242/jcs.111377

Gibbons, I. R., & Rowe, A. J. (1965). Dynein: A Protein with Adenosine Triphosphatase Activity from Cilia. *Science, 149*(3682), 424-426. doi:10.1126/science.149.3682.424

Gilbert-Barness, E., Kapur, R. P., Oligny, L. L., Siebert, J. R., & Optiz, J. M. (2007). *Potter's Pathology of the Fetus and Infant E-Book: 2-Volume Set*: Elsevier Health Sciences.

Glotzer, M. (2009). The 3Ms of central spindle assembly: microtubules, motors and MAPs. *Nat Rev Mol Cell Biol, 10*(1), 9-20. doi:10.1038/nrm2609

Goodyer, P. (2009). Renal Dysplasia/Hypoplasia. In E. Avner, W. Harmon, P. Niaudet, & N. Yoshikawa (Eds.), *Pediatric Nephrology: Sixth Completely Revised, Updated and Enlarged Edition* (pp. 107-120). Berlin, Heidelberg: Springer Berlin Heidelberg.

Gorbsky, G. J., Sammak, P. J., & Borisy, G. G. (1987). Chromosomes move poleward in anaphase along stationary microtubules that coordinately disassemble from their kinetochore ends. *J Cell Biol, 104*(1), 9-18.

Goshima, G., & Vale, R. D. (2003). The roles of microtubule-based motor proteins in mitosis: comprehensive RNAi analysis in the Drosophila S2 cell line. *J Cell Biol, 162*(6), 1003-1016. doi:10.1083/jcb.200303022

Gotz, M., & Huttner, W. B. (2005). The cell biology of neurogenesis. *Nat Rev Mol Cell Biol, 6*(10), 777-788. doi:10.1038/nrm1739

Gotz, M., Stoykova, A., & Gruss, P. (1998). Pax6 controls radial glia differentiation in the cerebral cortex. *Neuron, 21*(5), 1031-1044.

Grieshammer, U., Cebrian, C., Ilagan, R., Meyers, E., Herzlinger, D., & Martin, G. R. (2005). FGF8 is required for cell survival at distinct stages of nephrogenesis and for regulation of gene expression in nascent nephrons. *Development, 132*(17), 3847-3857. doi:10.1242/dev.01944

Grimes, D. T., Boswell, C. W., Morante, N. F., Henkelman, R. M., Burdine, R. D., & Ciruna, B. (2016). Zebrafish models of idiopathic scoliosis link cerebrospinal fluid flow defects to spine curvature. *Science, 352*(6291), 1341-1344. doi:10.1126/science.aaf6419

Groen In 't Woud, S., Renkema, K. Y., Schreuder, M. F., Wijers, C. H., van der Zanden, L. F., Knoers, N. V.*, et al.* (2016). Maternal risk factors involved in specific congenital anomalies of the kidney and urinary tract: A case-control study. *Birth Defects Res A Clin Mol Teratol, 106*(7), 596-603. doi:10.1002/bdra.23500

Gruber, R., Zhou, Z., Sukchev, M., Joerss, T., Frappart, P. O., & Wang, Z. Q. (2011). MCPH1 regulates the neuroprogenitor division mode by coupling the centrosomal cycle with mitotic entry through the Chk1-Cdc25 pathway. *Nat Cell Biol, 13*(11), 1325-1334. doi:10.1038/ncb2342

Gruneberg, U., Neef, R., Honda, R., Nigg, E. A., & Barr, F. A. (2004). Relocation of Aurora B from centromeres to the central spindle at the metaphase to anaphase transition requires MKlp2. *J Cell Biol, 166*(2), 167-172. doi:10.1083/jcb.200403084

Gruneberg, U., Neef, R., Li, X., Chan, E. H., Chalamalasetty, R. B., Nigg, E. A.*, et al.* (2006). KIF14 and citron kinase act together to promote efficient cytokinesis. *J Cell Biol, 172*(3), 363-372. doi:10.1083/jcb.200511061

Guemez-Gamboa, A., Coufal, N. G., & Gleeson, J. G. (2014). Primary cilia in the developing and mature brain. *Neuron, 82*(3), 511-521. doi:10.1016/j.neuron.2014.04.024

Guemez-Gamboa, A., Nguyen, L. N., Yang, H., Zaki, M. S., Kara, M., Ben-Omran, T.*, et al.* (2015). Inactivating mutations in MFSD2A, required for omega-3 fatty acid transport in brain, cause a lethal microcephaly syndrome. *Nat Genet, 47*(7), 809-813. doi:10.1038/ng.3311

Guernsey, D. L., Jiang, H., Hussin, J., Arnold, M., Bouyakdan, K., Perry, S.*, et al.* (2010). Mutations in centrosomal protein CEP152 in primary microcephaly families linked to MCPH4. *Am J Hum Genet, 87*(1), 40-51. doi:10.1016/j.ajhg.2010.06.003

Gupta, G. D., Coyaud, E., Goncalves, J., Mojarad, B. A., Liu, Y., Wu, Q.*, et al.* (2015). A Dynamic Protein Interaction Landscape of the Human Centrosome-Cilium Interface. *Cell, 163*(6), 1484-1499. doi:10.1016/j.cell.2015.10.065

Haas, P., & Gilmour, D. (2006). Chemokine signaling mediates self-organizing tissue migration in the zebrafish lateral line. *Dev Cell, 10*(5), 673-680. doi:10.1016/j.devcel.2006.02.019

Hackney, D. D. (1994). Evidence for alternating head catalysis by kinesin during microtubule-stimulated ATP hydrolysis. *Proc Natl Acad Sci U S A, 91*(15), 6865-6869.

Hamilton, F. (1822). *An Account of the Fishes Found in the River Ganges and Its Branches*: Constable.

Hammond, J. W., Blasius, T. L., Soppina, V., Cai, D., & Verhey, K. J. (2010). Autoinhibition of the kinesin-2 motor KIF17 via dual intramolecular mechanisms. *J Cell Biol, 189*(6), 1013-1025. doi:10.1083/jcb.201001057

Hammond, J. W., Cai, D., Blasius, T. L., Li, Z., Jiang, Y., Jih, G. T.*, et al.* (2009). Mammalian Kinesin-3 motors are dimeric in vivo and move by processive motility upon release of autoinhibition. *PLoS Biol, 7*(3), e72. doi:10.1371/journal.pbio.1000072

Hansen, D. V., Lui, J. H., Parker, P. R., & Kriegstein, A. R. (2010). Neurogenic radial glia in the outer subventricular zone of human neocortex. *Nature, 464*(7288), 554-561. doi:10.1038/nature08845

Harding, B. N., Moccia, A., Drunat, S., Soukarieh, O., Tubeuf, H., Chitty, L. S.*, et al.* (2016). Mutations in Citron Kinase Cause Recessive Microlissencephaly with Multinucleated Neurons. *Am J Hum Genet, 99*(2), 511-520. doi:10.1016/j.ajhg.2016.07.003

Harrington, M. J., Hong, E., & Brewster, R. (2009). Comparative analysis of neurulation: first impressions do not count. *Mol Reprod Dev, 76*(10), 954-965. doi:10.1002/mrd.21085

Hartfuss, E., Galli, R., Heins, N., & Gotz, M. (2001). Characterization of CNS precursor subtypes and radial glia. *Dev Biol, 229*(1), 15-30. doi:10.1006/dbio.2000.9962

Hatini, V., Huh, S. O., Herzlinger, D., Soares, V. C., & Lai, E. (1996). Essential role of stromal mesenchyme in kidney morphogenesis revealed by targeted disruption of Winged Helix transcription factor BF-2. *Genes Dev, 10*(12), 1467-1478.

Hawryluk, G. W., Ruff, C. A., & Fehlings, M. G. (2012). Development and maturation of the spinal cord: implications of molecular and genetic defects. *Handb Clin Neurol, 109*, 3-30. doi:10.1016/b978-0-444-52137-8.00001-2

Haydar, T. F., Ang, E., Jr., & Rakic, P. (2003). Mitotic spindle rotation and mode of cell division in the developing telencephalon. *Proc Natl Acad Sci U S A, 100*(5), 2890-2895. doi:10.1073/pnas.0437969100

He, M., Subramanian, R., Bangs, F., Omelchenko, T., Liem, K. F., Jr., Kapoor, T. M.*, et al.* (2014). The kinesin-4 protein Kif7 regulates mammalian Hedgehog signalling by organizing the cilium tip compartment. *Nat Cell Biol, 16*(7), 663-672. doi:10.1038/ncb2988

Hebert, J. M., & Fishell, G. (2008). The genetics of early telencephalon patterning: some assembly required. *Nat Rev Neurosci, 9*(9), 678-685. doi:10.1038/nrn2463

Heidet, L., Decramer, S., Pawtowski, A., Moriniere, V., Bandin, F., Knebelmann, B.*, et al.* (2010). Spectrum of HNF1B mutations in a large cohort of patients who harbor renal diseases. *Clin J Am Soc Nephrol, 5*(6), 1079-1090. doi:10.2215/cjn.06810909

Heidet, L., Moriniere, V., Henry, C., De Tomasi, L., Reilly, M. L., Humbert, C.*, et al.* (2017). Targeted Exome Sequencing Identifies PBX1 as Involved in Monogenic Congenital Anomalies of the Kidney and Urinary Tract. *J Am Soc Nephrol, 28*(10), 2901-2914. doi:10.1681/asn.2017010043

Hellmich, H. L., Kos, L., Cho, E. S., Mahon, K. A., & Zimmer, A. (1996). Embryonic expression of glial cell-line derived neurotrophic factor (GDNF) suggests multiple developmental roles in neural differentiation and epithelial-mesenchymal interactions. *Mech Dev, 54*(1), 95-105.

Hevner, R. F., Neogi, T., Englund, C., Daza, R. A., & Fink, A. (2003). Cajal-Retzius cells in the mouse: transcription factors, neurotransmitters, and birthdays suggest a pallial origin. *Brain Res Dev Brain Res, 141*(1-2), 39-53.

Hildebrandt, E. R., Gheber, L., Kingsbury, T., & Hoyt, M. A. (2006). Homotetrameric form of Cin8p, a Saccharomyces cerevisiae kinesin-5 motor, is essential for its in vivo function. *J Biol Chem, 281*(36), 26004-26013. doi:10.1074/jbc.M604817200

Hildebrandt, F. (2010). Genetic kidney diseases. *Lancet, 375*(9722), 1287-1295. doi:10.1016/s0140-6736(10)60236-x

Hinds, J. W., & Ruffett, T. L. (1971). Cell proliferation in the neural tube: an electron microscopic and golgi analysis in the mouse cerebral vesicle. *Z Zellforsch Mikrosk Anat, 115*(2), 226-264.

Hirokawa, N., Niwa, S., & Tanaka, Y. (2010). Molecular motors in neurons: transport mechanisms and roles in brain function, development, and disease. *Neuron, 68*(4), 610-638. doi:10.1016/j.neuron.2010.09.039

Hirokawa, N., Pfister, K. K., Yorifuji, H., Wagner, M. C., Brady, S. T., & Bloom, G. S. (1989). Submolecular domains of bovine brain kinesin identified by electron microscopy and monoclonal antibody decoration. *Cell, 56*(5), 867-878.

Hoijman, E., Rubbini, D., Colombelli, J., & Alsina, B. (2015). Mitotic cell rounding and epithelial thinning regulate lumen growth and shape. *Nat Commun, 6*, 7355. doi:10.1038/ncomms8355

Hong, E., & Brewster, R. (2006). N-cadherin is required for the polarized cell behaviors that drive neurulation in the zebrafish. *Development, 133*(19), 3895-3905. doi:10.1242/dev.02560

Horikawa, Y., Iwasaki, N., Hara, M., Furuta, H., Hinokio, Y., Cockburn, B. N.*, et al.* (1997). Mutation in hepatocyte nuclear factor-1 beta gene (TCF2) associated with MODY. *Nat Genet, 17*(4), 384-385. doi:10.1038/ng1297-384

Horne-Badovinac, S., Lin, D., Waldron, S., Schwarz, M., Mbamalu, G., Pawson, T.*, et al.* (2001). Positional cloning of heart and soul reveals multiple roles for PKC lambda in zebrafish organogenesis. *Curr Biol, 11*(19), 1492-1502.

Houart, C., Caneparo, L., Heisenberg, C., Barth, K., Take-Uchi, M., & Wilson, S. (2002). Establishment of the telencephalon during gastrulation by local antagonism of Wnt signaling. *Neuron, 35*(2), 255-265.

Houart, C., Westerfield, M., & Wilson, S. W. (1998). A small population of anterior cells patterns the forebrain during zebrafish gastrulation. *Nature, 391*(6669), 788-792. doi:10.1038/35853

Hu, C. K., Coughlin, M., Field, C. M., & Mitchison, T. J. (2011). KIF4 regulates midzone length during cytokinesis. *Curr Biol, 21*(10), 815-824. doi:10.1016/j.cub.2011.04.019

Hu, Q., Milenkovic, L., Jin, H., Scott, M. P., Nachury, M. V., Spiliotis, E. T.*, et al.* (2010). A septin diffusion barrier at the base of the primary cilium maintains ciliary membrane protein distribution. *Science, 329*(5990), 436-439. doi:10.1126/science.1191054

Hua, W., Young, E. C., Fleming, M. L., & Gelles, J. (1997). Coupling of kinesin steps to ATP hydrolysis. *Nature, 388*(6640), 390-393. doi:10.1038/41118

Huang, B., Rifkin, M. R., & Luck, D. J. (1977). Temperature-sensitive mutations affecting flagellar assembly and function in Chlamydomonas reinhardtii. *J Cell Biol, 72*(1), 67-85.

Huber, C., & Cormier-Daire, V. (2012). Ciliary disorder of the skeleton. *Am J Med Genet C Semin Med Genet, 160C*(3), 165-174. doi:10.1002/ajmg.c.31336

Humbert, C., Silbermann, F., Morar, B., Parisot, M., Zarhrate, M., Masson, C.*, et al.* (2014). Integrin alpha 8 recessive mutations are responsible for bilateral renal agenesis in humans. *Am J Hum Genet, 94*(2), 288-294. doi:10.1016/j.ajhg.2013.12.017

Huo, L., Yue, Y., Ren, J., Yu, J., Liu, J., Yu, Y.*, et al.* (2012). The CC1-FHA tandem as a central hub for controlling the dimerization and activation of kinesin-3 KIF1A. *Structure, 20*(9), 1550-1561. doi:10.1016/j.str.2012.07.002

Hussain, M. S., Baig, S. M., Neumann, S., Nurnberg, G., Farooq, M., Ahmad, I.*, et al.* (2012). A truncating mutation of CEP135 causes primary microcephaly and disturbed centrosomal function. *Am J Hum Genet, 90*(5), 871-878. doi:10.1016/j.ajhg.2012.03.016

Hussain, M. S., Baig, S. M., Neumann, S., Peche, V. S., Szczepanski, S., Nurnberg, G.*, et al.* (2013). CDK6 associates with the centrosome during mitosis and is mutated in a large Pakistani family with primary microcephaly. *Hum Mol Genet, 22*(25), 5199-5214. doi:10.1093/hmg/ddt374

Hutterer, A., Glotzer, M., & Mishima, M. (2009). Clustering of centralspindlin is essential for its accumulation to the central spindle and the midbody. *Curr Biol, 19*(23), 2043-2049. doi:10.1016/j.cub.2009.10.050

Huttner, W. B., & Kosodo, Y. (2005). Symmetric versus asymmetric cell division during neurogenesis in the developing vertebrate central nervous system. *Curr Opin Cell Biol, 17*(6), 648-657. doi:10.1016/j.ceb.2005.10.005

Imai, H., Oomiya, Y., Kikkawa, S., Shoji, W., Hibi, M., Terashima, T.*, et al.* (2012). Dynamic changes in the gene expression of zebrafish Reelin receptors during embryogenesis and hatching period. *Dev Growth Differ, 54*(2), 253-263. doi:10.1111/j.1440-169X.2012.01327.x

Insinna, C., Pathak, N., Perkins, B., Drummond, I., & Besharse, J. C. (2008). The homodimeric kinesin, Kif17, is essential for vertebrate photoreceptor sensory outer segment development. *Dev Biol, 316*(1), 160-170. doi:10.1016/j.ydbio.2008.01.025

Insolera, R., Bazzi, H., Shao, W., Anderson, K. V., & Shi, S. H. (2014). Cortical neurogenesis in the absence of centrioles. *Nat Neurosci, 17*(11), 1528-1535. doi:10.1038/nn.3831

Ishibe, S., Karihaloo, A., Ma, H., Zhang, J., Marlier, A., Mitobe, M.*, et al.* (2009). Met and the epidermal growth factor receptor act cooperatively to regulate final nephron number and maintain collecting duct morphology. *Development, 136*(2), 337-345. doi:10.1242/dev.024463

Ishikawa, H., & Marshall, W. F. (2011). Ciliogenesis: building the cell's antenna. *Nat Rev Mol Cell Biol, 12*(4), 222-234. doi:10.1038/nrm3085

Ishikawa, H., Thompson, J., Yates, J. R., 3rd, & Marshall, W. F. (2012). Proteomic analysis of mammalian primary cilia. *Curr Biol, 22*(5), 414-419. doi:10.1016/j.cub.2012.01.031

Jackson, A. P., Eastwood, H., Bell, S. M., Adu, J., Toomes, C., Carr, I. M.*, et al.* (2002). Identification of microcephalin, a protein implicated in determining the size of the human brain. *Am J Hum Genet, 71*(1), 136-142. doi:10.1086/341283

Jacquet, B. V., Salinas-Mondragon, R., Liang, H., Therit, B., Buie, J. D., Dykstra, M.*, et al.* (2009). FoxJ1-dependent gene expression is required for differentiation of radial glia into ependymal cells and a subset of astrocytes in the postnatal brain. *Development, 136*(23), 4021-4031. doi:10.1242/dev.041129

James, R. G., Kamei, C. N., Wang, Q., Jiang, R., & Schultheiss, T. M. (2006). Odd-skipped related 1 is required for development of the metanephric kidney and regulates formation and differentiation of kidney precursor cells. *Development, 133*(15), 2995-3004. doi:10.1242/dev.02442

James, R. G., & Schultheiss, T. M. (2005). Bmp signaling promotes intermediate mesoderm gene expression in a dose-dependent, cell-autonomous and translation-dependent manner. *Dev Biol, 288*(1), 113-125. doi:10.1016/j.ydbio.2005.09.025

Jamuar, S. S., & Walsh, C. A. (2015). Genomic variants and variations in malformations of cortical development. *Pediatr Clin North Am, 62*(3), 571-585. doi:10.1016/j.pcl.2015.03.002

Janson, M. E., Loughlin, R., Loiodice, I., Fu, C., Brunner, D., Nedelec, F. J.*, et al.* (2007). Crosslinkers and motors organize dynamic microtubules to form stable bipolar arrays in fission yeast. *Cell, 128*(2), 357-368. doi:10.1016/j.cell.2006.12.030

Jeppesen, G. M., & Hoerber, J. K. (2012). The mechanical properties of kinesin-1: a holistic approach. *Biochem Soc Trans, 40*(2), 438-443. doi:10.1042/bst20110768

Jiang, L., Tam, B. M., Ying, G., Wu, S., Hauswirth, W. W., Frederick, J. M.*, et al.* (2015). Kinesin family 17 (osmotic avoidance abnormal-3) is dispensable for photoreceptor morphology and function. *FASEB J, 29*(12), 4866-4880. doi:10.1096/fj.15-275677

Johnson, K., Barragan, J., Bashiruddin, S., Smith, C. J., Tyrrell, C., Parsons, M. J.*, et al.* (2016). Gfap-positive radial glial cells are an essential progenitor population for later-born neurons and glia in the zebrafish spinal cord. *Glia, 64*(7), 1170-1189. doi:10.1002/glia.22990

Jordan, S. N., & Canman, J. C. (2012). Rho GTPases in animal cell cytokinesis: an occupation by the one percent. *Cytoskeleton (Hoboken), 69*(11), 919-930. doi:10.1002/cm.21071

Kadir, R., Harel, T., Markus, B., Perez, Y., Bakhrat, A., Cohen, I.*, et al.* (2016). ALFY-Controlled DVL3 Autophagy Regulates Wnt Signaling, Determining Human Brain Size. *PLoS Genet, 12*(3), e1005919. doi:10.1371/journal.pgen.1005919

Kane, D. A., & Kimmel, C. B. (1993). The zebrafish midblastula transition. *Development, 119*(2), 447-456.

Kapitein, L. C., Peterman, E. J., Kwok, B. H., Kim, J. H., Kapoor, T. M., & Schmidt, C. F. (2005). The bipolar mitotic kinesin Eg5 moves on both microtubules that it crosslinks. *Nature, 435*(7038), 114-118. doi:10.1038/nature03503

Kapoor, T. M., Mayer, T. U., Coughlin, M. L., & Mitchison, T. J. (2000). Probing spindle assembly mechanisms with monastrol, a small molecule inhibitor of the mitotic kinesin, Eg5. *J Cell Biol, 150*(5), 975-988.

Kapoor, T. M., & Mitchison, T. J. (1999). Allele-specific activators and inhibitors for kinesin. *Proc Natl Acad Sci U S A, 96*(16), 9106-9111.

Kashina, A. S., Baskin, R. J., Cole, D. G., Wedaman, K. P., Saxton, W. M., & Scholey, J. M. (1996). A bipolar kinesin. *Nature, 379*(6562), 270-272. doi:10.1038/379270a0

Keller, G., Zimmer, G., Mall, G., Ritz, E., & Amann, K. (2003). Nephron number in patients with primary hypertension. *N Engl J Med, 348*(2), 101-108. doi:10.1056/NEJMoa020549

Kent, W. J., Sugnet, C. W., Furey, T. S., Roskin, K. M., Pringle, T. H., Zahler, A. M.*, et al.* (2002). The human genome browser at UCSC. *Genome Res, 12*(6), 996-1006. doi:10.1101/gr.229102

Kerecuk, L., Schreuder, M. F., & Woolf, A. S. (2008). Renal tract malformations: perspectives for nephrologists. *Nat Clin Pract Nephrol, 4*(6), 312-325. doi:10.1038/ncpneph0807

Kettleborough, R. N., Busch-Nentwich, E. M., Harvey, S. A., Dooley, C. M., de Bruijn, E., van Eeden, F.*, et al.* (2013). A systematic genome-wide analysis of zebrafish protein-coding gene function. *Nature, 496*(7446), 494-497. doi:10.1038/nature11992

Khan, M. A., Rupp, V. M., Orpinell, M., Hussain, M. S., Altmuller, J., Steinmetz, M. O.*, et al.* (2014). A missense mutation in the PISA domain of HsSAS-6 causes autosomal recessive primary microcephaly in a large consanguineous Pakistani family. *Hum Mol Genet, 23*(22), 5940-5949. doi:10.1093/hmg/ddu318

Kiecker, C., & Lumsden, A. (2012). The role of organizers in patterning the nervous system. *Annu Rev Neurosci, 35*, 347-367. doi:10.1146/annurev-neuro-062111-150543

Kim, H. T., Lee, M. S., Choi, J. H., Jung, J. Y., Ahn, D. G., Yeo, S. Y.*, et al.* (2011). The microcephaly gene aspm is involved in brain development in zebrafish. *Biochem Biophys Res Commun, 409*(4), 640-644. doi:10.1016/j.bbrc.2011.05.056

Kim, S., Lee, K., Choi, J. H., Ringstad, N., & Dynlacht, B. D. (2015). Nek2 activation of Kif24 ensures cilium disassembly during the cell cycle. *Nat Commun, 6*, 8087. doi:10.1038/ncomms9087

Kimmel, C. B., Ballard, W. W., Kimmel, S. R., Ullmann, B., & Schilling, T. F. (1995). Stages of embryonic development of the zebrafish. *Dev Dyn, 203*(3), 253-310. doi:10.1002/aja.1002030302

Kimmel, C. B., Hatta, K., & Eisen, J. S. (1991). Genetic control of primary neuronal development in zebrafish. *Dev Suppl, Suppl 2*, 47-57.

Kimmel, C. B., Warga, R. M., & Schilling, T. F. (1990). Origin and organization of the zebrafish fate map. *Development, 108*(4), 581-594.

Kishimoto, Y., Lee, K. H., Zon, L., Hammerschmidt, M., & Schulte-Merker, S. (1997). The molecular nature of zebrafish swirl: BMP2 function is essential during early dorsoventral patterning. *Development, 124*(22), 4457-4466.

Kline-Smith, S. L., Khodjakov, A., Hergert, P., & Walczak, C. E. (2004). Depletion of centromeric MCAK leads to chromosome congression and segregation defects due to improper kinetochore attachments. *Mol Biol Cell, 15*(3), 1146-1159. doi:10.1091/mbc.e03-08-0581

Knust, E., & Huttner, W. B. (2007). Cell polarity from cell division. *Dev Cell, 12*(5), 664-666. doi:10.1016/j.devcel.2007.04.006

Kobayashi, A., Kwan, K. M., Carroll, T. J., McMahon, A. P., Mendelsohn, C. L., & Behringer, R. R. (2005). Distinct and sequential tissue-specific activities of the LIM-class homeobox gene Lim1 for tubular morphogenesis during kidney development. *Development, 132*(12), 2809-2823. doi:10.1242/dev.01858

Kobayashi, A., Valerius, M. T., Mugford, J. W., Carroll, T. J., Self, M., Oliver, G.*, et al.* (2008). Six2 defines and regulates a multipotent self-renewing nephron progenitor population throughout mammalian kidney development. *Cell Stem Cell, 3*(2), 169-181. doi:10.1016/j.stem.2008.05.020

Kobayashi, T., Tsang, W. Y., Li, J., Lane, W., & Dynlacht, B. D. (2011). Centriolar kinesin Kif24 interacts with CP110 to remodel microtubules and regulate ciliogenesis. *Cell, 145*(6), 914-925. doi:10.1016/j.cell.2011.04.028

Koseki, C. (1993). Cell death programmed in uninduced metanephric mesenchymal cells. *Pediatr Nephrol, 7*(5), 609-611.

Kosodo, Y., & Huttner, W. B. (2009). Basal process and cell divisions of neural progenitors in the developing brain. *Dev Growth Differ, 51*(3), 251-261. doi:10.1111/j.1440-169X.2009.01101.x

Kosodo, Y., Roper, K., Haubensak, W., Marzesco, A. M., Corbeil, D., & Huttner, W. B. (2004). Asymmetric distribution of the apical plasma membrane during neurogenic divisions of mammalian neuroepithelial cells. *EMBO J, 23*(11), 2314-2324. doi:10.1038/sj.emboj.7600223

Kramer-Zucker, A. G., Wiessner, S., Jensen, A. M., & Drummond, I. A. (2005). Organization of the pronephric filtration apparatus in zebrafish requires Nephrin, Podocin and the FERM domain protein Mosaic eyes. *Dev Biol, 285*(2), 316-329. doi:10.1016/j.ydbio.2005.06.038

Kriegstein, A., & Alvarez-Buylla, A. (2009). The glial nature of embryonic and adult neural stem cells. *Annu Rev Neurosci, 32*, 149-184. doi:10.1146/annurev.neuro.051508.135600

Kudoh, T., Concha, M. L., Houart, C., Dawid, I. B., & Wilson, S. W. (2004). Combinatorial Fgf and Bmp signalling patterns the gastrula ectoderm into prospective neural and epidermal domains. *Development, 131*(15), 3581-3592. doi:10.1242/dev.01227

Kumar, A., Girimaji, S. C., Duvvari, M. R., & Blanton, S. H. (2009). Mutations in STIL, encoding a pericentriolar and centrosomal protein, cause primary microcephaly. *Am J Hum Genet, 84*(2), 286-290. doi:10.1016/j.ajhg.2009.01.017

Kuznetsov, S. A., Vaisberg, E. A., Shanina, N. A., Magretova, N. N., Chernyak, V. Y., & Gelfand, V. I. (1988). The quaternary structure of bovine brain kinesin. *EMBO J, 7*(2), 353-356.

Kwong, R. W., & Perry, S. F. (2013). The tight junction protein claudin-b regulates epithelial permeability and sodium handling in larval zebrafish, Danio rerio. *Am J Physiol Regul Integr Comp Physiol, 304*(7), R504-513. doi:10.1152/ajpregu.00385.2012

Lagutin, O. V., Zhu, C. C., Kobayashi, D., Topczewski, J., Shimamura, K., Puelles, L.*, et al.* (2003). Six3 repression of Wnt signaling in the anterior neuroectoderm is essential for vertebrate forebrain development. *Genes Dev, 17*(3), 368-379. doi:10.1101/gad.1059403

Lam, P. Y., Webb, S. E., Leclerc, C., Moreau, M., & Miller, A. L. (2009). Inhibition of stored Ca2+ release disrupts convergence-related cell movements in the lateral intermediate mesoderm resulting in abnormal positioning and morphology of the pronephric anlagen in intact zebrafish embryos. *Dev Growth Differ, 51*(4), 429-442. doi:10.1111/j.1440-169X.2009.01106.x

Lavdas, A. A., Grigoriou, M., Pachnis, V., & Parnavelas, J. G. (1999). The medial ganglionic eminence gives rise to a population of early neurons in the developing cerebral cortex. *J Neurosci, 19*(18), 7881-7888.

Lawrence, C. J., Dawe, R. K., Christie, K. R., Cleveland, D. W., Dawson, S. C., Endow, S. A.*, et al.* (2004). A standardized kinesin nomenclature. *J Cell Biol, 167*(1), 19-22. doi:10.1083/jcb.200408113

Lee, J. R., Shin, H., Choi, J., Ko, J., Kim, S., Lee, H. W.*, et al.* (2004). An intramolecular interaction between the FHA domain and a coiled coil negatively regulates the kinesin motor KIF1A. *EMBO J, 23*(7), 1506-1515. doi:10.1038/sj.emboj.7600164

Lee, S. H., Joo, K., Jung, E. J., Hong, H., Seo, J., & Kim, J. (2018). Export of membrane proteins from the Golgi complex to the primary cilium requires the kinesin motor, KIFC1. *FASEB J, 32*(2), 957-968. doi:10.1096/fj.201700563R

Lehtinen, M. K., & Walsh, C. A. (2011). Neurogenesis at the brain-cerebrospinal fluid interface. *Annu Rev Cell Dev Biol, 27*, 653-679. doi:10.1146/annurev-cellbio-092910-154026

Letinic, K., Zoncu, R., & Rakic, P. (2002). Origin of GABAergic neurons in the human neocortex. *Nature, 417*(6889), 645-649. doi:10.1038/nature00779

Levesque, A. A., & Compton, D. A. (2001). The chromokinesin Kid is necessary for chromosome arm orientation and oscillation, but not congression, on mitotic spindles. *J Cell Biol, 154*(6), 1135-1146. doi:10.1083/jcb.200106093

Lewis, T. R., Kundinger, S. R., Pavlovich, A. L., Bostrom, J. R., Link, B. A., & Besharse, J. C. (2017). Cos2/Kif7 and Osm-3/Kif17 regulate onset of outer segment development in zebrafish photoreceptors through distinct mechanisms. *Dev Biol, 425*(2), 176-190. doi:10.1016/j.ydbio.2017.03.019

Li, H., Bielas, S. L., Zaki, M. S., Ismail, S., Farfara, D., Um, K.*, et al.* (2016). Biallelic Mutations in Citron Kinase Link Mitotic Cytokinesis to Human Primary Microcephaly. *Am J Hum Genet, 99*(2), 501-510. doi:10.1016/j.ajhg.2016.07.004

Liem, K. F., Jr., Ashe, A., He, M., Satir, P., Moran, J., Beier, D.*, et al.* (2012). The IFT-A complex regulates Shh signaling through cilia structure and membrane protein trafficking. *J Cell Biol, 197*(6), 789-800. doi:10.1083/jcb.201110049

Liem, K. F., Jr., Tremml, G., Roelink, H., & Jessell, T. M. (1995). Dorsal differentiation of neural plate cells induced by BMP-mediated signals from epidermal ectoderm. *Cell, 82*(6), 969-979.

Lindstrom, N. O., De Sena Brandine, G., Tran, T., Ransick, A., Suh, G., Guo, J.*, et al.* (2018). Progressive Recruitment of Mesenchymal Progenitors Reveals a Time-Dependent Process of Cell Fate

Acquisition in Mouse and Human Nephrogenesis. *Dev Cell, 45*(5), 651-660.e654. doi:10.1016/j.devcel.2018.05.010

Lindstrom, N. O., Guo, J., Kim, A. D., Tran, T., Guo, Q., De Sena Brandine, G.*, et al.* (2018). Conserved and Divergent Features of Mesenchymal Progenitor Cell Types within the Cortical Nephrogenic Niche of the Human and Mouse Kidney. *J Am Soc Nephrol, 29*(3), 806-824. doi:10.1681/ASN.2017080890

Lindstrom, N. O., McMahon, J. A., Guo, J., Tran, T., Guo, Q., Rutledge, E.*, et al.* (2018). Conserved and Divergent Features of Human and Mouse Kidney Organogenesis. *J Am Soc Nephrol, 29*(3), 785-805. doi:10.1681/ASN.2017080887

Lindstrom, N. O., Tran, T., Guo, J., Rutledge, E., Parvez, R. K., Thornton, M. E.*, et al.* (2018). Conserved and Divergent Molecular and Anatomic Features of Human and Mouse Nephron Patterning. *J Am Soc Nephrol, 29*(3), 825-840. doi:10.1681/ASN.2017091036

Litingtung, Y., & Chiang, C. (2000). Specification of ventral neuron types is mediated by an antagonistic interaction between Shh and Gli3. *Nat Neurosci, 3*(10), 979-985. doi:10.1038/79916

Little, M. H. (2015). *Kidney Development, Disease, Repair and Regeneration*: Elsevier Science.

Liu, Y., Pathak, N., Kramer-Zucker, A., & Drummond, I. A. (2007). Notch signaling controls the differentiation of transporting epithelia and multiciliated cells in the zebrafish pronephros. *Development, 134*(6), 1111-1122. doi:10.1242/dev.02806

Loane, M., Dolk, H., Kelly, A., Teljeur, C., Greenlees, R., & Densem, J. (2011). Paper 4: EUROCAT statistical monitoring: identification and investigation of ten year trends of congenital anomalies in Europe. *Birth Defects Res A Clin Mol Teratol, 91 Suppl 1*, S31-43. doi:10.1002/bdra.20778

Logan, C. V., Abdel-Hamed, Z., & Johnson, C. A. (2011). Molecular genetics and pathogenic mechanisms for the severe ciliopathies: insights into neurodevelopment and pathogenesis of neural tube defects. *Mol Neurobiol, 43*(1), 12-26. doi:10.1007/s12035-010-8154-0

Lowery, L. A., & Sive, H. (2005). Initial formation of zebrafish brain ventricles occurs independently of circulation and requires the nagie oko and snakehead/atp1a1a.1 gene products. *Development, 132*(9), 2057-2067. doi:10.1242/dev.01791

Luders, J., & Stearns, T. (2007). Microtubule-organizing centres: a re-evaluation. *Nat Rev Mol Cell Biol, 8*(2), 161-167. doi:10.1038/nrm2100

Ludwig, K. S., & Landmann, L. (2005). Early development of the human mesonephros. *Anat Embryol (Berl), 209*(6), 439-447. doi:10.1007/s00429-005-0460-3

Lundberg, Y. W., Xu, Y., Thiessen, K. D., & Kramer, K. L. (2015). Mechanisms of otoconia and otolith development. *Dev Dyn, 244*(3), 239-253. doi:10.1002/dvdy.24195

Lyons, J. P., Miller, R. K., Zhou, X., Weidinger, G., Deroo, T., Denayer, T.*, et al.* (2009). Requirement of Wnt/beta-catenin signaling in pronephric kidney development. *Mech Dev, 126*(3-4), 142-159. doi:10.1016/j.mod.2008.11.007

Ma, D., & Liu, F. (2015). Genome Editing and Its Applications in Model Organisms. *Genomics Proteomics Bioinformatics, 13*(6), 336-344. doi:10.1016/j.gpb.2015.12.001

Ma, M., & Jiang, Y. J. (2007). Jagged2a-notch signaling mediates cell fate choice in the zebrafish pronephric duct. *PLoS Genet, 3*(1), e18. doi:10.1371/journal.pgen.0030018

Macumber, I., Schwartz, S., & Leca, N. (2017). Maternal obesity is associated with congenital anomalies of the kidney and urinary tract in offspring. *Pediatr Nephrol, 32*(4), 635-642. doi:10.1007/s00467-016-3543-x

Madariaga, L., Moriniere, V., Jeanpierre, C., Bouvier, R., Loget, P., Martinovic, J.*, et al.* (2013). Severe prenatal renal anomalies associated with mutations in HNF1B or PAX2 genes. *Clin J Am Soc Nephrol, 8*(7), 1179-1187. doi:10.2215/cjn.10221012

Mah, S. P., Saueressig, H., Goulding, M., Kintner, C., & Dressler, G. R. (2000). Kidney development in cadherin-6 mutants: delayed mesenchyme-to-epithelial conversion and loss of nephrons. *Dev Biol, 223*(1), 38-53. doi:10.1006/dbio.2000.9738

Majumdar, A., & Drummond, I. A. (1999). Podocyte differentiation in the absence of endothelial cells as revealed in the zebrafish avascular mutant, cloche. *Dev Genet, 24*(3-4), 220-229. doi:10.1002/(sici)1520-6408(1999)24:3/4<220::aid-dvg5>3.0.co;2-1

Majumdar, A., & Drummond, I. A. (2000). The zebrafish floating head mutant demonstrates podocytes play an important role in directing glomerular differentiation. *Dev Biol, 222*(1), 147-157. doi:10.1006/dbio.2000.9642

Majumdar, A., Lun, K., Brand, M., & Drummond, I. A. (2000). Zebrafish no isthmus reveals a role for pax2.1 in tubule differentiation and patterning events in the pronephric primordia. *Development, 127*(10), 2089-2098.

Makrythanasis, P., Maroofian, R., Stray-Pedersen, A., Musaev, D., Zaki, M. S., Mahmoud, I. G.*, et al.* (2018). Biallelic variants in KIF14 cause intellectual disability with microcephaly. *Eur J Hum Genet, 26*(3), 330-339. doi:10.1038/s41431-017-0088-9

Maliga, Z., Junqueira, M., Toyoda, Y., Ettinger, A., Mora-Bermudez, F., Klemm, R. W.*, et al.* (2013). A genomic toolkit to investigate kinesin and myosin motor function in cells. *Nat Cell Biol, 15*(3), 325-334. doi:10.1038/ncb2689

Mangale, V. S., Hirokawa, K. E., Satyaki, P. R., Gokulchandran, N., Chikbire, S., Subramanian, L.*, et al.* (2008). Lhx2 selector activity specifies cortical identity and suppresses hippocampal organizer fate. *Science, 319*(5861), 304-309. doi:10.1126/science.1151695

Manning, A. L., Ganem, N. J., Bakhoum, S. F., Wagenbach, M., Wordeman, L., & Compton, D. A. (2007). The kinesin-13 proteins Kif2a, Kif2b, and Kif2c/MCAK have distinct roles during mitosis in human cells. *Mol Biol Cell, 18*(8), 2970-2979. doi:10.1091/mbc.e07-02-0110

Marcus, R. C., & Easter, S. S., Jr. (1995). Expression of glial fibrillary acidic protein and its relation to tract formation in embryonic zebrafish (Danio rerio). *J Comp Neurol, 359*(3), 365-381. doi:10.1002/cne.903590302

Marin‐Valencia, I., Guerrini, R., & Gleeson, J. G. (2014). Pathogenetic mechanisms of focal cortical dysplasia. *Epilepsia, 55*(7), 970-978. doi:10.1111/epi.12650

Marose, T. D., Merkel, C. E., McMahon, A. P., & Carroll, T. J. (2008). Beta-catenin is necessary to keep cells of ureteric bud/Wolffian duct epithelium in a precursor state. *Dev Biol, 314*(1), 112-126. doi:10.1016/j.ydbio.2007.11.016

Marra, A. N., Li, Y., & Wingert, R. A. (2016). Antennas of organ morphogenesis: the roles of cilia in vertebrate kidney development. *Genesis, 54*(9), 457-469. doi:10.1002/dvg.22957

Marsh, D. J. (1983). Renal Physiology.

Marszalek, J. R., Ruiz-Lozano, P., Roberts, E., Chien, K. R., & Goldstein, L. S. (1999). Situs inversus and embryonic ciliary morphogenesis defects in mouse mutants lacking the KIF3A subunit of kinesin-II. *Proc Natl Acad Sci U S A, 96*(9), 5043-5048.

Martin, C. A., Murray, J. E., Carroll, P., Leitch, A., Mackenzie, K. J., Halachev, M.*, et al.* (2016). Mutations in genes encoding condensin complex proteins cause microcephaly through decatenation failure at mitosis. *Genes Dev, 30*(19), 2158-2172. doi:10.1101/gad.286351.116

Mayr, M. I., Hummer, S., Bormann, J., Gruner, T., Adio, S., Woehlke, G.*, et al.* (2007). The human kinesin Kif18A is a motile microtubule depolymerase essential for chromosome congression. *Curr Biol, 17*(6), 488-498. doi:10.1016/j.cub.2007.02.036

McCampbell, K. K., & Wingert, R. A. (2014). New tides: using zebrafish to study renal regeneration. *Transl Res, 163*(2), 109-122. doi:10.1016/j.trsl.2013.10.003

McDonald, H. B., Stewart, R. J., & Goldstein, L. S. (1990). The kinesin-like ncd protein of Drosophila is a minus end-directed microtubule motor. *Cell, 63*(6), 1159-1165.

McGregor, L., Makela, V., Darling, S. M., Vrontou, S., Chalepakis, G., Roberts, C.*, et al.* (2003). Fraser syndrome and mouse blebbed phenotype caused by mutations in FRAS1/Fras1 encoding a putative extracellular matrix protein. *Nat Genet, 34*(2), 203-208. doi:10.1038/ng1142

McHugh, T., Gluszek, A. A., & Welburn, J. P. I. (2018). Microtubule end tethering of a processive kinesin-8 motor Kif18b is required for spindle positioning. *J Cell Biol, 217*(7), 2403-2416. doi:10.1083/jcb.201705209

McMahon, A. P. (2016). Development of the Mammalian Kidney. *Curr Top Dev Biol, 117*, 31-64. doi:10.1016/bs.ctdb.2015.10.010

Meluh, P. B., & Rose, M. D. (1990). KAR3, a kinesin-related gene required for yeast nuclear fusion. *Cell, 60*(6), 1029-1041.

Meunier, A., & Azimzadeh, J. (2016). Multiciliated Cells in Animals. *Cold Spring Harb Perspect Biol, 8*(12). doi:10.1101/cshperspect.a028233

Meyer, G., & Goffinet, A. M. (1998). Prenatal development of reelin-immunoreactive neurons in the human neocortex. *J Comp Neurol, 397*(1), 29-40.

Meyer, G., Schaaps, J. P., Moreau, L., & Goffinet, A. M. (2000). Embryonic and early fetal development of the human neocortex. *J Neurosci, 20*(5), 1858-1868.

Michael, L., & Davies, J. A. (2004). Pattern and regulation of cell proliferation during murine ureteric bud development. *J Anat, 204*(4), 241-255. doi:10.1111/j.0021-8782.2004.00285.x

Michos, O., Cebrian, C., Hyink, D., Grieshammer, U., Williams, L., D'Agati, V.*, et al.* (2010). Kidney development in the absence of Gdnf and Spry1 requires Fgf10. *PLoS Genet, 6*(1), e1000809. doi:10.1371/journal.pgen.1000809

Michos, O., Goncalves, A., Lopez-Rios, J., Tiecke, E., Naillat, F., Beier, K.*, et al.* (2007). Reduction of BMP4 activity by gremlin 1 enables ureteric bud outgrowth and GDNF/WNT11 feedback signalling during kidney branching morphogenesis. *Development, 134*(13), 2397-2405. doi:10.1242/dev.02861

Mick, D. U., Rodrigues, R. B., Leib, R. D., Adams, C. M., Chien, A. S., Gygi, S. P.*, et al.* (2015). Proteomics of Primary Cilia by Proximity Labeling. *Dev Cell, 35*(4), 497-512. doi:10.1016/j.devcel.2015.10.015

Miki, H., Okada, Y., & Hirokawa, N. (2005). Analysis of the kinesin superfamily: insights into structure and function. *Trends Cell Biol, 15*(9), 467-476. doi:10.1016/j.tcb.2005.07.006

Miki, H., Setou, M., Kaneshiro, K., & Hirokawa, N. (2001). All kinesin superfamily protein, KIF, genes in mouse and human. *Proc Natl Acad Sci U S A, 98*(13), 7004-7011. doi:10.1073/pnas.111145398

Miller, M. S., Esparza, J. M., Lippa, A. M., Lux, F. G., 3rd, Cole, D. G., & Dutcher, S. K. (2005). Mutant kinesin-2 motor subunits increase chromosome loss. *Mol Biol Cell, 16*(8), 3810-3820. doi:10.1091/mbc.e05-05-0404

Mirzaa, G. M., & Annapurna, P. (2014). Megalencephaly and hemimegalencephaly: Breakthroughs in molecular etiology. *American Journal of Medical Genetics Part C: Seminars in Medical Genetics, 166*(2), 156-172. doi:doi:10.1002/ajmg.c.31401

Mirzaa, G. M., Vitre, B., Carpenter, G., Abramowicz, I., Gleeson, J. G., Paciorkowski, A. R.*, et al.* (2014). Mutations in CENPE define a novel kinetochore-centromeric mechanism for microcephalic primordial dwarfism. *Hum Genet, 133*(8), 1023-1039. doi:10.1007/s00439-014-1443-3

Mishima, M., Kaitna, S., & Glotzer, M. (2002). Central spindle assembly and cytokinesis require a kinesin-like protein/RhoGAP complex with microtubule bundling activity. *Dev Cell, 2*(1), 41-54.

Miyamoto, T., Hosoba, K., Ochiai, H., Royba, E., Izumi, H., Sakuma, T.*, et al.* (2015). The Microtubule-Depolymerizing Activity of a Mitotic Kinesin Protein KIF2A Drives Primary Cilia Disassembly Coupled with Cell Proliferation. *Cell Rep*. doi:10.1016/j.celrep.2015.01.003

Miyata, T., Kawaguchi, A., Okano, H., & Ogawa, M. (2001). Asymmetric inheritance of radial glial fibers by cortical neurons. *Neuron, 31*(5), 727-741.

Miyazaki, Y., Oshima, K., Fogo, A., Hogan, B. L., & Ichikawa, I. (2000). Bone morphogenetic protein 4 regulates the budding site and elongation of the mouse ureter. *J Clin Invest, 105*(7), 863-873. doi:10.1172/jci8256

Moawia, A., Shaheen, R., Rasool, S., Waseem, S. S., Ewida, N., Budde, B.*, et al.* (2017). Mutations of KIF14 cause primary microcephaly by impairing cytokinesis. *Ann Neurol, 82*(4), 562-577. doi:10.1002/ana.25044

Molina, I., Baars, S., Brill, J. A., Hales, K. G., Fuller, M. T., & Ripoll, P. (1997). A chromatin-associated kinesin-related protein required for normal mitotic chromosome segregation in Drosophila. *J Cell Biol, 139*(6), 1361-1371.

Mollinari, C., Kleman, J. P., Jiang, W., Schoehn, G., Hunter, T., & Margolis, R. L. (2002). PRC1 is a microtubule binding and bundling protein essential to maintain the mitotic spindle midzone. *J Cell Biol, 157*(7), 1175-1186. doi:10.1083/jcb.200111052

Molnar, Z., Metin, C., Stoykova, A., Tarabykin, V., Price, D. J., Francis, F.*, et al.* (2006). Comparative aspects of cerebral cortical development. *Eur J Neurosci, 23*(4), 921-934. doi:10.1111/j.1460-9568.2006.04611.x

Molyneaux, B. J., Arlotta, P., Menezes, J. R., & Macklis, J. D. (2007). Neuronal subtype specification in the cerebral cortex. *Nat Rev Neurosci, 8*(6), 427-437. doi:10.1038/nrn2151

Moore, K. L., Persaud, T. V. N., & Torchia, M. G. (2011). *The Developing Human E-Book*: Elsevier Health Sciences.

Mudumana, S. P., Hentschel, D., Liu, Y., Vasilyev, A., & Drummond, I. A. (2008). odd skipped related1 reveals a novel role for endoderm in regulating kidney versus vascular cell fate. *Development, 135*(20), 3355-3367. doi:10.1242/dev.022830

Mugford, J. W., Sipila, P., McMahon, J. A., & McMahon, A. P. (2008). Osr1 expression demarcates a multi-potent population of intermediate mesoderm that undergoes progressive restriction to an Osr1-dependent nephron progenitor compartment within the mammalian kidney. *Dev Biol, 324*(1), 88-98. doi:10.1016/j.ydbio.2008.09.010

Mugford, J. W., Yu, J., Kobayashi, A., & McMahon, A. P. (2009). High-resolution gene expression analysis of the developing mouse kidney defines novel cellular compartments within the nephron progenitor population. *Dev Biol, 333*(2), 312-323. doi:10.1016/j.ydbio.2009.06.043

Nachury, M. V., Loktev, A. V., Zhang, Q., Westlake, C. J., Peranen, J., Merdes, A.*, et al.* (2007). A core complex of BBS proteins cooperates with the GTPase Rab8 to promote ciliary membrane biogenesis. *Cell, 129*(6), 1201-1213. doi:10.1016/j.cell.2007.03.053

Nadarajah, B., Brunstrom, J. E., Grutzendler, J., Wong, R. O., & Pearlman, A. L. (2001). Two modes of radial migration in early development of the cerebral cortex. *Nat Neurosci, 4*(2), 143-150. doi:10.1038/83967

Nadarajah, B., & Parnavelas, J. G. (2002). Modes of neuronal migration in the developing cerebral cortex. *Nat Rev Neurosci, 3*(6), 423-432. doi:10.1038/nrn845

Neef, R., Gruneberg, U., Kopajtich, R., Li, X., Nigg, E. A., Sillje, H.*, et al.* (2007). Choice of Plk1 docking partners during mitosis and cytokinesis is controlled by the activation state of Cdk1. *Nat Cell Biol, 9*(4), 436-444. doi:10.1038/ncb1557

Nguyen, L. N., Ma, D., Shui, G., Wong, P., Cazenave-Gassiot, A., Zhang, X.*, et al.* (2014). Mfsd2a is a transporter for the essential omega-3 fatty acid docosahexaenoic acid. *Nature, 509*(7501), 503-506. doi:10.1038/nature13241

Nichane, M., Van Campenhout, C., Pendeville, H., Voz, M. L., & Bellefroid, E. J. (2006). The Na+/PO4 cotransporter SLC20A1 gene labels distinct restricted subdomains of the developing pronephros in Xenopus and zebrafish embryos. *Gene Expr Patterns, 6*(7), 667-672. doi:10.1016/j.modgep.2006.01.005

Nicholas, A. K., Khurshid, M., Desir, J., Carvalho, O. P., Cox, J. J., Thornton, G.*, et al.* (2010). WDR62 is associated with the spindle pole and is mutated in human microcephaly. *Nat Genet, 42*(11), 1010-1014. doi:10.1038/ng.682

Nicolaou, N., Renkema, K. Y., Bongers, E. M., Giles, R. H., & Knoers, N. V. (2015). Genetic, environmental, and epigenetic factors involved in CAKUT. *Nat Rev Nephrol, 11*(12), 720-731. doi:10.1038/nrneph.2015.140

Nieto, M., Monuki, E. S., Tang, H., Imitola, J., Haubst, N., Khoury, S. J.*, et al.* (2004). Expression of Cux-1 and Cux-2 in the subventricular zone and upper layers II-IV of the cerebral cortex. *J Comp Neurol, 479*(2), 168-180. doi:10.1002/cne.20322

Niwa, S., Nakajima, K., Miki, H., Minato, Y., Wang, D., & Hirokawa, N. (2012). KIF19A is a microtubule-depolymerizing kinesin for ciliary length control. *Dev Cell, 23*(6), 1167-1175. doi:10.1016/j.devcel.2012.10.016

Noctor, S. C., Flint, A. C., Weissman, T. A., Dammerman, R. S., & Kriegstein, A. R. (2001). Neurons derived from radial glial cells establish radial units in neocortex. *Nature, 409*(6821), 714-720. doi:10.1038/35055553

Noctor, S. C., Martinez-Cerdeno, V., Ivic, L., & Kriegstein, A. R. (2004). Cortical neurons arise in symmetric and asymmetric division zones and migrate through specific phases. *Nat Neurosci, 7*(2), 136-144. doi:10.1038/nn1172

Noctor, S. C., Martinez-Cerdeno, V., & Kriegstein, A. R. (2008). Distinct behaviors of neural stem and progenitor cells underlie cortical neurogenesis. *J Comp Neurol, 508*(1), 28-44. doi:10.1002/cne.21669

Nonaka, S., Tanaka, Y., Okada, Y., Takeda, S., Harada, A., Kanai, Y.*, et al.* (1998). Randomization of left-right asymmetry due to loss of nodal cilia generating leftward flow of extraembryonic fluid in mice lacking KIF3B motor protein. *Cell, 95*(6), 829-837.

Novas, R., Cardenas-Rodriguez, M., Lepanto, P., Fabregat, M., Rodao, M., Fariello, M. I.*, et al.* (2018). Kinesin 1 regulates cilia length through an interaction with the Bardet-Biedl syndrome related protein CCDC28B. *Sci Rep, 8*(1), 3019. doi:10.1038/s41598-018-21329-6

Novorol, C., Burkhardt, J., Wood, K. J., Iqbal, A., Roque, C., Coutts, N.*, et al.* (2013). Microcephaly models in the developing zebrafish retinal neuroepithelium point to an underlying defect in metaphase progression. *Open Biol, 3*(10), 130065. doi:10.1098/rsob.130065

Nunes Bastos, R., Gandhi, S. R., Baron, R. D., Gruneberg, U., Nigg, E. A., & Barr, F. A. (2013). Aurora B suppresses microtubule dynamics and limits central spindle size by locally activating KIF4A. *J Cell Biol, 202*(4), 605-621. doi:10.1083/jcb.201301094

O'Brien, L. L., Grimaldi, M., Kostun, Z., Wingert, R. A., Selleck, R., & Davidson, A. J. (2011). Wt1a, Foxc1a, and the Notch mediator Rbpj physically interact and regulate the formation of podocytes in zebrafish. *Dev Biol, 358*(2), 318-330. doi:10.1016/j.ydbio.2011.08.005

O'Rahilly, R., & Muller, F. (2008). Significant features in the early prenatal development of the human brain. *Ann Anat, 190*(2), 105-118. doi:10.1016/j.aanat.2008.01.001

Obara-Ishihara, T., Kuhlman, J., Niswander, L., & Herzlinger, D. (1999). The surface ectoderm is essential for nephric duct formation in intermediate mesoderm. *Development, 126*(6), 1103-1108.

Ohkura, H., Torok, T., Tick, G., Hoheisel, J., Kiss, I., & Glover, D. M. (1997). Mutation of a gene for a Drosophila kinesin-like protein, Klp38B, leads to failure of cytokinesis. *J Cell Sci, 110 (Pt 8)*, 945-954.

Ohuchi, H., Hori, Y., Yamasaki, M., Harada, H., Sekine, K., Kato, S.*, et al.* (2000). FGF10 acts as a major ligand for FGF receptor 2 IIIb in mouse multi-organ development. *Biochem Biophys Res Commun, 277*(3), 643-649. doi:10.1006/bbrc.2000.3721

Oliver, J., & MacDowell, M. (1968). *Nephrons and Kidneys: A Quantitative Study of Developmental and Evolutionary Mammalian Renal Architectonics*: Hoeber Medical Division, Harper & Row.

Ooshio, T., Fujita, N., Yamada, A., Sato, T., Kitagawa, Y., Okamoto, R.*, et al.* (2007). Cooperative roles of Par-3 and afadin in the formation of adherens and tight junctions. *J Cell Sci, 120*(Pt 14), 2352-2365. doi:10.1242/jcs.03470

Osathanondh, V., & Potter, E. L. (1963a). DEVELOPMENT OF HUMAN KIDNEY AS SHOWN BY MICRODISSECTION. II. RENAL PELVIS, CALYCES, AND PAPILLAE. *Arch Pathol, 76*, 277-289.

Osathanondh, V., & Potter, E. L. (1963b). DEVELOPMENT OF HUMAN KIDNEY AS SHOWN BY MICRODISSECTION. III. FORMATION AND INTERRELATIONSHIP OF COLLECTING TUBULES AND NEPHRONS. *Arch Pathol, 76*, 290-302.

Outtandy, P., Russell, C., Kleta, R., & Bockenhauer, D. (2018). Zebrafish as a model for kidney function and disease. *Pediatr Nephrol*. doi:10.1007/s00467-018-3921-7

Pachnis, V., Mankoo, B., & Costantini, F. (1993). Expression of the c-ret proto-oncogene during mouse embryogenesis. *Development, 119*(4), 1005-1017.

Packard, A., Georgas, K., Michos, O., Riccio, P., Cebrian, C., Combes, A. N.*, et al.* (2013). Luminal mitosis drives epithelial cell dispersal within the branching ureteric bud. *Dev Cell, 27*(3), 319-330. doi:10.1016/j.devcel.2013.09.001

Paek, H., Gutin, G., & Hebert, J. M. (2009). FGF signaling is strictly required to maintain early telencephalic precursor cell survival. *Development, 136*(14), 2457-2465. doi:10.1242/dev.032656

Panizzi, J. R., Jessen, J. R., Drummond, I. A., & Solnica-Krezel, L. (2007). New functions for a vertebrate Rho guanine nucleotide exchange factor in ciliated epithelia. *Development, 134*(5), 921-931. doi:10.1242/dev.02776

Paridaen, J. T., & Huttner, W. B. (2014). Neurogenesis during development of the vertebrate central nervous system. *EMBO Rep, 15*(4), 351-364. doi:10.1002/embr.201438447

Paridaen, J. T., Wilsch-Brauninger, M., & Huttner, W. B. (2013). Asymmetric inheritance of centrosome-associated primary cilium membrane directs ciliogenesis after cell division. *Cell, 155*(2), 333-344. doi:10.1016/j.cell.2013.08.060

Park, J. S., Valerius, M. T., & McMahon, A. P. (2007). Wnt/beta-catenin signaling regulates nephron induction during mouse kidney development. *Development, 134*(13), 2533-2539. doi:10.1242/dev.006155

Park, T. J., Mitchell, B. J., Abitua, P. B., Kintner, C., & Wallingford, J. B. (2008). Dishevelled controls apical docking and planar polarization of basal bodies in ciliated epithelial cells. *Nat Genet, 40*(7), 871-879. doi:10.1038/ng.104

Paul, B. M., & Vanden Heuvel, G. B. (2014). Kidney: polycystic kidney disease. *Wiley Interdiscip Rev Dev Biol, 3*(6), 465-487. doi:10.1002/wdev.152

Pavicic-Kaltenbrunner, V., Mishima, M., & Glotzer, M. (2007). Cooperative assembly of CYK-4/MgcRacGAP and ZEN-4/MKLP1 to form the centralspindlin complex. *Mol Biol Cell, 18*(12), 4992-5003. doi:10.1091/mbc.e07-05-0468

Pepicelli, C. V., Kispert, A., Rowitch, D. H., & McMahon, A. P. (1997). GDNF induces branching and increased cell proliferation in the ureter of the mouse. *Dev Biol, 192*(1), 193-198. doi:10.1006/dbio.1997.8745

Perantoni, A. O., Timofeeva, O., Naillat, F., Richman, C., Pajni-Underwood, S., Wilson, C.*, et al.* (2005). Inactivation of FGF8 in early mesoderm reveals an essential role in kidney development. *Development, 132*(17), 3859-3871. doi:10.1242/dev.01945

Perner, B., Englert, C., & Bollig, F. (2007). The Wilms tumor genes wt1a and wt1b control different steps during formation of the zebrafish pronephros. *Dev Biol, 309*(1), 87-96. doi:10.1016/j.ydbio.2007.06.022

Pezeron, G., Mourrain, P., Courty, S., Ghislain, J., Becker, T. S., Rosa, F. M.*, et al.* (2008). Live analysis of endodermal layer formation identifies random walk as a novel gastrulation movement. *Curr Biol, 18*(4), 276-281. doi:10.1016/j.cub.2008.01.028

Pfaff, K. L., Straub, C. T., Chiang, K., Bear, D. M., Zhou, Y., & Zon, L. I. (2007). The zebra fish cassiopeia mutant reveals that SIL is required for mitotic spindle organization. *Mol Cell Biol, 27*(16), 5887-5897. doi:10.1128/MCB.00175-07

Pfeffer, P. L., Gerster, T., Lun, K., Brand, M., & Busslinger, M. (1998). Characterization of three novel members of the zebrafish Pax2/5/8 family: dependency of Pax5 and Pax8 expression on the Pax2.1 (noi) function. *Development, 125*(16), 3063-3074.

Pickart, M. A., & Klee, E. W. (2014). Zebrafish approaches enhance the translational research tackle box. *Transl Res, 163*(2), 65-78. doi:10.1016/j.trsl.2013.10.007

Pohl, C., & Jentsch, S. (2009). Midbody ring disposal by autophagy is a post-abscission event of cytokinesis. *Nat Cell Biol, 11*(1), 65-70. doi:10.1038/ncb1813

Poirier, K., Lebrun, N., Broix, L., Tian, G., Saillour, Y., Boscheron, C.*, et al.* (2013). Mutations in TUBG1, DYNC1H1, KIF5C and KIF2A cause malformations of cortical development and microcephaly. *Nat Genet, 45*(6), 639-647. doi:10.1038/ng.2613

Porter, F. D., Drago, J., Xu, Y., Cheema, S. S., Wassif, C., Huang, S. P*., et al.* (1997). Lhx2, a LIM homeobox gene, is required for eye, forebrain, and definitive erythrocyte development. *Development, 124*(15), 2935-2944.

Postiglione, M. P., Juschke, C., Xie, Y., Haas, G. A., Charalambous, C., & Knoblich, J. A. (2011). Mouse inscuteable induces apical-basal spindle orientation to facilitate intermediate progenitor generation in the developing neocortex. *Neuron, 72*(2), 269-284. doi:10.1016/j.neuron.2011.09.022

Poureetezadi, S. J., & Wingert, R. A. (2016). Little fish, big catch: zebrafish as a model for kidney disease. *Kidney Int, 89*(6), 1204-1210. doi:10.1016/j.kint.2016.01.031

Prevo, B., Mangeol, P., Oswald, F., Scholey, J. M., & Peterman, E. J. (2015). Functional differentiation of cooperating kinesin-2 motors orchestrates cargo import and transport in C. elegans cilia. *Nat Cell Biol, 17*(12), 1536-1545. doi:10.1038/ncb3263

Pyati, U. J., Cooper, M. S., Davidson, A. J., Nechiporuk, A., & Kimelman, D. (2006). Sustained Bmp signaling is essential for cloaca development in zebrafish. *Development, 133*(11), 2275-2284. doi:10.1242/dev.02388

Qiao, J., Sakurai, H., & Nigam, S. K. (1999). Branching morphogenesis independent of mesenchymal-epithelial contact in the developing kidney. *Proc Natl Acad Sci U S A, 96*(13), 7330-7335.

Qiao, J., Uzzo, R., Obara-Ishihara, T., Degenstein, L., Fuchs, E., & Herzlinger, D. (1999). FGF-7 modulates ureteric bud growth and nephron number in the developing kidney. *Development, 126*(3), 547-554.

Qin, J., Lin, Y., Norman, R. X., Ko, H. W., & Eggenschwiler, J. T. (2011). Intraflagellar transport protein 122 antagonizes Sonic Hedgehog signaling and controls ciliary localization of pathway components. *Proc Natl Acad Sci U S A, 108*(4), 1456-1461. doi:10.1073/pnas.1011410108

Quaggin, S. E., & Kreidberg, J. A. (2008). Development of the renal glomerulus: good neighbors and good fences. *Development, 135*(4), 609-620. doi:10.1242/dev.001081

Rakic, P. (1974). Neurons in rhesus monkey visual cortex: systematic relation between time of origin and eventual disposition. *Science, 183*(4123), 425-427.

Rallu, M., Machold, R., Gaiano, N., Corbin, J. G., McMahon, A. P., & Fishell, G. (2002). Dorsoventral patterning is established in the telencephalon of mutants lacking both Gli3 and Hedgehog signaling. *Development, 129*(21), 4963-4974.

Ran, F. A., Hsu, P. D., Wright, J., Agarwala, V., Scott, D. A., & Zhang, F. (2013). Genome engineering using the CRISPR-Cas9 system. *Nat Protoc, 8*(11), 2281-2308. doi:10.1038/nprot.2013.143

Ray, S., Meyhofer, E., Milligan, R. A., & Howard, J. (1993). Kinesin follows the microtubule's protofilament axis. *J Cell Biol, 121*(5), 1083-1093.

Recuenco, M. C., Ohmori, T., Tanigawa, S., Taguchi, A., Fujimura, S., Conti, M. A*., et al.* (2015). Nonmuscle Myosin II Regulates the Morphogenesis of Metanephric Mesenchyme-Derived Immature Nephrons. *J Am Soc Nephrol, 26*(5), 1081-1091. doi:10.1681/asn.2014030281

Reiter, J. F., & Leroux, M. R. (2017). Genes and molecular pathways underpinning ciliopathies. *Nat Rev Mol Cell Biol, 18*(9), 533-547. doi:10.1038/nrm.2017.60

Renkema, K. Y., Stokman, M. F., Giles, R. H., & Knoers, N. V. (2014). Next-generation sequencing for research and diagnostics in kidney disease. *Nat Rev Nephrol, 10*(8), 433-444. doi:10.1038/nrneph.2014.95

Riccio, P., Cebrian, C., Zong, H., Hippenmeyer, S., & Costantini, F. (2016). Ret and Etv4 Promote Directed Movements of Progenitor Cells during Renal Branching Morphogenesis. *PLoS Biol, 14*(2), e1002382. doi:10.1371/journal.pbio.1002382

Rice, S., Lin, A. W., Safer, D., Hart, C. L., Naber, N., Carragher, B. O*., et al.* (1999). A structural change in the kinesin motor protein that drives motility. *Nature, 402*(6763), 778-784. doi:10.1038/45483

Rodriguez, M. M. (2014). Congenital Anomalies of the Kidney and the Urinary Tract (CAKUT). *Fetal Pediatr Pathol, 33*(5-6), 293-320. doi:10.3109/15513815.2014.959678

Rogers, G. C., Rogers, S. L., Schwimmer, T. A., Ems-McClung, S. C., Walczak, C. E., Vale, R. D*., et al.* (2004). Two mitotic kinesins cooperate to drive sister chromatid separation during anaphase. *Nature, 427*(6972), 364-370. doi:10.1038/nature02256

Rohde, L. A., & Heisenberg, C. P. (2007). Zebrafish Gastrulation: Cell Movements, Signals, and Mechanisms. *261*, 159-192. doi:10.1016/s0074-7696(07)61004-3

Romani, M., Micalizzi, A., & Valente, E. M. (2013). Joubert syndrome: congenital cerebellar ataxia with the molar tooth. *Lancet Neurol, 12*(9), 894-905. doi:10.1016/s1474-4422(13)70136-4

Romero, D. M., Bahi-Buisson, N., & Francis, F. (2018). Genetics and mechanisms leading to human cortical malformations. *Semin Cell Dev Biol, 76*, 33-75. doi:10.1016/j.semcdb.2017.09.031

Rosenfeld, S. S., Fordyce, P. M., Jefferson, G. M., King, P. H., & Block, S. M. (2003). Stepping and stretching. How kinesin uses internal strain to walk processively. *J Biol Chem, 278*(20), 18550-18556. doi:10.1074/jbc.M300849200

Ross, A. J., Dailey, L. A., Brighton, L. E., & Devlin, R. B. (2007). Transcriptional profiling of mucociliary differentiation in human airway epithelial cells. *Am J Respir Cell Mol Biol, 37*(2), 169-185. doi:10.1165/rcmb.2006-0466OC

Rubenstein, M., Meyer, R., & Bernstein, J. (1961). Congenital abnormalities of the urinary system. I. A postmortem survey of developmental anomalies and acquired congenital lesions in a children's hospital. *J Pediatr, 58*, 356-366.

Ruden, D. M., Cui, W., Sollars, V., & Alterman, M. (1997). A Drosophila kinesin-like protein, Klp38B, functions during meiosis, mitosis, and segmentation. *Dev Biol, 191*(2), 284-296. doi:10.1006/dbio.1997.8726

Ryan, R., Failler, M., Reilly, M. L., Garfa-Traore, M., Delous, M., Filhol, E*., et al.* (2018). Functional characterization of tektin-1 in motile cilia and evidence for TEKT1 as a new candidate gene for motile ciliopathies. *Hum Mol Genet, 27*(2), 266-282. doi:10.1093/hmg/ddx396

Sainio, K., Suvanto, P., Davies, J., Wartiovaara, J., Wartiovaara, K., Saarma, M*., et al.* (1997). Glial-cell-line-derived neurotrophic factor is required for bud initiation from ureteric epithelium. *Development, 124*(20), 4077-4087.

Sakurai, H., Bush, K. T., & Nigam, S. K. (2001). Identification of pleiotrophin as a mesenchymal factor involved in ureteric bud branching morphogenesis. *Development, 128*(17), 3283-3293.

Sanchez, I., & Dynlacht, B. D. (2016). Cilium assembly and disassembly. *Nat Cell Biol, 18*(7), 711-717. doi:10.1038/ncb3370

Sanna-Cherchi, S., Westland, R., Ghiggeri, G. M., & Gharavi, A. G. (2018). Genetic basis of human congenital anomalies of the kidney and urinary tract. *J Clin Invest, 128*(1), 4-15. doi:10.1172/JCI95300

Sanyanusin, P., Schimmenti, L. A., McNoe, L. A., Ward, T. A., Pierpont, M. E., Sullivan, M. J*., et al.* (1995). Mutation of the PAX2 gene in a family with optic nerve colobomas, renal anomalies and vesicoureteral reflux. *Nat Genet, 9*(4), 358-364. doi:10.1038/ng0495-358

Sarkisian, M. R., Li, W., Di Cunto, F., D'Mello, S. R., & LoTurco, J. J. (2002). Citron-kinase, a protein essential to cytokinesis in neuronal progenitors, is deleted in the flathead mutant rat. *J Neurosci, 22*(8), Rc217. doi:20026283

Satir, P., & Christensen, S. T. (2007). Overview of structure and function of mammalian cilia. *Annu Rev Physiol, 69*, 377-400. doi:10.1146/annurev.physiol.69.040705.141236

Sauer, F. C. (1935). Mitosis in the neural tube. *Journal of Comparative Neurology, 62*(2), 377-405. doi:doi:10.1002/cne.900620207

Saxen, L., Saxén, L., Bard, J. B. L., & Barlow, P. W. (1987). *Organogenesis of the Kidney*: Cambridge University Press.

Schedl, A. (2007). Renal abnormalities and their developmental origin. *Nat Rev Genet, 8*(10), 791-802. doi:10.1038/nrg2205

Schier, A. F., & Talbot, W. S. (2005). Molecular genetics of axis formation in zebrafish. *Annu Rev Genet, 39*, 561-613. doi:10.1146/annurev.genet.37.110801.143752

Schmid, B., Furthauer, M., Connors, S. A., Trout, J., Thisse, B., Thisse, C.*, et al.* (2000). Equivalent genetic roles for bmp7/snailhouse and bmp2b/swirl in dorsoventral pattern formation. *Development, 127*(5), 957-967.

Schmidt-Ott, K. M., & Barasch, J. (2008). WNT/beta-catenin signaling in nephron progenitors and their epithelial progeny. *Kidney Int, 74*(8), 1004-1008. doi:10.1038/ki.2008.322

Schmidt-Ott, K. M., Yang, J., Chen, X., Wang, H., Paragas, N., Mori, K.*, et al.* (2005). Novel regulators of kidney development from the tips of the ureteric bud. *J Am Soc Nephrol, 16*(7), 1993-2002. doi:10.1681/asn.2004121127

Schoenwolf, G. C., Bleyl, S. B., Brauer, P. R., & Francis-West, P. H. (2014). *Larsen's Human Embryology E-Book*: Elsevier Health Sciences.

Schoenwolf, G. C., & Delongo, J. (1980). Ultrastructure of secondary neurulation in the chick embryo. *Am J Anat, 158*(1), 43-63. doi:10.1002/aja.1001580106

Scholey, J. M. (2013). Kinesin-2: a family of heterotrimeric and homodimeric motors with diverse intracellular transport functions. *Annu Rev Cell Dev Biol, 29*, 443-469. doi:10.1146/annurev-cellbio-101512-122335

Scholey, J. M., Heuser, J., Yang, J. T., & Goldstein, L. S. (1989). Identification of globular mechanochemical heads of kinesin. *Nature, 338*(6213), 355-357. doi:10.1038/338355a0

Schou, K. B., Mogensen, J. B., Morthorst, S. K., Nielsen, B. S., Aleliunaite, A., Serra-Marques, A.*, et al.* (2017). KIF13B establishes a CAV1-enriched microdomain at the ciliary transition zone to promote Sonic hedgehog signalling. *Nat Commun, 8*, 14177. doi:10.1038/ncomms14177

Scott, R. P., & Quaggin, S. E. (2015). Review series: The cell biology of renal filtration. *J Cell Biol, 209*(2), 199-210. doi:10.1083/jcb.201410017

Seely, J. C. (2017). A brief review of kidney development, maturation, developmental abnormalities, and drug toxicity: juvenile animal relevancy. *J Toxicol Pathol, 30*(2), 125-133. doi:10.1293/tox.2017-0006

Self, M., Lagutin, O. V., Bowling, B., Hendrix, J., Cai, Y., Dressler, G. R.*, et al.* (2006). Six2 is required for suppression of nephrogenesis and progenitor renewal in the developing kidney. *EMBO J, 25*(21), 5214-5228. doi:10.1038/sj.emboj.7601381

Serluca, F. C., Drummond, I. A., & Fishman, M. C. (2002). Endothelial signaling in kidney morphogenesis: a role for hemodynamic forces. *Curr Biol, 12*(6), 492-497.

Serluca, F. C., & Fishman, M. C. (2001). Pre-pattern in the pronephric kidney field of zebrafish. *Development, 128*(12), 2233-2241.

Shah, M. M., Sampogna, R. V., Sakurai, H., Bush, K. T., & Nigam, S. K. (2004). Branching morphogenesis and kidney disease. *Development, 131*(7), 1449-1462. doi:10.1242/dev.01089

Shaheen, R., Hashem, A., Abdel-Salam, G. M., Al-Fadhli, F., Ewida, N., & Alkuraya, F. S. (2016). Mutations in CIT, encoding citron rho-interacting serine/threonine kinase, cause severe primary microcephaly in humans. *Hum Genet, 135*(10), 1191-1197. doi:10.1007/s00439-016-1722-2

Shakya, R., Watanabe, T., & Costantini, F. (2005). The role of GDNF/Ret signaling in ureteric bud cell fate and branching morphogenesis. *Dev Cell, 8*(1), 65-74. doi:10.1016/j.devcel.2004.11.008

Shimamura, K., & Rubenstein, J. L. (1997). Inductive interactions direct early regionalization of the mouse forebrain. *Development, 124*(14), 2709-2718.

Shimizu, T., Bae, Y. K., Muraoka, O., & Hibi, M. (2005). Interaction of Wnt and caudal-related genes in zebrafish posterior body formation. *Dev Biol, 279*(1), 125-141. doi:10.1016/j.ydbio.2004.12.007

Shitamukai, A., Konno, D., & Matsuzaki, F. (2011). Oblique radial glial divisions in the developing mouse neocortex induce self-renewing progenitors outside the germinal zone that resemble primate outer subventricular zone progenitors. *J Neurosci, 31*(10), 3683-3695. doi:10.1523/jneurosci.4773-10.2011

Short, K. M., Combes, A. N., Lefevre, J., Ju, A. L., Georgas, K. M., Lamberton, T.*, et al.* (2014). Global quantification of tissue dynamics in the developing mouse kidney. *Dev Cell, 29*(2), 188-202. doi:10.1016/j.devcel.2014.02.017

Sidman, R. L., & Rakic, P. (1973). Neuronal migration, with special reference to developing human brain: a review. *Brain Res, 62*(1), 1-35.

Skop, A. R., Liu, H., Yates, J., 3rd, Meyer, B. J., & Heald, R. (2004). Dissection of the mammalian midbody proteome reveals conserved cytokinesis mechanisms. *Science, 305*(5680), 61-66. doi:10.1126/science.1097931

Snow, J. J., Ou, G., Gunnarson, A. L., Walker, M. R., Zhou, H. M., Brust-Mascher, I.*, et al.* (2004). Two anterograde intraflagellar transport motors cooperate to build sensory cilia on C. elegans neurons. *Nat Cell Biol, 6*(11), 1109-1113. doi:10.1038/ncb1186

Solinet, S., Mahmud, K., Stewman, S. F., Ben El Kadhi, K., Decelle, B., Talje, L.*, et al.* (2013). The actin-binding ERM protein Moesin binds to and stabilizes microtubules at the cell cortex. *J Cell Biol, 202*(2), 251-260. doi:10.1083/jcb.201304052

Song, Z., Zhang, X., Jia, S., Yelick, P. C., & Zhao, C. (2016). Zebrafish as a Model for Human Ciliopathies. *J Genet Genomics, 43*(3), 107-120. doi:10.1016/j.jgg.2016.02.001

Sorokin, S. P. (1968). Reconstructions of centriole formation and ciliogenesis in mammalian lungs. *J Cell Sci, 3*(2), 207-230.

Spassky, N., & Meunier, A. (2017). The development and functions of multiciliated epithelia. *Nat Rev Mol Cell Biol, 18*(7), 423-436. doi:10.1038/nrm.2017.21

Squier, W., & Jansen, A. (2014). Polymicrogyria: pathology, fetal origins and mechanisms. *Acta Neuropathol Commun, 2*, 80. doi:10.1186/s40478-014-0080-3

Stancik, E. K., Navarro-Quiroga, I., Sellke, R., & Haydar, T. F. (2010). Heterogeneity in ventricular zone neural precursors contributes to neuronal fate diversity in the postnatal neocortex. *J Neurosci, 30*(20), 7028-7036. doi:10.1523/jneurosci.6131-09.2010

Stooke-Vaughan, G. A., Huang, P., Hammond, K. L., Schier, A. F., & Whitfield, T. T. (2012). The role of hair cells, cilia and ciliary motility in otolith formation in the zebrafish otic vesicle. *Development, 139*(10), 1777-1787. doi:10.1242/dev.079947

Stout, J. R., Yount, A. L., Powers, J. A., Leblanc, C., Ems-McClung, S. C., & Walczak, C. E. (2011). Kif18B interacts with EB1 and controls astral microtubule length during mitosis. *Mol Biol Cell, 22*(17), 3070-3080. doi:10.1091/mbc.E11-04-0363

Strnad, P., Leidel, S., Vinogradova, T., Euteneuer, U., Khodjakov, A., & Gonczy, P. (2007). Regulated HsSAS-6 levels ensure formation of a single procentriole per centriole during the centrosome duplication cycle. *Dev Cell, 13*(2), 203-213. doi:10.1016/j.devcel.2007.07.004

Stumpff, J., Wagenbach, M., Franck, A., Asbury, C. L., & Wordeman, L. (2012). Kif18A and chromokinesins confine centromere movements via microtubule growth suppression and spatial control of kinetochore tension. *Dev Cell, 22*(5), 1017-1029. doi:10.1016/j.devcel.2012.02.013

Sun, Z., Amsterdam, A., Pazour, G. J., Cole, D. G., Miller, M. S., & Hopkins, N. (2004). A genetic screen in zebrafish identifies cilia genes as a principal cause of cystic kidney. *Development, 131*(16), 4085-4093. doi:10.1242/dev.01240

Super, H., Soriano, E., & Uylings, H. B. (1998). The functions of the preplate in development and evolution of the neocortex and hippocampus. *Brain Res Brain Res Rev, 27*(1), 40-64.

Szczepanski, S., Hussain, M. S., Sur, I., Altmüller, J., Thiele, H., Abdullah, U.*, et al.* (2016). A novel homozygous splicing mutation of CASC5 causes primary microcephaly in a large Pakistani family. *Human Genetics, 135*(2), 157-170. doi:10.1007/s00439-015-1619-5

Tamamaki, N., Nakamura, K., Okamoto, K., & Kaneko, T. (2001). Radial glia is a progenitor of neocortical neurons in the developing cerebral cortex. *Neurosci Res, 41*(1), 51-60.

Tan, X., & Shi, S. H. (2013). Neocortical neurogenesis and neuronal migration. *Wiley Interdiscip Rev Dev Biol, 2*(4), 443-459. doi:10.1002/wdev.88

Tanenbaum, M. E., Macurek, L., Janssen, A., Geers, E. F., Alvarez-Fernandez, M., & Medema, R. H. (2009). Kif15 cooperates with eg5 to promote bipolar spindle assembly. *Curr Biol, 19*(20), 1703-1711. doi:10.1016/j.cub.2009.08.027

Tanenbaum, M. E., & Medema, R. H. (2010). Mechanisms of centrosome separation and bipolar spindle assembly. *Dev Cell, 19*(6), 797-806. doi:10.1016/j.devcel.2010.11.011

Tang, C. J., Fu, R. H., Wu, K. S., Hsu, W. B., & Tang, T. K. (2009). CPAP is a cell-cycle regulated protein that controls centriole length. *Nat Cell Biol, 11*(7), 825-831. doi:10.1038/ncb1889

Tanigawa, S., Wang, H., Yang, Y., Sharma, N., Tarasova, N., Ajima, R.*, et al.* (2011). Wnt4 induces nephronic tubules in metanephric mesenchyme by a non-canonical mechanism. *Dev Biol, 352*(1), 58-69. doi:10.1016/j.ydbio.2011.01.012

Taulet, N., Vitre, B., Anguille, C., Douanier, A., Rocancourt, M., Taschner, M.*, et al.* (2017). IFT proteins spatially control the geometry of cleavage furrow ingression and lumen positioning. *Nat Commun, 8*(1), 1928. doi:10.1038/s41467-017-01479-3

Taverna, E., & Huttner, W. B. (2010). Neural progenitor nuclei IN motion. *Neuron, 67*(6), 906-914. doi:10.1016/j.neuron.2010.08.027

Tawk, M., Araya, C., Lyons, D. A., Reugels, A. M., Girdler, G. C., Bayley, P. R.*, et al.* (2007). A mirror-symmetric cell division that orchestrates neuroepithelial morphogenesis. *Nature, 446*(7137), 797-800. doi:10.1038/nature05722

Thomas, J., Morle, L., Soulavie, F., Laurencon, A., Sagnol, S., & Durand, B. (2010). Transcriptional control of genes involved in ciliogenesis: a first step in making cilia. *Biol Cell, 102*(9), 499-513. doi:10.1042/bc20100035

Truebestein, L., & Leonard, T. A. (2016). Coiled-coils: The long and short of it. *Bioessays, 38*(9), 903-916. doi:10.1002/bies.201600062

Tsang, T. E., Shawlot, W., Kinder, S. J., Kobayashi, A., Kwan, K. M., Schughart, K.*, et al.* (2000). Lim1 activity is required for intermediate mesoderm differentiation in the mouse embryo. *Dev Biol, 223*(1), 77-90. doi:10.1006/dbio.2000.9733

Tucker, J. A., Mintzer, K. A., & Mullins, M. C. (2008). The BMP signaling gradient patterns dorsoventral tissues in a temporally progressive manner along the anteroposterior axis. *Dev Cell, 14*(1), 108-119. doi:10.1016/j.devcel.2007.11.004

Uy, N., & Reidy, K. (2016). Developmental Genetics and Congenital Anomalies of the Kidney and Urinary Tract. *J Pediatr Genet, 5*(1), 51-60. doi:10.1055/s-0035-1558423

Vale, R. D., Reese, T. S., & Sheetz, M. P. (1985). Identification of a novel force-generating protein, kinesin, involved in microtubule-based motility. *Cell, 42*(1), 39-50.

van Dam, T. J., Wheway, G., Slaats, G. G., Huynen, M. A., & Giles, R. H. (2013). The SYSCILIA gold standard (SCGSv1) of known ciliary components and its applications within a systems biology consortium. *Cilia, 2*(1), 7. doi:10.1186/2046-2530-2-7

van der Vaart, B., van Riel, W. E., Doodhi, H., Kevenaar, J. T., Katrukha, E. A., Gumy, L.*, et al.* (2013). CFEOM1-associated kinesin KIF21A is a cortical microtubule growth inhibitor. *Dev Cell, 27*(2), 145-160. doi:10.1016/j.devcel.2013.09.010

van der Ven, A. T., Vivante, A., & Hildebrandt, F. (2018). Novel Insights into the Pathogenesis of Monogenic Congenital Anomalies of the Kidney and Urinary Tract. *J Am Soc Nephrol, 29*(1), 36-50. doi:10.1681/asn.2017050561

Varga, Z. M., Wegner, J., & Westerfield, M. (1999). Anterior movement of ventral diencephalic precursors separates the primordial eye field in the neural plate and requires cyclops. *Development, 126*(24), 5533-5546.

Vasilyev, A., Liu, Y., Hellman, N., Pathak, N., & Drummond, I. A. (2012). Mechanical stretch and PI3K signaling link cell migration and proliferation to coordinate epithelial tubule morphogenesis in the zebrafish pronephros. *PLoS One, 7*(7), e39992. doi:10.1371/journal.pone.0039992

Vasilyev, A., Liu, Y., Mudumana, S., Mangos, S., Lam, P. Y., Majumdar, A.*, et al.* (2009). Collective cell migration drives morphogenesis of the kidney nephron. *PLoS Biol, 7*(1), e9. doi:10.1371/journal.pbio.1000009

Verhey, K. J., Kaul, N., & Soppina, V. (2011). Kinesin assembly and movement in cells. *Annu Rev Biophys, 40*, 267-288. doi:10.1146/annurev-biophys-042910-155310

Vitiello, E., Ferreira, J. G., Maiato, H., Balda, M. S., & Matter, K. (2014). The tumour suppressor DLC2 ensures mitotic fidelity by coordinating spindle positioning and cell-cell adhesion. *Nat Commun, 5*, 5826. doi:10.1038/ncomms6826

Vize, P. D., Woolf, A. S., & Bard, J. B. L. (2003). *The Kidney: From Normal Development to Congenital Disease*: Elsevier Science.

Vogel, P., Read, R. W., Hansen, G. M., Payne, B. J., Small, D., Sands, A. T.*, et al.* (2012). Congenital hydrocephalus in genetically engineered mice. *Vet Pathol, 49*(1), 166-181. doi:10.1177/0300985811415708

von Bartheld, C. S., Bahney, J., & Herculano-Houzel, S. (2016). The search for true numbers of neurons and glial cells in the human brain: A review of 150 years of cell counting. *J Comp Neurol, 524*(18), 3865-3895. doi:10.1002/cne.24040

Walczak, C. E., Gayek, S., & Ohi, R. (2013). Microtubule-depolymerizing kinesins. *Annu Rev Cell Dev Biol, 29*, 417-441. doi:10.1146/annurev-cellbio-101512-122345

Walczak, C. E., Mitchison, T. J., & Desai, A. (1996). XKCM1: a Xenopus kinesin-related protein that regulates microtubule dynamics during mitotic spindle assembly. *Cell, 84*(1), 37-47.

Walczak, C. E., Zong, H., Jain, S., & Stout, J. R. (2016). Spatial regulation of astral microtubule dynamics by Kif18B in PtK cells. *Mol Biol Cell, 27*(20), 3021-3030. doi:10.1091/mbc.E16-04-0254

Walker, K. A., & Bertram, J. F. (2011). Kidney development: core curriculum 2011. *Am J Kidney Dis, 57*(6), 948-958. doi:10.1053/j.ajkd.2011.03.009

Walther, Z., Vashishtha, M., & Hall, J. L. (1994). The Chlamydomonas FLA10 gene encodes a novel kinesin-homologous protein. *J Cell Biol, 126*(1), 175-188.

Wang, D., Nitta, R., Morikawa, M., Yajima, H., Inoue, S., Shigematsu, H.*, et al.* (2016). Motility and microtubule depolymerization mechanisms of the Kinesin-8 motor, KIF19A. *Elife, 5*. doi:10.7554/eLife.18101

Wang, W., Cao, L., Wang, C., Gigant, B., & Knossow, M. (2015). Kinesin, 30 years later: Recent insights from structural studies. *Protein Sci, 24*(7), 1047-1056. doi:10.1002/pro.2697

Wang, X., Tsai, J. W., Imai, J. H., Lian, W. N., Vallee, R. B., & Shi, S. H. (2009). Asymmetric centrosome inheritance maintains neural progenitors in the neocortex. *Nature, 461*(7266), 947-955. doi:10.1038/nature08435

Wang, Y. L. (2005). The mechanism of cortical ingression during early cytokinesis: thinking beyond the contractile ring hypothesis. *Trends Cell Biol, 15*(11), 581-588. doi:10.1016/j.tcb.2005.09.006

Warga, R. M., & Kimmel, C. B. (1990). Cell movements during epiboly and gastrulation in zebrafish. *Development, 108*(4), 569-580.

Watanabe, S., De Zan, T., Ishizaki, T., & Narumiya, S. (2013). Citron kinase mediates transition from constriction to abscission through its coiled-coil domain. *J Cell Sci, 126*(Pt 8), 1773-1784. doi:10.1242/jcs.116608

Wheway, G., Nazlamova, L., & Hancock, J. T. (2018). Signaling through the Primary Cilium. *Front Cell Dev Biol, 6*, 8. doi:10.3389/fcell.2018.00008

Wickstead, B., & Gull, K. (2006). A "holistic" kinesin phylogeny reveals new kinesin families and predicts protein functions. *Mol Biol Cell, 17*(4), 1734-1743. doi:10.1091/mbc.e05-11-1090

Wickstead, B., Gull, K., & Richards, T. A. (2010). Patterns of kinesin evolution reveal a complex ancestral eukaryote with a multifunctional cytoskeleton. *BMC Evol Biol, 10*, 110. doi:10.1186/1471-2148-10-110

Williams, C. L., McIntyre, J. C., Norris, S. R., Jenkins, P. M., Zhang, L., Pei, Q.*, et al.* (2014). Direct evidence for BBSome-associated intraflagellar transport reveals distinct properties of native mammalian cilia. *Nat Commun, 5*, 5813. doi:10.1038/ncomms6813

Wilson, C. W., Nguyen, C. T., Chen, M. H., Yang, J. H., Gacayan, R., Huang, J.*, et al.* (2009). Fused has evolved divergent roles in vertebrate Hedgehog signalling and motile ciliogenesis. *Nature, 459*(7243), 98-102. doi:10.1038/nature07883

Wilson, L., & Maden, M. (2005). The mechanisms of dorsoventral patterning in the vertebrate neural tube. *Dev Biol, 282*(1), 1-13. doi:10.1016/j.ydbio.2005.02.027

Wilson, S. I., & Edlund, T. (2001). Neural induction: toward a unifying mechanism. *Nat Neurosci, 4 Suppl*, 1161-1168. doi:10.1038/nn747

Wilson, S. W., & Houart, C. (2004). Early steps in the development of the forebrain. *Dev Cell, 6*(2), 167-181.

Winey, M., & O'Toole, E. (2014). Centriole structure. *Philos Trans R Soc Lond B Biol Sci, 369*(1650). doi:10.1098/rstb.2013.0457

Wingert, R. A., & Davidson, A. J. (2011). Zebrafish nephrogenesis involves dynamic spatiotemporal expression changes in renal progenitors and essential signals from retinoic acid and irx3b. *Dev Dyn, 240*(8), 2011-2027. doi:10.1002/dvdy.22691

Wingert, R. A., Selleck, R., Yu, J., Song, H. D., Chen, Z., Song, A.*, et al.* (2007). The cdx genes and retinoic acid control the positioning and segmentation of the zebrafish pronephros. *PLoS Genet, 3*(10), 1922-1938. doi:10.1371/journal.pgen.0030189

Winyard, P., & Chitty, L. S. (2008). Dysplastic kidneys. *Semin Fetal Neonatal Med, 13*(3), 142-151. doi:10.1016/j.siny.2007.10.009

Wittmann, T., Boleti, H., Antony, C., Karsenti, E., & Vernos, I. (1998). Localization of the kinesin-like protein Xklp2 to spindle poles requires a leucine zipper, a microtubule-associated protein, and dynein. *J Cell Biol, 143*(3), 673-685.

Wodarz, A., & Huttner, W. B. (2003). Asymmetric cell division during neurogenesis in Drosophila and vertebrates. *Mech Dev, 120*(11), 1297-1309.

Woehlke, G., Ruby, A. K., Hart, C. L., Ly, B., Hom-Booher, N., & Vale, R. D. (1997). Microtubule interaction site of the kinesin motor. *Cell, 90*(2), 207-216.

Wolf, M. T. (2015). Nephronophthisis and related syndromes. *Curr Opin Pediatr, 27*(2), 201-211. doi:10.1097/MOP.0000000000000194

Wood, K. W., Sakowicz, R., Goldstein, L. S., & Cleveland, D. W. (1997). CENP-E is a plus end-directed kinetochore motor required for metaphase chromosome alignment. *Cell, 91*(3), 357-366.

Woods, C. G. (2004). Human microcephaly. *Curr Opin Neurobiol, 14*(1), 112-117. doi:10.1016/j.conb.2004.01.003

Wullimann, M. F. (2009). Secondary neurogenesis and telencephalic organization in zebrafish and mice: a brief review. *Integr Zool, 4*(1), 123-133. doi:10.1111/j.1749-4877.2008.00140.x

Xu, P. X., Adams, J., Peters, H., Brown, M. C., Heaney, S., & Maas, R. (1999). Eya1-deficient mice lack ears and kidneys and show abnormal apoptosis of organ primordia. *Nat Genet, 23*(1), 113-117. doi:10.1038/12722

Yajima, J., Edamatsu, M., Watai-Nishii, J., Tokai-Nishizumi, N., Yamamoto, T., & Toyoshima, Y. Y. (2003). The human chromokinesin Kid is a plus end-directed microtubule-based motor. *EMBO J, 22*(5), 1067-1074. doi:10.1093/emboj/cdg102

Yamamoto, S., Jaiswal, M., Charng, W. L., Gambin, T., Karaca, E., Mirzaa, G.*, et al.* (2014). A drosophila genetic resource of mutants to study mechanisms underlying human genetic diseases. *Cell, 159*(1), 200-214. doi:10.1016/j.cell.2014.09.002

Yang, J. T., Laymon, R. A., & Goldstein, L. S. (1989). A three-domain structure of kinesin heavy chain revealed by DNA sequence and microtubule binding analyses. *Cell, 56*(5), 879-889.

Yang, Y. J., Baltus, A. E., Mathew, R. S., Murphy, E. A., Evrony, G. D., Gonzalez, D. M.*, et al.* (2012). Microcephaly gene links trithorax and REST/NRSF to control neural stem cell proliferation and differentiation. *Cell, 151*(5), 1097-1112. doi:10.1016/j.cell.2012.10.043

Yang, Z., Zimmerman, S., Brakeman, P. R., Beaudoin, G. M., 3rd, Reichardt, L. F., & Marciano, D. K. (2013). De novo lumen formation and elongation in the developing nephron: a central role for afadin in apical polarity. *Development, 140*(8), 1774-1784. doi:10.1242/dev.087957

Yildiz, A., Tomishige, M., Vale, R. D., & Selvin, P. R. (2004). Kinesin walks hand-over-hand. *Science, 303*(5658), 676-678. doi:10.1126/science.1093753

Yu, T. W., Mochida, G. H., Tischfield, D. J., Sgaier, S. K., Flores-Sarnat, L., Sergi, C. M.*, et al.* (2010). Mutations in WDR62, encoding a centrosome-associated protein, cause microcephaly with simplified gyri and abnormal cortical architecture. *Nat Genet, 42*(11), 1015-1020. doi:10.1038/ng.683

Yuce, O., Piekny, A., & Glotzer, M. (2005). An ECT2-centralspindlin complex regulates the localization and function of RhoA. *J Cell Biol, 170*(4), 571-582. doi:10.1083/jcb.200501097

Zaghloul, N. A., & Katsanis, N. (2011). Zebrafish assays of ciliopathies. *Methods Cell Biol, 105*, 257-272. doi:10.1016/b978-0-12-381320-6.00011-4

Zhadanov, A. B., Provance, D. W., Jr., Speer, C. A., Coffin, J. D., Goss, D., Blixt, J. A*., et al.* (1999). Absence of the tight junctional protein AF-6 disrupts epithelial cell-cell junctions and cell polarity during mouse development. *Curr Biol, 9*(16), 880-888.

Zhao, C., Omori, Y., Brodowska, K., Kovach, P., & Malicki, J. (2012). Kinesin-2 family in vertebrate ciliogenesis. *Proc Natl Acad Sci U S A, 109*(7), 2388-2393. doi:10.1073/pnas.1116035109

Zhao, H., Kegg, H., Grady, S., Truong, H. T., Robinson, M. L., Baum, M*., et al.* (2004). Role of fibroblast growth factor receptors 1 and 2 in the ureteric bud. *Dev Biol, 276*(2), 403-415. doi:10.1016/j.ydbio.2004.09.002

Zhao, W. M., Seki, A., & Fang, G. (2006). Cep55, a microtubule-bundling protein, associates with centralspindlin to control the midbody integrity and cell abscission during cytokinesis. *Mol Biol Cell, 17*(9), 3881-3896. doi:10.1091/mbc.e06-01-0015

Zhong, W., Feder, J. N., Jiang, M. M., Jan, L. Y., & Jan, Y. N. (1996). Asymmetric localization of a mammalian numb homolog during mouse cortical neurogenesis. *Neuron, 17*(1), 43-53.

Zhou, R., Niwa, S., Homma, N., Takei, Y., & Hirokawa, N. (2009). KIF26A is an unconventional kinesin and regulates GDNF-Ret signaling in enteric neuronal development. *Cell, 139*(4), 802-813. doi:10.1016/j.cell.2009.10.023

Zhou, W., Boucher, R. C., Bollig, F., Englert, C., & Hildebrandt, F. (2010). Characterization of mesonephric development and regeneration using transgenic zebrafish. *Am J Physiol Renal Physiol, 299*(5), F1040-1047. doi:10.1152/ajprenal.00394.2010

Zhou, Z. W., Tapias, A., Bruhn, C., Gruber, R., Sukchev, M., & Wang, Z. Q. (2013). DNA damage response in microcephaly development of MCPH1 mouse model. *DNA Repair (Amst), 12*(8), 645-655. doi:10.1016/j.dnarep.2013.04.017

Zhu, C., & Jiang, W. (2005). Cell cycle-dependent translocation of PRC1 on the spindle by Kif4 is essential for midzone formation and cytokinesis. *Proc Natl Acad Sci U S A, 102*(2), 343-348. doi:10.1073/pnas.0408438102

Zimmer, C., Tiveron, M. C., Bodmer, R., & Cremer, H. (2004). Dynamics of Cux2 expression suggests that an early pool of SVZ precursors is fated to become upper cortical layer neurons. *Cereb Cortex, 14*(12), 1408-1420. doi:10.1093/cercor/bhh102

Annexe

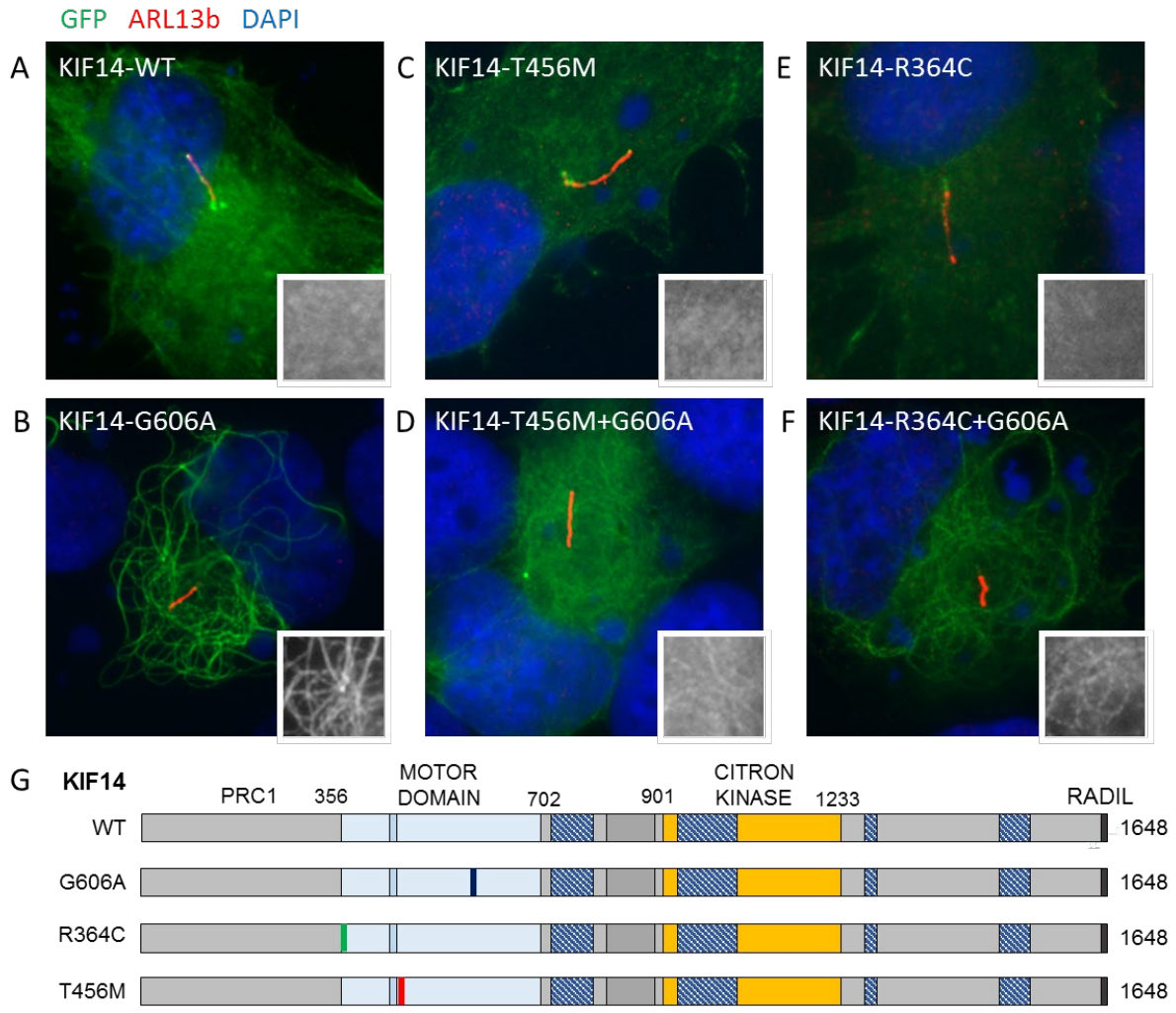

Figure A1. Effect of Missense Mutations on Microtubule Binding. *Representative images of RPE1 cells transfected with variant forms of KIF14 and immunostained for ARL13b (red) and Hoechst (blue). (A) KIF14-WT, (B) KIF14-G606A, (C) KIF14-T456M, (D) KIF14-T456M+G606A, (E) KIF14-R364C, (F) KIF14-R364C+G606A and (G) Schematic representation of the constructs used and the position of mutations.*

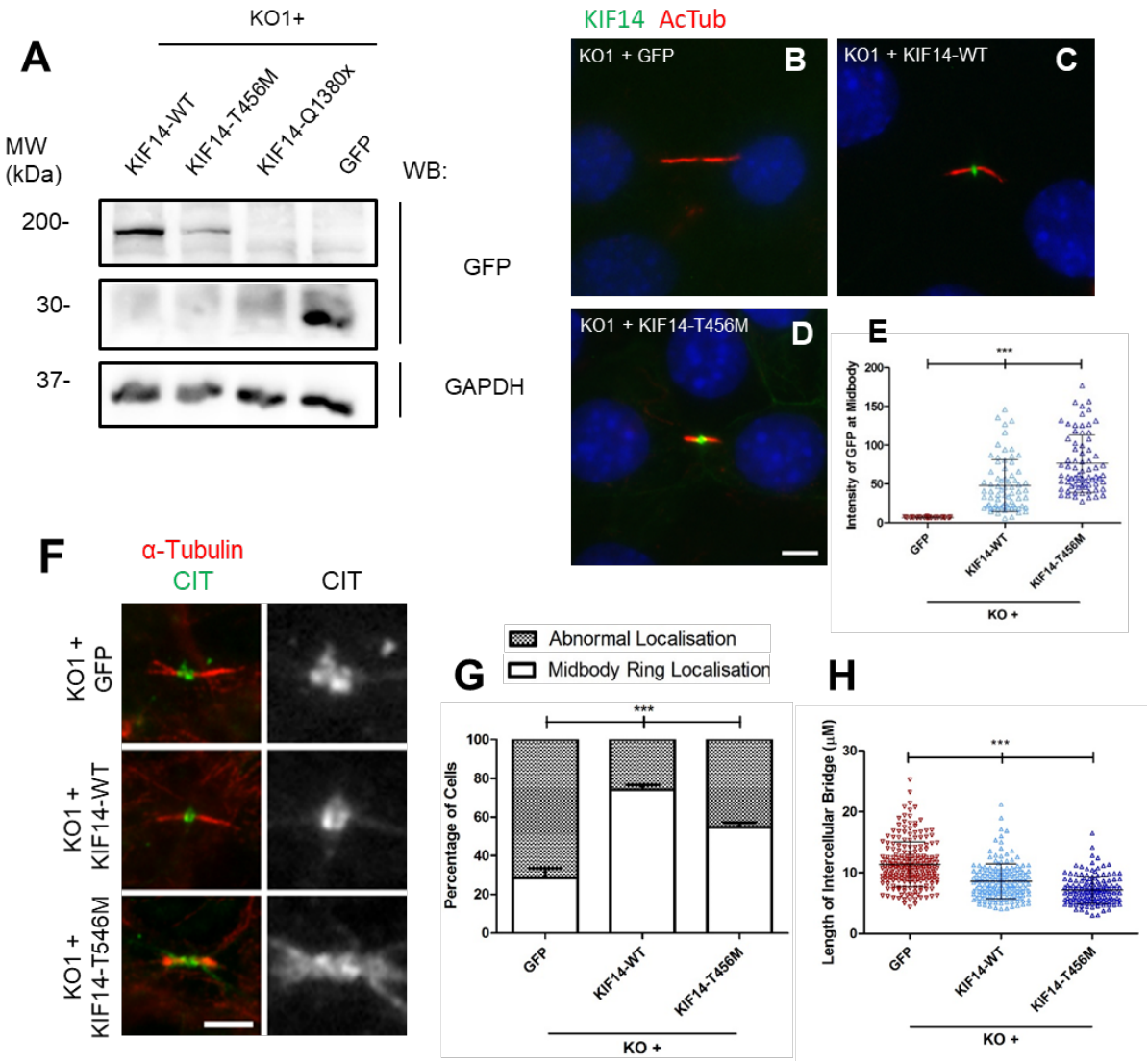

Figure A2. KIF14 re-expression in Kif14$^{-/-}$ mIMCD3 cells. *(A) mIMCD3 cells transduced with GFP-tagged KIF14 constructs were analysed by Western Blot using antibodies against GFP and GADPH, as a loading control. (B-D) Representative images of mitotic cells re-expressing GFP, KIF14-WT or KIF14-T456M immunostained for KIF14 (green) and acetylated α-tubulin (red). (E) Intensity of GFP localised at the midbody in cells re-expressing GFP, KIF14-WT or KIF14-T456M. (F) Immunostaining of α-tubulin (red) and CIT (green) at the midbody, and (G) quantification of the correct ring localisation of CIT. (H) Length of intercellular bridges as measured from the immunostaining of acetylated α-tubulin. ***P< 0.0001 from n=3 independent experiments, Dunn's Multiple Comparison Test following the Kruskal-Wallis ANOVA test for intensity of GFP (E) and length of intercellular bridges (H), and Fischer's exact test for CIT localisation (G). Scale bars: 5µm*

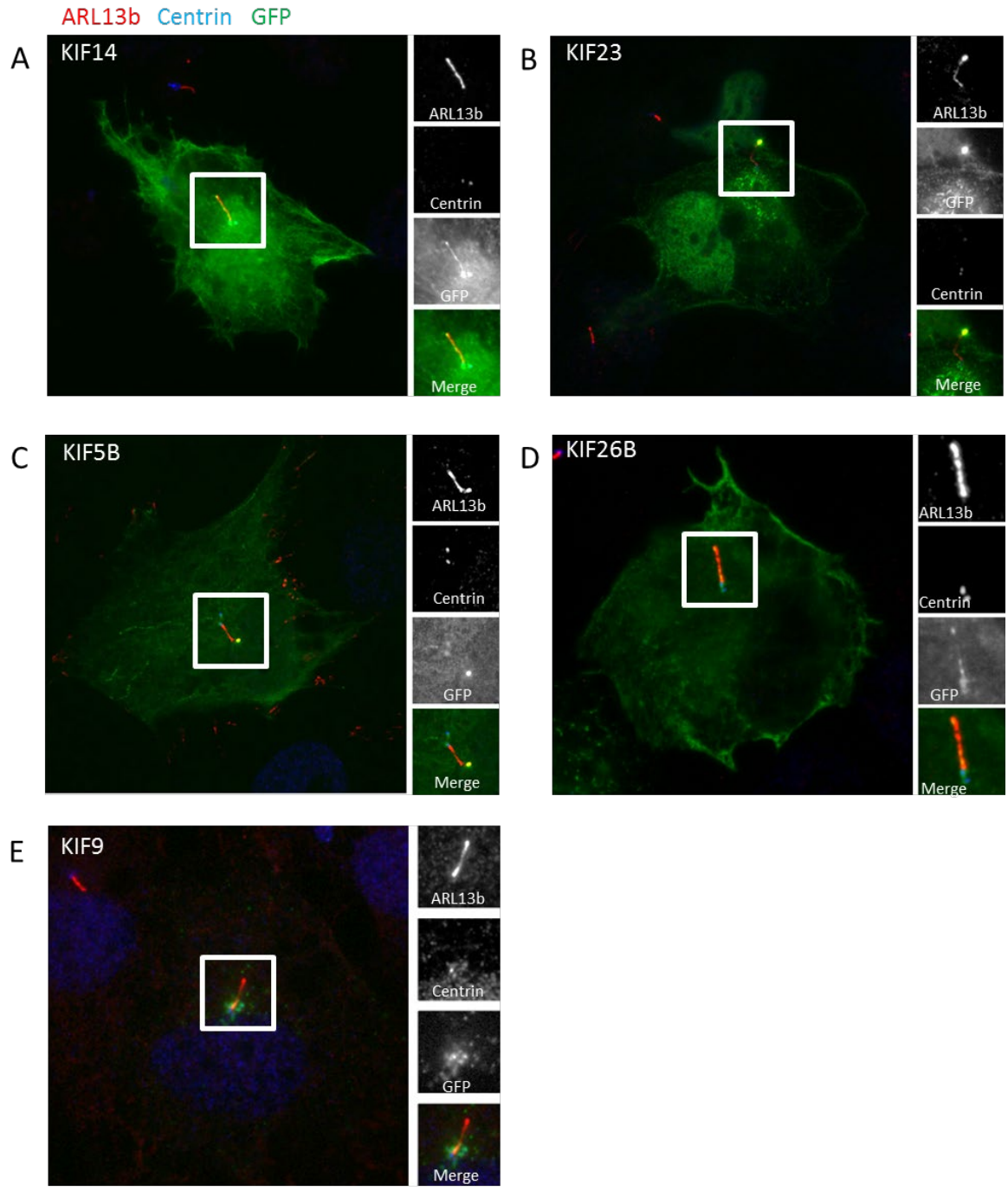

Figure A3. Localisation of novel ciliary kinesin. *Representative images of RPE1 cells transfected with GFP-tagged constructs of different kinesins, immunostained for ARL13b (red) and centrin (blue). (A) KIF14, (B) KIF23, (C) KIF5B, (D) KIF26B and (E) KIF9*

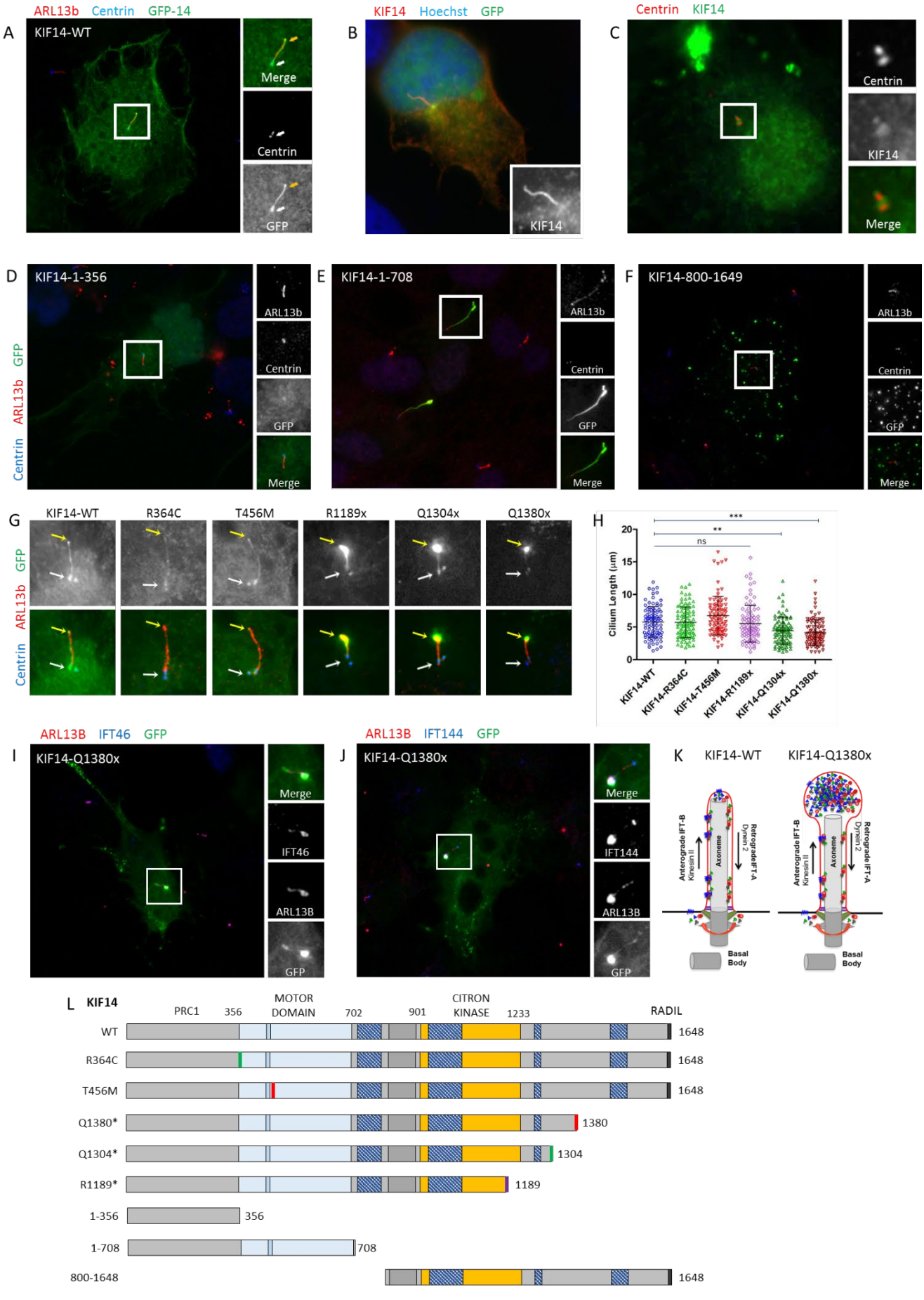
A
ARL13b Centrin GFP-14
KIF14-WT
Merge
Centrin
GFP
B
KIF14 Hoechst GFP
KIF14
C
Centrin KIF14
Centrin
KIF14
Merge
D
KIF14-1-356
GFP
ARL13b
Centrin
ARL13b
Centrin
GFP
Merge
E
KIF14-1-708
ARL13b
Centrin
GFP
Merge
F
KIF14-800-1649
ARL13b
Centrin
GFP
Merge
G
KIF14-WT
R364C
T456M
R1189x
Q1304x
Q1380x
GFP
ARL13b
Centrin
H
Cilium Length (µm)
***
**
ns
KIF14-WT
KIF14-R364C
KIF14-T456M
KIF14-R1189x
KIF14-Q1304x
KIF14-Q1380x
I
ARL13B IFT46 GFP
KIF14-Q1380x
Merge
IFT46
ARL13B
GFP
J
ARL13B IFT144 GFP
KIF14-Q1380x
Merge
IFT144
ARL13B
GFP
K
KIF14-WT
KIF14-Q1380x
Anterograde IFT-B
Kinesin II
Axoneme
Retrograde IFT-A
Dynein 2
Basal Body
L
KIF14
PRC1
356
MOTOR DOMAIN
702
901
CITRON KINASE
1233
RADIL
WT
R364C
T456M
Q1380*
Q1304*
R1189*
1-356
1-708
800-1648
1648
1380
1304
1189
356
708

Figure A4. KIF14 at cilia. *(A) Representative image of ciliary localisation of RPE1 cell transfected with GFP-tagged KIF14-WT. Cells were immunostained with ARL13b (red) and centrin (blue). Insets show higher magnification of cilia (B) Representative image of RPE1 cell immunostained for endogenous KIF14 (green) and centrin (red). Inset shows higher magnification of basal body. (C) Representative image of RPE1 cell transfected with construct encoding for unfused KIF14 and GFP. Cells were immunostained for KIF14 (red) and Hoechst (blue). Inset shows higher magnification of endogenously stained cilium. (D) Representative cilia from cells transfected with GFP-tagged WT and variant forms of KIF14. Cells were immunostained for ARL13b (red) and centrin (blue). (E) Quantification of the impact of transfection on the length of cilia. (F,G) Representative images of RPE1 cells transfected with GFP-tagged KIF14-Q1380x. Cells were immunostained with ARL13b (red) and with IFT46 (blue; F) or IFT144 (blue; G). Insets show higher magnification of cilia. (H) Schematic representation of the effect of overexpression of KIF14-Q1380x on cilia. (I) RPE1 cells were transfected with truncated forms of KIF14 and immunostained for ARL13b (red) and centrin (blue). Insets show higher magnification of cilia. (J) Schematic representation of constructs used throughout. NS = Not significant, **P< 0.001, ***P< 0.0001 from n=3 independent experiments, Dunn's Multiple Comparison Test following the Kruskal-Wallis ANOVA test for length of cilia.*

Abstract

Mutations in *KIF14* were previously shown to lead to either isolated microcephaly or to a developmental and lethal syndromic form associating severe microcephaly with renal hypodysplasia (RHD). The latter phenotype was considered reminiscent of a ciliopathy, relating to defects of the primary cilium, a signalling organelle present on the surface of many quiescent cells. *KIF14* encodes a mitotic kinesin which plays a key role at the midbody during cytokinesis, and was not previously shown to be involved in cilia-related functions. Here, we have analysed four families with foetuses presenting with the syndromic form and harbouring variations in *KIF14*. Our functional analyses show that the identified variations severely impact the activity of KIF14 and likely correspond to loss-of-function (LOF) mutations. Our analysis on human foetal kidney tissues revealed the accumulation of KIF14-positive midbody remnants in the lumen of ureteric bud tips, highlighting similarities between mitotic events during early brain and kidney development. Subsequently, analysis of a *kif14* mutant zebrafish line showed a conserved role for this mitotic kinesin. Interestingly, additional ciliopathy-associated phenotypes were also present in these mutant embryos, supporting a potential novel role for kif14 at cilia. However, our in vitro and in vivo analyses ultimately indicated that KIF14 does not have a direct role in ciliogenesis and that *kif14* LOF in zebrafish phenocopies ciliopathies through an accumulation of mitotic, non-ciliated cells in ciliated tissues. Altogether, our results demonstrate that KIF14 mutations result in a severe syndrome associating microcephaly and RHD through a conserved function in cytokinesis during kidney and brain development.

Keywords: KIF14 Cilia Ciliopathy Kidney Brain Microcephaly Mitosis Zebrafish Development

Targeted Exome Sequencing Identifies *PBX1* as Involved in Monogenic Congenital Anomalies of the Kidney and Urinary Tract

Laurence Heidet,*† Vincent Morinière,*‡ Charline Henry,§‖ Lara De Tomasi,§‖¶ Madeline Louise Reilly,§‖¶ Camille Humbert,§‖ Olivier Alibeu,** Cécile Fourrage,‡†† Christine Bole-Feysot,** Patrick Nitschké,†† Frédéric Tores,†† Marc Bras,†† Marc Jeanpierre,‖‡‡ Christine Pietrement,§§ Dominique Gaillard,‖‖ Marie Gonzales,¶¶ Robert Novo,*** Elise Schaefer,††† Joëlle Roume,‡‡‡ Jelena Martinovic,§§§ Valérie Malan,‖‖‖ Rémi Salomon,*†§‖ Sophie Saunier,§‖ Corinne Antignac,‡§‖ and Cécile Jeanpierre§‖

*Assistance Publique - Hôpitaux de Paris, Centre de référence des Maladies Rénales Héréditaires de l'Enfant et de l'Adulte, Paris, France; †Assistance Publique - Hôpitaux de Paris, Service de Néphrologie Pédiatrique, ‡Assistance Publique - Hôpitaux de Paris, Département de Génétique, and ‖‖‖Assistance Publique - Hôpitaux de Paris, Service de Cytogénétique, Hôpital Universitaire Necker-Enfants malades, Paris, France; §Institut National de la Santé et de la Recherche Médicale Unité Mixte de Recherche 1163, Laboratory of Hereditary Kidney Diseases, **Genomic Platform, Institut National de la Santé et de la Recherche Médicale Unité Mixte de Recherche 1163, Paris Descartes Sorbonne Paris Cité University, and ††Bioinformatic Plateform, Paris Descartes Sorbonne Paris Cité University, Imagine Institute, Paris, France; ‖Paris Descartes Sorbonne Paris Cité University, Paris, France; ¶Paris Diderot University, Paris, France; ‡‡Assistance Publique - Hôpitaux de Paris, Département de Génétique, Hôpital Cochin, Paris, France; §§Unité de néphrologie pédiatrique and ‖‖Service de Génétique clinique, Centre Hospitalo-Universitaire de Reims, Reims, France; ¶¶Assistance Publique - Hôpitaux de Paris, Département de Génétique Médicale, Hôpital Armand Trousseau and Université Pierre et Marie Curie, Paris, France; ***Centre Hospitalo-Universitaire de Lille, Hôpital Jeanne de Flandre, Service de Néphrologie Pédiatrique, Lille, France; †††Service de Génétique Médicale, Institut de Génétique Médicale d'Alsace, Hôpitaux Universitaires de Strasbourg, Strasbourg, France; ‡‡‡Unité de Génétique Médicale, Centre Hospitalier Intercommunal Poissy, St. Germain en Laye, Poissy, France; and §§§Assistance Publique - Hôpitaux de Paris, Unit of Fetal Pathology, Antoine Béclère Hospital, Clamart, France

ABSTRACT

Congenital anomalies of the kidney and urinary tract (CAKUT) occur in three to six of 1000 live births, represent about 20% of the prenatally detected anomalies, and constitute the main cause of CKD in children. These disorders are phenotypically and genetically heterogeneous. Monogenic causes of CAKUT in humans and mice have been identified. However, despite high-throughput sequencing studies, the cause of the disease remains unknown in most patients, and several studies support more complex inheritance and the role of environmental factors and/or epigenetics in the pathophysiology of CAKUT. Here, we report the targeted exome sequencing of 330 genes, including genes known to be involved in CAKUT and candidate genes, in a cohort of 204 unrelated patients with CAKUT; 45% of the patients were severe fetal cases. We identified pathogenic mutations in 36 of 204 (17.6%) patients. These mutations included five *de novo* heterozygous loss of function mutations/deletions in the PBX homeobox 1 gene (*PBX1*), a gene known to have a crucial role in kidney development. In contrast, the frequency of *SOX17* and *DSTYK* variants recently reported as pathogenic in CAKUT did not indicate causality. These findings suggest that *PBX1* is involved in monogenic CAKUT in humans and call into question the role of some gene variants recently reported as pathogenic in CAKUT. Targeted exome sequencing also proved to be an efficient and cost-effective strategy to identify pathogenic mutations and deletions in known CAKUT genes.

J Am Soc Nephrol 28: 2901–2914, 2017. doi: https://doi.org/10.1681/ASN.2017010043

Received January 14, 2017. Accepted April 20, 2017.

Published online ahead of print. Publication date available at www.jasn.org.

Correspondence: Dr. Cécile Jeanpierre, INSERM UMR 1163, Laboratory of Hereditary Kidney Diseases, Imagine Institute, 24 Boulevard du Montparnasse, 75015 Paris, France. Email: cecile.jeanpierre@inserm.fr

Congenital anomalies of the kidney and urinary tract (CAKUT) refer to a heterogeneous group of malformations of the kidney and the urinary tract due to defects in embryonic kidney development, a complex process that involves reciprocal interaction between the ureteric bud and the metanephric mesenchymal tissue. Prevalence of CAKUT has been estimated between three and six per 1000 live births. These kidney defects are frequently detected *in utero* by prenatal ultrasonography and account for 15%–20% of all of the prenatally detected congenital anomalies .[1] Their severity is extremely variable, but CAKUT represent the leading cause of CKD in children.[2] Genetic and environmental factors are proposed to be involved in CAKUT. Except for posterior urethral valves that usually appear as sporadic, familial clustering of CAKUT has been frequently described[3]; however, the heritability estimates remain unknown. In some families, CAKUT are inherited as a Mendelian monogenic disease, mostly transmitted as an autosomal dominant trait with variable expressivity. Although in these cases CAKUT are frequently associated with extrarenal anomalies (>100 syndromes including renal or urinary abnormalities, with a Mendelian transmission, have been described),[4] they can also present with isolated kidney diseases, particularly at prenatal ultrasound screening. Identification of the molecular defect in these patients is important to provide genetic counseling to the families. A monogenic cause of CAKUT was reported to be identified in approximately 10%–15% of patients presenting with isolated CAKUT.[5] Among the approximately 50 genes with reported mutations, *PAX2* and *HNF1B* are the two genes most frequently mutated in syndromic or isolated CAKUT.[6,7] Copy number variations (CNVs) have also been shown to be frequently associated with syndromic as well as isolated CAKUT; however, these CNVs are frequently attributable to known genomic disorders.[8–10] Recently, the simultaneous analysis of multiple candidate genes in parallel by next generation sequencing (NGS) was reported not to lead to a substantial increase in the proportion of patients with CAKUT with identified mutations,[11] suggesting that inheritance may frequently be more complex and/or involve noncoding regions, epigenetic modifications, or somatic mutations.

Here, we report targeted NGS of 330 genes known to be either involved in CAKUT or candidate genes in a large cohort of 204 unrelated patients with CAKUT, which led to the identification of a novel CAKUT gene, *PBX1*.

RESULTS

Patient Cohort

Two hundred four unrelated patients with CAKUT were included (K1–K204 in Supplemental Table 1). Criteria for inclusion were CAKUT involving both kidneys or unilateral CAKUT associated with either extrarenal defects or familial history of CAKUT (Table 1). Patients with posterior urethral valves were not included in the study. Fifty of the 204 patients had been previously tested for mutations in *HNF1B* (involved in renal cysts and diabetes syndrome) and/or *PAX2* (involved in papillorenal syndrome) and/or *EYA1* (involved in branchio-oto-renal syndrome) by Sanger sequencing and were revealed to be negative, and nine fetuses had been tested for mutations in *RET* (involved in bilateral kidney agenesis[12]), with one identified as carrying a variant of unknown significance.[13] In addition, we also tested 11 patients suspected to suffer from branchio-oto-renal syndrome because of branchial and/or ear abnormalities but without any renal phenotype (normal renal ultrasound) (BO1–BO11 in Supplemental Table 1). Sex ratio was 116 boys, 89 girls, and ten patients for which sex was unknown. Not including the 11 BO patients, 79 patients presented extrarenal anomalies. Fifty-five patients had familial history of renal disease affecting first-degree relative(s) (parents, children, or affected siblings), and eight additional patients had history of renal disease in more distant family. Moreover, seven patients had a parent with branchial defects and/or deafness (five), coloboma (one), or diabetes (one) without renal defect (Supplemental Table 1, Table 1). Ninety-three (45%) cases were fetuses affected with extremely severe renal anomalies at fetal ultrasound screening, which led to termination of pregnancy after parents' request and case by case evaluation by a multidisciplinary prenatal committee in accordance with the French law. Autopsy was performed after informed consent in all cases.

Screening the Candidate Genes and Identification of *PBX1* as a Novel Gene Involved in Monogenic CAKUT

Among the 330 genes, 275 were candidate genes with no mutation reported in patients with CAKUT so far (Supplemental Table 2). Analysis of these genes in the 204 individuals with renal involvement led to the identification of 125 heterozygous variants never reported in the Exome Aggregation Consortium (ExAC) database in a total of 88 genes in 92 patients (Supplemental Tables 1 and 3). In one of these genes, *PBX1*, we identified five heterozygous loss of function mutations/deletions (Figure 1, Table 2). The first mutation (family 1) was a frameshift mutation (p.Asn143Thrfs*37) in a 21-year-old adult affected with renal hypoplasia and deafness. She has an eGFR of 40 ml/min per 1.73 m^2. The second one (family 2) was a nonsense mutation (p.Arg184*) in a child presenting with small hyperechogenic kidneys with cysts, developmental delay, growth retardation, and long and narrow face. She had eGFR of 51 ml/min per 1.73 m^2 at the age of 11 years old. The third one (family 3) was a splice mutation (c.511–2A>G) in a fetus with renal hypoplasia and oligoamnios. The autopsy showed extremely severe oligonephronia. RNA was not available to study the effect of that mutation on splicing, but the mutation is predicted to lead to total loss of the 3′ splice site and skipping of exon 4, resulting in a frameshift. The two last patients presented with a heterozygous deletion removing the whole *PBX1* gene indicated by a reduced number of reads for the nine exons of the gene (Figure 1). The first one (family 4) was a 39-year-old adult woman followed for small and dysplastic horseshoe kidney also affected with profound deafness. She was the oldest patient of our series and had stage 3B renal failure (eGFR=40 ml/min per 1.73 m^2) at last evaluation. The second one (family 5) was an infant with a single small

Table 1. Renal and extrarenal phenotypes of the cohort encompassing 204 patients with CAKUT and 11 patients with branchial and/or ear defect (215 patients)

Phenotype	Patients	Extrarenal Phenotype[a]	Family History	
			Renal Defect	Nonrenal Defect
Main CAKUT phenotype				
Bilateral kidney agenesis	46	14	14	
Bilateral multicystic dysplasia	12	3	2	
Unilateral kidney agenesis	15	10	7	2[b,c]
Unilateral kidney agenesis plus secondary CAKUT phenotype[d]	23	7	6	1[b]
Unilateral multicystic dysplasia	5	3	2	
Unilateral multicystic dysplasia plus secondary CAKUT phenotype[d,e]	9	4	2	1[f]
Renal hypoplasia	22	10	6	1[b]
Renal hypoplasia plus secondary CAKUT phenotype[d,g]	34	12	9	2[c,h]
Renal dysplasia[i]	21	8	7	
Renal dysplasia plus secondary CAKUT phenotype[d,j]	6	1	2	
Other[k]	11	7	6	
Total	204	79	63	7
Branchial signs and/or ear defect without CAKUT phenotype	11	11	0	

[a]Includes Mullerian anomalies, urogenital sinus, testis agenesis, anal atresia, cardiopathy, VATER (vertebrae, anus, trachea, esophagus, renal) syndrome, diaphragmatic hernia, cystic adenomatoid lung malformation, lung isomerism, bone defect (ribs, vertebra, or polydactyly), eye defect (coloboma or morning glory syndrome), external ear abnormalities, deafness, branchial defect, pancreatic hypoplasia, abnormal teeth, liver defect, microcephaly, dysmorphic features, central nervous system anomaly, intellectual disability, and mellitus diabetes.
[b]Parent with BO without renal defect.
[c]Parent with deafness without renal defect.
[d]Includes all patients with two CAKUT phenotypes (*e.g.*, unilateral kidney agenesis plus contralateral multicystic dysplastic kidney and renal hypoplasia plus pelviureteric junction obstruction).
[e]Does not include unilateral multicystic dysplasia plus unilateral kidney agenesis, which is counted in the unilateral kidney agenesis plus secondary CAKUT diagnosis.
[f]Parent with diabetes without renal defect.
[g]Does not include renal hypoplasia plus unilateral kidney agenesis, which is counted in unilateral kidney agenesis plus secondary CAKUT diagnosis, or renal hypoplasia plus unilateral multicystic dysplasia, which is counted in multicystic kidney dysplasia plus secondary CAKUT.
[h]Parent with coloboma without renal defect.
[i]Renal dysplasia was defined by histology of the kidney and/or hyperechogenicity of the renal parenchyma at ultrasound with or without cysts.
[j]Does not include renal dysplasia plus unilateral multicystic dysplasia, plus unilateral renal agenesis, or plus renal hypoplasia and/or plus renal ectopy, plus hydronephrosis, or plus vesicoureteral reflux.
[k]Includes vesicoureteral reflux, pelviureteric junction obstruction, obstructive megaureter, hydronephrosis without further known diagnosis, and renal ectopy.

hyperechogenic kidney also presenting developmental delay, microcephaly, and facial dysmorphism (with long and narrow face as well as abnormal ear lobes). He had normal renal function at the age of 18 months old. Comparative Genomic Hybrization (CGH) array analysis (Agilent 60 K) performed on DNA from patients' lymphocytes confirmed presence of a 2.46-Mb deletion at 1q23.3q24.1 including *PBX1* and seven other genes in a family 4′ patient and a 9.1-Mb deletion on the long arm of a chromosome 1 including *PBX1* together with 130 other genes (Supplemental Figure 1) in a family 5′ patient. *De novo* occurrence of the deletion in patients K136 (family 5) was confirmed by fluorescence in situ hybridization on parents' lymphocytes, which was normal (Supplemental Figure 2). The pelviureteric junction obstruction in the patient's mother (shown in gray in Figure 1) is thus an incidental association. Sanger sequencing (families 1–3) or analysis of four microsatellite markers located in *PBX1* (family 4) allowed us to show that the mutations/deletion in these families also occurred *de novo* (Figure 1, Supplemental Table 4). In all five families, misclassification of the parents was excluded by analysis of at least 12 unlinked microsatellite markers located on various chromosomes (Supplemental Table 4) and the identification of a paternally inherited CNV on 1p (family 5) (Supplemental Figure 2). Moreover, by retrospective analysis of our cohort of patients with CAKUT, we identified another individual not included in the 204 patients screened by targeted NGS, in whom a *de novo* 6.2-Mb deletion, including *PBX1*, had been identified by CGH array analysis. This patient presented with small hyperechogenic kidneys, developmental delay, and facial dysmorphism, similar to the patient from family 5. He already had severe proteinuria associated with a rapidly progressing renal failure (eGFR=60 ml/min per 1.73 m^2) at the age of 10 years old.

To precisely evaluate the strength of association between *PBX1* mutations and CAKUT, we used a binomial probability test. The *P* value for identifying three *de novo* loss of function mutations in that gene among 204 patients was <0.001 (Supplemental Figure 3). The identification of three *de novo* loss of function mutations together with two *de novo* large deletions encompassing the gene among 204 patients with CAKUT strongly support the causal effect of the *PBX1* mutations.

Screening the Known CAKUT Genes

In 31 of the 204 patients, we identified 24 pathogenic mutations in seven known genes associated with highly penetrant

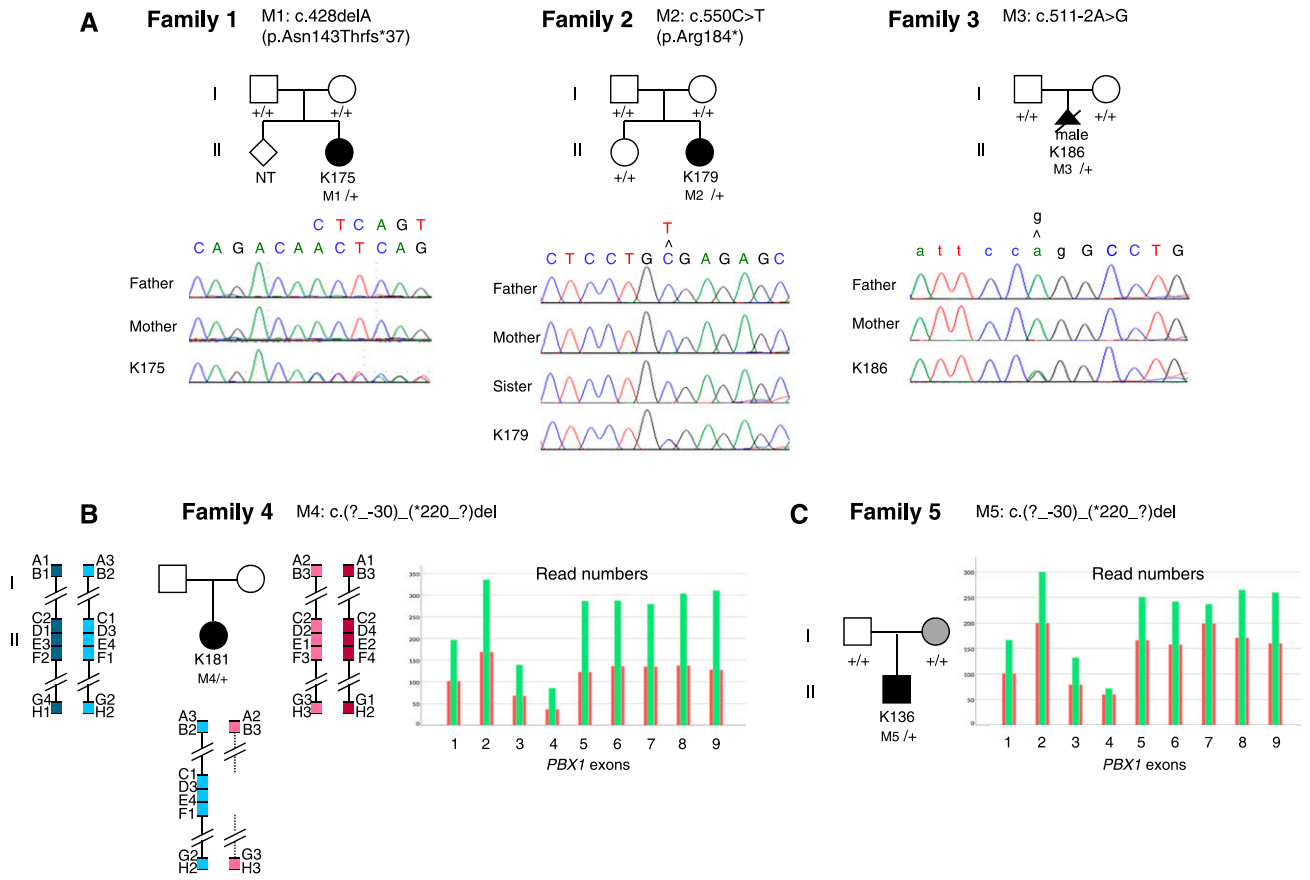

Figure 1. Identification of *de novo PBX1* mutations in three families and deletions in two families. (A) Pedigrees of three families with one affected individual (in black) carrying a *de novo* point mutations in *PBX1*. The affected individual in family 1 (K175) was a 21-year-old woman presenting with renal hypoplasia and deafness. The affected individual in family 2 (K179) was a 12-year-old girl presenting with small hyperechogenic kidneys with cysts, developmental delay, growth retardation, and long and narrow face. The affected individual in family 3 (K186) was a male fetus with extremely severe renal hypoplasia. Loss of function mutations (deletion of one base leading to a frameshift, nonsense mutation, or nucleotide change in the consensus acceptor splice site located in 3′ of intron 3) identified in patients K175, K179, and K186, respectively, were validated by Sanger sequencing. Absence of the mutation in the parents showed *de novo* occurrence in all patients. NT, not tested. (B) Pedigree of family 4 with a 40-year-old woman (K181) affected with small and dysplastic horseshoe kidney and deafness. NGS analysis of patient DNA revealed a reduced number of reads for all of the exons of *PBX1* (in red) compared with the mean number of reads for the 37 other DNAs analyzed in the same run (in green), suggesting deletion of one *PBX1* allele. Haplotypes of the affected woman and her parents were generated using four known microsatellite markers upstream and downstream of *PBX1* (markers A, B, G, and H) as well as four intragenic *PBX1* markers (markers C–F). Genomic positions of the microsatellite markers (on Human Genome version GRCh38.p7 from Ensembl) are A (D1S2675): chr1:162,240,203–162,240,364; B (D1S2844): chr1:162,979,036–162,979,218; C (in *PBX1* intron 1): chr1:164,562,253–164,562,694; D (in *PBX1* intron 2): chr1:164,651,731–164,652,170; E (in *PBX1* intron 2): chr1:164,707,219–164,707,656; F (in *PBX1* intron 8): chr1:164,833,830–164,834,270; G (D1S2762) chr1:166,986,900–166,987,137; and H (D1S196): chr1:167,635,063–167,635,195. Deletion of a <4-Mb region encompassing *PBX1* located on the maternally inherited chromosome was shown by the lack of maternal contribution for markers C–F (genotypes are in Supplemental Table 3). (C) Pedigree of family 5 with a 2-year-old infant boy (K136) presenting with a single hyperechogenic kidney associated with developmental delay, microcephaly, and facial dysmorphism (with long and narrow face as well as abnormal ear lobes). The mother was presenting pyeloureteric junction obstruction. NGS analysis of K136 DNA revealed a reduced number of reads for all of the exons of *PBX1* (in red) compared with the mean number of reads for the 38 other DNA analyzed in the same run (in green), suggesting deletion of one *PBX1* allele. Validation of this deletion and identification of its extent and *de novo* occurrence were performed by CGH analysis (Supplemental Figure 1).

CAKUT, namely *HNF1B*, *PAX2*, *EYA1*, *ANOS1*, *GATA3*, *CHD7*, and *KIF14* (Figure 2, Table 3). Three of the mutations/deletions, affecting *GATA3* or *KIF14*, were identified in patients who had been previously screened for *HNF1B*, *PAX2*, and/or *EYA1* by Sanger sequencing and remained unsolved. Renal phenotypes, extrarenal anomalies, and mutation inheritance are shown in Table 3 (Supplemental Table 1). As frequently observed for patients with mutations in these genes, 16 of the

Table 2. *De novo* loss of function variants in *PBX1* (NM_002585)

Patient	Kidney Phenotype	Renal Function	Extrarenal Phenotype	Nucleotide Change	Protein Change
K175	Bilateral hypoplasia	eGFR=40 ml/min per 1.73 m^2 (21 yr)	Deafness plus scoliosis	c.[428delA];[=]	p.[Asn143Thrfs*37];[=]
K179	Bilateral cystic hypodysplasia	eGFR=51 ml/min per 1.73 m^2 (11 yr)	Dysmorphic features plus developmental delay	c.[550C>T];[=]	p.[Arg184*];[=]
K186	Bilateral hypoplasia with oligonephronia	Oligoamnios	No	c.[511–2A>G];[=]	
K181	Hypoplasic horseshoe kidney, absence of corticomedullar differentiation	eGFR=40 ml/min per 1.73 m^2 (39 yr)	Deafness	c.[(?_−30)_(*220_?)del];[=]	
K136	Unilateral agenesis/small hyperechogenic kidney	Normal renal function (18 mo)	Dysmorphic features plus intellectual disability	c.[(?_−30)_(*220_?)del];[=]	

patients had extrarenal symptoms. Notably, the fetuses with biallelic *KIF14* mutations presented severe microcephaly and agenesis of the corpus callosum as recently reported.[14] Fourteen patients were sporadic, and *de novo* occurrence of the mutation was shown for the five families with available parental DNA. Somatic mosaicism in the mother was identified in one patient with a *PAX2* mutation. Ten patients had a family history of CAKUT (Supplemental Table 1, Table 3), and presence of the mutation was shown in the affected related individual in the seven tested families. In addition, in six patients with a family history of branchial and/or ear defect (three patients), deafness (one patient), diabetes (one patient), or coloboma (one patient), mutations were inherited from a parent with branchial and/or ear defect (*EYA1*), diabetes (*HNF1B*), coloboma (*PAX2*), or deafness (*GATA3*) but no renal defect in agreement with incomplete penetrance of the renal defect associated with mutations in these genes.[15–17] Altogether, 11 mutations were large deletions removing all exons of *HNF1B* (eight), *GATA3* (two), or *PAX2* (one); five were intragenic deletions removing few exons of *PAX2* (two), *EYA1* (one), *ANOS1* (one), or *KIF14* (one; homozygous); and 18 were point mutations (including small deletions up to 9 bp), all absent from the ExAC, except for one *EYA1* mutation that was present with a frequency of one of 66,722 in the European population. The 15 heterozygous large deletions were confirmed by either CGH or multiplex ligation–dependent probe amplification, and the homozygous deletion of *KIF14* was confirmed by sequencing of a cDNA synthesized from kidney RNA of the affected fetus (Supplemental Figure 4).

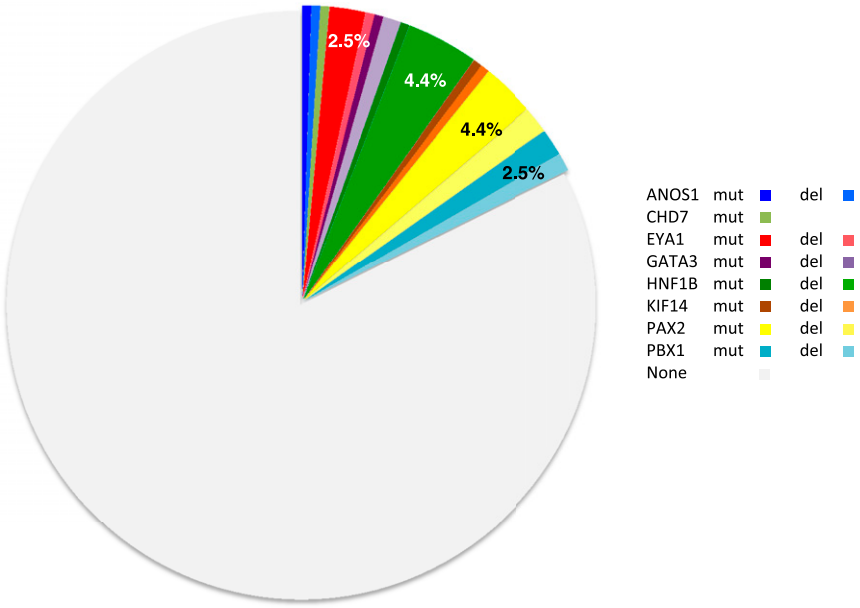

Figure 2. Identification of causative mutations/deletions in 36 of the 204 CAKUT cases. For each gene (*ANOS1*, *CHD7*, *EYA1*, *GATA3*, *HNF1B*, *KIF14*, *PAX2*, and *PBX1*), the proportions of patients with mutations and deletions are shown in dark and light colors, respectively. All of the mutations/deletions are heterozygous, except for *KIF4*, for which they are biallelic.

We also identified 21 rare heterozygous damaging variants in 12 genes reported as involved in dominant forms of CAKUT in a total of 17 individuals with CAKUT (Table 4). Extrarenal symptoms usually associated with mutations in some of these genes were never observed in these patients. All of the variants were missense predicted to be damaging by at least three of the five prediction programs used, and 13 of them, affecting a total of ten genes (*BICC1*, *CDC5L*, *CHD1L*, *NOTCH2*, *RET*, *SALL1*, *SALL4*, *TBC1D1*, *TBX18*, and *TNXB*),

Table 3. Causative mutations in known genes associated with highly penetrant CAKUT phenotype

Patient	Renal Phenotype[a]	Extrarenal Phenotype	Causal Gene	NM_ref	Nucleotide Change	Protein Change
Rare variants in individuals with CAKUT						
K4	RH	Bifid uterus	*HNF1B*	000458	c.[(?_−30)_(*220_?)del];[=]	
K50	UMD+	No	*HNF1B*	000458	c.[(?_−30)_(*220_?)del];[=]	
K103	RD+	No	*HNF1B*	000458	c.[(?_−30)_(*220_?)del];[=]	
K124	RD+	No	*HNF1B*	000458	c.[(?_−30)_(*220_?)del];[=]	
K143	RD+	No	*HNF1B*	000458	c.[(?_−30)_(*220_?)del];[=]	
K172	UMD+	Diabetes plus cryptorchidy	*HNF1B*	000458	c.[(?_−30)_(*220_?)del];[=]	
K185	RD	No	*HNF1B*	000458	c.[(?_−30)_(*220_?)del];[=]	
K203	RD	No	*HNF1B*	000458	c.[(?_−30)_(*220_?)del];[=]	
K170	RH+	No	*HNF1B*	000458	c.[344+2_+5del];[=]	
K72	RH	Papillary excavation	*PAX2*	003987	c.[(?_−30)_(*220_?)del];[=]	
K62	RH	Eye coloboma	*PAX2*	003987	c.[?−30_410+?del];[=]	
K79	RD	Papillary coloboma	*PAX2*	003987	c.[44−?_496+?del];[=]	
K117	RH	No	*PAX2*	003987	c.[183C>A];[=]	p.[Ser61Arg];[=]
K133	RH+	Papillary coloboma	*PAX2*	003987	c.[76del];[=]	p.[Val26Cysfs*3];[=]
K146	RH+	No	*PAX2*	003987	c.[446del];[=]	p.[Pro149Glnfs*10];[=]
K148	RH	No	*PAX2*	003987	c.[76dup];[=]	p.[Val26Glyfs*28];[=]
K176	RH+	No	*PAX2*	003987	c.[331G>A];[=]	p.[Ala111Thr];[=]
K199	Oth	Papillary coloboma	*PAX2*	003987	c.[212G>A];[=]	p.[Arg71Lys];[=]
K80	UKA+	Preauricular pit plus ear tag	*EYA1*	000503	c.[557−?_1597+?del];[=]	
K78	BKA	No	*EYA1*	000503	c.[967–1G>C];[=]	
K119	RH	Branchial defect plus deafness	*EYA1*	000503	c.[1459T>C];[=]	p.[Ser487Pro];[=]
K135	UKA	Preauricular pit	*EYA1*	000503	c.[553C>T];[=]	p.[Gln185*];[=]
K145	RH	Branchial defect	*EYA1*	000503	c.[1338_1346del];[=]	p.[Asn446_Tyr448del];[=]
K101	UKA	Ear tag plus external ear canal stenosis	*GATA3*	001002295	c.[(?_−30)_(*220_?)del];[=]	
K167	UKA	Deafness plus intellectual disability	*GATA3*	001002295	c.[(?_−30)_(*220_?)del];[=]	
K48	RH+	No	*GATA3*	001002295	c.[829C>T];[=]	p.[Arg277*];[=]
K158	BKA	No	*ANOS1*	000216	c.[?−30_255+?del]	
K26	BKA	No	*ANOS1*	000216	c.[769C>T];[=]	p.[Arg257*];[=]
K160	UKA	Deafness plus branchial defect plus colobomatous microphtalmia	*CHD7*	017780	c.[5050G>A];[=]	p.[Gly1684Ser];[=]
K73	RH+	Lissencephaly plus agenesis of corpus callosum	*KIF14*	014875	c.[3567−?_4072+?del]; [(3567-?_4072+?del)]	
K195	BKA	Craniostenosis plus microcephaly plus agenesis of corpus callosum	*KIF14*	014875	c.[3910C>T];[1090C>T]	p.[Gln1304*];[Arg364Cys]
Rare variants in individuals with branchial signs and/or ear defect without CAKUT phenotype						
BO4	No	Branchial defect plus preauricular pit plus deafness	*EYA1*	000503	c.[1081C>T];[=]	p.[Arg361*];[=]
BO5	No	Branchial defect plus deafness	*SIX1*	005982	c.[273_274insC];[=]	p.[Tyr92Leufs*62];[=]

PP2, Polyphen2; MT, MutationTaster; GVDV, Grantham variation score and Grantham difference score; RH, renal hypoplasia; NA, not available; UMD, unilateral multicystic dysplasia; RD, renal dysplasia; Oth, other; UKA, unilateral kidney agenesis; BKA, bilateral kidney agenesis; NFE, non-Finnish European population.
[a]Plus indicates presence of (a) secondary CAKUT phenotype(s).
[b]Considered as deleterious when ≥50.
[c]Considered as deleterious when ≥C25.
[d]Patient with sporadic case.
[e]Patient with familial case.
[f]Parent affected with diabetes without renal defect.
[g]Parent affected with coloboma without renal defect.
[h]Mutation transmitted to a son with coloboma without renal defect.
[i]Parent affected with BO without renal defect.
[j]Parent affected with deafness without renal defect.
[k]Clinical information not available.

Table 3. Continued

PP2	Sift	MT	Grantham[b]	GVDV[c]	No. of Missense Deleterious Scores	Splice Effect, %	ExAC	Inheritance	Ref.
							0	NA[d]	36
							0	Affected mother[e]	
							0	Affected mother[e]	
							0	*De novo*[d]	
							0	*De novo*[d]	
							0	Affected mother[f]	
							0	NA[d]	
							0	NA[e]	
						−100	0	NA[d]	
							0	Germinal mosaicism/ two affected children[e]	37
							0	NA[d]	
							0	*De novo*[d]	
1	0	dc	110	C0	4/5		0	*De novo*[d]	
							0	Affected mother[g]	38
							0	NA[d]	
							0	Unaffected mother (somatic mosaicism)[d]	39
0.998	0	dc	58	C0	4/5		0	Affected mother[e]	40
0.974	0	dc	26	C0	3/5	−49	0	NA[e,h]	41
							0	Affected mother[i]	
						−100	0	Affected father[e]	42
0.132	0.07	dc	74	C0	2/5		0.0015% NFE	Affected father[i]	43
							0	Affected mother[i]	44
							0	Affected father[e]	
							0	Affected father[j]	45
							0	NA[d]	
							0	*De novo*[d]	46
							0	Unaffected mother[e]	47
							0	NA[d]	48
0.929	0	dc	56	C55	5/5	−38	0	Father[k]	49
							0	NA[d]	
1	0	dc	180	C0	4/5		0	One mutation from each parent[e]	
							0	*De novo*[d]	50
							0	Affected mother[i]	

were absent from the ExAC. This suggests a causative effect for these variants, which remains to be shown. Of note, two of these variants were present in individuals with a pathogenic mutation identified (one variant in *CDC5L* in a child with a causative mutation in *CHD7* and one in *TBX18* in a fetus with a causative *de novo* mutation in *GATA3*), thus questioning the effect of these additional variants. Other patients were carrying variants in several genes, which may suggest oligogenic inheritance but also, highlights the arduousness of the interpretation of the variants (Table 4).

In addition, using less stringent criteria for variant filtering, we identified four previously reported mutations with frequency in the ExAC that was above the one to 5000 threshold (Table 4). The RET p.Asp567Gln variation in a fetus with bilateral kidney agenesis (that patient has already been reported[13]) was inherited from his unaffected father and not carried

Table 4. Variants in other genes reported in dominant forms of CAKUT, including previously reported variants and novel rare variants

Patient	Renal Phenotype[a]	Extrarenal Phenotype	Gene	NM_ref	Nucleotide Change
Novel rare variants in individuals with CAKUT					
K94	UKA+	Didelphys uterus	*BICC1*	001080512	c.[2264C>G];[=]
K127	UKA+	No	*BICC1*	001080512	c.[1052G>A];[=],
K160	UKA	Deafness plus branchial defect plus colobomatous microphtalmia	*CDC5L*	001253	c.[2240T>G];[=]
K162	RH+	Palate cleft plus preauticular pit	*CDC5L*	001253	c.[251C>G];[=]
K70	BMD	No	*CHD1L*	004284	c.[1557A>C];[=],
K127	UKA+	No	*DSTYK*	015375	c.[2674G>A];[=]
K32	RH	No	*NOTCH2*	024408	c.[1063G>A];[=]
K70	BMD	No	*NOTCH2*	024408	c.[5156G>A];[=]
K190	RH+	No	*NOTCH2*	024408	c.[854G>A];[5903C>T]
K83	BMD	No	*RET*	020975	c.[2063C>T];[=]
K91	UKA	No	*RET*	020975	c.[1903C>T];[=]
K69	BMD	No	*SALL1*	002968	c.[3771C>G];[=]
K70	BMD	No	*SALL4*	020436	c.[2492G>A];[=]
K29	BKA	Small testis	*SIX5*	175875	c.[2189C>T];[=]
K56	RD	Interventricular communication plus intrauterine growth retardation	*TBC1D1*	015173	c.[2790G>A];[=]
K105	RH+	No	*TBC1D1*	015173	c.[2152C>T];[=]
K21	BMD	No	*TBX18*	001080508	c.[610C>T]; [=]
K48	RH+	No	*TBX18*	001080508	c.[1483C>A];[=]
K192	BKA	No	*TBX18*	001080508	c.[772A>G]; [=]
K169	UKA+	No	*TNXB*	019105	c.[563C>T]; [=]
Previously reported variants[f] in individuals with CAKUT					
K3	BKA	Right ventricular dilation	*RET*	020975	c.[1699G>A];[=]
K32	RH	No	*RET*	020975	c.[2081G>A];[=]
K127	UKA+	No	*SOX17*	022454	c.[775T>A]; [=]
Previously reported variants[f] in individuals with BO					
BO11	No	Deafness	*DSTYK*	015375	c.[654+1G>A];[=]

UKA, unilateral kidney agenesis; NA, not available; RH, renal hypoplasia; BMD, bilateral multicystic dysplasia; NFE, non-Finnish European; EAS, East Asian; AMR, Latino; SAS, South Asian; BKA, bilateral kidney agenesis; RD, renal dysplasia; FIN, Finnish; OTH, Other populations.

[a]Plus indicates presence of (a) secondary phenotype(s).

[b]Number of programs that predicted the variant as damaging among Polyphen2 (probably and possibly damaging), Sift (deleterious), MutationTaster (deleterious), Grantham (considered as deleterious when ≥50), and Grantham variation score and Grantham difference score (considered as deleterious when ≥C25).

[c]Only variant frequencies in the population with the higher level are indicated.

[d]Sporadic.

[e]Familial.

[f]Variant reported in the literature with a frequency in the ExAC above the one to 5000 threshold.

[g]Clinical information not available.

[h]Mother affected with deafness without renal defect.

Table 4. Continued

Amino Acid Change	No. of Missense Deleterious Scores[b]	ExAC[c]	Inheritance	Ref.	Other Variant(s)
p.[Thr755Arg];[=]	4/5	0	NA[d]		
p.[Cys351Tyr];[=]	3/5	0	Unaffected mother plus affected brother[e]		*DSTYK*, *SOX17*[f]
p.[Leu747Trp];[=]	4/5	0	Father[g]		*CHD7* causative
p.[Thr84Ser]; [=]	5/5	0	NA[e]		
p.[Lys519Asn];[=]	4/5	0	NA[d]		*NOTCH2*, *SALL4*
p.[Asp892Asn];[=]	3/5	0.0075% NFE	Unaffected mother plus affected brother[e]		*BICC1*, *SOX17*[f]
p.[Asp355Asn];[=]	3/5	0.0015% NFE	NA[d]		*RET*[f]
p.[Arg1719Gln];[=]	3/5	0.012% EAS	NA[d]		*CHD1L*, *SALL4*
p.[Arg285His] [Ala1968Val]	4/5; 5/5	0.0087% AMR; 0	One from each parent[h]		
p.[Ser688Phe];[=]	5/5	0	Unaffected father[e]		
p.[Arg635Cys];[=]	5/5	0.012% SAS	Unaffected mother plus affected brother[e]		
p.[Asn1257Lys];[=]	4/5	0	NA[d]		
p.[Arg831Gln];[=]	3/5	0	NA[d]		*CHD1L*, *NOTCH2*
p.[Ser730Leu];[=]	4/5	0.012% NFE	NA[d]		
p.[Met930Ile];[=]	3/5	0	NA[d]		
p.[Arg718Cys];[=]	4/5	0.015% FIN	NA[d]		
p.[His204Tyr];[=]	5/5	0.0015% NFE	NA[d]		
p.[Gln495Leu];[=]	5/5	0	Unaffected father[d]		*GATA3* causative
p.[Ile258Val];[=]	3/5	0	NA[d]		
p.[Pro188Leu];[=]	3/5	0[g]	NA[d]		
p.[Asp567Asn];[=]	3/5	0.11% OTH	Unaffected father (absent in affected sister)[e]	13	
p.[Arg694Gln];[=]	2/5	0.049% SAS	NA[d]	18	*NOTCH2*
p.[Tyr259Asn];[=]	2/5	1.75% OTH	Unaffected father plus affected brother[e]	19	*BICC1*, *DSTYK*
		0.088% AMR	NA[d]	20	

by his sister, who presented with a less severe renal phenotype. This variant was identified in 19 individuals without CAKUT (seven being unrelated) from our in-house exome database (>8000 exomes). The RET p.Arg694Gln variation detected in a fetus with bilateral hypoplasia has been reported in a patient with Hirschsprung disease without associated renal involvement.[18] This mutation has low pathogenicity scores. The SOX17 p.Tyr259Asn variation, previously reported to be associated with vesicoureteral reflux,[19] was identified in a patient also carrying missense variants in *BICC1* and *DSTYK*. That *SOX17* variant was inherited from his unaffected father. It is found with a frequency of one in 181 in the European population in the ExAC and in 82 individuals without CAKUT in our in-house exome database. Finally, the *DSTYK* splice variant (c.654+1), recently reported in a large family with CAKUT,[20] was identified in a BO individual with normal renal ultrasound scan. That variant is found in the ExAC database with a frequency of one in 3563 in the European population

and was identified in 11 individuals without CAKUT (ten being unrelated) in our in-house exome database.

Burden Analyses of Rare Variants in Patients with Unsolved Cases

Finally, for the 168 patients with no mutation identified in *PBX1* or any of the highly penetrant CAKUT genes (*HNF1B*, *PAX2*, *EYA1*, *ANOS1*, *GATA3*, *CHD7*, or *KIF14*), we performed a burden test to look for genes with an enrichment in rare variants. When considering only loss of function variants, we did not identify any gene with nominal P value <0.05. When considering loss of function plus missense, we identified a few genes with nominal P value <0.05, but none of them reached significance with Bonferroni correction ($P<1.5\times10^{-4}$). These results are shown in Supplemental Table 5.

DISCUSSION

Whole-exome sequencing is currently considered as the optimal approach for identifying new genes involved in human diseases. However, targeted exome sequencing, because it offers the advantage to analyze larger series of patients for the same cost, may prove more efficient for mutation identification in the context of highly genetically heterogeneous diseases, such as CAKUT, provided that the gene selection is relevant. Analysis of candidate genes allowed us to identify five *de novo* *PBX1* mutations/deletions, including three loss of function point mutations, showing that this gene is a novel CAKUT gene. *PBX1* encodes the Pre-B Cell Leukemia Transcription Factor 1, a TALE homeodomain transcription factor known to play a crucial role in several developmental processes and modify *Hox* gene activity.[21] In the mouse, Pbx1 was notably shown to play a role during kidney development.[22,23] It is expressed in the nephrogenic mesenchyme, weakly in the induced mesenchyme and strongly in the stroma after ureteric bud invasion. Its expression decreases when cells undergo epithelial differentiation, whereas it increases in glomerular cells at the stage of capillary loop extension. Except for *Pdgfrb*, which was recently reported as a direct target gene during vascular patterning,[24] Pbx1 transcriptional targets in the kidney remain largely unknown. Although no defect was reported in $Pbx1^{+/-}$ kidneys, a majority of $Pbx1^{-/-}$ embryos exhibit hypoplastic kidneys (30% with unilateral kidney agenesis), poorly defined cortical and medullary regions (E13.0), and a reduced number of differentiating nephrons (E14.5). Mutant kidneys were also reported to be mispositioned caudally. Histologic analysis revealed defects in ureteric branching and abnormal expansion of induced mesenchyme, arising from a mesenchymal dysfunction that led to a reduced mesenchymal to epithelial differentiation.[23] $Pbx1^{-/-}$ mouse kidney phenotypes are thus highly reminiscent of those of the patients with heterozygous *PBX1* mutations (hypoplastic kidneys [all patients], unilateral agenesis [K136], oligonephronia [K186], and horseshoe kidney with absence of corticomedullar differentiation [K181]). A phenotype associated with haploinsufficiency in human but not in mouse has already been reported for other transcription factor–encoding genes involved in kidney development (*e.g.*, *HNF1B*, *SIX1*, and *SIX2*).

In 2012, Sanna-Cherchi *et al.*[9] reported a 0.5-Mb *de novo* deletion at 1q32, including *PBX1*, in a patient with renal hypoplasia. More recently, the study of overlapping deletions on the long arm of chromosome 1 in several patients presenting with renal malformation associated with other defects suggested that haploinsufficiency of *PBX1* might be responsible for the renal phenotype.[25] Our data confirm that hypothesis, because three *PBX1* mutations were *de novo* point mutations leading to a null allele. As for CAKUT associated with heterozygous mutations in genes encoding other transcription factors (*HNF1B*, *PAX2*, *EYA1*, and *SALL1*), the severity of the renal disease associated with *PBX1* defect seems variable: the oldest patient presents with stage 3 renal failure (eGFR of 40 ml/min per 1.73 m^2) at the age of 39 years old, whereas the fetal case showed major renal hypoplasia leading to oligohydramnios. This could be due to variants in modifier genes. Associated deafness was present in two of the five patients with *PBX1* mutation/deletion who were not carrying additional mutation or deletion of *PAX2*, *GATA3*, *EYA1*, or *SIX1*, four genes with mutations that may lead to deafness. In a mouse cochlear hair cell line, *Pbx1* is coexpressed with *Gata3*,[26] suggesting that *PBX1* mutations might be responsible for deafness. However, the majority of patients with large deletions at 1q23.3q24.1 removing *PBX1* do not have deafness.[25] Microcephaly, facial dysmorphism, ear anomalies, and developmental delay in a family 5 patient were reported in other patients with large deletions at that locus[25]; however, developmental delay and facial dysmorphism were also present in the patient from family 2 carrying a *PBX1* nonsense mutation. Screening of larger series of patients with CAKUT for mutations in *PBX1* will be necessary to more precisely evaluate their association with extrarenal phenotypes.

Our strategy of targeted exome sequencing also allowed us to improve the efficiency of identification of causative mutations in patients with known CAKUT compared with our previous workflow (by Sanger sequencing and MLPA analysis), in which only *HNF1B*, *PAX2*, and/or *EYA1* were screened. Altogether, causative mutations, including the five *PBX1* mutations, were identified in 36 of the 204 (17.6%) patients with CAKUT. This rate is far above that reported recently by a similar NGS approach (six of 453),[11] and this is likely due, at least in part, to the fact that the spectrum of phenotypes included was different. We only included CAKUT affecting both kidneys and/or familial and/or syndromic forms, excluding posterior urethral valves known to be most frequently sporadic, whereas Nicolaou *et al.*[11] included unilateral forms and many posterior urethral valves. The rate of mutation that we observed here is also higher than that reported by Thomas *et al.*[6] but close to that reported by Weber *et al.*[5] or Madariaga *et al.*[7] Of note, the proportion of patients with *HNF1B*, *PAX2*,

or *EYA1* mutations is probably slightly biased downward, because our cohort included 50 patients already known not to carry mutations in these genes. Interestingly, 40% of the identified mutations are deletions, removing either a few exons or the whole gene. Indeed, a major advantage of NGS is the identification of both point mutations and deletions (intragenic and whole-gene deletions) in a sole experiment. In addition to *HNF1B* deletions, heterozygous deletions, which would not have been diagnosed by our previous workflow, were identified in *PAX2*, *EYA1*, *GATA3*, and *ANOS1*. Also, one homozygous intragenic deletion of *KIF14* was shown in a consanguineous family. No mutation was identified in *ITGA8* or *FGF20*, two genes recently reported as responsible for autosomal recessive bilateral kidney agenesis.[27,28]

Among variants identified in this study, some are in other genes previously reported as responsible for dominant CAKUT (Table 4). However, although these variants met criteria supporting their pathogenicity (absence or low frequency in the ExAC and pathogenicity scores indicating deleterious effect), in the seven patients whose parents could be tested, the variants were inherited from an unaffected parent (Table 4), thus questioning their causality. In one patient with renal cystic hypodysplasia and deafness, compound heterozygous variants in *NOTCH2* were shown in the index patient, the significance of which is unknown. Growing numbers of available data regarding the frequency of variants among large control populations can lead variants initially considered as pathogenic to be reclassified. The frequency of the *SOX17* p.Tyr259Asn variation in the ExAC and our in-house database indicates that this variant is likely not causative, although it could be an at-risk allele as recently proposed.[29] As for the *DSTYK* splice variant (c.654+1)[20] that we identified in a BO individual without any renal involvement, the rate of this variant in the ExAC and our in-house database supports that, if involved in the development of a CAKUT phenotype, it has an incomplete penetrance. This highlights the fact that one must be cautious when interpreting variants reported as pathogenic in the literature. Indeed, some of them can reveal as low-penetrance alleles, modifiers, or even frequent polymorphisms instead of causative mutations.

Except for *KIF14*, no ballelic mutation was identified in any of the genes previously reported in recessive forms of CAKUT. As in the work by Nicolaou *et al.*,[11] we did not identify any significant increase in rare variants in any of the tested genes, reflecting the complexity of genetic studies in CAKUT. Moreover, no pathogenic mutation or rare variant of unknown significance was identified in 40% of our series (Supplemental Table 1). Although mutations or CNVs in gene(s), noncoding regions, or microRNAs not targeted by our capture library could be involved in some of these patients, somatic events and/or environmental factors or epigenetic mechanisms likely explain at least part of this large fraction of patients. The familial aggregation of CAKUT as well as the wide spectrum of severity of the phenotypes suggest a complex genetic architecture as observed in neurodevelopmental disorders.[30] This would fit with a model in which various combinations of variants as well as environmental factors will cause early kidney development insults and act together to alter renal and urinary tract formation. The timing, severity, location, and extent of the "deviation from an optimal renal developmental program" may determine the ultimate phenotype. Collaborative effort will be essential in the future to test a larger number of individuals by whole-exome sequencing, classify variants, and establish high-throughput functional assays to successfully decipher the complex genetic mechanisms of CAKUT and be able to propose appropriate genetic tests and counseling for the families.

During the review process of the paper, Le Tanno *et al.*[31] reported a novel series of *de novo* 1q23.3-q24.1 microdeletions in patients with syndromic CAKUT. The patient carrying the smallest deletion, limited to *PBX1*, presented with mild developmental delay and hearing loss, which was observed in two patients of our series harboring *PBX1* point mutations.

CONCISE METHODS

Design of the Targeted SureSelect Library

The 330 genes included in our panel are shown in Supplemental Table 2 and include 55 genes with mutations reported in the literature in patients with isolated and/or syndromic CAKUT and 275 candidate genes (including 104 genes with knockout in mouse that led to kidney developmental defects, 84 genes involved in cellular processes/signaling pathways relevant for kidney development, 11 genes with a role in ureter/bladder development, 57 genes encoding reported targets of transcription factors WT1 or HNF1B, and 19 homologs of genes in the sublists above expressed during kidney/lower urinary tract development). The custom SureSelect gene panel was designed using the SureDesign software (Agilent). The target regions covered 1.38 Mb, including coding exons and splice junctions.

Targeted Exome Sequencing and Prioritization of the Variants

DNA was extracted from blood cells (living patients) or frozen tissues (fetuses). The study was approved by the Comité de Protection des Personnes pour la Recherche Biomédicale Ile de France 2, and informed consent was obtained from the patients or parents. Illumina-compatible precapture barcoded genomic DNA libraries were constructed, and a series of 16 or 36 barcoded libraries was pooled at equimolar concentrations. The capture process was performed according to the SureSelect protocol (Agilent) and sequencing on an Illumina HiSeq2500. Sequences were aligned to the reference human genome hg19 using the Burrows–Wheeler Aligner.

The mean depth of coverage ranged from 215 to 719, with ≥98% of the bases covered at least 30× (Supplemental Material). Variants were prioritized according to their frequency in the ExAC database[32] and their predicted damaging effect. For known CAKUT genes, we selected previously published variants as well as nonsense, frameshift, splice variants, and missense predicted as damaging by at least three of five used prediction programs (Polyphen2, Sift, MutationTaster,

Grantham score, and Align-GVGD) (Supplemental Material) with a minor allele frequency ≤1/5000 for genes involved in dominant forms and ≤1/1000 for those involved in recessive forms. For candidate genes, only variants that were absent from the ExAC were retained.

To evaluate duplication and large deletion events, for each individual, the relative read count for each targeted region was determined as the ratio of the read count for that region divided by the total absolute read counts of all targeted regions of the design. The ratio of the relative read count of a region in a given individual over the average relative read counts in other individuals of the run resulted in the estimated copy number for that region in that individual (method adapted from ref. 33).

Burden Test

To look for an excess of rare variants in the 330 genes in patients with CAKUT, we conducted a burden test using the Madsen and Browning[34] Wilcoxon rank sum test and the SKAT-o test[35] as implemented in EPACTS software (http://genome.sph.umich.edu/wiki/EPACTS). For the patients, we included the 168 patients with no mutation identified in *PBX1* or any of the highly penetrant CAKUT genes (*HNF1B*, *PAX2*, *EYA1*, *ANOS1*, *GATA3*, *CHD7*, or *KIF14*). For the controls, we used 426 unrelated individuals who were unaffected parents of children presenting with immune deficiency that were sequenced by whole-exome sequencing on the same genomic platform. Variants in patients and controls were called together. Variants were filtered according to their frequency in public databases (the ExAC, dbSNP, 1000G, and EVS) using two different thresholds (<0.01% and <0.001%), and we then considered either loss of function variants (nonsense, frameshift, splice, start loss, and stop loss) or loss of function plus missense predicted as damaging by Polyphen2 (score >0.470) and Sift (score <0.05). Large deletions were not taken into account in this analysis.

ACKNOWLEDGMENTS

We thank patients and families for their participation. We also thank the foetopathologists of the SOciété Française de FOETopatholgie for providing us with fetal tissue samples and the pediatric nephrologists from the French Society of Pediatric Nephrology for referring the patients. We thank Marie-Claire Gubler for her help with histology analysis of fetal kidneys. We thank Olivier Gribouval for help with microsatellite analysis.

The research leading to these results has received funding from the European Union's Seventh Framework Programme (FP7/2007–2013) grant 305608 (EURenOmics). C. Humbert was funded by EURenOmics. This work was also supported by Programme Hospitalier de la Recherche Clinique Assistance Publique grant AOM07129 (to R.S.), Investments for the Future Program grant ANR-10-IAHY-01 (to S.S. and C.A.), and Fondation pour la Recherche Médicale grant DEQ20130326532 (to S.S.).

DISCLOSURES

None.

REFERENCES

1. Loane M, Dolk H, Kelly A, Teljeur C, Greenlees R, Densem J; EUROCAT Working Group: Paper 4: EUROCAT statistical monitoring: Identification and investigation of ten year trends of congenital anomalies in Europe. *Birth Defects Res A Clin Mol Teratol* 91[Suppl 1]: S31–S43, 2011
2. Ardissino G, Daccò V, Testa S, Bonaudo R, Claris-Appiani A, Taioli E, Marra G, Edefonti A, Sereni F; ItalKid Project: Epidemiology of chronic renal failure in children: Data from the ItalKid project. *Pediatrics* 111: e382–e387, 2003
3. Bulum B, Ozçakar ZB, Ustüner E, Düşünceli E, Kavaz A, Duman D, Walz K, Fitoz S, Tekin M, Yalçınkaya F: High frequency of kidney and urinary tract anomalies in asymptomatic first-degree relatives of patients with CAKUT. *Pediatr Nephrol* 28: 2143–2147, 2013
4. Limwongse C: Syndromes and malformations of the urinary tract. In: *Pediatric Nephrology*, Vol. 1, 6th Ed., edited by Avner ED, Harmon WE, Niaudet P, Yoshikawa N, Berlin, Springer, 2009, pp 121–156
5. Weber S, Moriniere V, Knüppel T, Charbit M, Dusek J, Ghiggeri GM, Jankauskiené A, Mir S, Montini G, Peco-Antic A, Wühl E, Zurowska AM, Mehls O, Antignac C, Schaefer F, Salomon R: Prevalence of mutations in renal developmental genes in children with renal hypodysplasia: Results of the ESCAPE study. *J Am Soc Nephrol* 17: 2864–2870, 2006
6. Thomas R, Sanna-Cherchi S, Warady BA, Furth SL, Kaskel FJ, Gharavi AG: HNF1B and PAX2 mutations are a common cause of renal hypodysplasia in the CKiD cohort. *Pediatr Nephrol* 26: 897–903, 2011
7. Madariaga L, Morinière V, Jeanpierre C, Bouvier R, Loget P, Martinovic J, Dechelotte P, Leporrier N, Thauvin-Robinet C, Jensen UB, Gaillard D, Mathieu M, Turlin B, Attie-Bitach T, Salomon R, Gübler MC, Antignac C, Heidet L: Severe prenatal renal anomalies associated with mutations in HNF1B or PAX2 genes. *Clin J Am Soc Nephrol* 8: 1179–1187, 2013
8. Lopez-Rivera E, Liu YP, Verbitsky M, Anderson BR, Capone VP, Otto EA, Yan Z, Mitrotti A, Martino J, Steers NJ, Fasel DA, Vukojevic K, Deng R, Racedo SE, Liu Q, Werth M, Westland R, Vivante A, Makar GS, Bodria M, Sampson MG, Gillies CE, Vega-Warner V, Maiorana M, Petrey DS, Honig B, Lozanovski VJ, Salomon R, Heidet L, Carpentier W, Gaillard D, Carrea A, Gesualdo L, Cusi D, Izzi C, Scolari F, van Wijk JA, Arapovic A, Saraga-Babic M, Saraga M, Kunac N, Samii A, McDonald-McGinn DM, Crowley TB, Zackai EH, Drozdz D, Miklaszewska M, Tkaczyk M, Sikora P, Szczepanska M, Mizerska-Wasiak M, Krzemien G, Szmigielska A, Zaniew M, Darlow JM, Puri P, Barton D, Casolari E, Furth SL, Warady BA, Gucev Z, Hakonarson H, Flogelova H, Tasic V, Latos-Bielenska A, Materna-Kiryluk A, Allegri L, Wong CS, Drummond IA, D'Agati V, Imamoto A, Barasch JM, Hildebrandt F, Kiryluk K, Lifton RP, Morrow BE, Jeanpierre C, Papaioannou VE, Ghiggeri GM, Gharavi AG, Katsanis N, Sanna-Cherchi S: Genetic drivers of kidney defects in the DiGeorge syndrome. *N Engl J Med* 376: 742–754, 2017
9. Sanna-Cherchi S, Kiryluk K, Burgess KE, Bodria M, Sampson MG, Hadley D, Nees SN, Verbitsky M, Perry BJ, Sterken R, Lozanovski VJ, Materna-Kiryluk A, Barlassina C, Kini A, Corbani V, Carrea A, Somenzi D, Murtas C, Ristoska-Bojkovska N, Izzi C, Bianco B, Zaniew M, Flogelova H, Weng PL, Kacak N, Giberti S, Gigante M, Arapovic A, Drnasin K, Caridi G, Curioni S, Allegri F, Ammenti A, Ferretti S, Goj V, Bernardo L, Jobanputra V, Chung WK, Lifton RP, Sanders S, State M, Clark LN, Saraga M, Padmanabhan S, Dominiczak AF, Foroud T, Gesualdo L, Gucev Z, Allegri L, Latos-Bielenska A, Cusi D, Scolari F, Tasic V, Hakonarson H, Ghiggeri GM, Gharavi AG: Copy-number disorders are a common cause of congenital kidney malformations. *Am J Hum Genet* 91: 987–997, 2012

10. Westland R, Verbitsky M, Vukojevic K, Perry BJ, Fasel DA, Zwijnenburg PJ, Bökenkamp A, Gille JJ, Saraga-Babic M, Ghiggeri GM, D'Agati VD, Schreuder MF, Gharavi AG, van Wijk JA, Sanna-Cherchi S: Copy number variation analysis identifies novel CAKUT candidate genes in children with a solitary functioning kidney. *Kidney Int* 88: 1402–1410, 2015
11. Nicolaou N, Pulit SL, Nijman IJ, Monroe GR, Feitz WF, Schreuder MF, van Eerde AM, de Jong TP, Giltay JC, van der Zwaag B, Havenith MR, Zwakenberg S, van der Zanden LF, Poelmans G, Cornelissen EA, Lilien MR, Franke B, Roeleveld N, van Rooij IA, Cuppen E, Bongers EM, Giles RH, Knoers NV, Renkema KY: Prioritization and burden analysis of rare variants in 208 candidate genes suggest they do not play a major role in CAKUT. *Kidney Int* 89: 476–486, 2016
12. Skinner MA, Safford SD, Reeves JG, Jackson ME, Freemerman AJ: Renal aplasia in humans is associated with RET mutations. *Am J Hum Genet* 82: 344–351, 2008
13. Jeanpierre C, Macé G, Parisot M, Morinière V, Pawtowsky A, Benabou M, Martinovic J, Amiel J, Attié-Bitach T, Delezoide AL, Loget P, Blanchet P, Gaillard D, Gonzales M, Carpentier W, Nitschke P, Tores F, Heidet L, Antignac C, Salomon R; Société Française de Foetopathologie: RET and GDNF mutations are rare in fetuses with renal agenesis or other severe kidney development defects. *J Med Genet* 48: 497–504, 2011
14. Filges I, Nosova E, Bruder E, Tercanli S, Townsend K, Gibson WT, Röthlisberger B, Heinimann K, Hall JG, Gregory-Evans CY, Wasserman WW, Miny P, Friedman JM: Exome sequencing identifies mutations in KIF14 as a novel cause of an autosomal recessive lethal fetal ciliopathy phenotype. *Clin Genet* 86: 220–228, 2014
15. Bower M, Salomon R, Allanson J, Antignac C, Benedicenti F, Benetti E, Binenbaum G, Jensen UB, Cochat P, DeCramer S, Dixon J, Drouin R, Falk MJ, Feret H, Gise R, Hunter A, Johnson K, Kumar R, Lavocat MP, Martin L, Morinière V, Mowat D, Murer L, Nguyen HT, Peretz-Amit G, Pierce E, Place E, Rodig N, Salerno A, Sastry S, Sato T, Sayer JA, Schaafsma GC, Shoemaker L, Stockton DW, Tan WH, Tenconi R, Vanhille P, Vats A, Wang X, Warman B, Weleber RG, White SM, Wilson-Brackett C, Zand DJ, Eccles M, Schimmenti LA, Heidet L: Update of PAX2 mutations in renal coloboma syndrome and establishment of a locus-specific database. *Hum Mutat* 33: 457–466, 2012
16. Krug P, Morinière V, Marlin S, Koubi V, Gabriel HD, Colin E, Bonneau D, Salomon R, Antignac C, Heidet L: Mutation screening of the EYA1, SIX1, and SIX5 genes in a large cohort of patients harboring branchio-oto-renal syndrome calls into question the pathogenic role of SIX5 mutations. *Hum Mutat* 32: 183–190, 2011
17. Lin YH, Wu CC, Hsu TY, Chiu WY, Hsu CJ, Chen PL: Identification of a novel GATA3 mutation in a deaf Taiwanese family by massively parallel sequencing. *Mutat Res* 771: 1–5, 2015
18. Garcia-Barceló M, Sham MH, Lee WS, Lui VC, Chen BL, Wong KK, Wong JS, Tam PK: Highly recurrent RET mutations and novel mutations in genes of the receptor tyrosine kinase and endothelin receptor B pathways in Chinese patients with sporadic Hirschsprung disease. *Clin Chem* 50: 93–100, 2004
19. Gimelli S, Caridi G, Beri S, McCracken K, Bocciardi R, Zordan P, Dagnino M, Fiorio P, Murer L, Benetti E, Zuffardi O, Giorda R, Wells JM, Gimelli G, Ghiggeri GM: Mutations in SOX17 are associated with congenital anomalies of the kidney and the urinary tract. *Hum Mutat* 31: 1352–1359, 2010
20. Sanna-Cherchi S, Sampogna RV, Papeta N, Burgess KE, Nees SN, Perry BJ, Choi M, Bodria M, Liu Y, Weng PL, Lozanovski VJ, Verbitsky M, Lugani F, Sterken R, Paragas N, Caridi G, Carrea A, Dagnino M, Materna-Kiryluk A, Santamaria G, Murtas C, Ristoska-Bojkovska N, Izzi C, Kacak N, Bianco B, Giberti S, Gigante M, Piaggio G, Gesualdo L, Kosuljandic Vukic D, Vukojevic K, Saraga-Babic M, Saraga M, Gucev Z, Allegri L, Latos-Bielenska A, Casu D, State M, Scolari F, Ravazzolo R, Kiryluk K, Al-Awqati Q, D'Agati VD, Drummond IA, Tasic V, Lifton RP, Ghiggeri GM, Gharavi AG: Mutations in DSTYK and dominant urinary tract malformations. *N Engl J Med* 369: 621–629, 2013
21. Moens CB, Selleri L: Hox cofactors in vertebrate development. *Dev Biol* 291: 193–206, 2006
22. Yu J, McMahon AP, Valerius MT: Recent genetic studies of mouse kidney development. *Curr Opin Genet Dev* 14: 550–557, 2004
23. Schnabel CA, Godin RE, Cleary ML: Pbx1 regulates nephrogenesis and ureteric branching in the developing kidney. *Dev Biol* 254: 262–276, 2003
24. Hurtado R, Zewdu R, Mtui J, Liang C, Aho R, Kurylo C, Selleri L, Herzlinger D: Pbx1-dependent control of VMC differentiation kinetics underlies gross renal vascular patterning. *Development* 142: 2653–2664, 2015
25. Mackenroth L, Hackmann K, Klink B, Weber JS, Mayer B, Schröck E, Tzschach A: Interstitial 1q23.3q24.1 deletion in a patient with renal malformation, congenital heart disease, and mild intellectual disability. *Am J Med Genet A* 170: 2394–2399, 2016
26. Rivolta MN, Halsall A, Johnson CM, Tones MA, Holley MC: Transcript profiling of functionally related groups of genes during conditional differentiation of a mammalian cochlear hair cell line. *Genome Res* 12: 1091–1099, 2002
27. Barak H, Huh SH, Chen S, Jeanpierre C, Martinovic J, Parisot M, Bole-Feysot C, Nitschké P, Salomon R, Antignac C, Ornitz DM, Kopan R: FGF9 and FGF20 maintain the stemness of nephron progenitors in mice and man. *Dev Cell* 22: 1191–1207, 2012
28. Humbert C, Silbermann F, Morar B, Parisot M, Zarhrate M, Masson C, Tores F, Blanchet P, Perez MJ, Petrov Y, Khau Van Kien P, Roume J, Leroy B, Gribouval O, Kalaydjieva L, Heidet L, Salomon R, Antignac C, Benmerah A, Saunier S, Jeanpierre C: Integrin alpha 8 recessive mutations are responsible for bilateral renal agenesis in humans. *Am J Hum Genet* 94: 288–294, 2014
29. Combes P, Planche V, Eymard-Pierre E, Sarret C, Rodriguez D, Boespflug-Tanguy O, Vaurs-Barriere C: Relevance of SOX17 variants for hypomyelinating leukodystrophies and congenital anomalies of the kidney and urinary tract (CAKUT). *Ann Hum Genet* 76: 261–267, 2012
30. Tordjman S, Somogyi E, Coulon N, Kermarrec S, Cohen D, Bronsard G, Bonnot O, Weismann-Arcache C, Botbol M, Lauth B, Ginchat V, Roubertoux P, Barburoth M, Kovess V, Geoffray MM, Xavier J: Gene × Environment interactions in autism spectrum disorders: Role of epigenetic mechanisms. *Front Psychiatry* 5: 53, 2014
31. Le Tanno P, Breton J, Bidart M, Satre V, Harbuz R, Ray PF, Bosson C, Dieterich K, Jaillard S, Odent S, Poke G, Beddow R, Digilio MC, Novelli A, Bernardini L, Pisanti MA, Mackenroth L, Hackmann K, Vogel I, Christensen R, Fokstuen S, Bena F, Amblard F, Devillard F, Vieville G, Apostolou A, Jouk PS, Guebre-Egziabher F, Sartelet H, Coutton C: PBX1 haploinsufficiency leads to syndromic congenital anomalies of the kidney and urinary tract (CAKUT) in humans [published online ahead of print March 7, 2017]. *J Med Genet* doi:10.1136/jmedgenet-2016-104435
32. Lek M, Karczewski KJ, Minikel EV, Samocha KE, Banks E, Fennell T, O'Donnell-Luria AH, Ware JS, Hill AJ, Cummings BB, Tukiainen T, Birnbaum DP, Kosmicki JA, Duncan LE, Estrada K, Zhao F, Zou J, Pierce-Hoffman E, Berghout J, Cooper DN, Deflaux N, DePristo M, Do R, Flannick J, Fromer M, Gauthier L, Goldstein J, Gupta N, Howrigan D, Kiezun A, Kurki MI, Moonshine AL, Natarajan P, Orozco L, Peloso GM, Poplin R, Rivas MA, Ruano-Rubio V, Rose SA, Ruderfer DM, Shakir K, Stenson PD, Stevens C, Thomas BP, Tiao G, Tusie-Luna MT, Weisburd B, Won HH, Yu D, Altshuler DM, Ardissino D, Boehnke M, Danesh J, Donnelly S, Elosua R, Florez JC, Gabriel SB, Getz G, Glatt SJ, Hultman CM, Kathiresan S, Laakso M, McCarroll S, McCarthy MI, McGovern D, McPherson R, Neale BM, Palotie A, Purcell SM, Saleheen D, Scharf JM, Sklar P, Sullivan PF, Tuomilehto J, Tsuang MT, Watkins HC, Wilson JG, Daly MJ, MacArthur DG; Exome Aggregation Consortium: Analysis of protein-coding genetic variation in 60,706 humans. *Nature* 536: 285–291, 2016
33. Goossens D, Moens LN, Nelis E, Lenaerts AS, Glassee W, Kalbe A, Frey B, Kopal G, De Jonghe P, De Rijk P, Del-Favero J: Simultaneous

mutation and copy number variation (CNV) detection by multiplex PCR-based GS-FLX sequencing. *Hum Mutat* 30: 472–476, 2009
34. Madsen BE, Browning SR: A groupwise association test for rare mutations using a weighted sum statistic. *PLoS Genet* 5: e1000384, 2009
35. Lee S, Wu MC, Lin X: Optimal tests for rare variant effects in sequencing association studies. *Biostatistics* 13: 762–775, 2012
36. Bellanné-Chantelot C, Clauin S, Chauveau D, Collin P, Daumont M, Douillard C, Dubois-Laforgue D, Dusselier L, Gautier JF, Jadoul M, Laloi-Michelin M, Jacquesson L, Larger E, Louis J, Nicolino M, Subra JF, Wilhem JM, Young J, Velho G, Timsit J: Large genomic rearrangements in the hepatocyte nuclear factor-1beta (TCF2) gene are the most frequent cause of maturity-onset diabetes of the young type 5. *Diabetes* 54: 3126–3132, 2005
37. Benetti E, Artifoni L, Salviati L, Pinello L, Perrotta S, Zuffardi O, Zacchello G, Murer L: Renal hypoplasia without optic coloboma associated with PAX2 gene deletion. *Nephrol Dial Transplant* 22: 2076–2078, 2007
38. Schimmenti LA, Shim HH, Wirtschafter JD, Panzarino VA, Kashtan CE, Kirkpatrick SJ, Wargowski DS, France TD, Michel E, Dobyns WB: Homonucleotide expansion and contraction mutations of PAX2 and inclusion of Chiari 1 malformation as part of renal-coloboma syndrome. *Hum Mutat* 14: 369–376, 1999
39. Sanyanusin P, McNoe LA, Sullivan MJ, Weaver RG, Eccles MR: Mutation of PAX2 in two siblings with renal-coloboma syndrome. *Hum Mol Genet* 4: 2183–2184, 1995
40. Sellick GS, Longman C, Tolmie J, Newbury-Ecob R, Geenhalgh L, Hughes S, Whiteford M, Garrett C, Houlston RS: Genomewide linkage searches for Mendelian disease loci can be efficiently conducted using high-density SNP genotyping arrays. *Nucleic Acids Res* 32: e164, 2004
41. Higashide T, Wada T, Sakurai M, Yokoyama H, Sugiyama K: Macular abnormalities and optic disk anomaly associated with a new PAX2 missense mutation. *Am J Ophthalmol* 139: 203–205, 2005
42. Rickard S, Boxer M, Trompeter R, Bitner-Glindzicz M: Importance of clinical evaluation and molecular testing in the branchio-oto-renal (BOR) syndrome and overlapping phenotypes. *J Med Genet* 37: 623–627, 2000
43. Abdelhak S, Kalatzis V, Heilig R, Compain S, Samson D, Vincent C, Levi-Acobas F, Cruaud C, Le Merrer M, Mathieu M, König R, Vigneron J, Weissenbach J, Petit C, Weil D: Clustering of mutations responsible for branchio-oto-renal (BOR) syndrome in the eyes absent homologous region (eyaHR) of EYA1. *Hum Mol Genet* 6: 2247–2255, 1997
44. Orten DJ, Fischer SM, Sorensen JL, Radhakrishna U, Cremers CW, Marres HA, Van Camp G, Welch KO, Smith RJ, Kimberling WJ: Branchio-oto-renal syndrome (BOR): Novel mutations in the EYA1 gene, and a review of the mutational genetics of BOR. *Hum Mutat* 29: 537–544, 2008
45. Fukami M, Muroya K, Miyake T, Iso M, Kato F, Yokoi H, Suzuki Y, Tsubouchi K, Nakagomi Y, Kikuchi N, Horikawa R, Ogata T: GATA3 abnormalities in six patients with HDR syndrome. *Endocr J* 58: 117–121, 2011
46. Van Esch H, Groenen P, Nesbit MA, Schuffenhauer S, Lichtner P, Vanderlinden G, Harding B, Beetz R, Bilous RW, Holdaway I, Shaw NJ, Fryns JP, Van de Ven W, Thakker RV, Devriendt K: GATA3 haploinsufficiency causes human HDR syndrome. *Nature* 406: 419–422, 2000
47. Montenegro LR, Silveira LF, Tusset C, de Castro M, Versiani BR, Latronico AC, Mendonca BB, Trarbach EB: Combined use of multiplex ligation-dependent probe amplification and automatic sequencing for identification of KAL1 defects in patients with Kallmann syndrome. *Fertil Steril* 100: 854–859, 2013
48. Hardelin JP, Levilliers J, del Castillo I, Cohen-Salmon M, Legouis R, Blanchard S, Compain S, Bouloux P, Kirk J, Moraine C, Chaussain JL, Weissenbach J, Petit C: X chromosome-linked Kallmann syndrome: Stop mutations validate the candidate gene. *Proc Natl Acad Sci U S A* 89: 8190–8194, 1992
49. Asakura Y, Toyota Y, Muroya K, Kurosawa K, Fujita K, Aida N, Kawame H, Kosaki K, Adachi M: Endocrine and radiological studies in patients with molecularly confirmed CHARGE syndrome. *J Clin Endocrinol Metab* 93: 920–924, 2008
50. Spruijt L, Hoefsloot LH, van Schaijk GH, van Waardenburg D, Kremer B, Brackel HJ, de Die-Smulders CE: Identification of a novel EYA1 mutation presenting in a newborn with laryngomalacia, glossoptosis, retrognathia, and pectus excavatum. *Am J Med Genet A* 140: 1343–1345, 2006

This article contains supplemental material online at http://jasn.asnjournals.org/lookup/suppl/doi:10.1681/ASN.2017010043/-/DCSupplemental.

Supplemental methods

Targeted exome sequencing: design, sequencing, and prioritization of the variants

We developed a targeted exome sequencing strategy focusing on 330 genes (Table S2) including (a) known causative or likely causative genes, with mutations reported in the literature in cases with isolated and/or syndromic CAKUT (55 genes),[1-50] (b) genes whose knock-out in mouse lead to kidney developmental defects (104 genes),[51-142] (c) genes involved in cellular processes/signaling pathways relevant for kidney development (84 genes),[143-200] (d) genes with a role in ureter/bladder development (11 genes),[201,202] (e) potential targets of transcription factors WT1 or HNF1B (57 genes),[204-206] and (f) gene related to gene(s) in group (a) to (e), expressed during kidney/LUT development (19 genes). A custom SureSelect gene panel was designed using the SureDesign software (Agilent). The target regions covered 1.38 Mb, including coding exons and splice junctions of the 330 genes. Illumina compatible precapture barecoded genomic DNA libraries were constructed according to the manufacturer's protocol (Ovation Ultralow, Nugen Technologies). Briefly, 1 to 3 µg of each double strand genomic DNA was mechanically fragmented to a median size of 200 pb using a Covaris, 100 ng was end-repaired and Illumina compatible adaptors containing a specific 8 bases barecode were ligated to the repaired ends (one specific barecode per patient). DNA fragments were PCR amplified to get the final precapture barecoded libraries and series of 16 or 36 barecoded libraries were pooled at equimolar concentrations. The capture process was performed according to the SureSelect protocol (Agilent) using 750 ng of the pool and 2µl or 3µl of biotinylated probes from the SureSelect panel (for pools of 16 or 36 libraries respectively). The barecoded libraries molecules complementary to the biotinylated probes retained by streptavidine coated magnetic beads were PCR amplified to generate a final pool of postcapture libraries. Sequencing was performed on an Illumina HiSeq2500 (Paired-End sequencing 130 x130 bases, High

Throughput Mode, 36 libraries per lane). After demultiplexing, sequences were aligned to the reference human genome hg19 using the Burrows-Wheeler Aligner. Downstream processing was carried out with the Genome Analysis Toolkit (GATK), SAMtools and Picard, following documented best practices (https://software.broadinstitute.org/gatk/best-practices/). Variant calls were made with the GATK Unified Genotyper. The annotation process was based on the latest release of the Ensembl database. Variants were annotated and analysed using the Polyweb software interface designed by the Bioinformatics platform of University Paris Descartes.

Prioritization of the variants was performed thanks to the polyweb interface. For known CAKUT genes, we filtered the variants whose frequency in ExAC was higher than 0,02% for genes reported in dominant CAKUT, or higher than 0,1% for those reported in recessive forms. For candidate genes, more stringent criteria were used in order to focus on the most promising genes and only variants absent in ExAC were retained. In addition, all variants identified in our in-house database (> 8000 exomes) in more than 5 independent sequencing projects of patients with various non-CAKUT phenotypes were eliminated. For missense variants, prediction of damaging effect was based on PolyPhen2,[207] Sift,[208] Mutation Taster,[209] Grantham score,[210] and GVGD.[211] Prediction of the effect of variants on splicing were based on SpliceSiteFinder, MaxEntScan, NNSPLICE, GeneSplicer and HumanSplicingFinder through Alamut.[212]

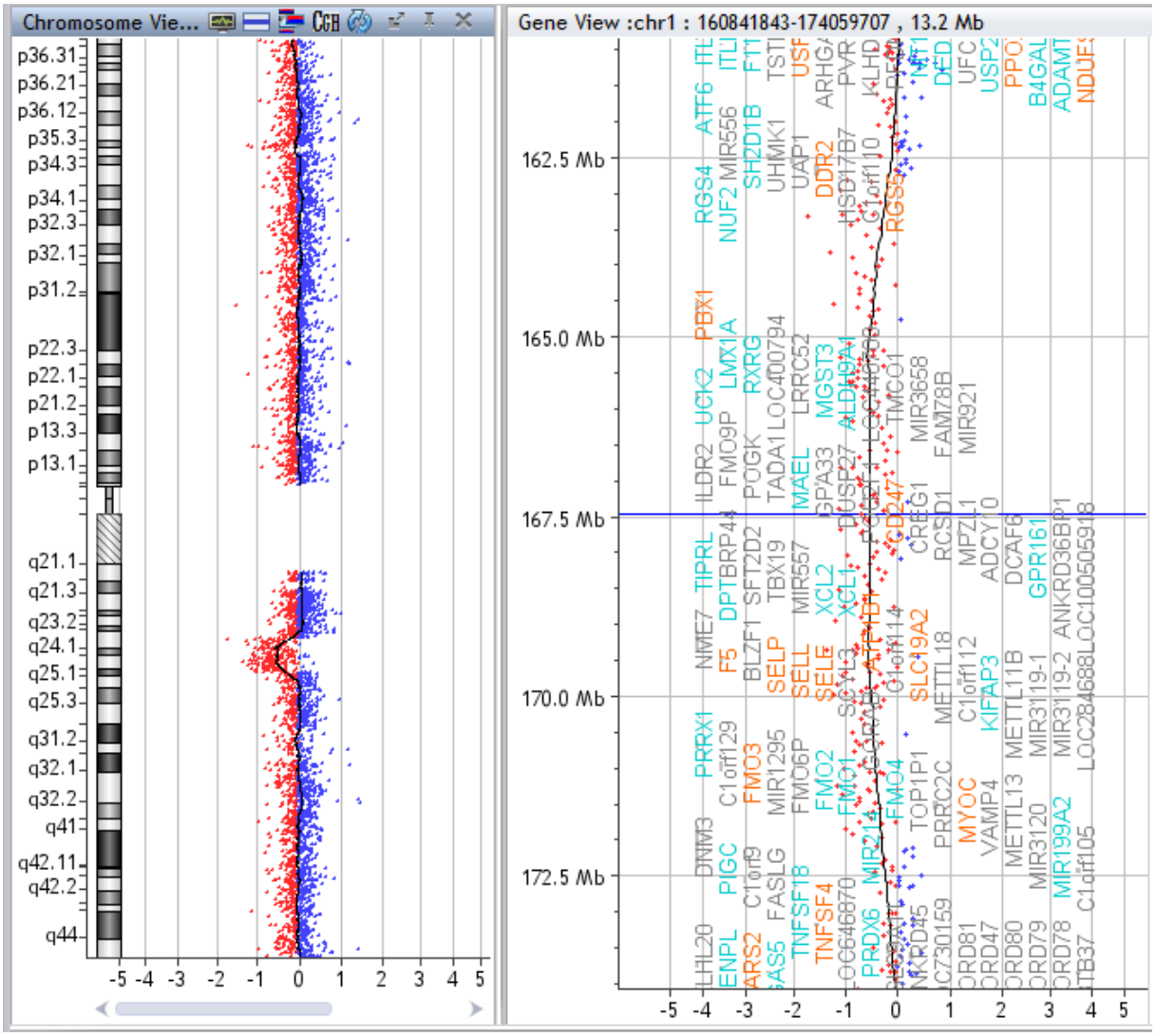

Figure S1 : Identification of a mosaic deletion including *PBX1* in the long arm of chromosome 1 in case K136 by CGH array

Array CGH analysis of DNA extracted from lymphocytes of case K136 was performed on an Agilent 60K oligonucleotide microarray (Agilent Technologies, Santa Clara, CA, USA). Result showing the 1q23.3q24.3 deletion (left). Vertical and horizontal axes indicate the genomic location and signal log2 ratio, respectively. The mean log2 ratio of the aberration region is −0.465, indicating mosaic deletion (right). The aneusomic segment was approximately 9.1 Mb in size, with proximal and distal breakpoints at 162,824,523 bp and 172,011,180 bp (GRCh 37, Hg19). This region includes *PBX1* and ~ 130 other genes.

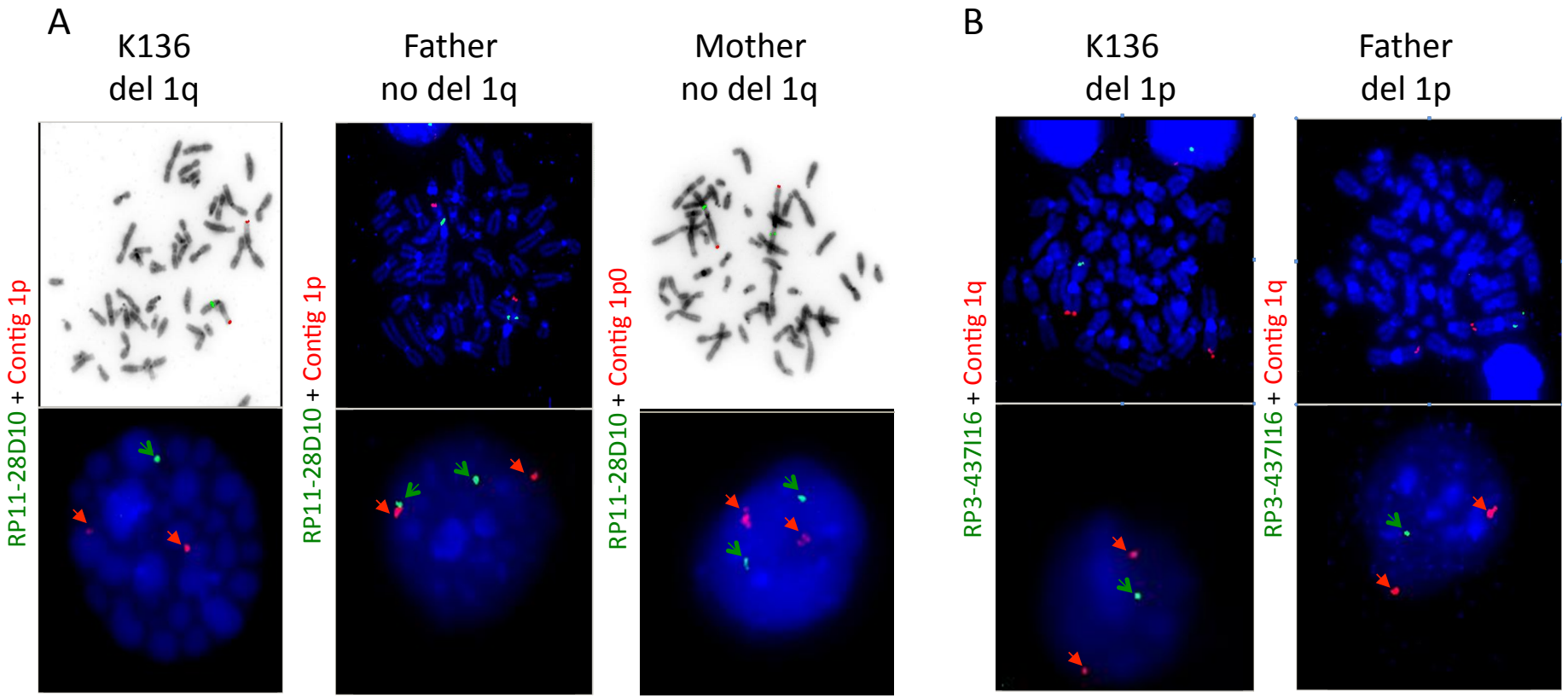

Figure S2: Fluorescent in situ hybridization experiments showing (A) *de novo* occurrence of the 1q deletion including *PBX1* and (B) inheritance of a paternal 1p deletion in case K136 (family 5)

BAC clones RP11-28D10 located in chr1:167,722,147 - 167,722,642; RP3-437I16 located in chr1:29,528,719-29,549,213

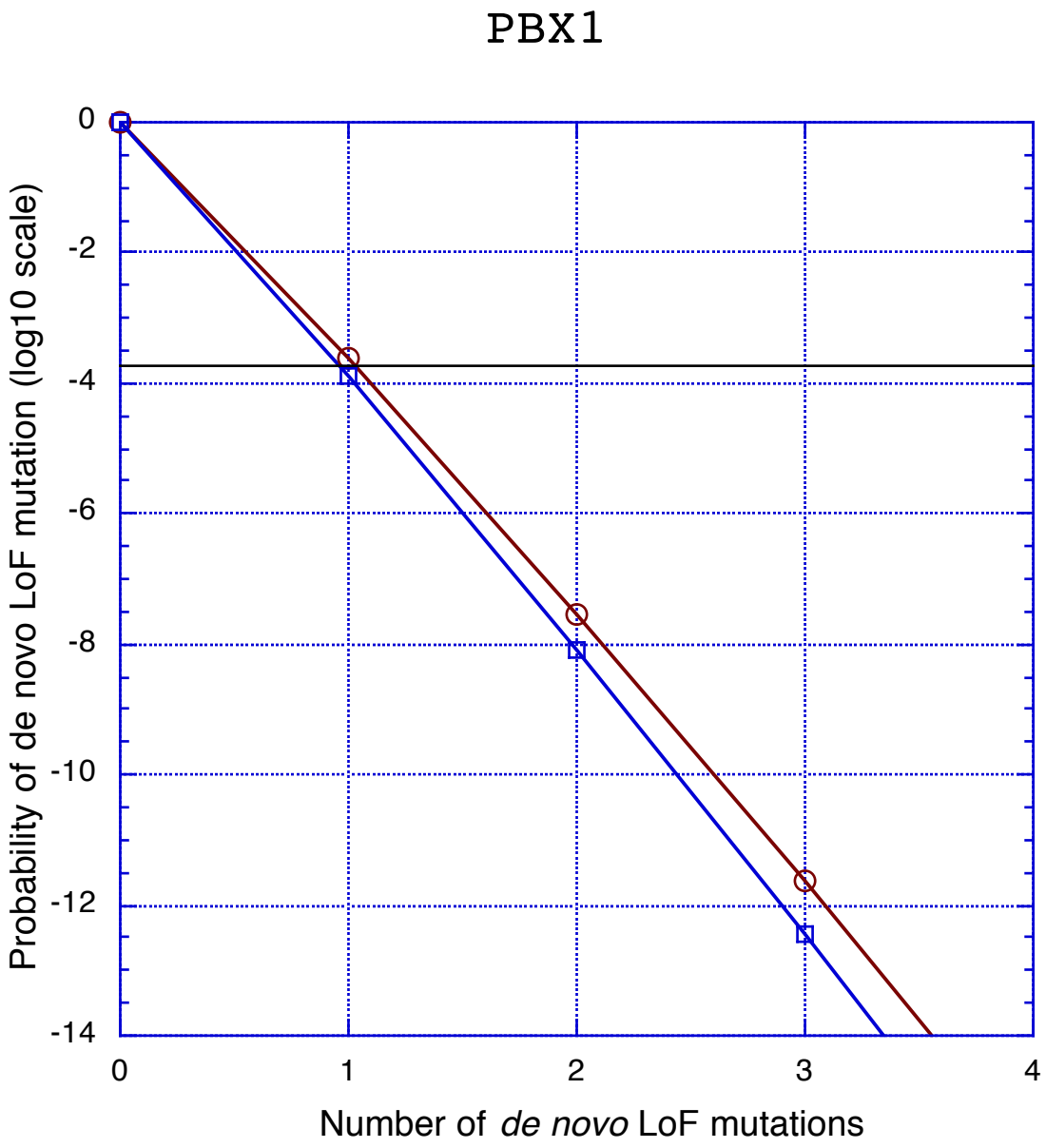

Figure S3: Result of a binomial test showing the probability that one or more *de novo* loss of function mutations in *PBX1* would occur by chance only in a cohort of 204 CAKUT cases.

Calculated and empirical values of probability for *de novo* loss-of-function mutations in *PBX1* were considered: (1) blue line: $p = 6.4 \times 10^{-7}$ = mean of values computed by Samocha et al for nonsense (7.8×10^{-7}), frameshift (8.2×10^{-7}) and splice site mutations (3.3×10^{-7}) in *PBX1*;[213] (2) red line: $p = 1.2 \times 10^{-6}$, corresponding to empirical frequency of *de novo* loss of function mutations per exome per generation (0.03 per-generation),[214] according to the size of the coding sequence of *PBX1* (1293 bp). The black line indicates the Bonferroni corrected significance threshold (1.5×10^{-4}) for 330 genes. The p-value for 3 mutations is 3.6×10^{-13}.

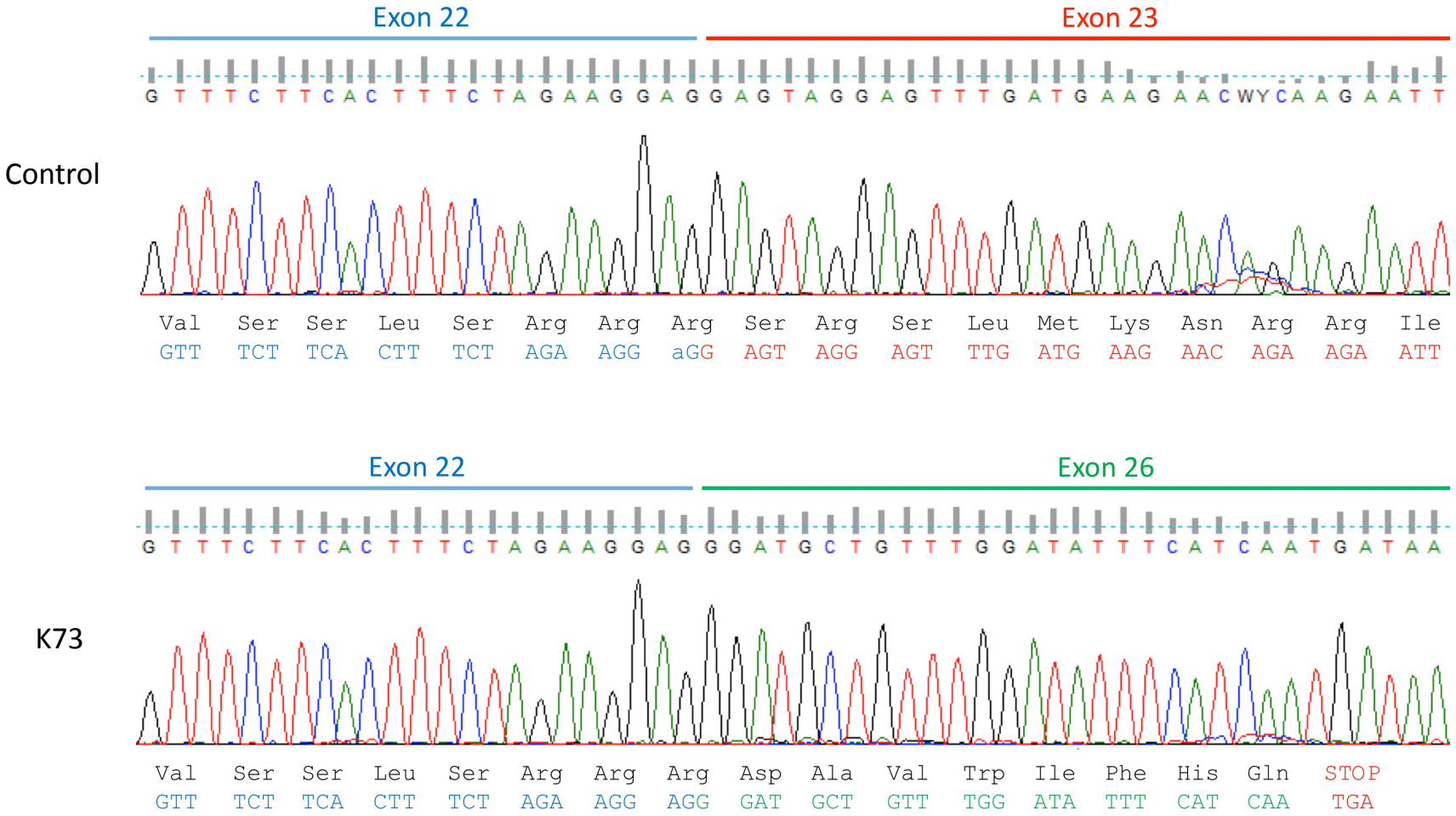

Figure S4: cDNA sequencing showing deletion of exons 23-25 with creation of a premature stop codon in case K73

Table S1. Phenotypes of all cases and variants identified																							
Case	Sex	Fetus	Renal phenotype acronym	RHa	RDb	Cysts	UMDc	BMDd	UKAe	BKAf	VURg	ObMegaUh	Duplexi	PUOj	Unprecised hydronephrosis	Renal ectopy	Family (1st degree)k	Family (other)l	Extra-renal phenotype	Causative mutations	Rare damaging variants in dominant CAKUT genes(<1/5000 in ExAC)	Reported variants in dominant CAKUT genes (>1/5000, <1/100 in ExAC)	Rare damaging variants in candidate genes[m] (absent from ExAC)
Cases with CAKUT phenotype																							
K1	F		RH	1																			MMP9, p.[Arg322Trp];[=] PDE3B, p.[Leu92Argfs*241];[=] HIC1, p.[Pro230Ser];[=]
K2	M		RH	1															hypospadias + polydactyly				CDKN1C, p.[Leu6Pro];[=]
K3	M	fetus	BKA							1							1		rigth ventricular dilation			RET, p.[Asp567Asn];[=]	
K4	F		RH	1															bifid uterus	HNF1B, c.[(?_-30)_(*220_?)del];[=]			
K5	M	fetus	BKA							1													LHX1, p.[Thr90Ile];[=]
K6	F		UKA						1										mullerian duplication				
K7	M	fetus	BKA							1									aortic stenosis				
K8	F	fetus	BKA							1									ephageal atresia + imperforate anus + 13th pair of ribs + vertebral fusion				
K9	M	fetus	BKA							1							1						SHH, p.[Val366Ala];[=]
K10	M	fetus	BKA							1													SPOCK2, p.[Lys398Glu];[=]
K11	M	fetus	UKA+				1		1														KIF3A, p.[Glu379Lys];[=]
K12	M	fetus	BKA							1													
K13	NA	fetus	BMD					1															DCHS1, p.[Ala2216Val];[=]
K14	F		RH	1													1		urogenital sinus				MAGED1, p.[Ala738Val];[=]
K15	M	fetus	BKA							1							1		pulmonary isomerisme + 11 pairs of ribs				
K16	M	fetus	BKA							1													
K17	F		UKA+						1		1		1				1						FRY, p.[Ala1643Val];[=]
K18	M	fetus	BMD					1															
K19	F	fetus	BKA							1									uterus and fallopian tubes agenesis				
K20	M	fetus	RD		1	1													liver cysts + pancreatitis				ENC1, p.[Tyr220His];[=]
K21	M	fetus	BMD					1													TBX18, p.[His204Tyr];[=]		
K22	M		RH+	1	1						1						1						
K23	F	fetus	BKA							1									left diaphragmatic hernia				
K24	M	fetus	BKA							1													
K25	M	fetus	UKA+				1		1										intrauterine growth retardation				
K26	M	fetus	BKA							1										ANOS1, p.[Arg257*];[=]			
K27	M	fetus	UKA+		1	1			1										left diaphragmatic hernia + imperforate anus + hypospadias				
K28	M	fetus	BKA							1									ear tag				LHX1, p.[Asn230His];[=] WNT6, p.[Gly196Alafs*123];[=]
K29	M	fetus	BKA							1											SIX5, p.[Ser730Leu];[=]		
K30	M		UMD+		1		1																
K31	M		RH+	1	1												1						WNT9B, p.[Cys145Tyr];[=]
K32	F	fetus	RH	1																	NOTCH2, p.[Asp355Asn];[=]	RET, p.[Arg694Gln];[=]	
K33	M		UMD+		1	1	1							1									
K34	M	fetus	BKA							1									testis agenesis				CRIM1, p.[Gly634Glu];[=]
K35	M		RH+	1							1						1						
K36	F		UKA+	1					1														
K37	F	fetus	UKA+				1		1														
K38	M	fetus	UKA+				1		1														
K39	F	fetus	UKA+				1		1								1	1	megalourethra				PIK3C3, p.[Phe597His];[=] RSPO3, p.[Lys161Gln];[=]
K40	F	fetus	BKA							1													
K41	M	fetus	BKA							1													
K42	F	fetus	Oth												1		1						
K43	F	fetus	RH+	1	1														heart defect + partial pancreas agenesis				ETV4, p.[Tyr209Cys];[=]
K44	NA	fetus	UKA+						1							1							GNB3, p.[Val276Gly];[=]
K45	F	fetus	BMD					1											accessory spleen				TGM5, p.[Thr590Arg];[=]
K46	M	fetus	BMD					1															KISS1R, p.[Ala135Ser];[=]
K47	M		RH+	1	1						1						1						
K48	M	fetus	RH+	1	1	1														GATA3, p.[Arg277*];[=]	TBX18, p.[Gln495Lys];[=]		
K49	M	fetus	BKA							1													
K50	F		UMD+				1				1						1			HNF1B, c.[(?_-30)_(*220_?)del];[=]			
K51	F	fetus	BMD					1											unicornuate uterus				SULF2, p.[Thr766Ile];[=]
K52	F	fetus	RD		1	1																	
K53	NA	fetus	UKA+	1					1								1						GREM1, p.[Gly9Cysfs*16];[=]

K54	NA	fetus	RD		1																		
K55	M		UKA						1									1					SOX4, p.[Phe334His];[=] WNT2B, p.[Ser136Ile];[=]
K56	NA	fetus	RD		1														interventricular communication + intrauterine growth retardation		TBC1D1, p.[Met930Ile];[=]		
K57	F	fetus	BKA							1													
K58	M	fetus	BKA							1								1					SPOCK2, p.[Gly372Trp];[=]
K59	F	fetus	RH+	1	1	1													uterus hypoplasia				
K60	F	fetus	RD		1	1													pancreas hypoplasia				DCHS1, p.[Thr930Ser];[=]
K61	NA	fetus	BKA							1													ECM1, p.[Asn176Ile];[=]
K62	M		RH	1															eye coloboma	PAX2, c.[?-30_305+?];[=]			
K63	F	fetus	BKA							1													
K64	M		Oth								1							1					KIF26B, p.[Arg1930Gly];[=]
K65	M	fetus	BMD					1															LAMC1, c.[1427+1G>C];[=] DACT1, p.[Glu57Lys];[=]
K66	M	fetus	BKA							1													
K67	M	fetus	UMD+				1								1				interventricular communication + single ombilical artery + small gallblader				
K68	M		RH+	1	1													1					
K69	F	fetus	BMD					1													SALL1, p.[Asn1257Lys];[=]		
K70	M	fetus	BMD					1													CHD1L, p.[Lys519Asn];[=] NOTCH2, p.[Arg1719Gln];[=] SALL4, p.[Arg831Gln];[=]		
K71	M	fetus	UMD				1											1					HIC1, p.[Gly702Asp];[=]
K72	M		RH	1														1	papillary excavation	PAX2, c.[(?_-30)_(*220_?)del];[=]			
K73	F	fetus	RH+	1	1	1													lissencephaly + agenesis of corpus callosum	KIF14, p.[1189Argfs*9];[(1189Argfs*9)]			CRLF1, p.[Lys285Glu];[=]
K74	M	fetus	BKA							1													HOXB1, p.[Ala294Val];[=]
K75	F		RH+	1	1	1																	
K76	M		RD		1	1													hypertelorism				
K77	F		RH	1														1					MDM4, p.[Ala398Thr];[=]
K78	NA	fetus	BKA							1								1	external ear anomaly	EYA1, c.[967-1G>C]:[=],			SOX4, p.[Ser136Ala];[=]
K79	F		RD		1	1													papillary coloboma	PAX2, c.[26-?_503+?del];[=]			
K80	F		UKA+		1	1			1									1 (BO)	preauricular pit + ear tag	EYA1, c.[557-?_1597+?del];[=]			GBX2, p.[Arg51Gly];[=]
K81	F	fetus	BKA							1													AMOTL1, p.[Glu507Lys];[=]
K82	M	fetus	BKA							1								1	1				HOXC11, p.[Pro62Arg];[=] SULF2, p.[Arg656Leu];[=]
K83	M		BMD					1											1			RET, p.[Ser688Phe];[=]		
K84	F	fetus	UKA+	1					1														AMOT, p.[Arg534Lys];[=]
K85	M		UKA						1									1	abnormal teeth				
K86	M		UMD+				1				1								morning glory syndrome + intellectual disability				DCHS1, p.[Val290Leu];[=]
K87	NA	fetus	BKA							1									1				HOXB5, p.[Arg181Trp];[=] HCN3, p.[Arg685Trp];[=]
K88	F	fetus	BKA							1								1					
K89	F		RH	1															1				
K90	F	fetus	RH+	1	1	1																	
K91	M		UKA						1									1			RET, p.[Arg635Cys];[=]		
K92	M	fetus	BKA							1													RCSD1, p.[Arg167Lys];[=]
K93	F		RH+	1	1														intellectual disability				LAMA5, p.[Leu1930Pro];[=] NTN1, p.[605Trpext*84];[=]
K94	M	fetus	UKA+				1		1										didelphys uterus		BICC1, p.[Thr755Arg];[=]		
K95	F	fetus	BKA							1													MET, p.[Ala119Val];[=]
K96	F		Oth											1				1	persistent left vena cava				HPSE, p.[Met1?];[=]
K97	F		Oth								1								optic atrophia + hyperlaxity				
K98	M	fetus	BKA							1								1	1				
K99	F	fetus	RH	1																			
K100	M		RD		1																		BMPR1A, p.[Phe397Ser];[=]
K101	F		UKA						1									1 (deafness)	ear tag + external ear canal stenosis	GATA3, c.[(?_-30)_(*220_?)del];[=]			
K102	M		RD		1	1																	MMP9, p.[Arg267Glyfs*71];[=]
K103	M		RD+		1										1			1		HNF1B, c.[(?_-30)_(*220_?)del];[=]			
K104	F		RH+	1	1	1																	
K105	M		RH+	1	1						1										TBC1D1, p.[Arg718Cys];[=]		
K106	M		RH+	1	1	1																	FAT4, p.[Ala2178Val];[=] FOXC1, p.[Ser339Phe];[=]

K107	F		RH	1															preauricular pits				ZEB2, p.[Thr350Met];[=] MYOCD, p.[Lys241Arg(;)Ser435Phe] GPR173, p.[Val143Ala];[=]
K108	M		RD		1	1											1							
K109	M		RH+	1	1	1								1										
K110	M		RD		1	1											1							
K111	F	fetus	BKA							1														
K112	M		RH+	1	1	1																		
K113	F		Oth								1						1		preauricular pits + deafness				GRHL2, p.[Lys419Glu];[=] PTGIR, p.[Pro17Argfs*6];[=]
K114	M		Oth									1							preauricular pits + cryptorchidy				AMOTL1, p.[Pro420Ser];[=]
K115	M		UMD				1												retina and iris coloboma					
K116	F	fetus	RH	1															intrauterine growth retardation + aortic anomaly				SCRIB, p.[Ser118Pro];[=]
K117	M	fetus	RH	1																PAX2, p.[Ser61Arg];[=]			CRLF1, p.[Trp144*];[=]
K118	F		RD		1	1																		
K119	F		RH	1													1 (BO)		branchial defect + deafness	EYA1, p.[Ser487Pro];[=]			LGR4, p.[Phe864*];[=] FAT1, p.[Glu1920Ala];[=] GAS1, p.[Ala216Glyfs*52];[=]
K120	M		RD		1														preauricular pit + deafness + growth retardation				NPNT, p.[Arg484Cys];[=]
K121	M	fetus	BKA							1									anus atresia + 13th pair of ribs					
K122	M	fetus	RD		1	1																		
K123	M		RH+	1	1														deafness					
K124	M		RD+		1	1								1						HNF1B, c.[(?_-30)_(*220_?)del];[=]			SCRIB, p.[Ala1516Val];[=]
K125	M		Oth												1			1					MATN4, p.[Ser44Asn];[=]
K126	NA	fetus	BKA							1													FAT4, p.[Glu3862Gln];[=] HOXD13, p.[Glu81*];[=]
K127	M		UKA+				1		1								1				BICC1, p.[Cys351Tyr];[=] DSTYK, p.[Asp892Asn];[=]	SOX17, p.[Tyr259Asn];[=]	
K128	F		UKA						1										bicornuate uterus					
K129	F		RD		1	1													diabetes				EGFR, p.[Gly573Arg];[=] FOXC2, p.[Pro204Ser];[=] HOXA11, p.[Met294Thr];[=]
K130	F	fetus	BMD					1									1							
K131	M		RD+		1	1									1		1						FZD7, p.[Pro217Leu];[=]
K132	F		UKA+		1	1			1										mullerian duplication				MMP9, p.[Ser335*];[=]
K133	F		RH+	1	1						1						1 (coloboma)		papillary coloboma	PAX2, p.[Val26Cysfs*3];[=]				
K134	F	fetus	BKA							1									cardiomyopathy + didelphys uterus					
K135	M		UKA						1								1 (BO)		preauricular pit	EYA1, p.[Gln185*];[=]			FZD4, p.[Leu443Met];[=]
K136	M		UKA+		1				1								1		dysmorphic features + intellectual disability + microcephaly	**PBX1, c.[(?_-30)_(*220_?)del];[=]**				
K137	M		RD+		1											1			papillary excavation				TFCP2L1, p.[Cys52Phe];[=]
K138	M		UKA+						1		1						1						SPOCK2, p.[Leu207Arg];[=]
K139	M		UKA						1								1							
K140	F		UMD+	1	1		1												dysmorphic features + intellectual disability					
K141	M		UMD+				1					1					1							
K142	M		RH+	1	1																			
K143	M		RD+		1										1					HNF1B, c.[(?_-30)_(*220_?)del];[=]				
K144	F	fetus	BMD					1											pulmonary cystic adenomatoid malformation				LAMA5, p.[Gly3067Alafs*40];[=] LAMC1, c.[3850-1G>A];[=] IRX2, p.[Leu398Ser];[=]
K145	M		RH	1													1		branchial defect	EYA1, p.[Asn446_Tyr448del];[=]			FZD8, p.[Pro105Arg];[=] ZNF106, p.[Phe1857Leu];[=] WNT6, p.[Glu221Asp];[=]
K146	F		RH+	1	1	1														PAX2, p.[Pro149Glnfs*10];[=]				
K147	F	fetus	UKA+				1		1															
K148	F	fetus	RH	1																PAX2, p.[Val26Glyfs*28];[=]				
K149	M		Oth									1											FAT4, p.[Arg1804Gly];[=]
K150	F		UKA						1										branchial defect					
K151	M		RH+	1	1	1																		
K152	M		UMD				1												preauicular pit				FAT3, p.[Thr3272Ser];[=]
K153	F		UKA+						1					1										
K154	M	fetus	BKA							1														
K155	F		UKA						1								1							
K156	M		RD+		1	1					1												TJP2, p.[Pro826Gln];[=]

K157	F		UKA						1											deafness				
K158	M	fetus	BKA							1								1			ANOS1, c.[?-30_255+?del]				
K159	M		UKA+		1	1			1																DCHS1, p.[Gln1714*];[=]
K160	F		UKA						1											deafness + branchial defect + colobomatous microphtalmia	CHD7, p.[Gly1684Ser];[=]	CDC5L, p.[Leu747Trp];[=]		
K161	F		RH	1																					MMP9, p.[Gly605Alafs*9];[=]
K162	F		RH+	1							1							1	1	palate cleft + preauticular pit		CDC5L, p.[Thr84Ser];[=]		FGFR1, p.[Arg91Trp];[=]
K163	M	fetus	BKA							1									1	interventricular communication				
K164	M	fetus	UMD+		1	1	1																		
K165	F	fetus	UKA+	1					1																
K166	F		Oth														1			deafness + preauricular pit				
K167	M		UKA						1											deafness + intellectual disability	GATA3, c.[(?_-30)_(*220_?)del];[=]			HIC1, p.[Gly386Arg];[=]
K168	M	fetus	BKA							1										intrauterine growth retardation				
K169	M	fetus	UKA+				1		1													TNXB, p.[Pro188Leu];[=]		
K170	M		RH+	1	1	1															HNF1B, c.[344+2_+5del];[=]			
K171	M		RD		1	1												1						
K172	M	fetus	UMD+		1	1	1											1 (diabetes)		diabetes + cryptorchidy	HNF1B, c.[(?_-30)_(*220_?)del];[=]			
K173	M		RH+	1	1	1												1	1	hypomagnesemia				FGF8, p.[Thr121Ser];[=] SLC6A18, p.[Thr221Ser];[=] FAT3, p.[Leu577Val];[=]
K174	NA	fetus	BKA							1														FRY, p.[Thr2366Ile];[=]
K175	F		RH	1																deafness + scoliosis	**PBX1, p.[Asn143Thrfs*37];[=]**			HOXD11, p.[Gly87Arg];[=]
K176	M		RH+	1	1	1												1			PAX2, p.[Ala111Thr];[=]			SCRIB, p.[Leu396Phe];[=]
K177	F		Oth												1					preauricular pit				ROBO1, p.[Ala1414Asp];[=] HS6ST1, p.[Lys84Asn];[=]
K178	F		RH+	1									1											
K179	F		RH+	1	1	1														dysmorphic features + intellectual disability	**PBX1, p.[Arg184*];[=]**			
K180	M		RH	1														1						NR2F2, p.[Gly44Ser];[=] WNT11, p.[Glu345Ala];[=] MECOM, p.[Ala311Val];[=]
K181	F		RH+	1	1												1			deafness	**PBX1, c.[(?_-30)_(*220_?)del];[=]**			
K182	F		RD		1	1												1		interauricular communication + osophageal atresia				SEMA3A, p.[Thr134Met];[=]
K183	M	fetus	UKA+				1		1								1							FAT1, p.[His2123Tyr];[=] GLI1, p.[Arg323Gln];[=]
K184	M		RH+	1	1						1									ear tag				ADCY8, p.[Ile868Ser];[=]
K185	F		RD		1																HNF1B, c.[(?_-30)_(*220_?)del];[=]			CITED1, p.[Gln6*];[=]
K186	M	fetus	RH	1																	**PBX1, c.[511-2A>G];[=],**			
K187	M	fetus	BKA							1								1	1					
K188	M		RD		1	1												1	1					FAT3, p.[Val1242Leu];[=]
K189	F		RD		1													1						ZNF106, p.[Ser482Phefs*17];[=]
K190	F		RH+	1	1	1												1 (deafness)				NOTCH2, p.[Ala1968Val];[Arg285His]		GRHL2, p.[Gly386Arg];[=] PAXIP1, p.[His358Gln];[=] DEAF1, p.[Glu232Glyfs*10];[=]
K191	F		RH+	1	1	1																		GBX2, p.[Pro62Leu];[=]
K192	F	fetus	BKA							1												TBX18, p.[Ile258Val];[=]		
K193	M		RH	1																				
K194	M		RH	1																				
K195	F	fetus	BKA							1								1		craniostenosis + microcephaly + agenesis of corpus callosum	KIF14, p.[Gln1304*];[Arg364Cys]			FAT4, p.[Glu4734Gly];[=]
K196	F		UMD				1													diabetes				GLI1, p.[Pro1080Leu];[=] HNF1A, p.[Gly319Ser];[=]
K197	M		UKA						1										1					RAI2, p.[Leu169Pro]
K198	F		UKA						1										1	VACTER syndrome				
K199	M		Oth								1							1		papillary coloboma	PAX2, p.[Arg71Lys];[=]			
K200	M		UMD				1											1						
K201	F	fetus	BKA							1								1						LAMA5, p.[Pro1082Leu];[=]
K202	M		RH+	1										1										
K203	F		RD		1	1												1			HNF1B, c.[(?_-30)_(*220_?)del];[=]			RARG, p.[Pro82Leu];[=]
K204	M		RH+	1	1													1		diabetes				
Cases with branchial signs and/or ear defect without CAKUT phenotype																								
BO1	F																			branchial defect + deafness				
BO2	F																			deafness				WNT11, p.[Cys59Alafs*19];[=]
BO3	F																			ear tag + ear tag + intellectual diability + thumb hypoplasia		WNT4, p.[Arg83Gln];[=]		PAXIP1, p.[Gln404_Ala407del];[=]

BO4	F																	branchial defect + preauricular pit + deafness	EYA1, p.[Arg361*];[=]			
BO5	M																	branchial defect + deafness	SIX1, p.[Tyr92Leufs*62];[=]			SCRIB, p.[Arg1641Cys];[=] FAT1, p.[His1190Tyr];[=]
BO6	M																	ear tag + deafness				
BO7	M																	preauricular pit + deafness		TNXB, p.[Pro2490Arg];[=]		
BO8	M																	external ear hypoplasia				
BO9	F																	branchial defect				
BO10	F																	external ear defect + preauricular pit + ear tag				
BO11	M																	deafness			DSTYK, c.[654+1G>A];[=]	

(a) Renal Hypoplasia
(b) Renal Dysplasia
(c) Unilateral Multicystic Dysplasia
(d) Bilateral Multicystic Dysplasia
(e) Unilateral Kidney Agenesis
(f) Bilateral Kidney Agenesis
(g) Vesico-Ureteral Reflux
(h) Obstructive Megaureter
(i) Duplex kidney
(j) Pelvi-ureteric junction Obstruction
(k) Parents, children and/or siblings
(l) Grand parents, uncles, aunts, cousins
(m) *PBX1* mutations are in the "Causative mutations" column

Table S2.List of genes for targeted exome sequencing

gene	Name	Phenotype/Syndrome	OMIM#	MGI#	References
a- Human mutations in CAKUT +/- syndrome					
ACE	angiotensin I converting enzyme (peptidyl-dipeptidase A) 1	Renal tubular dysgenesis	106180		1
ACTA2	actin, alpha 2, smooth muscle, aorta	Prune Belly			2
ACTG2	actin, gamma 2, smooth muscle, enteric	Megacystis Microcolon Intestinal Hypoperistalsis	155310		3
AGT	angiotensinogen (serpin peptidase inhibitor, clade A, member 8)	Renal tubular dysgenesis	106165		1
AGTR1	angiotensin II receptor, type 1a	Renal tubular dysgenesis	106180		1
ANOS1	Anosmin	Kallmann	308700		4
BICC1	BicC family RNA binding protein 1	Cystic renal dysplasia	601331		5
BMP4	bone morphogenetic protein 4	Isolated CAKUT			6
CDC5L	cell division cycle 5-like (S. pombe)	Isolated CAKUT			7
CHD1L	chromodomain helicase DNA binding protein 1-like	Isolated CAKUT			8
CHD7	chromodomain helicase DNA binding protein 7	Charge/Kallmann	214880/612370		9
CHRM3	cholinergic receptor, muscarinic 3, cardiac	Prune belly like	100100		10
DACH1	dachshund 1 (Drosophila)	Cystic renal dysplasia			11
DHCR7	7-dehydrocholesterol reductase	Smith-Lemli-Opitz	270400		12
DSTYK	dual serine/threonine and tyrosine protein kinase	Isolated CAKUT	610805		13
ESRRG	estrogen-related receptor gamma	Kidney agenesis			14
EYA1	EYA transcriptional coactivator and phosphatase 1	Branchio oto renal	113650		15
FAM58A	family with sequence similarity 58, member B	Toe syndactyly, telecanthus, anogenital and renal malformations	300707		16
FGF20	fibroblast growth factor 20	Kidney agenesis	615721		17
FRAS1	Fraser extracellular matrix complex subunit 1	Fraser/isolated CAKUT	219000		18
FREM1	Fras1 related extracellular matrix protein 1	Bifid nose, renal agenesis & anorectal malformations syndrome/isolated CAKUT	608980		19
FREM2	Fras1 related extracellular matrix protein 2	Fraser/isolated CAKUT	219000		18
GATA3	GATA binding protein 3	Hypoparathyroidism, sensorineural deafness and renal dysplasia	146255		20
GDF6	growth differentiation factor 6	Klippel-Feil	118180		21
GLI3	GLI-Kruppel family member GLI3	Pallister Hall	146510		22
GPC3	glypican 3	Simpson Golabi Behmel	312870		23
GRIP1	glutamate receptor interacting protein 1	Fraser/isolatedCAKUT	219000		24
HNF1B	HNF1 homeobox B	Renal cysts and diabetes	137920		25
HPSE2	heparanase 2	Urofacial	236730		26
ITGA3	integrin alpha 3	nephrotic syndrome	614748		27
ITGA8	integrin alpha 8	Kidney agenesis	191830		28
JAG1	jagged 1	Allagile	118450		29
KIF14	kinesin family member 14	Multicystic renal dysplasia/renal agenesis and microcephaly	616258		30
LRIG2	leucine-rich repeats and immunoglobulin-like domains 2	Urofacial	615112		31
LRP4	low density lipoprotein receptor-related protein 4	Cenani-Lenz	212780		32
NEK8	NIMA (never in mitosis gene a)-related expressed kinase 8	Renal cystic dysplasia, situs inversus, cardiopathy, bile duct paucity	615415		33
NOTCH2	notch 2	Allagille/Hadju Cheney	610205		34
PAX2	paired box 2	Renal coloboma	120330		35
REN	renin 1 structural	Renal tubular dysgenesis	179820		36
RET	ret proto-oncogene	Kidney agenesis, Hirschsprung	142623		37
ROBO2	roundabout guidance receptor 2	Vesico ureteral reflux	610878		38
SALL1	sal-like 1 (Drosophila)	Townes Brocks	107480		39
SALL4	sal-like 4 (Drosophila)	Duane-radial ray	607323		40
SIX1	sine oculis-related homeobox 1	Branchio oto renal	608389		41
SIX2	sine oculis-related homeobox 2	Isolated CAKUT			6
SIX5	sine oculis-related homeobox 5	Branchio oto renal	610896		42
SLIT2	slit homolog 2 (Drosophila)	Vesico ureteral reflux			38
SOX17	SRY (sex determining region Y)-box 17	isolated CAKUT	613674		43
TBC1D1	TBC1 domain family, member 1	isolated CAKUT			44
TBX18	T-box18	pelvi-ureteric jonction obstruction	143400		45
TNXB	tenascin XB	Vesico ureteral reflux	615963		46
TRAP1	TNF receptor-associated protein 1	VACTERL/isolated CAKUT			47
UMOD	uromodulin	Hyperuricemia, Medullary cystic kidney disease	162000, 603860		48
UPK3A	uroplakin 3A	Vesico ureteral reflux			49
WNT4	wingless-type MMTV integration site family, member 4	Hypodysplasia			50
b- Mouse models with kidney developmental defects					
AGTR2	angiotensin II receptor, type 2			MGI:87966	51
ALDH1A2	aldehyde dehydrogenase family 1, subfamily A2			MGI:107928	52
AMER1	APC membrane recruitment 1			MGI:1919595	53
AQP2	aquaporin 2			MGI:1096865	54

ATMIN	ATM interactor			MGI:2682328	55
BCL2	B cell leukemia/lymphoma 2			MGI:88138	56
BDKRB2	bradykinin receptor, beta 2			MGI:102845	57
BMP7	bone morphogenetic protein 7			MGI:103302	58
BMPER	BMP-binding endothelial regulator			MGI:1920480	59
CDH6	cadherin 6			MGI:107435	60
CER1	alkaline ceramidase 1				61
CFL1	cofilin 1				62
CRIM1	cysteine rich transmembrane BMP regulator 1 (chordin like)			MGI:1354756	63
CTNNB1	catenin (cadherin associated protein), beta 1			MGI:88276	64
CTNNBIP1	catenin beta interacting protein 1			MGI:1915756	65
CXCR4	chemokine (C-X-C motif) receptor 4			MGI:109563	66
DACT1	dishevelled-binding antagonist of beta-catenin 1			MGI:1891740	67
DCHS1	dachsous 1 (Drosophila)			MGI:2685011	68
DCN	decorin			MGI:94872	69
DLG1	discs, large homolog 1 (Drosophila)			MGI:107231	70
DLL1	delta-like 1 (Drosophila)			MGI:104659	71
DSTN	destrin				62
ECM1	extracellular matrix protein 1				72
EGFR	epidermal growth factor receptor			MGI:95294	73
EMX2	empty spiracles homeobox 2			MGI:95388	74
EPHA4	Eph receptor A4				75
EPHA7	Eph receptor A7				75
ETV4	ets variant 4			MGI:99423	76
ETV5	ets variant 5			MGI:1096867	76
EXOC5	exocyst complex component 5			MGI:2145645	77
FAT1	FAT atypical cadherin 1			MGI:109168	78
FAT4	FAT atypical cadherin 4			MGI:3045256	79
FGF10	fibroblast growth factor 10			MGI:1099809	80
FGF7	fibroblast growth factor 7			MGI:95521	81
FGF8	fibroblast growth factor 8			MGI:99604	82
FGF9	fibroblast growth factor 9				17
FGFR1	fibroblast growth factor receptor 1	Kallmann	147950		83
FGFR2	fibroblast growth factor receptor 2			MGI:95523	83
FGFRL1	fibroblast growth factor receptor-like 1			MGI:2150920	84
FMN1	formin 1			MGI:101815	85
FOXC1	forkhead box C1			MGI:1347466	86
FOXC2	forkhead box C2			MGI:1347481	86
FOXD1	forkhead box D1			MGI:1347463	87
FSTL1	follistatin-like 1			MGI:102793	88
GATA2	GATA binding protein 2			MGI:95662	89
GDF11	growth differentiation factor 11			MGI:1338027	90
GDNF	glial cell line derived neurotrophic factor			MGI:107430	91
GFRA1	glial cell line derived neurotrophic factor family receptor alpha 1			MGI:1100842	92
GLCE	glucuronyl C5-epimerase			MGI:2136405	93
GREM1	gremlin 1, DAN family BMP antagonist			MGI:1344337	94
GRHL2	grainyhead-like 2 (Drosophila)				95
HOXA11	homeobox A10				96
HOXD11	homeobox D11				96
HS2ST1	heparan sulfate 2-O-sulfotransferase 1			MGI:1346049	97
ILK	integrin linked kinase			MGI:1195267	98
ISL1	ISL1 transcription factor, LIM/homeodomain				99
ITGB1	integrin beta 1 (fibronectin receptor beta)			MGI:96610	100
KIF26B	kinesin family member 26B			MGI:2447076	101
KIF3A	kinesin family member 3A			MGI:107689	102
KISS1R	KISS1 receptor			MGI:2148793	103
LAMA5	laminin, alpha 5			MGI:105382	104
LAMC1	laminin, gamma 1			MGI:99914	105
LGR4	leucine-rich repeat-containing G protein-coupled receptor 4			MGI:1891468	106
LHX1	LIM homeobox protein 1			MGI:99783	107
LZTS2	leucine zipper, putative tumor suppressor 2			MGI:2385095	108
MMP9	matrix metallopeptidase 9				109
MYCN	v-myc avian myelocytomatosis viral related oncogene, neuroblastoma derived			MGI:97357	110
NFIA	nuclear factor I/A			MGI:108056	111
NPNT	nephronectin			MGI:2148811	112
NR2F2	nuclear receptor subfamily 2, group F, member 2				113
OSR1	odd-skipped related 1 (Drosophila)			MGI:1344424	114
PARVA	parvin, alpha			MGI:1931144	115
PAX8	paired box 8				116
PBX1	pre B cell leukemia homeobox 1			MGI:97495	117
POU3F3	POU domain, class 3, transcription factor 3			MGI:102564	118
PPP3R1	protein phosphatase 3, regulatory subunit B, alpha isoform (calcineurin B, type I)			MGI:107172	119
PTCH1	patched 1			MGI:105373	120
PTGS2	prostaglandin-endoperoxide synthase 2			MGI:97798	121
RARA	retinoic acid receptor, alpha				122

RARB	retinoic acid receptor, beta				122
RBPJ	recombination signal binding protein for immunoglobulin kappa J region			MGI:96522	123
RERE	arginine glutamic acid dipeptide (RE) repeats			MGI:2683486	124
ROBO1	roundabout guidance receptor 1			MGI:1274781	66
SEMA3A	sema domain, immunoglobulin domain (Ig), short basic domain, secreted, (semaphorin) 3A	Kallmann	614897	MGI:107558	125
SHH	sonic hedgehog			MGI:98297	126
SMAD4	SMAD family member 4			MGI:894293	127
SOX11	SRY (sex determining region Y)-box 11				128
SOX12	SRY (sex determining region Y)-box 12				129
SOX4	SRY (sex determining region Y)-box 4				129
SOX8	SRY (sex determining region Y)-box 8				130
SOX9	SRY (sex determining region Y)-box 9			MGI:98371	130
SPRY1	sprouty homolog 1 (Drosophila)			MGI:1345139	131
TCF21	transcription factor 21			MGI:1202715	132
TFCP2L1	transcription factor CP2-like 1			MGI:2444691	133
TGFB2	transforming growth factor, beta 2			MGI:98726	134
TGFBR3	transforming growth factor, beta receptor III				135
TRPS1	trichorhinophalangeal syndrome I (human)			MGI:1927616	136
TSHZ3	teashirt zinc finger family member 3			MGI:2442819	137
WNT11	wingless-type MMTV integration site family, member 11			MGI:101948	138
WNT5A	wingless-type MMTV integration site family, member 5A			MGI:98958	66
WNT7B	wingless-type MMTV integration site family, member 7B			MGI:98962	139
WNT9B	wingless-type MMTV integration site family, member 9B			MGI:1197020	140
WT1	Wilms tumor 1 homolog	Denys Drash syndrome	194080/256370		141
YAP1	yes-associated protein 1			MGI:103262	142

c- Relevant functional data (cellular and/or non-mouse models)

ALCAM	activated leukocyte cell adhesion molecule	143
ALX1	ALX homeobox 1	144
AMOT	angiomotin	145
AMOTL1	angiomotin-like 1	145
AMOTL2	angiomotin-like 2	145
ATF2	glial cell line derived neurotrophic factor	143
BCL2L11	BCL2-like 11 (apoptosis facilitator)	146
CD151	CD151 antigen	147
CDKN1C	cyclin-dependent kinase inhibitor 1C (P57)	148
CITED1	Cbp/p300-interacting transactivator with Glu/Asp-rich carboxy-terminal domain 1	149
CRLF1	cytokine receptor-like factor 1	150
DCHS2	dachsous 2 (Drosophila)	151
DKK1	dickkopf WNT signaling pathway inhibitor 1	64
ELF5	E74-like factor 5	152
ESRP1	epithelial splicing regulatory protein 1	unpublished
ESRP2	epithelial splicing regulatory protein 2	unpublished
FJX1	four jointed box 1 (Drosophila)	79
FRS2	fibroblast growth factor receptor substrate 2	153
FRY	FRY microtubule binding protein	unpublished
FZD3	frizzled class receptor 9	143
FZD4	frizzled class receptor 4	154
FZD7	frizzled class receptor 7	155
FZD8	frizzled class receptor 8	154
GLI1	GLI-Kruppel family member GLI1	156
GNB3	guanine nucleotide binding protein (G protein), beta 3	49
GPC1	glypican 1	157
HAS3	hyaluronan synthase 3	158
HCN3	hyperpolarization-activated, cyclic nucleotide-gated K+ 3	159
HGF	interleukin 6	160
HOXB5	homeobox B5	161
HOXB6	homeobox B6	161
HOXC11	homeobox C11	96
HOXD10	homeobox D10	162
HOXD3	homeobox D3	161
HOXD8	homeobox D8	161
HOXD9	homeobox D9	161
IRX3	Iroquois related homeobox 3	163
KDR	kinase insert domain protein receptor	164
KEAP1	kelch-like ECH-associated protein 1	unpublished
KIT	kit oncogene	165
LATS1	large tumor suppressor	166
LLGL1	lethal giant larvae homolog 1 (Drosophila)	167
MAGED1	melanoma antigen, family D, 1	168
MDM2	transformed mouse 3T3 cell double minute 2	169
MDM4	transformed mouse 3T3 cell double minute 4	unpublished
MECOM	MDS1 and EVI1 complex locus	170
MEOX2	mesenchyme homeobox 2	171

MET	met proto-oncogene				172
MMP13	matrix metallopeptidase 13				173
NCAM1	neural cell adhesion molecule 1				174
NF2	neurofibromatosis 2				175
NKX2-1	NK2 homeobox 1				176
NR2F1	nuclear receptor subfamily 2, group F, member 2				177
NR4A2	nuclear receptor subfamily 4, group A, member 2				178
OSR2	odd-skipped related 2				179
PAXIP1	PAX interacting (with transcription-activation domain) protein 1				180
Pik3c3	phosphoinositide-3-kinase, class 3				unpublished
PLAC8	placenta-specific 8				181
PPM1B	protein phosphatase 1B, magnesium dependent, beta isoform				182
PRKX	protein kinase, X-linked				183
PTPN11	protein tyrosine phosphatase, non-receptor type 11				184
RARG	retinoic acid receptor, gamma				122
RSPO3	R-spondin 3				185
RXRA	retinoid X receptor alpha				177
SCRIB	scribbled planar cell polarity				186
SH2B1	SH2B adaptor protein 1				187
SHOX2	short stature homeobox 2				188
SIM1	single-minded homolog 1 (Drosophila)				189
SMO	smoothened, frizzled class receptor				190
SNAI1	snail family zinc finger 1				191
SOST	sclerostin				192
SPRY2	sprouty homolog 2 (Drosophila)				193
SULF1	sulfatase 1				194
SULF2	sulfatase 2				194
TAZ	WW domain containing transcription regulator 1				178
TBX1	T-box 1				162
TBX3	T-box 3	Ulnar mammary	181450		195
TIMP1	tissue inhibitor of metalloproteinase 1				173
TJP2	tight junction protein 2				196
USF2	upstream transcription factor 2				14
VEGFA	vascular endothelial growth factor A				197
VSNL1	visinin-like 1				198
WNT5B	wingless-type MMTV integration site family, member 5B				199
ZEB2	zinc finger E-box binding homeobox 2				200

d- Role in ureter/bladder development

ADAMTS1	a disintegrin-like and metallopeptidase (reprolysin type) with thrombospondin type 1 motif, 1			MGI:109249	201
AHR	aryl-hydrocarbon receptor			MGI:105043	202
BMP5	bone morphogenetic protein 5			MGI:88181	202
BMPR1A	bone morphogenetic protein receptor, type 1A				202
BMPR1B	bone morphogenetic protein receptor, type 1B				202
BMPR2	bone morphogenetic protein receptor, type II (serine/threonine kinase)			MGI:1095407	202
HOXD13	homeobox D13				202
ID2	inhibitor of DNA binding 2			MGI:96397	202
KLF5	Kruppel-like factor 5				203
MYOCD	myocardin				202
SCARB2	scavenger receptor class B, member 2			MGI:1196458	202

e- Potential targets of WT1 or HNF1B

ACTN3	actinin alpha 3				204
ADCY8	adenylate cyclase 8				204
Aip	aryl-hydrocarbon receptor-interacting protein				204
ASIC4	acid-sensing (proton-gated) ion channel family member 4				204
C1QTNF3	C1q and tumor necrosis factor related protein 3				204
CALCR	calcitonin receptor				204
CEBPA	CCAAT/enhancer binding protein (C/EBP), alpha				204
CHST9	carbohydrate (N-acetylgalactosamine 4-0) sulfotransferase 9				204
CRYM	crystallin, mu				204
DEAF1	asparagine-linked glycosylation 10B (alpha-1,2-glucosyltransferase)				204
DES	desmin				204
DUSP6	dual specificity phosphatase 6				204
EGR1	early growth response 1				204
ENC1	ectodermal-neural cortex 1				204
FGF14	fibroblast growth factor 14				204
FGF16	fibroblast growth factor 16				204
FGF18	fibroblast growth factor 18				204
FST	follistatin				204
GAS1	growth arrest specific 1				205
GBX2	gastrulation brain homeobox 2				204
GPR173	G-protein coupled receptor 173				204
GPX6	glutathione peroxidase 7				204

HIC1	hypermethylated in cancer 1	204
HOXA3	homeobox A3	204
HOXB1	homeobox B1	204
HOXB3	homeobox B3	204
HS3ST6	heparan sulfate (glucosamine) 3-O-sulfotransferase 6	204
IRX1	Iroquois related homeobox 1 (Drosophila)	206
IRX2	Iroquois related homeobox 2 (Drosophila)	206
KRT23	keratin 23	204
LRFN2	leucine rich repeat and fibronectin type III domain containing 2	204
MATN4	matrilin 2	204
Mybph	myosin binding protein H	204
NRXN3	neurexin III	204
NTN1	netrin 1	204
PDE3B	phosphodiesterase 3B, cGMP-inhibited	204
PHF19	PHD finger protein 19	204
PPP1R1B	protein phosphatase 1, regulatory (inhibitor) subunit 1B	204
PTGIR	prostaglandin I receptor (IP)	204
RAI2	retinoic acid induced 2	204
RCSD1	RCSD domain containing 1	204
REM1	rad and gem related GTP binding protein 1	204
RORA	RAR-related orphan receptor alpha	204
RSPO1	R-spondin 1	204
SLC16A6	solute carrier family 16 (monocarboxylic acid transporters), member 6	204
SLC6A18	solute carrier family 6 (neurotransmitter transporter), member 18	204
SNAP91	synaptosomal-associated protein 91	204
SPACA4	sperm acrosome associated 4	204
SPOCK2	sparc/osteonectin, cwcv and kazal-like domains proteoglycan 2	204
STMN4	stathmin-like 4	204
SYPL2	synaptophysin-like 2	204
TGM5	transglutaminase 5	204
TNNT2	troponin T2, cardiac	204
TRAF1	TNF receptor-associated factor 1	204
UNCX	UNC homeobox	204
WNT8B	wingless-type MMTV integration site family, member 8B	204
ZNF106	zinc finger protein 106	204

f- gene related to gene(s) in group (a) to (e), expressed during kidney/LUT development

ALDH1A3	aldehyde dehydrogenase family 1, subfamily A3
BMP2	bone morphogenetic protein 2
BMP6	bone morphogenetic protein 6
FAT3	FAT atypical cadherin 3
FGF1	fibroblast growth factor 1
FGF2	fibroblast growth factor 13
GRIP2	glutamate receptor interacting protein 2
HNF1A	HNF1 homeobox A
HNF4A	hepatic nuclear factor 4, alpha
HPSE	heparanase
HS6ST1	heparan sulfate 6-O-sulfotransferase 1
SIX4	sine oculis-related homeobox 4
TBX2	T-box 2
UPK1A	uroplakin 1A
UPK1B	uroplakin 1B
UPK2	uroplakin 2
UPK3B	uroplakin 3B
WNT2B	wingless-type MMTV integration site family, member 2B
WNT6	wingless-type MMTV integration site family, member 6

Table S3. List of the 120 variants of unknown significance identified in candidate genes in CAKUT cases, that are absent in ExAC and our in-house database

Gene	Ref seq	Nucleotide change	Protein change	Number of damaging scores for missense variants [a]
ADCY8	NM_001115	c.2603T>G	p.Ile868Ser	4/5
AMOT	NM_001113490	c.1601G>A	p.Arg534Lys	3/5
AMOTL1	NM_130847	c.1519G>A	p.Glu507Lys	5/5
AMOTL1	NM_130847	c.1258C>T	p.Pro420Ser	3/5
BMPR1A	NM_004329	c.1189C>T	p.Phe397Ser	5/5
CDKN1C	NM_000076	c.17T>C	p.Leu6Pro	3/5
CITED1	NM_001144885	c.16C>T	p.Gln6*	
CRIM1	NM_016441	c.1901G>A	p.Gly634Glu	5/5
CRLF1	NM_004750	c.853A>G	p.Lys285Glu	3/5
CRLF1	NM_004750	c.431G>A	p.Trp144*	
DACT1	NM_016651	c.169G>A	p.Glu57Lys	5/5
DCHS1	NM_003737	c.6647C>T	p.Ala2216Val	3/5
DCHS1	NM_003737	c.5140C>T	p.Gln1714*	
DCHS1	NM_003737	c.2789C>G	p.Thr930Ser	4/5
DCHS1	NM_003737	c.868G>T,	p.Val290Leu	4/5
DEAF1	NM_021008	c.694dup	p.Glu232Glyfs*10	
ECM1	NM_004425	c.527A>T	p.Asn176Ile	4/5
EGFR	NM_005228	c.1717G>A	p.Gly573Arg	5/5
ENC1	NM_003633	c.658T>C	p.Tyr220His	4/5
ETV4	NM_001986	c.626A>G	p.Tyr209Cys	5/5
FAT1	NM_005245	c.5759A>C	p.Glu1920Ala	4/5
FAT1	NM_005245	c.6367C>T	p.His2123Tyr	5/5
FAT3	NM_001008781	c.1729C>G	p.Leu577Val	3/5
FAT3	NM_001008781	c.9814A>T	p.Thr3272Ser	3/5
FAT3	NM_001008781	c.3724G>C	p.Val1242Leu	3/5
FAT4	NM_001291303	c.6533C>T	p.Ala2178Val	4/4
FAT4	NM_001291303	c.5410A>G	p.Arg1804Gly	4/4
FAT4	NM_001291303	c.11584G>C	p.Glu3862Gln	4/4
FAT4	NM_001291303	c.14201A>G	p.Glu4734Gly	4/5
FGF8	NM_033163	c.362C>G	p.Thr121Ser	3/5
FGFR1	NM_001174067	c.271C>T	p.Arg91Trp	4/5
FOXC1	NM_001453	c.1016C>T	p.Ser339Phe	3/5
FOXC2	NM_005251	c.610C>T	p.Pro204Ser	3/5
FRY	NM_023037	c.4928C>T	p.Ala1643Val	3/5
FRY	NM_023037	c.7097C>T	p.Thr2366Ile	4/5
FZD4	NM_012193	c.1327C>A	p.Leu443Met	3/5
FZD7	NM_003507	c.650C>T	p.Pro217Leu	4/5
FZD8	NM_031866	c.314C>G	p.Pro105Arg	3/5
GAS1	NM_002048	c.644dup	p.Ala216Glyfs*52	
GBX2	NM_001485	c.151C>G	p.Arg51Gly	4/5
GBX2	NM_001485	c.185C>T	p.Pro62Leu	3/5
GLI1	NM_005269	c.968G>A	p.Arg323Gln	4/5
GLI1	NM_005269	c.3239C>T	p.Pro1080Leu	4/5

GNB3	NM_002075	c.827T>G	p.Val276Gly	4/5
GPR173	NM_018969	c.428T>C	p.Val143Ala	4/5
GREM1	NM_013372	c.24-25insTGTA	p.Gly9Cysfs*16	
GRHL2	NM_024915	c.1156G>A	p.Gly386Arg	5/5
GRHL2	NM_024915	c.1255A>G	p.Lys419Glu	5/5
HCN3	NM_020897	c.2053C>T	p.Arg685Trp	4/5
HIC1	NM_006497	c.1099G>C	p.Gly386Arg	3/5
HIC1	NM_006497	c.2105G>A	p.Gly702Asp	4/5
HIC1	NM_006497	c.688C>T	p.Pro230Ser	3/5
HNF1A	NM_001306179	c.955G>A	p.Gly319Ser	3/4
HOXA11	NM_005523	c.881T>C	p.Met294Thr	3/5
HOXB1	NM_002144	c.881C>T	p.Ala294Val	4/5
HOXB5	NM_002147	c.542G>C	p.Arg181Trp	5/5
HOXC11	NM_014212	c.185C>G	p.Pro62Arg	4/5
HOXD11	NM_021192	c.259G>C	p.Gly87Arg	3/5
HOXD13	NM_000523	c.241G>T	p.Glu81*	
HPSE	NM_006665	c.2T>C	p.Met1?	
HS6ST1	NM_004807	c.252G>T	p.Lys84Asn	3/5
IRX2	NM_033267	c.1193T>C	p.Leu398Ser	3/5
KIF26B	NM_018012	c.5788C>G	p.Arg1930Gly	4/5
KIF3A	NM_007054	c.1135G>A	p.Glu379Lys	3/5
KISS1R	NM_032551	c.403G>T	p.Ala135Ser	5/5
LAMA5	NM_005560	c.9200del	p.Gly3067Alafs*40	
LAMA5	NM_005560	c.5789T>C	p.Leu1930Pro	3/5
LAMA5	NM_005560	c.3245C>T	p.Pro1082Leu	4/5
LAMC1	NM_002293	c.1427+1G>C	c.1427+1G>C	
LAMC1	NM_002293	c.3850-1G>A	c.3850-1G>A	
LGR4	NM_018490	c.2590_2591insAA	p.Phe864*	
LHX1	NM_005568	c.688A>C	p.Asn230His	4/4
LHX1	NM_005568	c.269C>T	p.Thr90Ile	4/4
MAGED1	NM_001005333	c.2213C>T	p.Ala738Val	4/5
MATN4	NM_003833	c.131G>A	p.Ser44Asn	3/5
MDM4	NM_002393	c.1192G>A	p.Ala398Thr	3/5
MECOM	NM_001105077	c.932C>T	p.Ala311Val	3/5
MET	NM_001127500	c.356C>T	p.Ala119Val	5/5
MMP9	NM_004994	c.798delC	p.Arg267Glyfs*71	
MMP9	NM_004994	c.964C>T	p.Arg322Trp	3/5
MMP9	NM_004994	c.1814del	p.Gly605Alafs*9	
MMP9	NM_004994	c.1004C>A	p.Ser335*	
MYOCD	NM_001146312	c.722A>G	p.Lys241Arg	3/5
MYOCD	NM_001146312	c.1304C>T	p.Ser435Phe	4/5
NPNT	NM_001184690	c.1450C>T	p.Arg484Cys	4/5
NR2F2	NM_021005	c.130G>A	p.Gly44Ser	3/5
NTN1	NM_004822	c.1814A>G	p.605Trpext*84	
PAXIP1	NM_007349	c.1074T>G	p.His358Gln	3/5
PDE3B	NM_000922	c.275_194del	p.Leu92Argfs*241	
PIK3C3	NM_002647	c.1790C>A	p.Phe597His	4/4
PTGIR	NM_000960	c.48del	p.Pro17Argfs*6	
RAI2	NM_001172739	c.506T>C	p.Leu169Pro	4/5

RARG	NM_000966	c.245C>T	p.Pro82Leu	4/5
RCSD1	NM_052862	c.500G>A	p.Arg167Lys	4/5
ROBO1	NM_002941	c.4241C>A	p.Ala1414Asp	3/5
RSPO3	NM_032784	c.481A>C	p.Lys161Gln	3/5
SCRIB	NM_182706	c.4547C>T	p.Ala1516Val	5/5
SCRIB	NM_182706	c.1186C>T	p.Leu396Phe	3/5
SCRIB	NM_182706	c.352T>C	p.Ser118Pro	3/5
SEMA3A	NM_006080	c.401C>T	p.Thr134Met	4/5
SHH	NM_000193	c.1097T>C	p.Val366Ala	3/5
SLC6A18	NM_182632	c.661A>T	p.Thr221Ser	3/5
SOX4	NM_003107	c.1001C>A	p.Phe334His	3/5
SOX4	NM_003107	c.406T>G	p.Ser136Ala	3/5
SPOCK2	NM_014767	c.1114G>T	p.Gly372Trp	4/5
SPOCK2	NM_014767	c.620T>G	p.Leu207Arg	4/5
SPOCK2	NM_014767	c.1192A>G	p.Lys398Glu	4/5
SULF2	NM_018837	c.1967G>T	p.Arg656Leu	4/5
SULF2	NM_018837	c.2297C>T	p.Thr766Ile	5/5
TFCP2L1	NM_014553	c.155G>T	p.Cys52Phe	4/5
TGM5	NM_201631	c.1769C>G	p.Thr590Arg	4/5
TJP2	NM_001170416	c.2477C>A	p.Pro826Gln	3/5
WNT11	NM_004626	c.1034A>C	p.Glu345Ala	3/5
WNT2B	NM_024494	c.407G>T	p.Ser136Ile	5/5
WNT6	NM_006522	c.663G>C	p.Glu221Asp	4/5
WNT6	NM_006522	c.568_586dup	p.Gly196Alafs*123	
WNT9B	NM_003396	c.434G>A	p.Cys145Tyr	5/5
ZEB2	NM_014795	c.1049C>T	p.Thr350Met	3/5
ZNF106	NM_022473	c.5569T>C	p.Phe1857Leu	3/5
ZNF106	NM_022473	c.1444dup	p.Ser482Phefs*17	

(a) according to Polyphen2 (probably and possibly damaging), Sift (deleterious), Mutation Taster (deleterious), Grantham (considered as deleterious when ≥ 50) and GVGD (considered as deleterious when ≥ C25)

Table S4. Analysis of microsatellite markers for validation of *de novo PBX1* deletion in family 4 and paternity and maternity testing in the 5 families

Microsatellite markers	Position (Ensembl GrCh38)	nb alleles	% het	Family 1			Family 2			Family 3			Family 4			Family 5		
				Father	Mother	K175	Father	Mother	K179	Father	Mother	K186	Father	Mother	K181	Mother	K136	
D1S2675	ch1:162240203-162240364	8	72										140	158	140			Those 8 markers are refered to as A-H in Figure 1B
													160	160	158			
D1S2844	ch1:162979036-162979218	9	81										175	173	173			
													177	173	175			
D1S_PBX1_intron1	chr1:164562453-164562494	UK	UK										286	286	288			
													288	286	del			
D1S_PBX1_intron2-1	chr1:164651931-164651970	UK	UK										214	212	214			
													230	226	del			
D1S_PBX1_intron2-2	chr1:164707419-164707456	UK	UK										156	164	156			
													162	166	del			
D1S_PBX1_intron8	chr1:164834030-164834070	UK	UK										330	320	332			
													332	322	del			
D1S2762	ch1:166986900-166987137	8	81										228	240	240			
													242	244	242			
D1S196	ch1:167635063-167635195	5	73										271	269	269			
													273	271	271			
D1S433	ch1: 168398939-168399082	6	59	146	146	148							146	148	146			
				148	150	150							150	150	150			
D1S2643	ch1: 175553723-175553898	9	75	172	178	172	182	174	178	170	170	170	172	172	172	170	170	
				172	178	178	182	178	182	170	170	170	172	178	178	178	172	
D3S1270	ch3:1406588-1406749	9	75	165	165	165	165	165	165	165	165	165	165	163	165	153	153	
				165	173	173	169	169	165	173	165	165	165	165	165	167	167	
D3S2446	ch3: 81919331-81919574	UK	69	238	238	238	238	238	238	234	234	238	238	234	234	238	238	
				246	246	246	246	238	246	238	238	238	242	242	238	238	238	
D3S4554	ch3: 82542137-82542386	UK	65	248	248	248	256	248	248	252	248	248	248	248	248	248	256	
				248	252	252	256	248	256	260	256	252	260	256	256	260	260	
D4S3351	ch4: 158626043-158626231	UK	82	182	198	198	186	176	186	174	182	174	178	178	178	182	182	
				202	198	202	210	202	202	186	190	182	186	178	178	182	182	
D6S1572	ch6: 131016434-131016547	9	84	112	104	104	112	112	112	104	104	104	104	114	114	100	118	
				112	120	112	122	122	122	104	114	104	114	114	114	118	118	
D8S1820	ch8: 28140086-28140196	7	73	98	106	106	104	104	104	98	98	98	98	98	98	106	106	
				106	108	106	104	104	104	106	98	106	108	106	98	106	106	
D13S1268	ch13:66939348-66939481	9	80	122	118	118	118	120	136	120	130	120	118	134	134	120	120	
				136	140	136	136	140	140	120	136	136	140	136	140	142	120	
D14S997	ch14:62233775-62233986	8	76	210	204	204	214	204	212	202	202	202	212	202	202	206	202	
				212	214	210	216	212	216	212	210	212	214	212	214	216	206	
D15S1510	ch15: 80528302-80528551	UK	52	244	248	248	248	248	248	244	248	248	244	248	244	252	248	
				256	248	256	252	248	252	248	248	248	252	248	248	252	252	
D15S211	ch15:80900569-80900799	25	94				226	220	242	220	224	228						
							246	242	246	246	228	246						
D21S1903	ch21:44721130-44721407	14	83	245	255	245	255	249	257	255	245	245	241	245	245	241	241	
				257	261	261	257	257	257	257	257	257	253	245	253	249	259	
D21S1446	ch21: 46617673-46617893	UK	76										206	206	206	206	206	
													210	210	210	206	206	

Table S5. Burden analysis of rare variants in the unsolved CAKUT cases[a] (n=168) versus controls (n=426)					
		Madsen		Skat	
GENE	number of variants	PVALUE	STAT	PVALUE	STATRHO
Variant frequency < 0.1%, LOF + Missense damaging with polyphen 2 and Sift					
DCHS2	6	0.003261	34677	0.0037375	0.2
FZD3	2	0.02437	35358	0.037478	1
GRHL2	2	0.02437	35358	0.037478	1
HOXD13	4	0.037197	35228	0.067466	0.8
ANOS1[b]	3	0.037197	35228	0.042087	1
ECM1	4	0.03771	35229	0.064325	0.7
SULF1	4	0.03771	35229	0.064325	0.7
SPOCK2	4	0.038232	35230	0.065785	0.7
TBC1D1	3	ns	ns	0.037546	1
Variant frequency < 0.01%, LOF + Missense damaging with polyphen 2 and Sift					
ECM1	2	0.02437	35358	0.037478	1
FZD3	2	0.02437	35358	0.037478	1
GNB3	2	0.02437	35358	0.037478	1
GRHL2	2	0.02437	35358	0.037478	1
HOXD13	2	0.024371	35358	0.03938	1
DCHS2	3	0.037884	35230	0.039858	0.2
TBC1D1	3	ns	ns	0.037546	1

(a) cases with no mutation identified in *PBX1* and highly penetrant CAKUT genes *(HNF1B, PAX2, EYA1, ANOS1, GATA3, CHD7 or KIF14)*

(b) heterozygous variants in female cases

ns: non significant

Supplemental references

1. Gribouval, O., Moriniere, V., Pawtowski, A., Arrondel, C., Sallinen, S.L., Saloranta, C., Clericuzio, C., Viot, G., Tantau, J., Blesson, S., et al. (2012). Spectrum of mutations in the renin-angiotensin system genes in autosomal recessive renal tubular dysgenesis. Hum Mutat 33, 316-326.
2. Richer, J., Milewicz, D.M., Gow, R., de Nanassy, J., Maharajh, G., Miller, E., Oppenheimer, L., Weiler, G., and O'Connor, M. (2012). R179H mutation in ACTA2 expanding the phenotype to include prune-belly sequence and skin manifestations. Am J Med Genet A 158A, 664-668.
3. Thorson, W., Diaz-Horta, O., Foster, J., 2nd, Spiliopoulos, M., Quintero, R., Farooq, A., Blanton, S., and Tekin, M. (2014). De novo ACTG2 mutations cause congenital distended bladder, microcolon, and intestinal hypoperistalsis. Hum Genet 133, 737-742.
4. Hardelin, J.P., Levilliers, J., del Castillo, I., Cohen-Salmon, M., Legouis, R., Blanchard, S., Compain, S., Bouloux, P., Kirk, J., Moraine, C., et al. (1992). X chromosome-linked Kallmann syndrome: stop mutations validate the candidate gene. Proc Natl Acad Sci U S A 89, 8190-8194.
5. Kraus, M.R., Clauin, S., Pfister, Y., Di Maio, M., Ulinski, T., Constam, D., Bellanne-Chantelot, C., and Grapin-Botton, A. (2012). Two mutations in human BICC1 resulting in Wnt pathway hyperactivity associated with cystic renal dysplasia. Hum Mutat 33, 86-90.
6. Weber, S., Taylor, J.C., Winyard, P., Baker, K.F., Sullivan-Brown, J., Schild, R., Knuppel, T., Zurowska, A.M., Caldas-Alfonso, A., Litwin, M., et al. (2008). SIX2 and BMP4 mutations associate with anomalous kidney development. J Am Soc Nephrol 19, 891-903.
7. Hwang, D.Y., Dworschak, G.C., Kohl, S., Saisawat, P., Vivante, A., Hilger, A.C., Reutter, H.M., Soliman, N.A., Bogdanovic, R., Kehinde, E.O., et al. (2014). Mutations in 12 known dominant disease-causing genes clarify many congenital anomalies of the kidney and urinary tract. Kidney Int 85, 1429-1433.
8. Brockschmidt, A., Chung, B., Weber, S., Fischer, D.C., Kolatsi-Joannou, M., Christ, L., Heimbach, A., Shtiza, D., Klaus, G., Simonetti, G.D., et al. (2012). CHD1L: a new candidate gene for congenital anomalies of the kidneys and urinary tract (CAKUT). Nephrol Dial Transplant 27, 2355-2364.
9. Lalani, S.R., Safiullah, A.M., Fernbach, S.D., Harutyunyan, K.G., Thaller, C., Peterson, L.E., McPherson, J.D., Gibbs, R.A., White, L.D., Hefner, M., et al. (2006). Spectrum of CHD7 mutations in 110 individuals with CHARGE syndrome and genotype-phenotype correlation. Am J Hum Genet 78, 303-314.
10. Weber, S., Thiele, H., Mir, S., Toliat, M.R., Sozeri, B., Reutter, H., Draaken, M., Ludwig, M., Altmuller, J., Frommolt, P., et al. (2011). Muscarinic Acetylcholine Receptor M3 Mutation Causes Urinary Bladder Disease and a Prune-Belly-like Syndrome. Am J Hum Genet 89, 668-674.
11. Schild, R., Knuppel, T., Konrad, M., Bergmann, C., Trautmann, A., Kemper, M.J., Wu, K., Yaklichkin, S., Wang, J., Pestell, R., et al. (2013). Double homozygous missense mutations in DACH1 and BMP4 in a patient with bilateral cystic renal dysplasia. Nephrol Dial Transplant 28, 227-232.
12. Quelin, C., Loget, P., Verloes, A., Bazin, A., Bessieres, B., Laquerriere, A., Patrier, S., Grigorescu, R., Encha-Razavi, F., Delahaye, S., et al. (2012). Phenotypic spectrum of fetal Smith-Lemli-Opitz syndrome. Eur J Med Genet 55, 81-90.

13. Sanna-Cherchi, S., Sampogna, R.V., Papeta, N., Burgess, K.E., Nees, S.N., Perry, B.J., Choi, M., Bodria, M., Liu, Y., Weng, P.L., et al. (2013). Mutations in DSTYK and dominant urinary tract malformations. N Engl J Med 369, 621-629.
14. Harewood, L., Liu, M., Keeling, J., Howatson, A., Whiteford, M., Branney, P., Evans, M., Fantes, J., and Fitzpatrick, D.R. (2010). Bilateral renal agenesis/hypoplasia/dysplasia (BRAHD): postmortem analysis of 45 cases with breakpoint mapping of two de novo translocations. PLoS One 5, e12375.
15. Abdelhak, S., Kalatzis, V., Heilig, R., Compain, S., Samson, D., Vincent, C., Levi-Acobas, F., Cruaud, C., Le Merrer, M., Mathieu, M., et al. (1997). Clustering of mutations responsible for branchio-oto-renal (BOR) syndrome in the eyes absent homologous region (eyaHR) of EYA1. Hum Mol Genet 6, 2247-2255.
16. Unger, S., Bohm, D., Kaiser, F.J., Kaulfuss, S., Borozdin, W., Buiting, K., Burfeind, P., Bohm, J., Barrionuevo, F., Craig, A., et al. (2008). Mutations in the cyclin family member FAM58A cause an X-linked dominant disorder characterized by syndactyly, telecanthus and anogenital and renal malformations. Nat Genet 40, 287-289.
17. Barak, H., Huh, S.H., Chen, S., Jeanpierre, C., Martinovic, J., Parisot, M., Bole-Feysot, C., Nitschke, P., Salomon, R., Antignac, C., et al. (2012). FGF9 and FGF20 maintain the stemness of nephron progenitors in mice and man. Dev Cell 22, 1191-1207.
18. Saisawat, P., Tasic, V., Vega-Warner, V., Kehinde, E.O., Gunther, B., Airik, R., Innis, J.W., Hoskins, B.E., Hoefele, J., Otto, E.A., et al. (2012). Identification of two novel CAKUT-causing genes by massively parallel exon resequencing of candidate genes in patients with unilateral renal agenesis. Kidney Int 81, 196-200.
19. Alazami, A.M., Shaheen, R., Alzahrani, F., Snape, K., Saggar, A., Brinkmann, B., Bavi, P., Al-Gazali, L.I., and Alkuraya, F.S. (2009). FREM1 mutations cause bifid nose, renal agenesis, and anorectal malformations syndrome. Am J Hum Genet 85, 414-418.
20. Van Esch, H., Groenen, P., Nesbit, M.A., Schuffenhauer, S., Lichtner, P., Vanderlinden, G., Harding, B., Beetz, R., Bilous, R.W., Holdaway, I., et al. (2000). GATA3 haplo-insufficiency causes human HDR syndrome. Nature 406, 419-422.
21. Tassabehji, M., Fang, Z.M., Hilton, E.N., McGaughran, J., Zhao, Z., de Bock, C.E., Howard, E., Malass, M., Donnai, D., Diwan, A., et al. (2008). Mutations in GDF6 are associated with vertebral segmentation defects in Klippel-Feil syndrome. Hum Mutat 29, 1017-1027.
22. Johnston, J.J., Olivos-Glander, I., Killoran, C., Elson, E., Turner, J.T., Peters, K.F., Abbott, M.H., Aughton, D.J., Aylsworth, A.S., Bamshad, M.J., et al. (2005). Molecular and clinical analyses of Greig cephalopolysyndactyly and Pallister-Hall syndromes: robust phenotype prediction from the type and position of GLI3 mutations. Am J Hum Genet 76, 609-622.
23. Pilia, G., Hughes-Benzie, R.M., MacKenzie, A., Baybayan, P., Chen, E.Y., Huber, R., Neri, G., Cao, A., Forabosco, A., and Schlessinger, D. (1996). Mutations in GPC3, a glypican gene, cause the Simpson-Golabi-Behmel overgrowth syndrome. Nat Genet 12, 241-247.
24. Vogel, M.J., van Zon, P., Brueton, L., Gijzen, M., van Tuil, M.C., Cox, P., Schanze, D., Kariminejad, A., Ghaderi-Sohi, S., Blair, E., et al. (2012). Mutations in GRIP1 cause Fraser syndrome. J Med Genet 49, 303-306.
25. Heidet, L., Decramer, S., Pawtowski, A., Moriniere, V., Bandin, F., Knebelmann, B., Lebre, A.S., Faguer, S., Guigonis, V., Antignac, C., et al. (2010). Spectrum of HNF1B mutations in a large cohort of patients who harbor renal diseases. Clin J Am Soc Nephrol 5, 1079-1090.

26. Daly, S.B., Urquhart, J.E., Hilton, E., McKenzie, E.A., Kammerer, R.A., Lewis, M., Kerr, B., Stuart, H., Donnai, D., Long, D.A., et al. (2010). Mutations in HPSE2 cause urofacial syndrome. Am J Hum Genet 86, 963-969.
27. Has, C., Sparta, G., Kiritsi, D., Weibel, L., Moeller, A., Vega-Warner, V., Waters, A., He, Y., Anikster, Y., Esser, P., et al. (2012). Integrin alpha3 mutations with kidney, lung, and skin disease. N Engl J Med 366, 1508-1514.
28. Humbert, C., Silbermann, F., Morar, B., Parisot, M., Zarhrate, M., Masson, C., Tores, F., Blanchet, P., Perez, M.J., Petrov, Y., et al. (2014). Integrin alpha 8 recessive mutations are responsible for bilateral renal agenesis in humans. Am J Hum Genet 94, 288-294.
29. Oda, T., Elkahloun, A.G., Pike, B.L., Okajima, K., Krantz, I.D., Genin, A., Piccoli, D.A., Meltzer, P.S., Spinner, N.B., Collins, F.S., et al. (1997). Mutations in the human Jagged1 gene are responsible for Alagille syndrome. Nat Genet 16, 235-242.
30. Filges, I., Nosova, E., Bruder, E., Tercanli, S., Townsend, K., Gibson, W.T., Rothlisberger, B., Heinimann, K., Hall, J.G., Gregory-Evans, C.Y., et al. (2014). Exome sequencing identifies mutations in KIF14 as a novel cause of an autosomal recessive lethal fetal ciliopathy phenotype. Clin Genet 86, 220-228.
31. Stuart, H.M., Roberts, N.A., Burgu, B., Daly, S.B., Urquhart, J.E., Bhaskar, S., Dickerson, J.E., Mermerkaya, M., Silay, M.S., Lewis, M.A., et al. (2013). LRIG2 mutations cause urofacial syndrome. Am J Hum Genet 92, 259-264.
32. Khan, T.N., Klar, J., Ali, Z., Khan, F., Baig, S.M., and Dahl, N. (2013). Cenani-Lenz syndrome restricted to limb and kidney anomalies associated with a novel LRP4 missense mutation. Eur J Med Genet 56, 371-374.
33. Grampa, V., Delous, M., Zaidan, M., Odye, G., Thomas, S., Elkhartoufi, N., Filhol, E., Niel, O., Silbermann, F., Lebreton, C., et al. (2016). Novel NEK8 Mutations Cause Severe Syndromic Renal Cystic Dysplasia through YAP Dysregulation. PLoS Genet 12, e1005894.
34. Kamath, B.M., Spinner, N.B., and Rosenblum, N.D. (2013). Renal involvement and the role of Notch signalling in Alagille syndrome. Nat Rev Nephrol 9, 409-418.
35. Bower, M., Salomon, R., Allanson, J., Antignac, C., Benedicenti, F., Benetti, E., Binenbaum, G., Jensen, U.B., Cochat, P., DeCramer, S., et al. (2012). Update of PAX2 mutations in renal coloboma syndrome and establishment of a locus-specific database. Hum Mutat 33, 457-466.
36. Gribouval, O., Gonzales, M., Neuhaus, T., Aziza, J., Bieth, E., Laurent, N., Bouton, J.M., Feuillet, F., Makni, S., Ben Amar, H., et al. (2005). Mutations in genes in the renin-angiotensin system are associated with autosomal recessive renal tubular dysgenesis. Nat Genet 37, 964-968.
37. Skinner, M.A., Safford, S.D., Reeves, J.G., Jackson, M.E., and Freemerman, A.J. (2008). Renal aplasia in humans is associated with RET mutations. Am J Hum Genet 82, 344-351.
38. Hwang, D.Y., Kohl, S., Fan, X., Vivante, A., Chan, S., Dworschak, G.C., Schulz, J., van Eerde, A.M., Hilger, A.C., Gee, H.Y., et al. (2015). Mutations of the SLIT2-ROBO2 pathway genes SLIT2 and SRGAP1 confer risk for congenital anomalies of the kidney and urinary tract. Hum Genet 134, 905-916.
39. Botzenhart, E.M., Green, A., Ilyina, H., Konig, R., Lowry, R.B., Lo, I.F., Shohat, M., Burke, L., McGaughran, J., Chafai, R., et al. (2005). SALL1 mutation analysis in Townes-Brocks syndrome: twelve novel mutations and expansion of the phenotype. Hum Mutat 26, 282.
40. Kohlhase, J., Heinrich, M., Schubert, L., Liebers, M., Kispert, A., Laccone, F., Turnpenny, P., Winter, R.M., and Reardon, W. (2002). Okihiro syndrome is caused by SALL4 mutations. Hum Mol Genet 11, 2979-2987.

41. Weber, S., Moriniere, V., Knuppel, T., Charbit, M., Dusek, J., Ghiggeri, G.M., Jankauskiene, A., Mir, S., Montini, G., Peco-Antic, A., et al. (2006). Prevalence of mutations in renal developmental genes in children with renal hypodysplasia: results of the ESCAPE study. J Am Soc Nephrol 17, 2864-2870.
42. Krug, P., Moriniere, V., Marlin, S., Koubi, V., Gabriel, H.D., Colin, E., Bonneau, D., Salomon, R., Antignac, C., and Heidet, L. (2011). Mutation screening of the EYA1, SIX1, and SIX5 genes in a large cohort of patients harboring branchio-oto-renal syndrome calls into question the pathogenic role of SIX5 mutations. Hum Mutat 32, 183-190.
43. Gimelli, S., Caridi, G., Beri, S., McCracken, K., Bocciardi, R., Zordan, P., Dagnino, M., Fiorio, P., Murer, L., Benetti, E., et al. (2010). Mutations in SOX17 are associated with congenital anomalies of the kidney and the urinary tract. Hum Mutat 31, 1352-1359.
44. Kosfeld, A., Kreuzer, M., Daniel, C., Brand, F., Schafer, A.K., Chadt, A., Weiss, A.C., Riehmer, V., Jeanpierre, C., Klintschar, M., et al. (2016). Whole-exome sequencing identifies mutations of TBC1D1 encoding a Rab-GTPase-activating protein in patients with congenital anomalies of the kidneys and urinary tract (CAKUT). Hum Genet 135, 69-87.
45. Vivante, A., Kleppa, M.J., Schulz, J., Kohl, S., Sharma, A., Chen, J., Shril, S., Hwang, D.Y., Weiss, A.C., Kaminski, M.M., et al. (2015). Mutations in TBX18 Cause Dominant Urinary Tract Malformations via Transcriptional Dysregulation of Ureter Development. Am J Hum Genet 97, 291-301.
46. Gbadegesin, R.A., Brophy, P.D., Adeyemo, A., Hall, G., Gupta, I.R., Hains, D., Bartkowiak, B., Rabinovich, C.E., Chandrasekharappa, S., Homstad, A., et al. (2013). TNXB mutations can cause vesicoureteral reflux. J Am Soc Nephrol 24, 1313-1322.
47. Saisawat, P., Kohl, S., Hilger, A.C., Hwang, D.Y., Yung Gee, H., Dworschak, G.C., Tasic, V., Pennimpede, T., Natarajan, S., Sperry, E., et al. (2014). Whole-exome resequencing reveals recessive mutations in TRAP1 in individuals with CAKUT and VACTERL association. Kidney Int 85, 1310-1317.
48. Dahan, K., Devuyst, O., Smaers, M., Vertommen, D., Loute, G., Poux, J.M., Viron, B., Jacquot, C., Gagnadoux, M.F., Chauveau, D., et al. (2003). A cluster of mutations in the UMOD gene causes familial juvenile hyperuricemic nephropathy with abnormal expression of uromodulin. J Am Soc Nephrol 14, 2883-2893.
49. van Eerde, A.M., Duran, K., van Riel, E., de Kovel, C.G., Koeleman, B.P., Knoers, N.V., Renkema, K.Y., van der Horst, H.J., Bokenkamp, A., van Hagen, J.M., et al. (2012). Genes in the ureteric budding pathway: association study on vesico-ureteral reflux patients. PLoS One 7, e31327.
50. Vivante, A., Mark-Danieli, M., Davidovits, M., Harari-Steinberg, O., Omer, D., Gnatek, Y., Cleper, R., Landau, D., Kovalski, Y., Weissman, I., et al. (2013). Renal hypodysplasia associates with a WNT4 variant that causes aberrant canonical WNT signaling. J Am Soc Nephrol 24, 550-558.
51. Ichiki, T., Labosky, P.A., Shiota, C., Okuyama, S., Imagawa, Y., Fogo, A., Niimura, F., Ichikawa, I., Hogan, B.L., and Inagami, T. (1995). Effects on blood pressure and exploratory behaviour of mice lacking angiotensin II type-2 receptor. Nature 377, 748-750.
52. Mic, F.A., Haselbeck, R.J., Cuenca, A.E., and Duester, G. (2002). Novel retinoic acid generating activities in the neural tube and heart identified by conditional rescue of Raldh2 null mutant mice. Development 129, 2271-2282.
53. Moisan, A., Rivera, M.N., Lotinun, S., Akhavanfard, S., Coffman, E.J., Cook, E.B., Stoykova, S., Mukherjee, S., Schoonmaker, J.A., Burger, A., et al. (2011). The WTX

tumor suppressor regulates mesenchymal progenitor cell fate specification. Dev Cell 20, 583-596.
54. McDill, B.W., Li, S.Z., Kovach, P.A., Ding, L., and Chen, F. (2006). Congenital progressive hydronephrosis (cph) is caused by an S256L mutation in aquaporin-2 that affects its phosphorylation and apical membrane accumulation. Proc Natl Acad Sci U S A 103, 6952-6957.
55. Goggolidou, P., Hadjirin, N.F., Bak, A., Papakrivopoulou, E., Hilton, H., Norris, D.P., and Dean, C.H. (2014). Atmin mediates kidney morphogenesis by modulating Wnt signaling. Hum Mol Genet 23, 5303-5316.
56. Veis, D.J., Sorenson, C.M., Shutter, J.R., and Korsmeyer, S.J. (1993). Bcl-2-deficient mice demonstrate fulminant lymphoid apoptosis, polycystic kidneys, and hypopigmented hair. Cell 75, 229-240.
57. Fan, H., Stefkova, J., and El-Dahr, S.S. (2006). Susceptibility to metanephric apoptosis in bradykinin B2 receptor null mice via the p53-Bax pathway. Am J Physiol Renal Physiol 291, F670-682.
58. Jena, N., Martin-Seisdedos, C., McCue, P., and Croce, C.M. (1997). BMP7 null mutation in mice: developmental defects in skeleton, kidney, and eye. Exp Cell Res 230, 28-37.
59. Ikeya, M., Fukushima, K., Kawada, M., Onishi, S., Furuta, Y., Yonemura, S., Kitamura, T., Nosaka, T., and Sasai, Y. (2010). Cv2, functioning as a pro-BMP factor via twisted gastrulation, is required for early development of nephron precursors. Dev Biol 337, 405-414.
60. Mah, S.P., Saueressig, H., Goulding, M., Kintner, C., and Dressler, G.R. (2000). Kidney development in cadherin-6 mutants: delayed mesenchyme-to-epithelial conversion and loss of nephrons. Dev Biol 223, 38-53.
61. Chi, L., Saarela, U., Railo, A., Prunskaite-Hyyrylainen, R., Skovorodkin, I., Anthony, S., Katsu, K., Liu, Y., Shan, J., Salgueiro, A.M., et al. (2011). A secreted BMP antagonist, Cer1, fine tunes the spatial organization of the ureteric bud tree during mouse kidney development. PLoS One 6, e27676.
62. Kuure, S., Cebrian, C., Machingo, Q., Lu, B.C., Chi, X., Hyink, D., D'Agati, V., Gurniak, C., Witke, W., and Costantini, F. (2010). Actin depolymerizing factors cofilin1 and destrin are required for ureteric bud branching morphogenesis. PLoS Genet 6, e1001176.
63. Wilkinson, L., Kurniawan, N.D., Phua, Y.L., Nguyen, M.J., Li, J., Galloway, G.J., Hashitani, H., Lang, R.J., and Little, M.H. (2012). Association between congenital defects in papillary outgrowth and functional obstruction in Crim1 mutant mice. J Pathol 227, 499-510.
64. Bridgewater, D., Di Giovanni, V., Cain, J.E., Cox, B., Jakobson, M., Sainio, K., and Rosenblum, N.D. (2011). beta-catenin causes renal dysplasia via upregulation of Tgfbeta2 and Dkk1. J Am Soc Nephrol 22, 718-731.
65. Hasegawa, Y., Satoh, K., Iizuka-Kogo, A., Shimomura, A., Nomura, R., Akiyama, T., and Senda, T. (2007). Loss of ICAT gene function leads to arrest of ureteric bud branching and renal agenesis. Biochem Biophys Res Commun 362, 988-994.
66. San Agustin, J.T., Klena, N., Granath, K., Panigrahy, A., Stewart, E., Devine, W., Strittmatter, L., Jonassen, J.A., Liu, X., Lo, C.W., et al. (2016). Genetic link between renal birth defects and congenital heart disease. Nat Commun 7, 11103.
67. Suriben, R., Kivimae, S., Fisher, D.A., Moon, R.T., and Cheyette, B.N. (2009). Posterior malformations in Dact1 mutant mice arise through misregulated Vangl2 at the primitive streak. Nat Genet 41, 977-985.
68. Mao, Y., Mulvaney, J., Zakaria, S., Yu, T., Morgan, K.M., Allen, S., Basson, M.A., Francis-West, P., and Irvine, K.D. (2011). Characterization of a Dchs1 mutant mouse

reveals requirements for Dchs1-Fat4 signaling during mammalian development. Development 138, 947-957.
69. Fetting, J.L., Guay, J.A., Karolak, M.J., Iozzo, R.V., Adams, D.C., Maridas, D.E., Brown, A.C., and Oxburgh, L. (2014). FOXD1 promotes nephron progenitor differentiation by repressing decorin in the embryonic kidney. Development 141, 17-27.
70. Naim, E., Bernstein, A., Bertram, J.F., and Caruana, G. (2005). Mutagenesis of the epithelial polarity gene, discs large 1, perturbs nephrogenesis in the developing mouse kidney. Kidney Int 68, 955-965.
71. Liu, Z., Chen, S., Boyle, S., Zhu, Y., Zhang, A., Piwnica-Worms, D.R., Ilagan, M.X., and Kopan, R. (2013). The extracellular domain of Notch2 increases its cell-surface abundance and ligand responsiveness during kidney development. Dev Cell 25, 585-598.
72. Paroly, S.S., Wang, F., Spraggon, L., Merregaert, J., Batourina, E., Tycko, B., Schmidt-Ott, K.M., Grimmond, S., Little, M., and Mendelsohn, C. (2013). Stromal protein Ecm1 regulates ureteric bud patterning and branching. PLoS One 8, e84155.
73. Zhang, Z., Pascuet, E., Hueber, P.A., Chu, L., Bichet, D.G., Lee, T.C., Threadgill, D.W., and Goodyer, P. (2010). Targeted inactivation of EGF receptor inhibits renal collecting duct development and function. J Am Soc Nephrol 21, 573-578.
74. Miyamoto, N., Yoshida, M., Kuratani, S., Matsuo, I., and Aizawa, S. (1997). Defects of urogenital development in mice lacking Emx2. Development 124, 1653-1664.
75. Weiss, A.C., Airik, R., Bohnenpoll, T., Greulich, F., Foik, A., Trowe, M.O., Rudat, C., Costantini, F., Adams, R.H., and Kispert, A. (2014). Nephric duct insertion requires EphA4/EphA7 signaling from the pericloacal mesenchyme. Development 141, 3420-3430.
76. Kuure, S., Chi, X., Lu, B., and Costantini, F. (2010). The transcription factors Etv4 and Etv5 mediate formation of the ureteric bud tip domain during kidney development. Development 137, 1975-1979.
77. Fogelgren, B., Polgar, N., Lui, V.H., Lee, A.J., Tamashiro, K.K., Napoli, J.A., Walton, C.B., Zuo, X., and Lipschutz, J.H. (2015). Urothelial Defects from Targeted Inactivation of Exocyst Sec10 in Mice Cause Ureteropelvic Junction Obstructions. PLoS One 10, e0129346.
78. Ciani, L., Patel, A., Allen, N.D., and ffrench-Constant, C. (2003). Mice lacking the giant protocadherin mFAT1 exhibit renal slit junction abnormalities and a partially penetrant cyclopia and anophthalmia phenotype. Mol Cell Biol 23, 3575-3582.
79. Saburi, S., Hester, I., Fischer, E., Pontoglio, M., Eremina, V., Gessler, M., Quaggin, S.E., Harrison, R., Mount, R., and McNeill, H. (2008). Loss of Fat4 disrupts PCP signaling and oriented cell division and leads to cystic kidney disease. Nat Genet 40, 1010-1015.
80. Michos, O., Cebrian, C., Hyink, D., Grieshammer, U., Williams, L., D'Agati, V., Licht, J.D., Martin, G.R., and Costantini, F. (2010). Kidney development in the absence of Gdnf and Spry1 requires Fgf10. PLoS Genet 6, e1000809.
81. Qiao, J., Uzzo, R., Obara-Ishihara, T., Degenstein, L., Fuchs, E., and Herzlinger, D. (1999). FGF-7 modulates ureteric bud growth and nephron number in the developing kidney. Development 126, 547-554.
82. Perantoni, A.O., Timofeeva, O., Naillat, F., Richman, C., Pajni-Underwood, S., Wilson, C., Vainio, S., Dove, L.F., and Lewandoski, M. (2005). Inactivation of FGF8 in early mesoderm reveals an essential role in kidney development. Development 132, 3859-3871.
83. Poladia, D.P., Kish, K., Kutay, B., Hains, D., Kegg, H., Zhao, H., and Bates, C.M. (2006). Role of fibroblast growth factor receptors 1 and 2 in the metanephric mesenchyme. Dev Biol 291, 325-339.

84. Gerber, S.D., Steinberg, F., Beyeler, M., Villiger, P.M., and Trueb, B. (2009). The murine Fgfrl1 receptor is essential for the development of the metanephric kidney. Dev Biol 335, 106-119.
85. Chao, C.W., Chan, D.C., Kuo, A., and Leder, P. (1998). The mouse formin (Fmn) gene: abundant circular RNA transcripts and gene-targeted deletion analysis. Mol Med 4, 614-628.
86. Kume, T., Deng, K., and Hogan, B.L. (2000). Murine forkhead/winged helix genes Foxc1 (Mf1) and Foxc2 (Mfh1) are required for the early organogenesis of the kidney and urinary tract. Development 127, 1387-1395.
87. Hatini, V., Huh, S.O., Herzlinger, D., Soares, V.C., and Lai, E. (1996). Essential role of stromal mesenchyme in kidney morphogenesis revealed by targeted disruption of Winged Helix transcription factor BF-2. Genes Dev 10, 1467-1478.
88. Adams, D., Larman, B., and Oxburgh, L. (2007). Developmental expression of mouse Follistatin-like 1 (Fstl1): Dynamic regulation during organogenesis of the kidney and lung. Gene Expr Patterns 7, 491-500.
89. Hoshino, T., Shimizu, R., Ohmori, S., Nagano, M., Pan, X., Ohneda, O., Khandekar, M., Yamamoto, M., Lim, K.C., and Engel, J.D. (2008). Reduced BMP4 abundance in Gata2 hypomorphic mutant mice result in uropathies resembling human CAKUT. Genes Cells 13, 159-170.
90. Esquela, A.F., and Lee, S.J. (2003). Regulation of metanephric kidney development by growth/differentiation factor 11. Dev Biol 257, 356-370.
91. Sanchez, M.P., Silos-Santiago, I., Frisen, J., He, B., Lira, S.A., and Barbacid, M. (1996). Renal agenesis and the absence of enteric neurons in mice lacking GDNF. Nature 382, 70-73.
92. Tomac, A.C., Grinberg, A., Huang, S.P., Nosrat, C., Wang, Y., Borlongan, C., Lin, S.Z., Chiang, Y.H., Olson, L., Westphal, H., et al. (2000). Glial cell line-derived neurotrophic factor receptor alpha1 availability regulates glial cell line-derived neurotrophic factor signaling: evidence from mice carrying one or two mutated alleles. Neuroscience 95, 1011-1023.
93. Li, J.P., Gong, F., Hagner-McWhirter, A., Forsberg, E., Abrink, M., Kisilevsky, R., Zhang, X., and Lindahl, U. (2003). Targeted disruption of a murine glucuronyl C5-epimerase gene results in heparan sulfate lacking L-iduronic acid and in neonatal lethality. J Biol Chem 278, 28363-28366.
94. Michos, O., Panman, L., Vintersten, K., Beier, K., Zeller, R., and Zuniga, A. (2004). Gremlin-mediated BMP antagonism induces the epithelial-mesenchymal feedback signaling controlling metanephric kidney and limb organogenesis. Development 131, 3401-3410.
95. Aue, A., Hinze, C., Walentin, K., Ruffert, J., Yurtdas, Y., Werth, M., Chen, W., Rabien, A., Kilic, E., Schulzke, J.D., et al. (2015). A Grainyhead-Like 2/Ovo-Like 2 Pathway Regulates Renal Epithelial Barrier Function and Lumen Expansion. J Am Soc Nephrol 26, 2704-2715.
96. Wellik, D.M., Hawkes, P.J., and Capecchi, M.R. (2002). Hox11 paralogous genes are essential for metanephric kidney induction. Genes Dev 16, 1423-1432.
97. Bullock, S.L., Fletcher, J.M., Beddington, R.S., and Wilson, V.A. (1998). Renal agenesis in mice homozygous for a gene trap mutation in the gene encoding heparan sulfate 2-sulfotransferase. Genes Dev 12, 1894-1906.
98. Smeeton, J., Zhang, X., Bulus, N., Mernaugh, G., Lange, A., Karner, C.M., Carroll, T.J., Fassler, R., Pozzi, A., Rosenblum, N.D., et al. (2010). Integrin-linked kinase regulates p38 MAPK-dependent cell cycle arrest in ureteric bud development. Development 137, 3233-3243.

99. Kaku, Y., Ohmori, T., Kudo, K., Fujimura, S., Suzuki, K., Evans, S.M., Kawakami, Y., and Nishinakamura, R. (2013). Islet1 deletion causes kidney agenesis and hydroureter resembling CAKUT. J Am Soc Nephrol 24, 1242-1249.
100. Zhang, X., Mernaugh, G., Yang, D.H., Gewin, L., Srichai, M.B., Harris, R.C., Iturregui, J.M., Nelson, R.D., Kohan, D.E., Abrahamson, D., et al. (2009). beta1 integrin is necessary for ureteric bud branching morphogenesis and maintenance of collecting duct structural integrity. Development 136, 3357-3366.
101. Uchiyama, Y., Sakaguchi, M., Terabayashi, T., Inenaga, T., Inoue, S., Kobayashi, C., Oshima, N., Kiyonari, H., Nakagata, N., Sato, Y., et al. (2010). Kif26b, a kinesin family gene, regulates adhesion of the embryonic kidney mesenchyme. Proc Natl Acad Sci U S A 107, 9240-9245.
102. Lin, F., Hiesberger, T., Cordes, K., Sinclair, A.M., Goldstein, L.S., Somlo, S., and Igarashi, P. (2003). Kidney-specific inactivation of the KIF3A subunit of kinesin-II inhibits renal ciliogenesis and produces polycystic kidney disease. Proc Natl Acad Sci U S A 100, 5286-5291.
103. Yi, T., Tan, K., Cho, S.G., Wang, Y., Luo, J., Zhang, W., Li, D., and Liu, M. (2010). Regulation of embryonic kidney branching morphogenesis and glomerular development by KISS1 receptor (Gpr54) through NFAT2- and Sp1-mediated Bmp7 expression. J Biol Chem 285, 17811-17820.
104. Shannon, M.B., Patton, B.L., Harvey, S.J., and Miner, J.H. (2006). A hypomorphic mutation in the mouse laminin alpha5 gene causes polycystic kidney disease. J Am Soc Nephrol 17, 1913-1922.
105. Willem, M., Miosge, N., Halfter, W., Smyth, N., Jannetti, I., Burghart, E., Timpl, R., and Mayer, U. (2002). Specific ablation of the nidogen-binding site in the laminin gamma1 chain interferes with kidney and lung development. Development 129, 2711-2722.
106. Kinzel, B., Pikiolek, M., Orsini, V., Sprunger, J., Isken, A., Zietzling, S., Desplanches, M., Dubost, V., Breustedt, D., Valdez, R., et al. (2014). Functional roles of Lgr4 and Lgr5 in embryonic gut, kidney and skin development in mice. Dev Biol 390, 181-190.
107. Kobayashi, A., Kwan, K.M., Carroll, T.J., McMahon, A.P., Mendelsohn, C.L., and Behringer, R.R. (2005). Distinct and sequential tissue-specific activities of the LIM-class homeobox gene Lim1 for tubular morphogenesis during kidney development. Development 132, 2809-2823.
108. Peng, Y., Clark, C., Luong, R., Tu, W.H., Lee, J., Johnson, D.T., Das, A., Carroll, T.J., and Sun, Z. (2011). The leucine zipper putative tumor suppressor 2 protein LZTS2 regulates kidney development. J Biol Chem 286, 40331-40342.
109. Arnould, C., Lelievre-Pegorier, M., Ronco, P., and Lelongt, B. (2009). MMP9 limits apoptosis and stimulates branching morphogenesis during kidney development. J Am Soc Nephrol 20, 2171-2180.
110. Bates, C.M., Kharzai, S., Erwin, T., Rossant, J., and Parada, L.F. (2000). Role of N-myc in the developing mouse kidney. Dev Biol 222, 317-325.
111. Lu, W., Quintero-Rivera, F., Fan, Y., Alkuraya, F.S., Donovan, D.J., Xi, Q., Turbe-Doan, A., Li, Q.G., Campbell, C.G., Shanske, A.L., et al. (2007). NFIA haploinsufficiency is associated with a CNS malformation syndrome and urinary tract defects. PLoS Genet 3, e80.
112. Linton, J.M., Martin, G.R., and Reichardt, L.F. (2007). The ECM protein nephronectin promotes kidney development via integrin alpha8beta1-mediated stimulation of Gdnf expression. Development 134, 2501-2509.

113. Yu, C.T., Tang, K., Suh, J.M., Jiang, R., Tsai, S.Y., and Tsai, M.J. (2012). COUP-TFII is essential for metanephric mesenchyme formation and kidney precursor cell survival. Development 139, 2330-2339.
114. Wang, Q., Lan, Y., Cho, E.S., Maltby, K.M., and Jiang, R. (2005). Odd-skipped related 1 (Odd 1) is an essential regulator of heart and urogenital development. Dev Biol 288, 582-594.
115. Lange, A., Wickstrom, S.A., Jakobson, M., Zent, R., Sainio, K., and Fassler, R. (2009). Integrin-linked kinase is an adaptor with essential functions during mouse development. Nature 461, 1002-1006.
116. Narlis, M., Grote, D., Gaitan, Y., Boualia, S.K., and Bouchard, M. (2007). Pax2 and pax8 regulate branching morphogenesis and nephron differentiation in the developing kidney. J Am Soc Nephrol 18, 1121-1129.
117. Schnabel, C.A., Godin, R.E., and Cleary, M.L. (2003). Pbx1 regulates nephrogenesis and ureteric branching in the developing kidney. Dev Biol 254, 262-276.
118. Nakai, S., Sugitani, Y., Sato, H., Ito, S., Miura, Y., Ogawa, M., Nishi, M., Jishage, K., Minowa, O., and Noda, T. (2003). Crucial roles of Brn1 in distal tubule formation and function in mouse kidney. Development 130, 4751-4759.
119. Chang, C.P., McDill, B.W., Neilson, J.R., Joist, H.E., Epstein, J.A., Crabtree, G.R., and Chen, F. (2004). Calcineurin is required in urinary tract mesenchyme for the development of the pyeloureteral peristaltic machinery. J Clin Invest 113, 1051-1058.
120. Maezawa, Y., Binnie, M., Li, C., Thorner, P., Hui, C.C., Alman, B., Taketo, M.M., and Quaggin, S.E. (2012). A new Cre driver mouse line, Tcf21/Pod1-Cre, targets metanephric mesenchyme. PLoS One 7, e40547.
121. Slattery, P., Frolich, S., Schreiber, Y., and Nusing, R.M. (2016). COX-2 gene dosage-dependent defects in kidney development. Am J Physiol Renal Physiol 310, F1113-1122.
122. Batourina, E., Gim, S., Bello, N., Shy, M., Clagett-Dame, M., Srinivas, S., Costantini, F., and Mendelsohn, C. (2001). Vitamin A controls epithelial/mesenchymal interactions through Ret expression. Nat Genet 27, 74-78.
123. Bonegio, R.G., Beck, L.H., Kahlon, R.K., Lu, W., and Salant, D.J. (2011). The fate of Notch-deficient nephrogenic progenitor cells during metanephric kidney development. Kidney Int 79, 1099-1112.
124. Kim, B.J., Zaveri, H.P., Shchelochkov, O.A., Yu, Z., Hernandez-Garcia, A., Seymour, M.L., Oghalai, J.S., Pereira, F.A., Stockton, D.W., Justice, M.J., et al. (2013). An allelic series of mice reveals a role for RERE in the development of multiple organs affected in chromosome 1p36 deletions. PLoS One 8, e57460.
125. Reidy, K., and Tufro, A. (2011). Semaphorins in kidney development and disease: modulators of ureteric bud branching, vascular morphogenesis, and podocyte-endothelial crosstalk. Pediatr Nephrol 26, 1407-1412.
126. Yu, J., Carroll, T.J., and McMahon, A.P. (2002). Sonic hedgehog regulates proliferation and differentiation of mesenchymal cells in the mouse metanephric kidney. Development 129, 5301-5312.
127. Oxburgh, L., Chu, G.C., Michael, S.K., and Robertson, E.J. (2004). TGFbeta superfamily signals are required for morphogenesis of the kidney mesenchyme progenitor population. Development 131, 4593-4605.
128. Murugan, S., Shan, J., Kuhl, S.J., Tata, A., Pietila, I., Kuhl, M., and Vainio, S.J. (2012). WT1 and Sox11 regulate synergistically the promoter of the Wnt4 gene that encodes a critical signal for nephrogenesis. Exp Cell Res 318, 1134-1145.
129. Huang, J., Arsenault, M., Kann, M., Lopez-Mendez, C., Saleh, M., Wadowska, D., Taglienti, M., Ho, J., Miao, Y., Sims, D., et al. (2013). The transcription factor Sry-

related HMG box-4 (SOX4) is required for normal renal development in vivo. Dev Dyn 242, 790-799.
130. Reginensi, A., Clarkson, M., Neirijnck, Y., Lu, B., Ohyama, T., Groves, A.K., Sock, E., Wegner, M., Costantini, F., Chaboissier, M.C., et al. (2011). SOX9 controls epithelial branching by activating RET effector genes during kidney development. Hum Mol Genet 20, 1143-1153.
131. Basson, M.A., Akbulut, S., Watson-Johnson, J., Simon, R., Carroll, T.J., Shakya, R., Gross, I., Martin, G.R., Lufkin, T., McMahon, A.P., et al. (2005). Sprouty1 is a critical regulator of GDNF/RET-mediated kidney induction. Dev Cell 8, 229-239.
132. Quaggin, S.E., Schwartz, L., Cui, S., Igarashi, P., Deimling, J., Post, M., and Rossant, J. (1999). The basic-helix-loop-helix protein pod1 is critically important for kidney and lung organogenesis. Development 126, 5771-5783.
133. Yamaguchi, Y., Yonemura, S., and Takada, S. (2006). Grainyhead-related transcription factor is required for duct maturation in the salivary gland and the kidney of the mouse. Development 133, 4737-4748.
134. Short, K.M., Hodson, M.J., and Smyth, I.M. (2010). Tomographic quantification of branching morphogenesis and renal development. Kidney Int 77, 1132-1139.
135. Walker, K.A., Sims-Lucas, S., Caruana, G., Cullen-McEwen, L., Li, J., Sarraj, M.A., Bertram, J.F., and Stenvers, K.L. (2011). Betaglycan is required for the establishment of nephron endowment in the mouse. PLoS One 6, e18723.
136. Gui, T., Sun, Y., Gai, Z., Shimokado, A., Muragaki, Y., and Zhou, G. (2013). The loss of Trps1 suppresses ureteric bud branching because of the activation of TGF-beta signaling. Dev Biol 377, 415-427.
137. Caubit, X., Lye, C.M., Martin, E., Core, N., Long, D.A., Vola, C., Jenkins, D., Garratt, A.N., Skaer, H., Woolf, A.S., et al. (2008). Teashirt 3 is necessary for ureteral smooth muscle differentiation downstream of SHH and BMP4. Development 135, 3301-3310.
138. Majumdar, A., Vainio, S., Kispert, A., McMahon, J., and McMahon, A.P. (2003). Wnt11 and Ret/Gdnf pathways cooperate in regulating ureteric branching during metanephric kidney development. Development 130, 3175-3185.
139. Yu, J., Carroll, T.J., Rajagopal, J., Kobayashi, A., Ren, Q., and McMahon, A.P. (2009). A Wnt7b-dependent pathway regulates the orientation of epithelial cell division and establishes the cortico-medullary axis of the mammalian kidney. Development 136, 161-171.
140. Carroll, T.J., Park, J.S., Hayashi, S., Majumdar, A., and McMahon, A.P. (2005). Wnt9b plays a central role in the regulation of mesenchymal to epithelial transitions underlying organogenesis of the mammalian urogenital system. Dev Cell 9, 283-292.
141. Kreidberg, J.A., Sariola, H., Loring, J.M., Maeda, M., Pelletier, J., Housman, D., and Jaenisch, R. (1993). WT-1 is required for early kidney development. Cell 74, 679-691.
142. Reginensi, A., Scott, R.P., Gregorieff, A., Bagherie-Lachidan, M., Chung, C., Lim, D.S., Pawson, T., Wrana, J., and McNeill, H. (2013). Yap- and Cdc42-dependent nephrogenesis and morphogenesis during mouse kidney development. PLoS Genet 9, e1003380.
143. Cizelsky, W., Tata, A., Kuhl, M., and Kuhl, S.J. (2014). The Wnt/JNK signaling target gene alcam is required for embryonic kidney development. Development 141, 2064-2074.
144. Ranghini, E.J., and Dressler, G.R. (2015). Evidence for intermediate mesoderm and kidney progenitor cell specification by Pax2 and PTIP dependent mechanisms. Dev Biol 399, 296-305.
145. Mana-Capelli, S., Paramasivam, M., Dutta, S., and McCollum, D. (2014). Angiomotins link F-actin architecture to Hippo pathway signaling. Mol Biol Cell 25, 1676-1685.

146. Phua, Y.L., Chu, J.Y., Marrone, A.K., Bodnar, A.J., Sims-Lucas, S., and Ho, J. (2015). Renal stromal miRNAs are required for normal nephrogenesis and glomerular mesangial survival. Physiol Rep 3.
147. Nicolaou, N., Margadant, C., Kevelam, S.H., Lilien, M.R., Oosterveld, M.J., Kreft, M., van Eerde, A.M., Pfundt, R., Terhal, P.A., van der Zwaag, B., et al. (2012). Gain of glycosylation in integrin alpha3 causes lung disease and nephrotic syndrome. J Clin Invest 122, 4375-4387.
148. Goldman, M., Smith, A., Shuman, C., Caluseriu, O., Wei, C., Steele, L., Ray, P., Sadowski, P., Squire, J., Weksberg, R., et al. (2002). Renal abnormalities in beckwith-wiedemann syndrome are associated with 11p15.5 uniparental disomy. J Am Soc Nephrol 13, 2077-2084.
149. Metsuyanim, S., Harari-Steinberg, O., Buzhor, E., Omer, D., Pode-Shakked, N., Ben-Hur, H., Halperin, R., Schneider, D., and Dekel, B. (2009). Expression of stem cell markers in the human fetal kidney. PLoS One 4, e6709.
150. Sims-Lucas, S., Di Giovanni, V., Schaefer, C., Cusack, B., Eswarakumar, V.P., and Bates, C.M. (2012). Ureteric morphogenesis requires Fgfr1 and Fgfr2/Frs2alpha signaling in the metanephric mesenchyme. J Am Soc Nephrol 23, 607-617.
151. Bagherie-Lachidan, M., Reginensi, A., Pan, Q., Zaveri, H.P., Scott, D.A., Blencowe, B.J., Helmbacher, F., and McNeill, H. (2015). Stromal Fat4 acts non-autonomously with Dchs1/2 to restrict the nephron progenitor pool. Development 142, 2564-2573.
152. Takayama, M., Miyatake, K., and Nishida, E. (2014). Identification and characterization of retinoic acid-responsive genes in mouse kidney development. Genes Cells 19, 637-649.
153. Kurokawa, K., Kawai, K., Hashimoto, M., Ito, Y., and Takahashi, M. (2003). Cell signalling and gene expression mediated by RET tyrosine kinase. J Intern Med 253, 627-633.
154. Ye, X., Wang, Y., Rattner, A., and Nathans, J. (2011). Genetic mosaic analysis reveals a major role for frizzled 4 and frizzled 8 in controlling ureteric growth in the developing kidney. Development 138, 1161-1172.
155. Zhang, B., Tran, U., and Wessely, O. (2011). Expression of Wnt signaling components during Xenopus pronephros development. PLoS One 6, e26533.
156. Hu, M.C., Mo, R., Bhella, S., Wilson, C.W., Chuang, P.T., Hui, C.C., and Rosenblum, N.D. (2006). GLI3-dependent transcriptional repression of Gli1, Gli2 and kidney patterning genes disrupts renal morphogenesis. Development 133, 569-578.
157. Weber, S., Landwehr, C., Renkert, M., Hoischen, A., Wuhl, E., Denecke, J., Radlwimmer, B., Haffner, D., Schaefer, F., and Weber, R.G. (2011). Mapping candidate regions and genes for congenital anomalies of the kidneys and urinary tract (CAKUT) by array-based comparative genomic hybridization. Nephrol Dial Transplant 26, 136-143.
158. Rilla, K., Pasonen-Seppanen, S., Karna, R., Karjalainen, H.M., Torronen, K., Koistinen, V., Tammi, M.I., Tammi, R.H., Teravainen, T., and Manninen, A. (2012). HAS3-induced accumulation of hyaluronan in 3D MDCK cultures results in mitotic spindle misorientation and disturbed organization of epithelium. Histochem Cell Biol 137, 153-164.
159. Hurtado, R., Bub, G., and Herzlinger, D. (2010). The pelvis-kidney junction contains HCN3, a hyperpolarization-activated cation channel that triggers ureter peristalsis. Kidney Int 77, 500-508.
160. Santos, O.F., Barros, E.J., Yang, X.M., Matsumoto, K., Nakamura, T., Park, M., and Nigam, S.K. (1994). Involvement of hepatocyte growth factor in kidney development. Dev Biol 163, 525-529.

161. Brunskill, E.W., Park, J.S., Chung, E., Chen, F., Magella, B., and Potter, S.S. (2014). Single cell dissection of early kidney development: multilineage priming. Development 141, 3093-3101.
162. Fu, Y., Li, F., Zhao, D.Y., Zhang, J.S., Lv, Y., and Li-Ling, J. (2014). Interaction between Tbx1 and Hoxd10 and connection with TGFbeta-BMP signal pathway during kidney development. Gene 536, 197-202.
163. Reggiani, L., Raciti, D., Airik, R., Kispert, A., and Brandli, A.W. (2007). The prepattern transcription factor Irx3 directs nephron segment identity. Genes Dev 21, 2358-2370.
164. McGrath-Morrow, S., Cho, C., Molls, R., Burne-Taney, M., Haas, M., Hicklin, D.J., Tuder, R., and Rabb, H. (2006). VEGF receptor 2 blockade leads to renal cyst formation in mice. Kidney Int 69, 1741-1748.
165. Rangel, E.B., Gomes, S.A., Dulce, R.A., Premer, C., Rodrigues, C.O., Kanashiro-Takeuchi, R.M., Oskouei, B., Carvalho, D.A., Ruiz, P., Reiser, J., et al. (2013). C-kit(+) cells isolated from developing kidneys are a novel population of stem cells with regenerative potential. Stem Cells 31, 1644-1656.
166. Oka, T., Mazack, V., and Sudol, M. (2008). Mst2 and Lats kinases regulate apoptotic function of Yes kinase-associated protein (YAP). J Biol Chem 283, 27534-27546.
167. Yamanaka, T., Horikoshi, Y., Izumi, N., Suzuki, A., Mizuno, K., and Ohno, S. (2006). Lgl mediates apical domain disassembly by suppressing the PAR-3-aPKC-PAR-6 complex to orient apical membrane polarity. J Cell Sci 119, 2107-2118.
168. Nikopoulos, G.N., Martins, J.F., Adams, T.L., Karaczyn, A., Adams, D., Vary, C., Oxburgh, L., and Verdi, J.M. (2009). NRAGE: a potential rheostat during branching morphogenesis. Mech Dev 126, 337-349.
169. Hilliard, S., Aboudehen, K., Yao, X., and El-Dahr, S.S. (2011). Tight regulation of p53 activity by Mdm2 is required for ureteric bud growth and branching. Dev Biol 353, 354-366.
170. Li, Y., Cheng, C.N., Verdun, V.A., and Wingert, R.A. (2014). Zebrafish nephrogenesis is regulated by interactions between retinoic acid, mecom, and Notch signaling. Dev Biol 386, 111-122.
171. Schwab, K., Hartman, H.A., Liang, H.C., Aronow, B.J., Patterson, L.T., and Potter, S.S. (2006). Comprehensive microarray analysis of Hoxa11/Hoxd11 mutant kidney development. Dev Biol 293, 540-554.
172. Woolf, A.S., Kolatsi-Joannou, M., Hardman, P., Andermarcher, E., Moorby, C., Fine, L.G., Jat, P.S., Noble, M.D., and Gherardi, E. (1995). Roles of hepatocyte growth factor/scatter factor and the met receptor in the early development of the metanephros. J Cell Biol 128, 171-184.
173. Hellman, N.E., Spector, J., Robinson, J., Zuo, X., Saunier, S., Antignac, C., Tobias, J.W., and Lipschutz, J.H. (2008). Matrix metalloproteinase 13 (MMP13) and tissue inhibitor of matrix metalloproteinase 1 (TIMP1), regulated by the MAPK pathway, are both necessary for Madin-Darby canine kidney tubulogenesis. J Biol Chem 283, 4272-4282.
174. Harari-Steinberg, O., Metsuyanim, S., Omer, D., Gnatek, Y., Gershon, R., Pri-Chen, S., Ozdemir, D.D., Lerenthal, Y., Noiman, T., Ben-Hur, H., et al. (2013). Identification of human nephron progenitors capable of generation of kidney structures and functional repair of chronic renal disease. EMBO Mol Med 5, 1556-1568.
175. Piccolo, S., Dupont, S., and Cordenonsi, M. (2014). The biology of YAP/TAZ: hippo signaling and beyond. Physiol Rev 94, 1287-1312.
176. Grasberger, H., Ringkananont, U., Lefrancois, P., Abramowicz, M., Vassart, G., and Refetoff, S. (2005). Thyroid transcription factor 1 rescues PAX8/p300 synergism

impaired by a natural PAX8 paired domain mutation with dominant negative activity. Mol Endocrinol 19, 1779-1791.
177. Thiagarajan, R.D., Georgas, K.M., Rumballe, B.A., Lesieur, E., Chiu, H.S., Taylor, D., Tang, D.T., Grimmond, S.M., and Little, M.H. (2011). Identification of anchor genes during kidney development defines ontological relationships, molecular subcompartments and regulatory pathways. PLoS One 6, e17286.
178. Zhao, D., Desai, S., and Zeng, H. (2011). VEGF stimulates PKD-mediated CREB-dependent orphan nuclear receptor Nurr1 expression: role in VEGF-induced angiogenesis. Int J Cancer 128, 2602-2612.
179. Lan, Y., Kingsley, P.D., Cho, E.S., and Jiang, R. (2001). Osr2, a new mouse gene related to Drosophila odd-skipped, exhibits dynamic expression patterns during craniofacial, limb, and kidney development. Mech Dev 107, 175-179.
180. Lechner, M.S., Levitan, I., and Dressler, G.R. (2000). PTIP, a novel BRCT domain-containing protein interacts with Pax2 and is associated with active chromatin. Nucleic Acids Res 28, 2741-2751.
181. Boualia, S.K., Gaitan, Y., Tremblay, M., Sharma, R., Cardin, J., Kania, A., and Bouchard, M. (2013). A core transcriptional network composed of Pax2/8, Gata3 and Lim1 regulates key players of pro/mesonephros morphogenesis. Dev Biol 382, 555-566.
182. Abraham, S., Paknikar, R., Bhumbra, S., Luan, D., Garg, R., Dressler, G.R., and Patel, S.R. (2015). The Groucho-associated phosphatase PPM1B displaces Pax transactivation domain interacting protein (PTIP) to switch the transcription factor Pax2 from a transcriptional activator to a repressor. J Biol Chem 290, 7185-7194.
183. Li, X., Hyink, D.P., Polgar, K., Gusella, G.L., Wilson, P.D., and Burrow, C.R. (2005). Protein kinase X activates ureteric bud branching morphogenesis in developing mouse metanephric kidney. J Am Soc Nephrol 16, 3543-3552.
184. Willecke, R., Heuberger, J., Grossmann, K., Michos, O., Schmidt-Ott, K., Walentin, K., Costantini, F., and Birchmeier, W. (2011). The tyrosine phosphatase Shp2 acts downstream of GDNF/Ret in branching morphogenesis of the developing mouse kidney. Dev Biol 360, 310-317.
185. Rong, X., Chen, C., Zhou, P., Zhou, Y., Li, Y., Lu, L., Liu, Y., Zhou, J., and Duan, C. (2014). R-spondin 3 regulates dorsoventral and anteroposterior patterning by antagonizing Wnt/beta-catenin signaling in zebrafish embryos. PLoS One 9, e99514.
186. Yates, L.L., Papakrivopoulou, J., Long, D.A., Goggolidou, P., Connolly, J.O., Woolf, A.S., and Dean, C.H. (2010). The planar cell polarity gene Vangl2 is required for mammalian kidney-branching morphogenesis and glomerular maturation. Hum Mol Genet 19, 4663-4676.
187. Sampson, M.G., Coughlin, C.R., 2nd, Kaplan, P., Conlin, L.K., Meyers, K.E., Zackai, E.H., Spinner, N.B., and Copelovitch, L. (2010). Evidence for a recurrent microdeletion at chromosome 16p11.2 associated with congenital anomalies of the kidney and urinary tract (CAKUT) and Hirschsprung disease. Am J Med Genet A 152A, 2618-2622.
188. Kiefer, S.M., Robbins, L., Barina, A., Zhang, Z., and Rauchman, M. (2008). SALL1 truncated protein expression in Townes-Brocks syndrome leads to ectopic expression of downstream genes. Hum Mutat 29, 1133-1140.
189. Cheng, C.N., and Wingert, R.A. (2015). Nephron proximal tubule patterning and corpuscles of Stannius formation are regulated by the sim1a transcription factor and retinoic acid in zebrafish. Dev Biol 399, 100-116.

190. Cain, J.E., Islam, E., Haxho, F., Chen, L., Bridgewater, D., Nieuwenhuis, E., Hui, C.C., and Rosenblum, N.D. (2009). GLI3 repressor controls nephron number via regulation of Wnt11 and Ret in ureteric tip cells. PLoS One 4, e7313.
191. Grande, M.T., Sanchez-Laorden, B., Lopez-Blau, C., De Frutos, C.A., Boutet, A., Arevalo, M., Rowe, R.G., Weiss, S.J., Lopez-Novoa, J.M., and Nieto, M.A. (2015). Snail1-induced partial epithelial-to-mesenchymal transition drives renal fibrosis in mice and can be targeted to reverse established disease. Nat Med 21, 989-997.
192. Wang, L.F., Wu, H., Xu, Y., Deng, M., Han, X.L., and Bai, D. (2015). Effect of SOST gene deletion on the progression of renal interstitial fibrosis in obstructive kidney injury. Ren Fail 37, 1514-1517.
193. Chi, L., Zhang, S., Lin, Y., Prunskaite-Hyyrylainen, R., Vuolteenaho, R., Itaranta, P., and Vainio, S. (2004). Sprouty proteins regulate ureteric branching by coordinating reciprocal epithelial Wnt11, mesenchymal Gdnf and stromal Fgf7 signalling during kidney development. Development 131, 3345-3356.
194. Takashima, Y., Keino-Masu, K., Yashiro, H., Hara, S., Suzuki, T., van Kuppevelt, T.H., Masu, M., and Nagata, M. (2016). Heparan sulfate 6-O-endosulfatases, Sulf1 and Sulf2, regulate glomerular integrity by modulating growth factor signaling. Am J Physiol Renal Physiol 310, F395-408.
195. Wensing, L.A., and Campos, A.H. (2014). TBX3, a downstream target of TGF-beta1, inhibits mesangial cell apoptosis. Exp Cell Res 328, 340-350.
196. Qiao, X., Roth, I., Feraille, E., and Hasler, U. (2014). Different effects of ZO-1, ZO-2 and ZO-3 silencing on kidney collecting duct principal cell proliferation and adhesion. Cell Cycle 13, 3059-3075.
197. Tufro, A., Norwood, V.F., Carey, R.M., and Gomez, R.A. (1999). Vascular endothelial growth factor induces nephrogenesis and vasculogenesis. J Am Soc Nephrol 10, 2125-2134.
198. Ola, R., Jakobson, M., Kvist, J., Perala, N., Kuure, S., Braunewell, K.H., Bridgewater, D., Rosenblum, N.D., Chilov, D., Immonen, T., et al. (2011). The GDNF target Vsnl1 marks the ureteric tip. J Am Soc Nephrol 22, 274-284.
199. Patel, N., Sharpe, P.T., and Miletich, I. (2011). Coordination of epithelial branching and salivary gland lumen formation by Wnt and FGF signals. Dev Biol 358, 156-167.
200. Xiong, M., Jiang, L., Zhou, Y., Qiu, W., Fang, L., Tan, R., Wen, P., and Yang, J. (2012). The miR-200 family regulates TGF-beta1-induced renal tubular epithelial to mesenchymal transition through Smad pathway by targeting ZEB1 and ZEB2 expression. Am J Physiol Renal Physiol 302, F369-379.
201. Mittaz, L., Russell, D.L., Wilson, T., Brasted, M., Tkalcevic, J., Salamonsen, L.A., Hertzog, P.J., and Pritchard, M.A. (2004). Adamts-1 is essential for the development and function of the urogenital system. Biol Reprod 70, 1096-1105.
202. Bohnenpoll, T., and Kispert, A. (2014). Ureter growth and differentiation. Semin Cell Dev Biol 36, 21-30.
203. Bell, S.M., Zhang, L., Mendell, A., Xu, Y., Haitchi, H.M., Lessard, J.L., and Whitsett, J.A. (2011). Kruppel-like factor 5 is required for formation and differentiation of the bladder urothelium. Dev Biol 358, 79-90.
204. Motamedi, F.J., Badro, D.A., Clarkson, M., Lecca, M.R., Bradford, S.T., Buske, F.A., Saar, K., Hubner, N., Brandli, A.W., and Schedl, A. (2014). WT1 controls antagonistic FGF and BMP-pSMAD pathways in early renal progenitors. Nat Commun 5, 4444.
205. Kann, M., Bae, E., Lenz, M.O., Li, L., Trannguyen, B., Schumacher, V.A., Taglienti, M.E., Bordeianou, L., Hartwig, S., Rinschen, M.M., et al. (2015). WT1 targets Gas1 to

maintain nephron progenitor cells by modulating FGF signals. Development 142, 1254-1266.
206. Heliot, C., Desgrange, A., Buisson, I., Prunskaite-Hyyrylainen, R., Shan, J., Vainio, S., Umbhauer, M., and Cereghini, S. (2013). HNF1B controls proximal-intermediate nephron segment identity in vertebrates by regulating Notch signalling components and Irx1/2. Development 140, 873-885.
207. Adzhubei, I.A., Schmidt, S., Peshkin, L., Ramensky, V.E., Gerasimova, A., Bork, P., Kondrashov, A.S., and Sunyaev, S.R. (2010). A method and server for predicting damaging missense mutations. Nat Methods 7, 248-249.
208. Kumar, P., Henikoff, S., and Ng, P.C. (2009). Predicting the effects of coding non-synonymous variants on protein function using the SIFT algorithm. Nat Protoc 4, 1073-1081.
209. Schwarz, J.M., Cooper, D.N., Schuelke, M., and Seelow, D. (2014). MutationTaster2: mutation prediction for the deep-sequencing age. Nat Methods 11, 361-362.
210. Grantham, R. (1974). Amino acid difference formula to help explain protein evolution. Science 185, 862-864.
211. Tavtigian, S.V., Deffenbaugh, A.M., Yin, L., Judkins, T., Scholl, T., Samollow, P.B., de Silva, D., Zharkikh, A., and Thomas, A. (2006). Comprehensive statistical study of 452 BRCA1 missense substitutions with classification of eight recurrent substitutions as neutral. J Med Genet 43, 295-305.
212. Houdayer, C. (2011). In silico prediction of splice-affecting nucleotide variants. Methods Mol Biol 760, 269-281.
213. Samocha, K.E., Robinson, E.B., Sanders, S.J., Stevens, C., Sabo, A., McGrath, L.M., Kosmicki, J.A., Rehnström, K., Mallick, S., Kirby, A., et al. (2014). A framework for the interpretation of de novo mutation in human disease. Nat Genet 46, 944-950.
214. Velman, J.A., and Brunner, H.G. (2012). De novo mutations in human genetic disease. Nat Rev Genet 13, 565-575